PB93-114817

REPORT NO.
UCB/EERC-91/13
OCTOBER 1991

EARTHQUAKE ENGINEERING RESEARCH CENTER

SHAKING TABLE – STRUCTURE INTERACTION

by

ABDULKARIM M. RINAWI
RAY W. CLOUGH

Report to the National Science Foundation

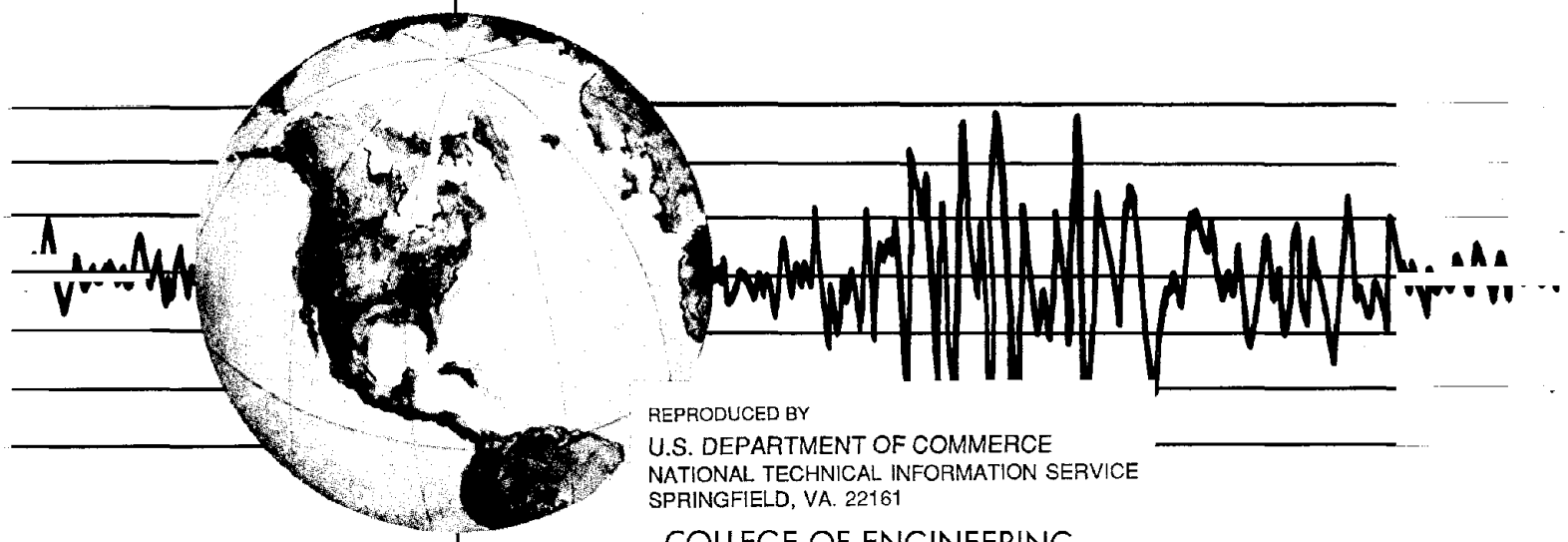

REPRODUCED BY
U.S. DEPARTMENT OF COMMERCE
NATIONAL TECHNICAL INFORMATION SERVICE
SPRINGFIELD, VA. 22161

COLLEGE OF ENGINEERING

UNIVERSITY OF CALIFORNIA AT BERKELEY

For sale by the National Technical Information Service, U.S. Department of Commerce, Springfield, Virginia 22161

See back of report for up to date listing of EERC reports.

DISCLAIMER

Any opinions, findings, and conclusions or recommendations expressed in this publication are those of the authors and do not necessarily reflect the views of the National Science Foundation or the Earthquake Engineering Research Center, University of California at Berkeley.

50272-101

REPORT DOCUMENTATION PAGE	1. REPORT NO. NSF/ENG-91014	2.	3. PB93-114817

4. Title and Subtitle

"Shaking Table-Structure Interaction"

5. Report Date

October 1991

6.

7. Author(s)

A. M. Rinawi and R. W. Clough

8. Performing Organization Rept. No.

UCB/EERC-91/13

9. Performing Organization Name and Address

Earthquake Engineering Research Center
University of California, Berkeley
1301 So. 46th Street
Richmond, Calif. 94804

10. Project/Task/Work Unit No.

11. Contract(C) or Grant(G) No.

(C)

(G) CEE 8316662

12. Sponsoring Organization Name and Address

National Science Foundation
1800 G. Street, N.W.
Washington, D.C. 20550

13. Type of Report & Period Covered

14.

15. Supplementary Notes

16. Abstract (Limit: 200 words)

The 20x20 ft shaking table at the Earthquake Engineering Research Center in Berkeley is tested for interaction effects. The tests include three loading configurations: a bare table, a table loaded with a 70 kip mass and a table loaded with a 68 kip single degree-of-freedom structure with a height of 219 inches. The shaking table has 5 degrees of freedom: one horizontal, one vertical and 3 rotational. When loaded with heavy and tall structures, it undergoes pitching (rocking) motion even in the absence of a pitch degree of freedom. It is observed that the interaction effects are negligible for the bare table and the rigid mass case. For the tall and heavy structure the pitching of the seismic simulator was evident when a horizontal signal was used; in addition, a change in frequency component of the horizontal table motion near the structural frequency was observed. Mathematical models are derived for analyzing the table-structure system. Simplified spring-mass-damper models are discussed. Methods for avoiding modeling of the table flexibilities are presented. Interaction effects are studied using response spectra and the equivalent coupled single degree-of- freedom table-structure system. It is concluded that the interaction effects are very similar to those encountered in soil structure interaction studies. The interaction causes a reduction in the structural frequency component of the command signal near the structural frequency and usually, but not always, an increase in damping. The change in the frequency component of the command signal near the structural frequency due to interaction does not significantly affect the ability of the shaking table to produce damaging motions to the test structure.

17. Document Analysis a. Descriptors

b. Identifiers/Open-Ended Terms

c. COSATI Field/Group

18. Availability Statement	19. Security Class (This Report)	21. No. of Pages
Release Unlimited	unclassified	289
	20. Security Class (This Page) unclassified	22. Price

SHAKING TABLE — STRUCTURE INTERACTION

by

Abdulkarim M. Rinawi

and

Ray W. Clough

Report to the National Science Foundation

Report No. UCB/EERC-91/13
Earthquake Engineering Research Center
College of Engineering
University of California at Berkeley

October 1991

| B

ABSTRACT

The 20x20 ft shaking table at the Earthquake Engineering Research Center in Berkeley (EERC) is tested for interaction effects. The tests include three loading configurations: a bare table, a table loaded with 70 kips mass and a table loaded with 68 kips single degree of freedom structure with a height of 219 inches. The shaking table has 5 degrees of freedom, one horizontal, one vertical and 3 rotational degrees of freedom. When loaded with heavy and tall structures, the shaking table undergoes pitching (rocking) motion even in the absence of a pitch command signal. This is mainly due to the flexibility in the pitch degree of freedom. It is observed that the interaction effects are negligible for the bare table and the table with rigid mass case. In the case of the tall and heavy structure the pitching of the seismic simulator was evident when using a table horizontal command signal; in addition, a change in the frequency component of the horizontal table motion near the structural frequency was observed. Mathematical models are derived for analyzing the table-structure system. These include a shaking table with a horizontal actuator, a pitching actuator and a passive pitch stabilizer. Simplified spring-mass-damper models are also discussed. Methods for avoiding modeling of the table flexibilities are presented. These include the use of a two-directional base input motion and the simpler uni-directional effective base motion. Interaction effects are studied using response spectra and the equivalent coupled single degree of freedom table-structure system. It is concluded that the interaction effects are very similar to those encountered in soil structure interaction studies. The interaction causes a reduction in the structural frequency and usually, but not always, an increase in damping. The change in the frequency component of the command signal near the structural frequency due to interaction does not significantly affect the ability of the shaking table to produce damaging motions to the test structure.

ACKNOWLEDGMENTS

This report is based on the Ph.D. thesis written by the first author at the University of California at Berkeley; Professor R.W. Clough was the thesis advisor. The authors would like to acknowledge the contribution made by Dr. Marcial Blondet in the earlier stages of this project. The help of Dr. Ian Aiken, Dr. Chia-Ming Uang, Dr. Rakesh Goel, and Dr. A.S. Whittaker is also appreciated. The staff of the Earthquake Engineering Research Center, especially Mr. Don Clyde provided invaluable assistance and advice over the course of the experimental program.

The research reported herein was supported by the National Science Foundation and by the Nishkian Chair in Structural Engineering held by Professor R.W. Clough. The support from both sources is gratefully acknowledged.

TABLE OF CONTENTS

Chapter One
INTRODUCTION

1.1 INTRODUCTORY REMARKS

Shaking tables are increasingly being used to test the seismic performance of structures. At present, the shaking table at the Earthquake Engineering Research Center at Berkeley (EERC) can provide two component input motions, horizontal and vertical. In order to allow such input motions, the table is supported by four vertical actuators and three horizontal actuators (Fig 1.1). No locking mechanism is provided to prevent the table from pitching, rolling or twisting; only one of the horizontal degrees of freedom is locked. The undesirable motions are usually minimized by feedback control mechanisms that provide different force levels to the actuators based on the amount of the undesirable motion. In the original design of the table, it was realized that the control system was unable to completely eliminate these movements; for that reason a system of passive stabilizers was designed to provide additional resistance to the undesirable pitching motion.

In spite of the presence of the passive stabilizer system, the EERC table still has some flexibility in the rotational degrees of freedom, and large overturning moments resulting from testing tall and heavy structures can cause undesirable table pitch, roll and twist motions as shown by the results of recent tests [1].

Even in the absence of the rotational degrees of freedom, system reproduction of the horizontal and vertical command signals can be significantly influenced by the addition of the test structure. This is due to shaking table-structure interaction. This interaction effect causes the frequency content of the table displacement to be very different from that of the desired command signal, near the resonance frequency of the test structure.

In planning this research effort, it was hoped that by reproducing the conditions under which the first significant pitching interaction was observed, enough information could be gathered to understand the interaction

problem. In order to accomplish this goal, a steel test frame was constructed with a fundamental frequency of 2.5 Hz. This frequency is the same as that of the reinforced concrete test structure for which significant amounts of undesirable pitch and roll motions were observed in a standard experimental research program [1].

1.2 LITERATURE REVIEW

Shaking table pitching and interaction effects were traditionally dealt with by adding two vertical springs to the mathematical model to represent the pitching flexibility [2,3,4,5,6]. The passive stabilizer system was added to the EERC table in 1977 to reduce the flexibility in the pitching degree of freedom. For this reason springs in the mathematical model used by Tang [2] are different from the ones used by later researchers. The required properties of the springs were typically derived from trial and error analysis, so that the coupled structure frequency matches the measured frequency. This approach, though convenient, can lead to serious errors because the springs will hide other modeling errors.

The performance of shaking tables was the subject of several researchers at U.C. Berkeley in the past. Rea et al. [7] tested a small unidirectional shaking table and the EERC table. Mathematical models were formulated to represent these shaking tables; however the models did not include the pitch effects. Rea found that:

> "... The magnitudes of the peak and notch distortions in the frequency response of shaking tables are sensitive to the amount of force feedback employed by the control system. In addition, the magnitudes depend on the ratio of the mass of the structure to mass of the shaking table, and to the transmissibility function of the structure with respect to the table.
>
> Although the peak and notch effect may cause difficulties in determining the frequency response of structures by means of shaking tables, it has little effect on the accuracy to which a shaking table can reproduce earthquake-type motions..."

Rea also studied the effect of foundation compliance on a shaking table frequency response and found that foundation compliance affects the frequency response of the EERC shaking table only at low frequencies, and that the magnitude of the effect depends on the transmissibility function of the foundation with respect to the table.

Blondet el al. performed a similar study on the unidirectional shaking table at the Catholic University of Peru [8]. In addition to Rea's model, a two degree of freedom mass-spring-damper system was used to simulate the shaking table-structure interaction. Blondet et al. concluded the following

(1) The main aspects of the interaction problem can be studied from a mechanical viewpoint using a 2DOF spring-mass-damper system.

(2) The interaction effects are mainly manifested by a peak and notch in the amplitude frequency response with the maximum attenuation occurring precisely at the natural vibration frequency of the test structure. This is particularly undesirable since the purpose of earthquake simulation tests is to excite the structure at its own frequency in order to cause damage.

1.3 RESEARCH OBJECTIVES

The objective of this research project was to evaluate the EERC shaking table performance and to establish analytical models for the shaking table that can be used to account for and predict the shaking table-structure interaction effects.

More specifically the objectives can be stated as:

(1) to evaluate the table reproduction of typical earthquake records and to study the effects of the pitch motion on the structural response;

(2) to establish a simplified mass-spring-damper system that can account for shaking table-structure interaction effects and can be easily incorporated in analytical models of the test structures; also to devise ways for identifying the model parameters;

(3) to develop an analytical model for a unidirectional shaking table system that includes the feedback control loops;

(4) to extend the mathematical model to include table pitching effects by means of

   (a) a mass-spring-damper system (hybrid model), and

   (b) a feedback control loop similar to that of the horizontal actuators;

   (Such models can be used to predict table performance and stability.)

(5) to investigate ways of improving system performance through modification of the command signal, the addition of actuators, etc; and

(6) to study methods of analyzing tested structures on the shaking table, that may avoid dealing with interaction altogether.

1.4 SCOPE

This report consists of nine main sections. Chapter 2 introduces the shaking table system, test structure and instrumentation. Chapter 3 presents some preliminary data analysis and describes the techniques used in data processing and identification of structural properties: it also presents a list of the acquired data. Transfer functions and response spectra of measured motions are also shown. Chapter 4, an introductory chapter for the rest of the report, illustrates the different ways of dealing with shaking table interaction including methods of avoiding the interaction problem through use of the effective base horizontal acceleration or two-directional base input analysis. Chapter 5 deals with representing the shaking table by a simple spring-damper system, and describes means of identifying the properties of the springs and dampers used in this model. Chapter 6 presents the derivation for the feedback control system representing the bare unidirectional table. Chapter 7 extends the model of Chapter 6 to include a single degree-of-freedom test structure system. Chapter 8 deals with a two-directional feedback control system loaded with a single degree-of-freedom structure. It also introduces a hybrid model that combines a simple spring-damper model with a control system model. Chapter 9 illustrates the effect of shaking table interaction on the response of a test structure

using analytical models. Response spectra and coupled system parameters are derived and discussed. Chapter 10 presents a summary and the conclusions of this study.

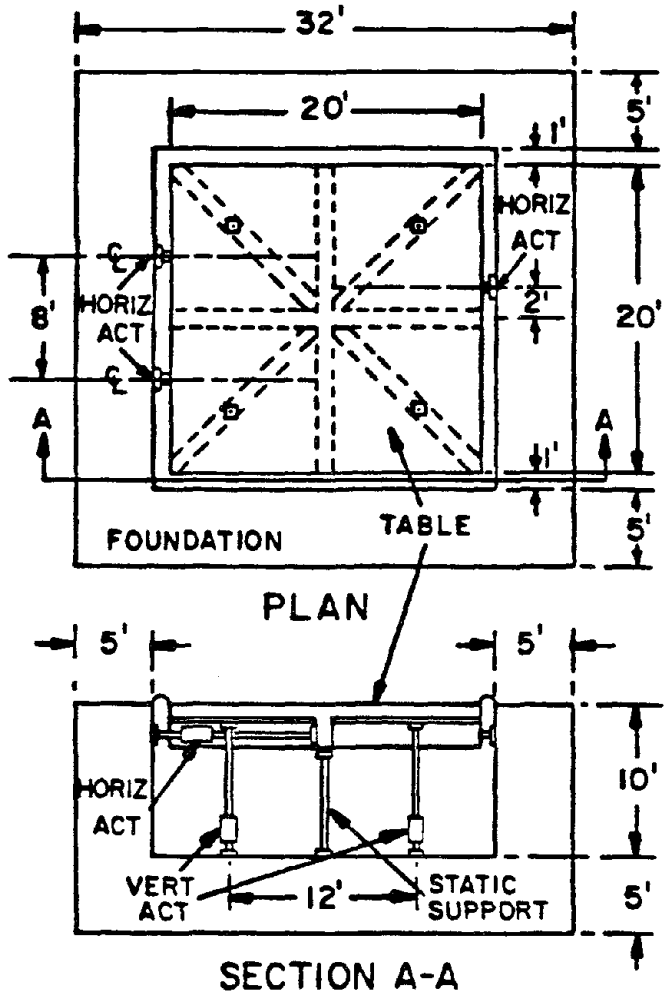

Fig. 1.1 Actuator locations for EERC shaking table.

Chapter Two
TEST EQUIPMENT AND PROCEDURE

2.1 INTRODUCTION

The earthquake simulator performance tests consisted of testing the bare table system, the table with a heavy mass rigidly attached to the table, and the table with a single degree-of-freedom test structure. A nine-story steel structure was also tested, both with fixed and isolated bases, but this structure is not covered in this report. The primary objective of the tests was to obtain measurements of the motions induced in the table by specified inputs so that a comparison could be made between the input signal and the measured responses.

2.2 EARTHQUAKE SIMULATOR

The Earthquake Engineering Research Center (EERC) earthquake simulator consists of a 20 ft by 20 ft reinforced concrete platform. The table is a one foot thick reinforced concrete slab stiffened by heavy central transverse ribs at the bottom. The weight of the slab is about 100,000 lb. The slab is designed to have a fundamental vibration frequency above 20 Hz, so that it can be considered rigid within the usual operating frequency range (0-10 Hz) of the shaking table.

At the time of the test, the EERC table could be programmed to produce a specified vertical and a horizontal component of motion. The table, however, has additional flexibilities in the pitch, roll and twist directions. The shaking table is supported vertically by 4 active actuators located in a square pattern, 12 ft apart; four passive actuators, in a 17-ft square pattern, were added in the late seventies to reduce the flexibility in the pitch degree of freedom and to increase the overturning moment capacity. The horizontal motion is produced by three active actuators. Figure 2.1 shows a sketch of the table with the locations of actuators. Figure 2.2 shows a schematic of the hydraulic interconnection of the passive pitch stabilizers. The actuator

capacities are 25,000 lb for each vertical actuator and 70,000 lb for each horizontal actuator. The horizontal actuators have 170 gpm (gal/min) servovalves; the vertical actuators have 90 gpm servovalves. Table 2.1 lists the specifications for the various EERC shaking table actuators.

The two translational degrees of freedom can be programmed to produce any type of wave form within the limits of the displacement, velocity and force capacity and the frequency bandwidth of the table. With these capacities, the table is able to produce motions about twice those recorded during the El Centro earthquake of 1940, including both the N-S horizontal, and the vertical components combined. The displacement is limited by the actuator stroke and the table clearance, $\mp$ 5 inches in the horizontal and $\mp$ 2 inches in the vertical directions. The flow rate in the servovalves limits the maximum velocities produced in the horizontal and vertical directions to 25 in/sec and 15 in/sec, respectively. The maximum acceleration is limited by the force limits of the actuators together with the mass of the table-structure system. Figure 2.3 shows the acceleration limits for the unloaded table as a function of frequency.

During operation, the air in the pit beneath the shaking table is pressurized so that the total weight of the table and the structure being tested is balanced by the difference between the air pressure in the pit and the ambient air pressure. The pit entrance is sealed by two airtight doors that provide a lock chamber and thus permit access to the pit while the air in the pit is pressurized. The one foot horizontal gap between the edge of the table and the interior foundation walls is sealed by a 24-inch wide strip of vinyl-covered nylon fabric. A differential air pressure of 1.55 psi is required to balance the weight of the shaking table alone.

Oil at 3,000 psi is supplied by four 90 gpm pressure regulated pumps, each of which is driven by a 120 hp electric motor. Accumulators that can double the peak instantaneous flow rates are installed in the main oil line, but the oil supply is not sufficient to produce maximum horizontal and vertical velocities simultaneously. However, it is considered unlikely that the maximum horizontal and vertical components of an earthquake would occur

simultaneously.

The actuator forces are reacted by a massive foundation block, which is a reinforced concrete structure in the form of an open box with 5 ft thick sides. The outside dimensions of the box are 32 x 32 x 15 ft, and the inside dimensions are 22 x 22 x 10 ft. The foundation weighs 1,580,000 lb. Specifications of the shaking table are given in Table 2.2.

Table 2.3 is a list of the signals measured during the tests on the SDOF structure.

2.3 DATA ACQUISITION SYSTEM

The data acquisition system can acquire up to 128 data channels. An analog to digital converter converts the filtered data into digital form to be stored and processed by a VAX 11/750 computer. Data analysis and display are mainly done through the S Statistical Software available on the VAX. The data acquisition system samples data at 50 KHZ, and when acquiring data on all 128 channels, the maximum sampling rate per channel is 50,000/128 = 390 samples per second. During the current tests an analog lowpass filter with cut-off frequency of 100 Hz was applied to all output channels before they were digitized. Sampling was normally done at twice the filter frequency in order to avoid aliasing in the digitized signals. Aliasing is a phenomenon that occurs when sampling a high frequency signal at a sampling rate less that twice that frequency. Undersampling would cause the digitized signal to have lower frequency signals generated from the high frequency data. It is usually very difficult to get rid of these aliased frequencies once the data is collected, and simple filtering would not help in this case.

2.4 TEST STRUCTURE

Figure 2.4 shows the single degree-of-freedom structure mounted on the EERC shaking table in tests performed for this investigation. The structure is a four story, braced steel frame weighing 6.45 kips and supporting a weight of 62.5 kips. This test frame is the lower part of the steel frame tested by Hucklebridge [3].

The structure consists mainly of W6x8.5 beams and W4x13 steel columns. A W8x31 base beam connects it to the shaking table by means of pre-stressed steel rods spaced at 3 ft intervals which pass through 2-in diameter holes in the 1-ft thick reinforced-concrete table. The two identical parallel frames that form the steel structure are spaced 6 ft apart, and the total length of the frame in the test direction is 18 ft. The height of the first floor is 4 ft above the base beam; all the other floors are 3-ft high except for the top floor. That floor consists of 1.5-ft high columns supporting 16-inch deep beams, on which are placed eight concrete blocks weighing 4 kips each. The height of the concrete blocks is 15 inches. The concrete blocks support 26.4 kips of lead blocks. The center of mass of the lead blocks is 11 inches above the upper face of the concrete blocks.

A sketch of the instrumentation is shown in Fig. 2.5. Four accelerometers at the top of the structure were attached to the top deep beams to measure the structure responses -- two sensing motion in the direction of the table movement and two oriented to indicate accelerations perpendicular to the table motion. The accelerometers were 189.3 inches above the top face of the shaking table. Two displacement meters were also used in the lateral direction (direction of table motion), and the displacements were measured with respect to a reference frame which was supported on the laboratory floor away from the table.

2.5 TEST MASS

The table was loaded with three concrete blocks (WxHxL=48x21.5x240 inches) having a total weight of 70.5 kips. Each block was anchored to the table by post-tensioned steel rods. The long direction of the blocks was aligned perpendicular to the horizontal direction of shaking. This total mass was used to determine the effect on the table performance of a rigid test specimen with relatively low overturning moment. The center of gravity of the mass was only 10.75 inches above the table surface, as shown in Fig. 2.6.

2.6 OTHER TEST EQUIPMENT

A small shaker driving a weight of 50 lb was placed on the top of the test structure; this produced a random input force that was used to evaluate the uncoupled structure frequency and damping.

A GenRad 2515 vibration analysis system was used for the generation of random command signals, for data acquisition and for transfer function evaluation. The system can acquire 4 channels of data at a maximum sampling rate of 25000 samples per second. It has a built in Fast Fourier Transform (FFT) analyzer to perform frequency domain computations. The FFT frame can be varied from 512 points to 8192 points. Four transfer functions can be calculated and averaged in real time. Overlapping windows are used for noise reduction in transfer function and power spectra computations; other features include cross spectra, auto and cross correlation and coherence function computations. Very efficient "circle fitting" is also available for resonance frequency, damping and amplitude computation. The system has capabilities for storing the test data on a disk for further analysis with either TSL2 (Time Series Language), or MODAL software. MODAL is a program developed by SDRC (Structural Dynamics Research Corporation) to do multi-mode transfer function fitting, mode shapes estimation and display. Frequencies and damping ratios were calculated using the RTA (Real Time Analysis) program on the GenRad system.

ACTUATOR (as in Fig. 2.1)	MODEL NUM.	AREA (in^2)	STROKE (in)	SERVOVALVE (MODEL #)	FLOW (gpm) CAPACITY	CAPACITY (kips)
H1	204.32	25.4	12	251.42	170	50
H2	204.32	25.4	12	251.42	170	50
H3	204.32	25.4	12	251.42	170	50
V1	204.25	9.6	4	251.32	90	25
V2	204.25	9.6	4	251.32	90	25
V3	204.25	9.6	4	251.32	90	25
V4	204.25	9.6	4	251.32	90	25
P1	204.72	26.0	4	N/A	N/A	50
P2	204.72	26.0	4	N/A	N/A	50
P3	204.72	26.0	4	N/A	N/A	50
P4	204.72	26.0	4	N/A	N/A	50

Table 2.1: Specifications for MTS actuators used in EERC earthquake simulator.

Plan dimensions	20 x 20 ft (6.1 x 6.1 meters)
Model tie down locations	2-inch diameter holes @ 36 inches on center (914 mm)
Model weight capacity	130,000 lb (578 KN)
Overhead clearance	40 ft to ceiling (12.2 meters) 32 ft to 10 ton crane (9.75 meters)
Overturning resistance	3,343 kip-ft (229 NM)
Displacement	Horizontal ∓ 5 inches (∓ 152 mm) Vertical ∓ 2 inches (∓ 76 mm)
Velocity	Horizontal ∓ 25 ips (∓ 635 mm/sec) Vertical ∓ 15 ips (∓ 381 mm/sec)
Acceleration	Horizontal ∓ 1.5 G (∓ 1472 gal) Vertical ∓ 1.0 G (∓ 981 gal)
Bandwidth	0 - 20 Hz

Table 2.2: Specifications of EERC Shaking Table

CHANNEL ID	CHANNEL NAME	FULL NAME	UNITS
1	avg hdisp	Average Horizontal Displacement	inches
2	avg vdisp	Average Vertical Displacement	inches
3	avg hacc	Average Horizontal Acceleration	G
4	avg vacc	Average Vertical Acceleration	G
5	pitch acc	Pitch Acceleration	rad/sec2
6	roll acc	Roll Acceleration	rad/sec2
7	twist acc	Twist Acceleration	rad/sec2
8	v2 disp	V2 Vertical Actuator Displacement	inches
9	v3 disp	V3 Vertical Actuator Displacement	inches
10	v4 disp	V4 Vertical Actuator Displacement	inches
11	h span	Command Displacement	inches
12	h1 force	H1 Horizontal Actuator Force	kips
13	h2 force	H2 Horizontal Actuator Force	kips
14	h3 force	H3 Horizontal Actuator Force	kips
15	v1 force	V1 Vertical Actuator Force	kips
16	v2 force	V2 Vertical Actuator Force	kips
17	v3 force	V3 Vertical Actuator Force	kips
18	v4 force	V4 Vertical Actuator Force	kips
19	h1 disp	H1 Horizontal Actuator Displacement	inches
20	h2 disp	H2 Horizontal Actuator Displacement	inches
21	p1 stab	P1 Passive Stabilizer Force	kips
22	p2 stab	P2 Passive Stabilizer Force	kips
23	p3 stap	P3 Passive Stabilizer Force	kips
24	p4 stab	P4 Passive Stabilizer Force	kips
25	h vel	Table Horizontal Velocity	in/sec
26	accN-NE	Accelerometer	G
27	accN-NW	Accelerometer	G
28	accW-NW	Accelerometer	G
29	accW-SW	Accelerometer	G
30	potN-SW	Potentiometer	inches
31	potN-SE	Potentiometer	inches
32	accCMD	Accelerometer	G

Table 2.3: Identification of Test Channels

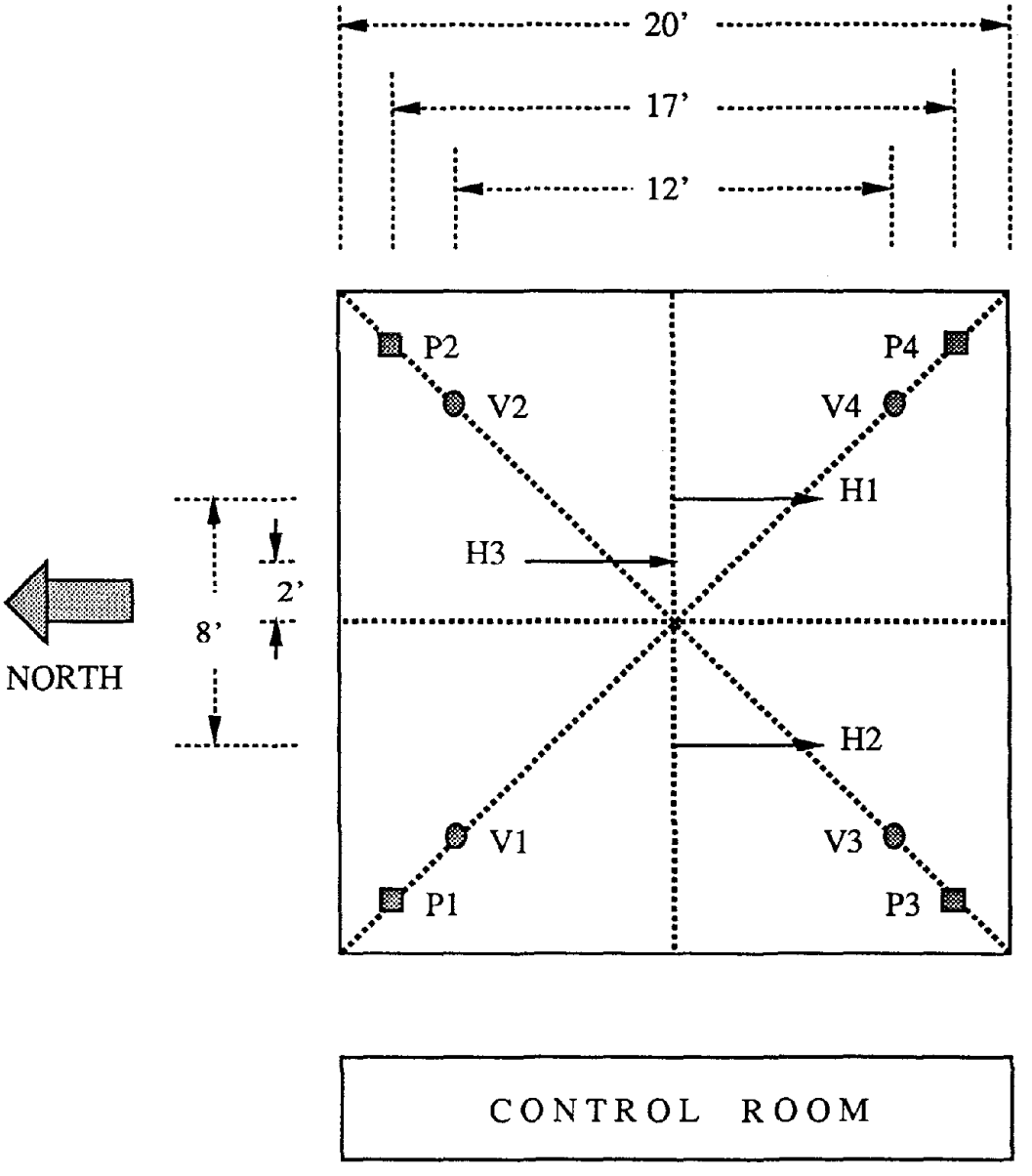

V1, V2, V3, V4 : Vertical Actuators
P1, P2, P3, P4 : Passive Stabilizers
H1, H2, H3 : Horizontal Actuators

Fig. 2.1: Actuator locations in EERC earthquake simulator.

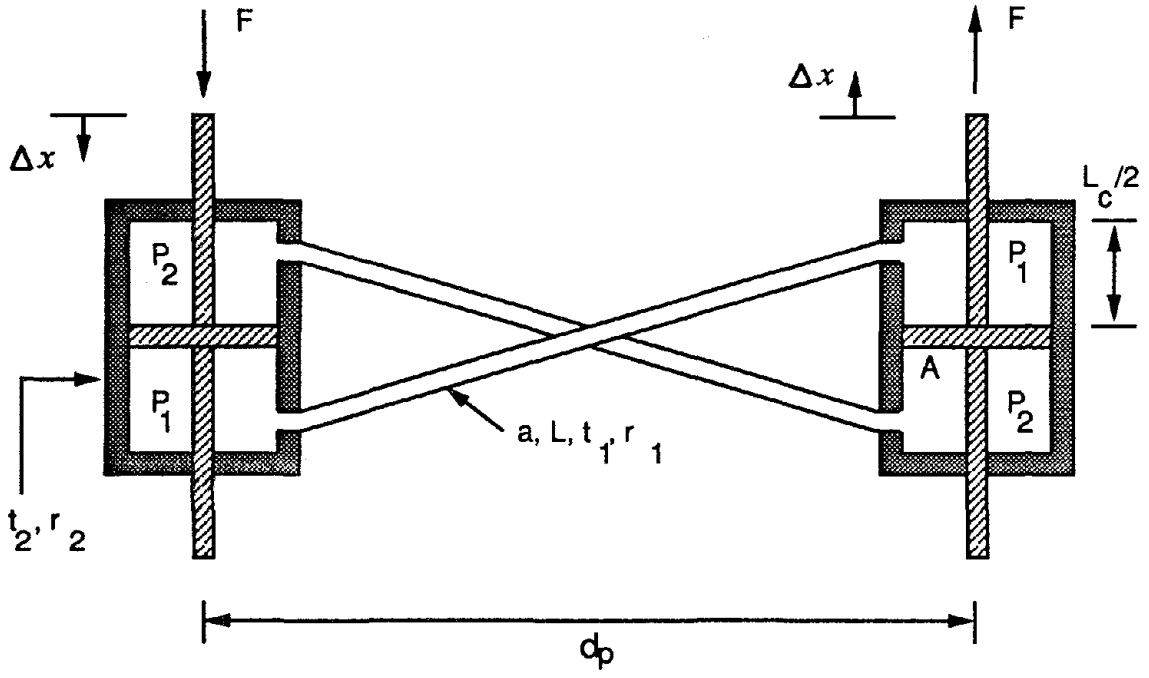

Fig. 2.2: Hydraulic Passive Stabilizer Unit.

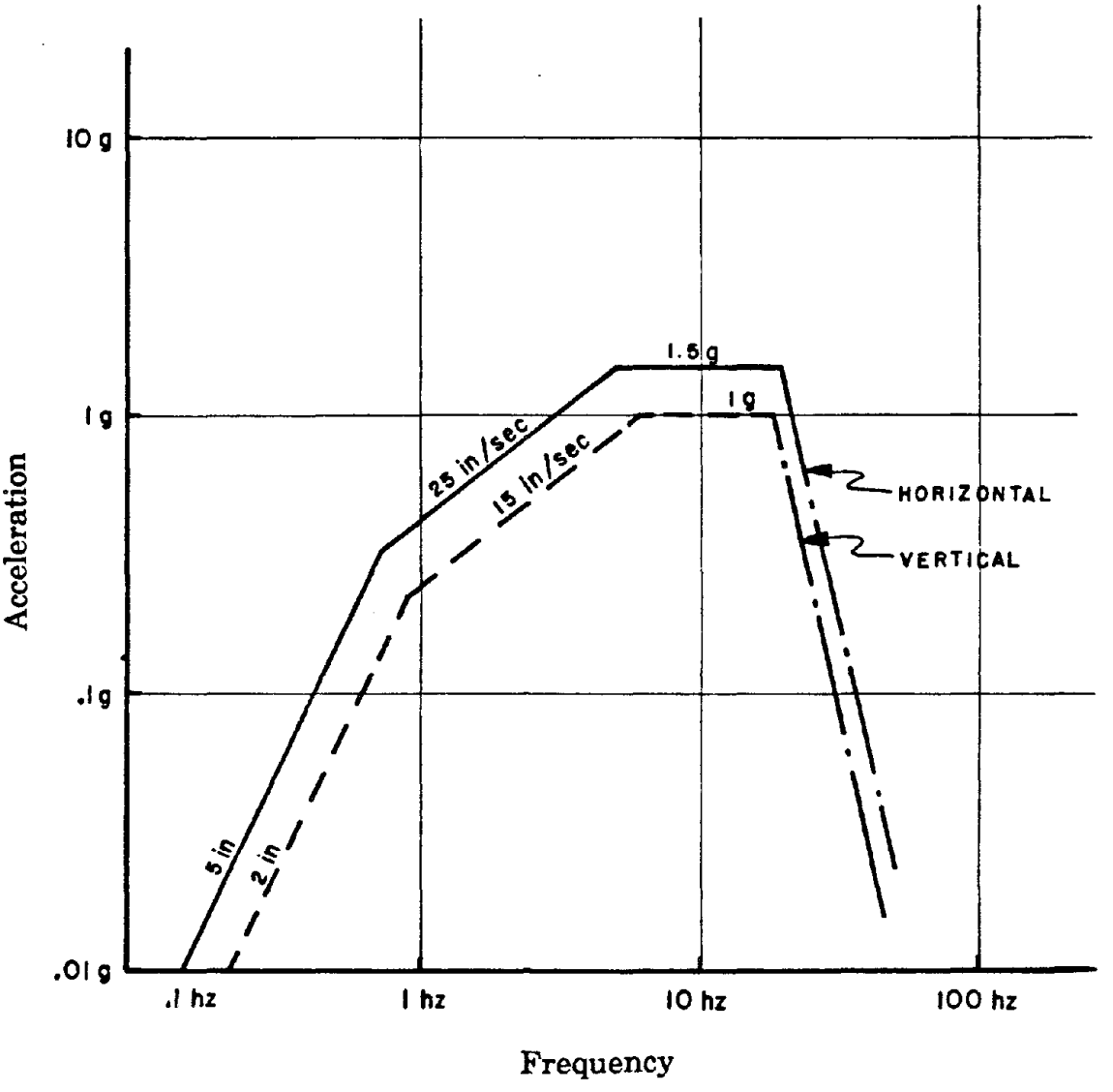

Fig. 2.3: EERC Shaking Table Motion Limits. Bare Table.

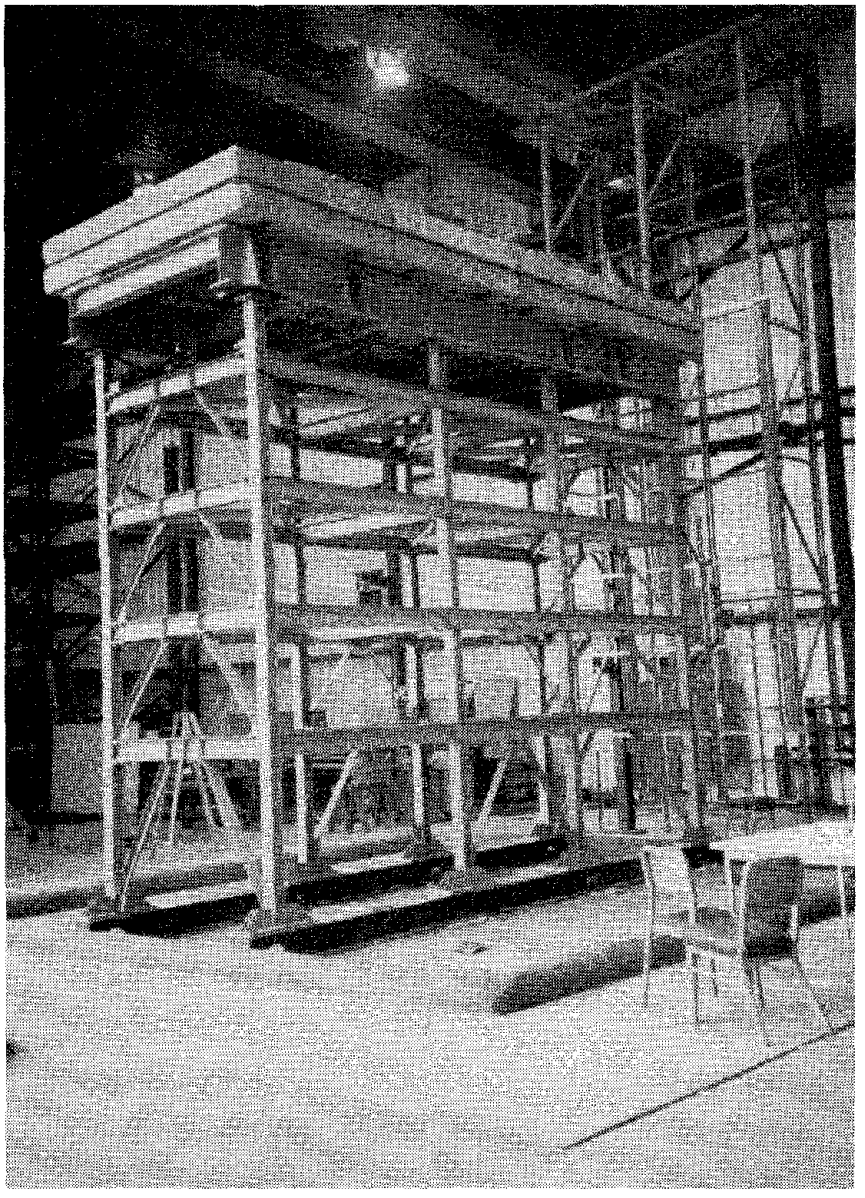

Fig. 2.4: SDOF Structure Mounted on EERC Shaking Table.

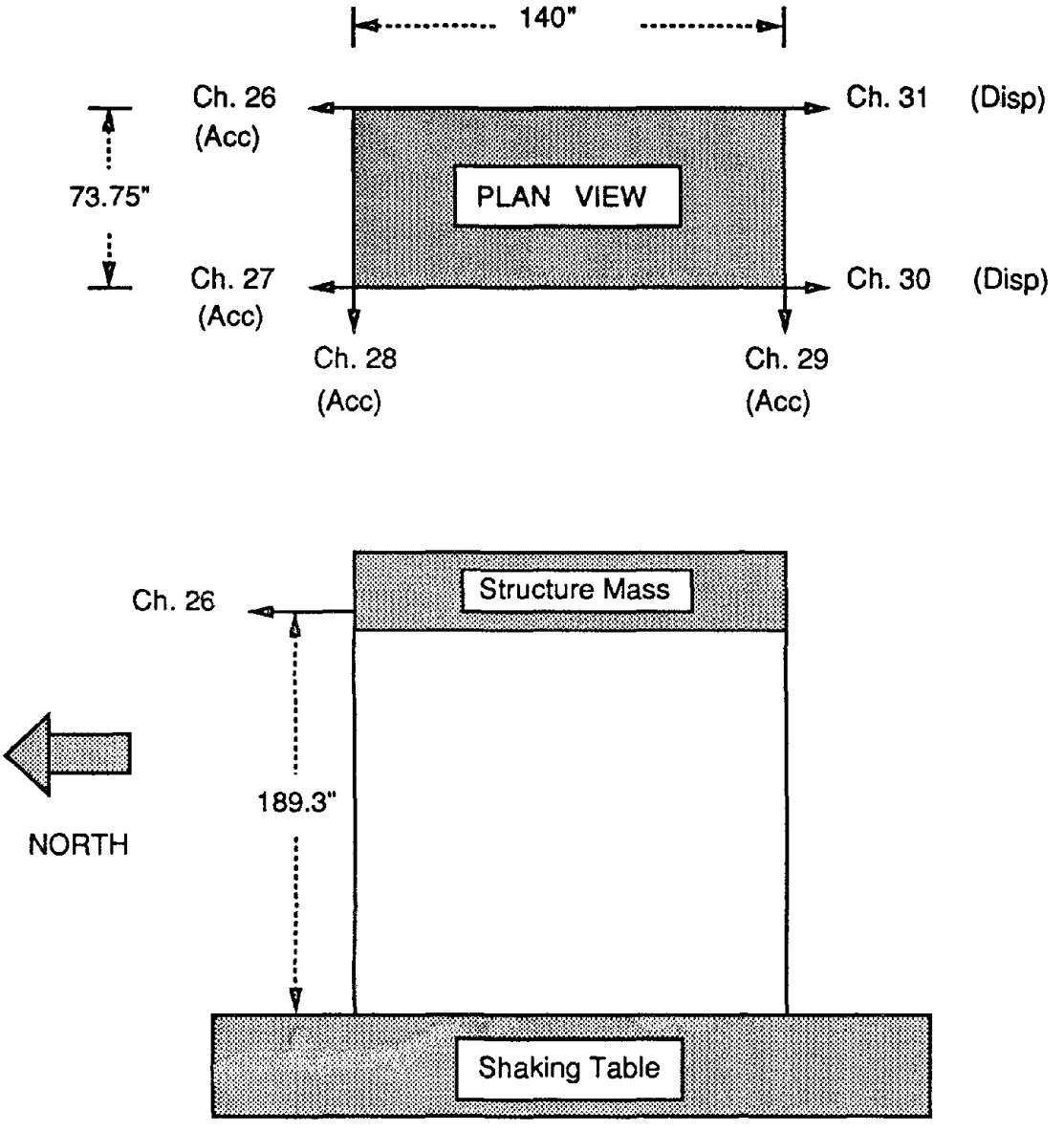

Fig. 2.5: Locations of accelerometers and displacement meters.

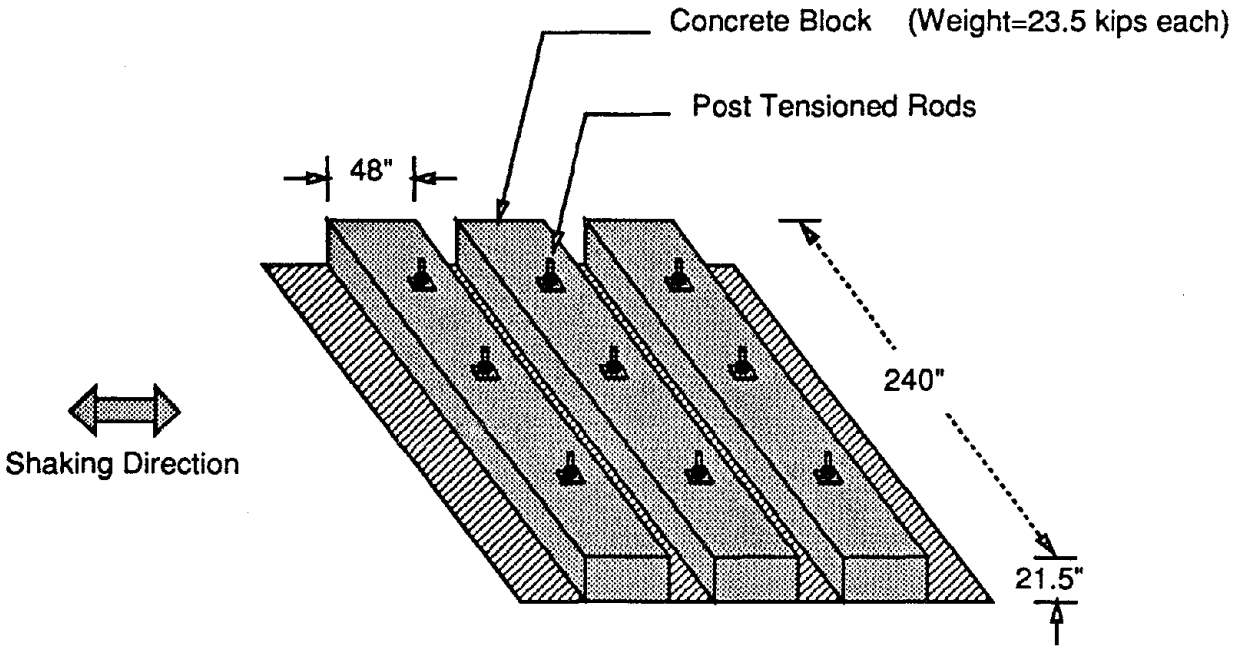

Fig. 2.6: Concrete blocks on EERC shaking table.

Chapter Three
PRELIMINARY DATA ANALYSIS

3.1 INTRODUCTION

Tables 3.3-3.6 are lists of tests performed on the VAX computer. The random test signals recorded on the VAX consisted of short duration signals of 11 seconds each. Normally a random signal test lasted for a period of more that 1 minute and the GenRad system collected the data through successive averaging of auto and cross spectra, transfer functions and coherence functions. The VAX random signal record was done for reference purposes only. Four channels were normally recorded on the GenRad system while 32 channels were written to the VAX storage disk. A list of the VAX data acquisition channels is provided in Table 2.3.

One way of studying the shaking table system performance is by means of transfer functions which give an indication of the system reproduction of the command signal, the frequency bandwidth and stability of the table motion. In this chapter some of the transfer functions produced by the GenRad system from the shaking table test signals are described.

Transfer functions are presented for three loading conditions: bare table, 70 kip mass attached rigidly to the table, and 62.5 kip SDOF structure having a height of 190 inches. The transfer functions show the output table horizontal displacement and table pitch displacement as a function of the inputted table command displacement.

The natural frequencies and damping ratios of the test structure were evaluated. Two cases are considered, first the base of the structure is completely fixed, and second the structure and the table are acting as a coupled system. The fixed-base structure case is obtained by locking all the motions of the shaking table. Also presented are response spectra comparisons including some showing the shaking table interaction effects.

3.2 DATA PROCESSING

Transfer function measurements of the shaking table horizontal displacement, the table pitch acceleration and the test structure top acceleration relative to the command displacement were performed using the RTA 2.0 program running under the RT-11 operating system of the GenRad 2515. During data acquisition each signal of length 16 seconds (called a frame) is represented by 2048 data points in the GenRad system. In the frequency domain it has a frequency band of 0-32 Hz with 512 complex frequency points. The GenRad system has a built-in anti-aliasing filter that automatically filters any frequencies higher than half the sampling frequency. A "Hanning Window" was used to minimize the leakage by eliminating the abrupt discontinuities at the ends of each data frame. Leakage causes the amplitude spectrum at a given frequency to decrease by transferring some of the energy at that frequency to adjacent frequencies. The Hanning function also reduces the total energy contained in the frame, but this can be corrected by a factor such that the total energy is the same as that of the original input frame. In order to minimize the effect of noise in the measured transfer functions, successive measurements are taken and averaged. Typically a total of 40 averages were made. Overlapping segments were used in order to minimize the time needed for averaging and smoothing out the data. In this case the system does not wait until a completely new data frame is obtained, it simply uses part of the old frame to complete the number of points needed for the FFT.

3.2.1 Method Of Estimating Transfer Functions

In order to get the best estimate of the transfer function H_{xy} between two channels x & y, the GenRad system uses the following calculation procedure:

$$H_{xy} = \frac{G_{xy}}{G_{xx}} \tag{3.1a}$$

where

$$G_{xy} = \sum(S_x \bar{S}_y) \tag{3.1b}$$

$$G_{xx} = \sum(S_x \bar{S}_x) = \sum(S_x)^2 \tag{3.1c}$$

S_x =Fourier Spectrum of Input x

S_y =Fourier Spectrum of Output y

$\bar{S}_x, \bar{S}_y$ =Complex Conjugates of S_x and S_y, respectively

In the GenRad system, transfer functions are evaluated and added to the current average values to obtain an updated average which is displayed.

In order to estimate the degree of noise present as well as the nonlinearity and repeatability in the system transfer function, the coherence function was also measured. The coherence function between input x and response y is defined as

$$Coherence\,(x,y) = \frac{(G_{xy})^2}{G_{xx} G_{yy}} \tag{3.2}$$

The coherence function is meaningful only for averaged data and it is always less than or equal to unity. A value close to one indicates good quality transfer function data. Mitchell [9] discusses more improved methods for transfer function estimation.

3.3 IDENTIFICATION OF STRUCTURAL PROPERTIES

Random signals provide input energy that is relatively uniform over the frequency range of interest; therefore these signals can be useful in frequency and damping identification. In addition to the random signals, two earthquake records, the 1952 Taft and the 1978 Miyagi-Ken-Oki were used for structural identification.

3.3.1 Fixed Base Case

3.3.1.1 Identification using random signals: The fixed-base case was studied by placing a small shaker at the top of the structure while the shaking table was completely blocked against motion. A random signal was applied to the small shaker mass (50 lb) and the inertia forces induced in the structure were used to estimate the frequency (2.87 Hz) and damping (0.3 percent).

3.3.1.2 Identification using earthquake records: The method using a small shaker involved locking the base of the structure from motion and applying a very small amplitude load to the top of the structure. In actual tests the forces applied to the structure are large enough so as to produce yielding and damage in the tested specimen. The fixed-base characteristics of the model under such severe loads could be very different from those corresponding to small amplitude vibrations. An updated estimate of the structural characteristics during the actual test becomes important.

During a horizontal earthquake motion simulation test with the EERC shaking table, the table would move horizontally and would undergo some pitching due the high overturning moment induced by the test structure. The equation of motion for a single degree-of-freedom structure subjected to a rigid base translation x_t and rigid base rotation θ as shown in Fig. 3.1 can be written as

$$m_s \ddot{x}_s^t + c_s \dot{x}_s + k_s x_s = 0 \tag{3.3}$$

where m_s, c_s and k_s are, respectively, the values for the structural mass, damping and stiffness. The absolute displacement of the mass of the structure consists of a rigid body component due to the base motions and a deformation or relative displacement component x_s as

$$x_s^t = (x_t + \theta h) + x_s = x_{eff} + x_s \tag{3.4}$$

where x_{eff} is the effective rigid body translation of the structural mass and is written as

$$x_{eff} = x_t + h\theta \tag{3.5}$$

Equation (3.4) can be substituted in Eq. (3.3) to get

$$m_s\ddot{x}_s + c_s\dot{x}_s + k_s x_s = -m_s(\ddot{x}_{eff}) \tag{3.6}$$

and in terms of the structural frequency and damping parameters it can be rewritten as

$$\ddot{x}_s + 2\xi_s\omega_s\dot{x}_s + \omega_s^2 x_s = -\ddot{x}_{eff} \tag{3.7}$$

where ω_s and ξ_s are the fixed-base frequency and damping of the structure, and are given by the relations

$$\omega_s^2 = \frac{k_s}{m_s} \tag{3.8}$$

$$2\xi_s\omega_s = \frac{c_s}{m_s} \tag{3.9}$$

In the frequency domain Eq. (3.7) can be written as

$$(-\omega^2 + 2\xi_s\omega_s\omega j + \omega_s^2)x_s(\omega) = \omega^2 x_{eff}(\omega) \tag{3.10}$$

where j is $\sqrt{-1}$. The transfer function between the structural relative displacement and the effective displacement can be written as

$$H(j\omega) = \frac{x_s(\omega)}{x_{eff}(\omega)} = \frac{\omega^2}{(\omega_s^2 - \omega^2) + j(2\xi_s\omega_s\omega)} \tag{3.11}$$

This transfer function is the focal point in identifying the fixed-base frequency and damping. Damping can be estimated using the half power or bandwidth method [11]; but in most cases a linear least squares circle fitting [10] or amplitude fitting [Appendix D] were used to identify the fixed-base characteristics. The transfer function $H(j\omega)$ was estimated from the measured relative structural displacement and the measured effective acceleration for each earthquake simulation test.

Much larger damping values were determined from the earthquake tests than were observed in the random signal tests with the small shaker. These damping values increased with the amplitude of earthquake excitation and this significant change in damping can be attributed to the fact that the

mass was not rigidly attached to the structure. The relative movement of the 264 lead weights which were stacked on three layers can lead to friction and hence energy dissipation. The fixed-base structural frequency and damping during the different earthquake tests are shown in Figs. 3.2a and 3.2b. Figure 3.2b shows clearly the damping dependence on the response amplitude. The procedure used for fixed-base frequency and damping identification as described here is exact for SDOF systems and also can give a good approximation of the first fixed-base frequency for MDOF systems, as discussed in Chapter 4.

3.3.2 Coupled Table-Structure Properties

The coupled shaking table-structure properties were evaluated by subjecting the table-structure system to a random horizontal table command displacement. The transfer function of the relative mass acceleration with respect to the command signal was evaluated and circle fitting [10] was performed to evaluate the system frequency (2.54 Hz) and damping (3.33 percent). These properties reflect the coupling due to both the horizontal and pitching degree of freedom. In order to evaluate the coupled parameters in the pitching degrees of freedom only, another transfer function, the relative mass acceleration with respect to the horizontal table acceleration was used.

The frequency and damping determined for the SDOF test structure for the two earthquake signals used are listed in Table 3.1 for the fixed-base case, for the pitch coupling case, and for the pitch and horizontal coupling case. The estimation of the coupled system parameters and their usefulness will be explained in more detail in Section 5.3.1.

3.4 TRANSFER FUNCTIONS OF THE SHAKING TABLE SYSTEM

In this section the experimentally measured transfer functions are presented for three cases: bare table, table with 70 kip mass rigidly attached to the table, and table with a SDOF structure. In all cases the EERC table was subjected to a random command displacement signal. The resulting transfer function between the table displacement and the

command displacement was instantaneously calculated using the GenRad system. In this section only the experimental results corresponding to the standard settings of the shaking table control system (Table 3.2) are presented, although additional tests were performed to investigate the influence of the control system settings as shown in Tables 3.3-3.6. The effect of some control system settings will be dealt with in Chapters 6 and 7.

3.4.1 Bare Table Transfer Function

The transfer function of the bare table horizontal displacement relative to the command displacement is shown in Fig. 3.3. It has characteristics similar to a low-pass filter of about 10 Hz, almost completely attenuating all frequencies above 25 Hz. The phase curve of the transfer function shows that frequencies in the table displacement above about 12.6 Hz are out of phase with those of the command displacement. The transfer function of the pitch displacement θ relative to the command displacement is shown in Fig. 3.4. Pitch displacement was obtained from the measured pitch acceleration by dividing the Fourier amplitude at each frequency by ω^2. The bare table pitch consists mainly of high frequency response. It is out of phase with the command displacement at about 11.5 Hz, it has a peak around 12.5 Hz, and it shows a notch at about 24 Hz.

3.4.2 Table Loaded With 70 Kip Mass

The transfer function for the horizontal displacement of the table loaded with a 70 kip weight is shown in Fig. 3.5. Also shown in the figure for comparison is the bare table transfer function (taken from Fig. 3.3). The addition of the mass caused a decrease in the system frequency bandwidth. The table displacement becomes out of phase with the command signal at about 8.5 Hz frequency.

The pitch transfer function for the table loaded with a rigid mass is shown in Fig. 3.6 . It has two prominent peaks, at about 8 and 15 Hz. The figure also indicates that the pitch becomes out of phase with the command displacement at about 8 Hz.

3.4.3 Table Loaded With SDOF Structure

The transfer function of the shaking table horizontal displacement over the command displacement for the loaded table case with SDOF structure is shown in Fig. 3.7 together with the bare table transfer function from Fig. 3.3. This transfer function shows a significant peak (resonance) with an amplitude of 2.2 and a notch (anti-resonance) with an amplitude of 0.7, occurring near the coupled table-structure frequency. A significant phase lag is clearly seen near the peak and notch frequencies.

Compared with the bare table transfer function, in addition to the peak and notch effects, the transfer function with the SDOF structure showed amplification of response for frequencies between 5 and 8 Hz, and attenuation for frequencies higher than 8 Hz. In addition, the out-of-phase frequency (frequency at which the phase is 180 degrees) was significantly lower (9.6 Hz). All of the effects contributed to reducing the bandwidth.

The transfer function of the shaking table pitch displacement over table horizontal command displacement for the loaded table with SDOF structure is shown in Fig. 3.8. In this case the shaking table pitch motion is dominated by the response at the coupled table-structure frequency. The phase shift frequency is about 9.6 Hz together with a small peak near 15 Hz and a notch at about 24 Hz.

3.5 GENERAL COMMENTS ON TRANSFER FUNCTIONS

From the bare table transfer functions (Fig. 3.3), it can be seen that the table horizontal displacement gives a good representation of the command displacement if the command displacement has no frequencies higher than 10 Hz. Frequencies higher than 10 Hz are significantly attenuated and are almost eliminated above 25 Hz. It also can be seen that in the range of 3-10 Hz the table displacements are only about 80 percent of the command displacements. Very long period signals (0-3 Hz) are reproduced much better than the higher frequency signals.

In the case of the 70 kip added mass (Fig. 3.5), the command signals having frequencies between 0 and 8 Hz are reproduced with less than a 5 percent

error in the amplitude. However, the phase is not as well reproduced because at frequencies higher than 8.5 Hz the response is out of phase with the command signal.

The addition of the SDOF structure changed the horizontal table transfer function significantly (Fig. 3.7). The peak and notch in this function are due to interaction effects and in this case, system reproduction of the command signal is questionable. At frequencies just below the coupled table-structure frequency, the table displacement amplitudes are more than twice the command displacements. At frequencies just higher than the coupled frequency (which also happened to be the fixed-base structural frequency) the table displacement amplitudes are significantly lower than those of the command displacement. In addition, a close look at the pitch transfer function (Fig. 3.8) shows a clear significant response near the same coupled frequency. This is undesirable since most of the structural response is concentrated around this frequency. It was for this reason that this investigation was undertaken in order to see how accurately the system reproduces the command displacement and whether the real table motion produces greater or less damaging effects to the test structure.

Although the rigid mass had some eccentricity, with respect to the table mass, the maximum table pitch in this case (Fig. 3.6) was only twice as much as for the bare table (Fig. 3.4). The addition of the SDOF structure however caused the pitch motion to have a peak near the coupled table-structure frequency (Fig. 3.8) with an amplitude ten times higher than the maximum amplitude in the bare table transfer function (Fig. 3.4).

3.6 COMPARISONS OF MEASURED ACCELERATION SPECTRA

One way to look at the extent of interaction is to compare the command acceleration spectra with that of the measured horizontal table acceleration, and more important, with that of the effective acceleration spectra which was defined in Section 3.3.1.2. The effective acceleration spectrum represents the peak response of a SDOF test structure with no coupling effects (i.e. with fixed-base properties). The response spectrum of the

horizontal table acceleration represents the peak responses of a SDOF structure with pitch coupling only. The command acceleration spectrum in this case represents the maximum responses of a SDOF test structure taking into account coupling in both the horizontal and pitching degrees of freedom.

Figure 3.9a shows the response spectra of the original Taft acceleration record and the measured table acceleration record. All the spectra are for 5 percent of critical damping. It is clear that the spectrum of the table acceleration is slightly higher than that of the earthquake record near the coupled table-structure period T_c. The spectrum evaluated from the effective table acceleration $\ddot{x}_t + h\ddot{\theta}$ can be compared with the original Taft spectrum in Fig. 3.9b. Clearly the effective acceleration has a much higher response at periods greater than the fixed-base structure period T_f. This spectrum has a very significant peak at the coupled period T_c of the system at which period the pitch motion is mainly concentrated. It should be noted here that only the value at the fixed-base frequency applies to this structure. Furthermore, with respect to the original spectrum shown in Fig. 3.9b, only the spectral value corresponding to the coupled period T_c applies to this particular structure. This latest observation suggests that although the effective acceleration spectra differ significantly from the original spectra, the peak response for the tested structure did not vary significantly.

It should be noted here that since the effective motion is a function of the tested structure and its effective height, simple comparisons of this type are not very useful in studying the interaction effects. In addition, damping is an important factor as it varies from the uncoupled to the coupled case. Damping was taken as a constant value of 5 percent in this case. The response spectrum approach will be discussed in more detail in Chapter 9.

EARTHQUAKE RECORD	Fixed base		Base rotation coupling		Transl. and rot. coupling	
	FREQ (Hz)	DAMP (%)	FREQ (Hz)	DAMP (%)	FREQ (Hz)	DAMP (%)
Miyagi span 270	2.87	1.2	2.71	2.3	2.62	2.0
Miyagi span 350	2.86	1.4	2.71	2.5	2.59	1.8
Taft span 200	2.86	1.7	2.70	1.0	2.58	2.4

Table 3.1: Vibration characteristics of the structure for three boundary conditions and three different records.

DIRECTION	GAIN	DELTA-P	RATE
Horizontal Control	9	1.5	5
Pitch Control	0	2.0	0
Vertical Control	4	2.0	10
Roll Control	4	2.0	10
Twist Control	5	2.0	0

Table 3.2 : Standard Shaking Table Control Settings (1985-1986).

RUN NUM	RUN ID	DURATION	Time Step	Comments
				BARE TABLE
850802.01	RANDOM 0-25hz	15	.005	span=50
850802.02	RANDOM 0-25hz	15	.005	span=100
850802.03	RANDOM 0-25hz	15	.005	span=150
850802.04	MIYAGI	15	.005	span=270
850802.05	MIYAGI	15	.005	span=500
850802.06	TAFT.s	25	.005	span=400
850802.07	TAFT.s	20	.005	span=800
850802.08	TAFT.s	20	.005	span=800
ADDED STRUCTURE 60kips 200 inches				SDOF STEEL STRUCTURE
850809.01	RANDOM 0-25hz	1	.002	ADD SMALL SHAKER
850809.02	RANDOM 0-25hz	11	.005	small shaker
850812.01	RANDOM 0-25hz	25	.01	small shaker
INCREASES GAINS ON CHANNELS 26-29 from 50 to 500				
850812.02	RANDOM 0-25hz	25	.01	
MOVED CHANNELS 27 TO SHAKER & PUT GAIN BACK TO 50				
850812.03	RANDOM 0-50hz	25	.01	transv excit
850813.01	RANDOM 0-25hz	25	.01	skewed excit
CHANNEL 27 GAIN AT 500				SDOF STEEL STRUCTURE
850813.02	RANDOM 0-50hz	25	.01	skewed excit
850813.03	RANDOM 0-50hz	25	.01	skewed excit
850813.04	RANDOM 0-50hz	9	.004	skewed excit
850813.05	RANDOM 0-50hz	10.5	.0025	skewed excit
850814.17	RANDOM 0-25hz	11	.005	skewed excit
850814.18	RANDOM 0-25hz	11	.005	stopped @t=-5sec
850814.18	RANDOM 0-25hz	11	.005	stopped @t=-5sec
850814.19	RANDOM 0-10hz	11	.005	filters@10hz
850814.20	RANDOM 0-10hz	11	.005	stopped @t=-5sec
850815.01	RANDOM 0-25hz	22	.005	SMALL SHAKER REMOVED
CHANNELS 26-29 GAIN AT 50				SDOF STEEL STRUCTURE
850816.01	sine	11	.005	1.0hz
850816.02	sine	11	.005	7.5hz span=20
850816.03	sine	11	.005	10hz span=20
850816.04	RANDOM 0-25hz	11	.005	span=500
VERTICAL EXCITATION				SDOF STEEL STRUCTURE
850816.05	RANDOM 0-25hz	11	.005	vertical spv=70
850816.06	RANDOM 0-25hz	11	.005	spv=700 rg=0

Table 3.3: A List of EERC Shaking Table Tests

RUN NUM	RUN ID	DURATION	Time Step	Comments
HP GENERATOR 0-25 Hz HSPAN=400				SDOF STEEL STRUCTURE
850819.01	RANDOM 0-25hz	11	.005	HC: std sp=150
850819.02	RANDOM 0-25hz	11	.005	HC: std sp=400
850819.03	RANDOM 0-25hz	11	.005	HC: gain=10
850819.04	RANDOM 0-25hz	11	.005	HC: gain=8
850819.05	RANDOM 0-25hz	11	.005	HC: p=0
850819.06	RANDOM 0-25hz	11	.005	HC: p=5
850819.07	RANDOM 0-25hz	11	.005	PC: gain=3
850819.08	RANDOM 0-25hz	11	.005	PC: gain=3 p=0
HP GENERATOR 0-25 Hz VSPAN=400				SDOF STEEL STRUCTURE
850819.09	RANDOM 0-25hz	11	.005	std vertical
850819.10	RANDOM 0-25hz	11	.005	RC: gain=0
850819.11	RANDOM 0-25hz	11	.005	RC: gain=5
850819.12	RANDOM 0-25hz	11	.005	RC: p=6.0
850819.13	RANDOM 0-25hz	11	.005	RC: p=0
850819.14	RANDOM 0-25hz	11	.005	VC: gain=2
850819.15	RANDOM 0-25hz	11	.005	VC: gain=6.0
850819.16	RANDOM 0-25hz	11	.005	VC: p=1
850819.17	RANDOM 0-25hz	11	.005	VC: p=3
850819.18	RANDOM 0-25hz	11	.005	VC: r=5
HP GENERATOR 0-25 Hz HSPAN=500				SDOF STEEL STRUCTURE
850819.19	RANDOM 0-25hz	11	.005	TC: gain=0
850819.20	RANDOM 0-25hz	11	.005	TC: gain=8
850819.21	RANDOM 0-25hz	11	.005	TC: p=0
850819.22	RANDOM 0-25hz	11	.005	TC: p=5
850819.23	MIYAGI	22	.005	span=270
850819.24	MIYAGI	22	.005	span=350
850819.25	TAFT.s	22	.005	span=400
850819.26	TAFT.s	22	.005	span=200

Table 3.4: A List of EERC Shaking Table Tests

RUN NUM	RUN ID	DURATION	Time Step	Comments
CHANGED SIGN OF CALIBRATION ON CHAN 21-24 (PASSIVE STAB.) GENRAD HSPAN = 50				SDOF STEEL STRUCTURE
850822.01	RANDOM 0-32hz	128secs	.07813	HC: std span=30
850822.02	RANDOM 0-32hz	128secs	.005	HC: std span=30
850822.03	RANDOM 0-32hz	11	.005	HC: std span=30
850822.04	RANDOM 0-32hz	11	.005	HC: std span=50
850822.05	RANDOM 0-32hz	11	.005	HC: gain=10
850822.06	RANDOM 0-32hz	11	.005	HC: p=0
850822.07	RANDOM 0-32hz	11	.005	HC: p=5
850822.08	RANDOM 0-32hz	11	.005	PC: gain=1
850822.09	RANDOM 0-32hz	11	.005	PC: gain=3
850822.10	RANDOM 0-32hz	11	.005	PC: gain=3 p=0
850822.11	RANDOM 0-32hz	11	.005	TC: gain=8
850822.12	RANDOM 0-32hz	11	.005	TC: p=0
CHANGED CH11 FROM HSPAN TO VSPAN = 100				SDOF STEEL STRUCTURE
850822.13	RANDOM 0-32hz	11	.005	VC: stand span=100
850823.01	RANDOM 0-32hz	11	.005	VC: gain=6.0
850823.02	RANDOM 0-32hz	11	.005	VC: p=1
850823.03	RANDOM 0-32hz	11	.005	VC: p=5.0
850823.04	RANDOM 0-32hz	11	.005	RC: gain=0,
850823.05	RANDOM 0-32hz	11	.005	RC: gain=6,
850823.06	RANDOM 0-32hz	11	.005	RC: p=0,
850823.07	RANDOM 0-32hz	11	.005	RC: p=6,
CHANGED 11 to HSPAN=50				SDOF STEEL STRUCTURE
850823.08	RANDOM 0-32hz	11	.005	HC: std, VC: gain=6
850823.09	MIYAGI	22	.005	Hspan=350, Vspan=0
850823.10	TAFT.s	22	.005	Hspan=400, Vspan=0
850823.11	RANDOM 0-32hz	11	.005	PC: pstab=off,
850823.12	RANDOM 0-32hz	11	.005	PC: pstab=off g=4
DISCONNECTED PASSIVE STABILIZERS				SDOF STEEL STRUCTURE
850823.13	RANDOM 0-32hz	11	.005	PC: gain=2.0 sp=30,
850823.14	RANDOM 0-32hz	11	.005	PC: gain=0 sp=30,
850823.15	RANDOM 0-32hz	11	.005	PC: g=2,p=1,sp=30

Table 3.5: A List of EERC Shaking Table Tests

RUN NUM	RUN ID	DURATION	Time Step	Comments
RECONNECTED STABILIZERS, INCREASED STAB. PRESS FROM 1000 TO 2000				SDOF STEEL STRUCTURE
850827.01	TAFT.s	22	.005	PC: g=6 span=100
850827.02	RANDOM 0-32hz	11	.005	PC: gain=0 span=400
850827.03	RANDOM 0-32hz	11	.005	PC: g=4 p=2 span=400
850827.04	RANDOM 0-32hz	11	.005	PC: g=6 p=2 span=400
850827.05	RANDOM 0-32hz	11	.005	PC: g=6 p=0 span=400
				BARE TABLE
860821.01	random 0-32Hz	128	.004	sph=500
860821.02	random 0-32Hz	128	.004	sph=400
860821.03	ec2	18	.004	sph=200 ts=1/4
860821.04	ec2.corr	18	.004	sph=200ts=1/4
860821.05	ec2.corr2	18	.004	sph=200ts=1/4
ANCHORED 3 CONCRETE BLKS @ 25 kips each				TABLE WITH MASS
860822.01	random 0-32Hz	128	.004	sph=500
860822.02	random 0-32Hz	128	.004	sph=400
CONCRETE BLOCKS REMOVED				BARE TABLE
860826.01	ec2	18	.004	sph=200
860826.02	ec2.c1	18	.004	sph=200
860827.01	ec2	18	.004	sph=200
860827.02	ec2.c1	18	.004	sph=200
860827.03	ec2.c2	18	.004	sph=200
860828.01	random 0-32Hz	10	.004	sph=600
860828.02	random 0-32Hz	10	.004	sph=700
860828.03	random 0-32Hz	10	.004	sph=900
860828.04	random 0-32Hz	10	.004	sph=1000
870121.01	pulse	10	.0025	HC: p=1.5 AS
870121.02	pulse	10	.0025	HC: p=0.0 AES
870121.03	pulse	10	.0025	HC: p=5.0 AES
SLAVE SPOOL VALVE TESTS all calibrated except slave rate slave calib 0.25in/5volts int=.005				BARE TABLE
890331.02	r.30 random 0-32Hz	32	0.005	sph=50 ignore h2disp&force
890331.03	r.30 random 0-32Hz	32	0.005	sph=25 ignore h2disp&force
890331.04	r.30 random 0-32Hz	32	0.005	spv=50 ignore V3disp&force
890331.05	r.30.filt@30Hz	32	0.005	spv=50 ignore V3disp&force

Table 3.6: A List of EERC Shaking Table Tests

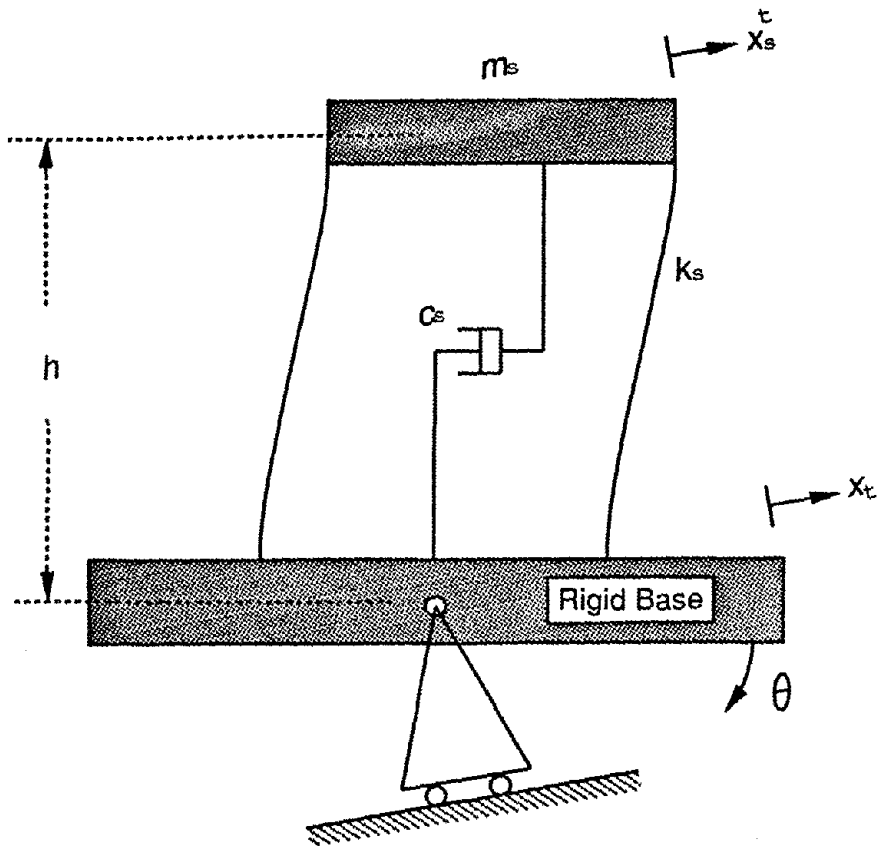

Fig. 3.1: Single–Degree–of–Freedom Structure with Rigid Base Translation and Rotation.

(a) Frequency

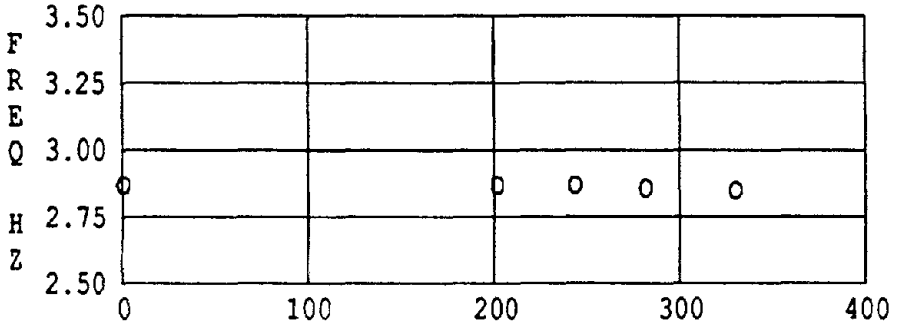

(b) Damping

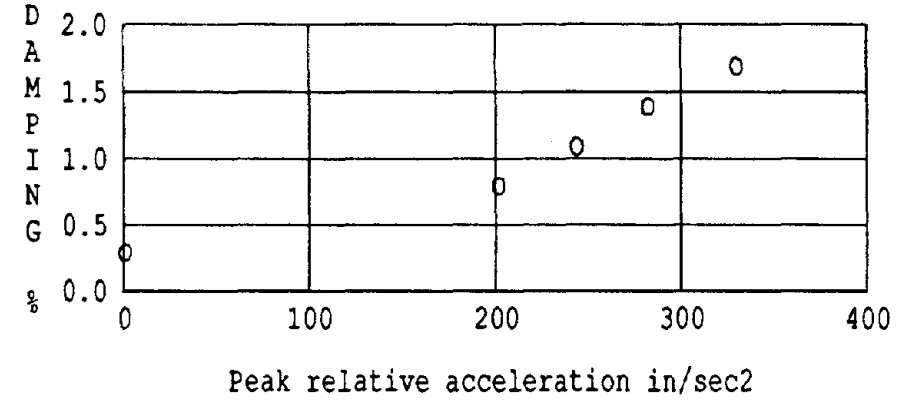

Fig. 3.2: Variation of Structural Frequency and Damping with Response Amplitude.

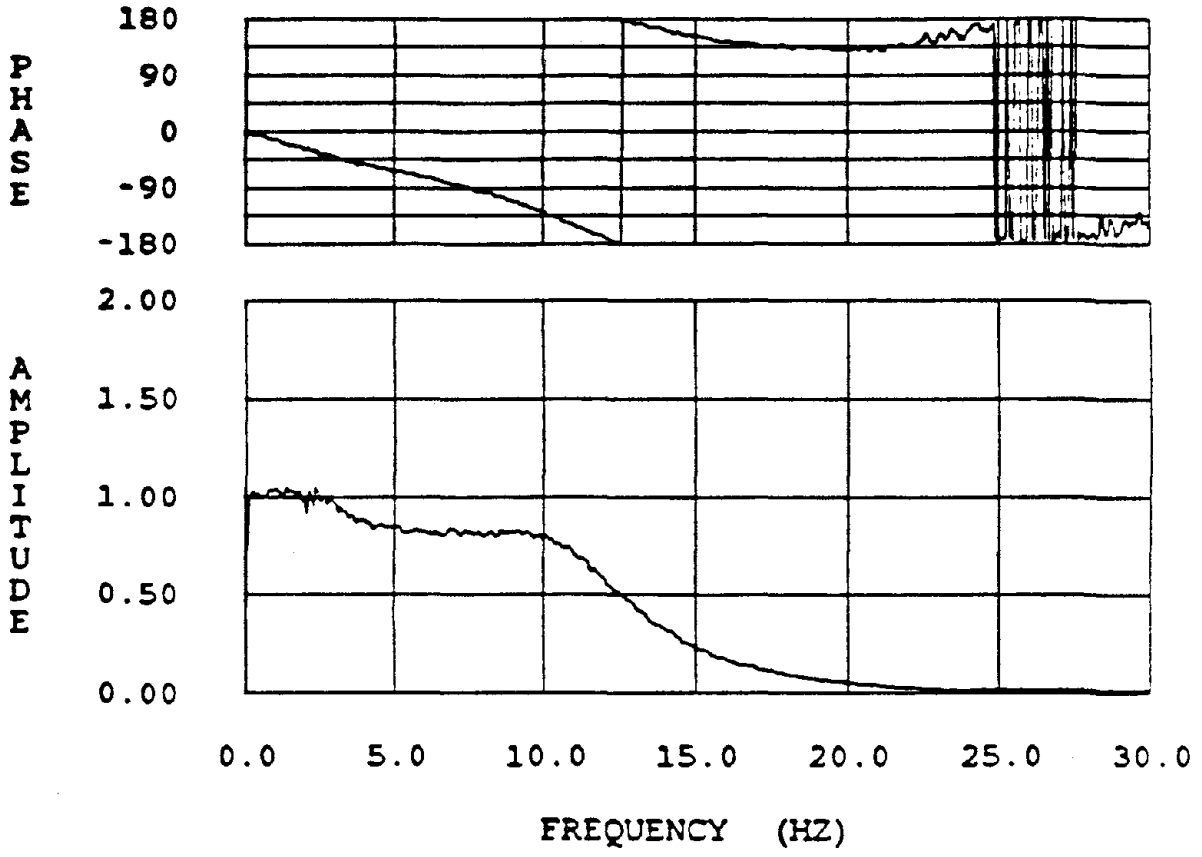

Fig. 3.3: Transfer Function of Table Horizontal Displacement over Horizontal Command Displacement.
Bare Table

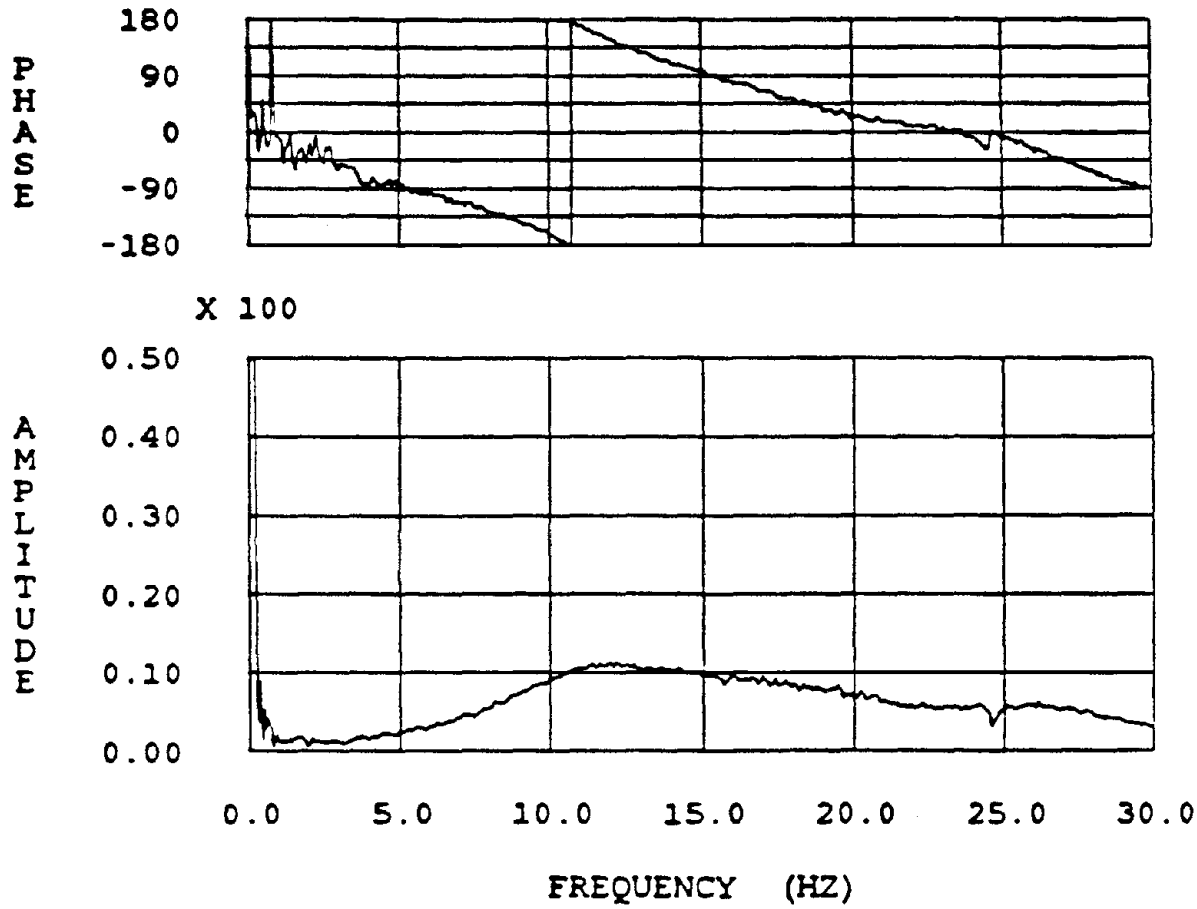

Fig. 3.4: Transfer Function of Table Pitch Displacement over Horizontal Command Displacement (rad/inch).
Bare Table.

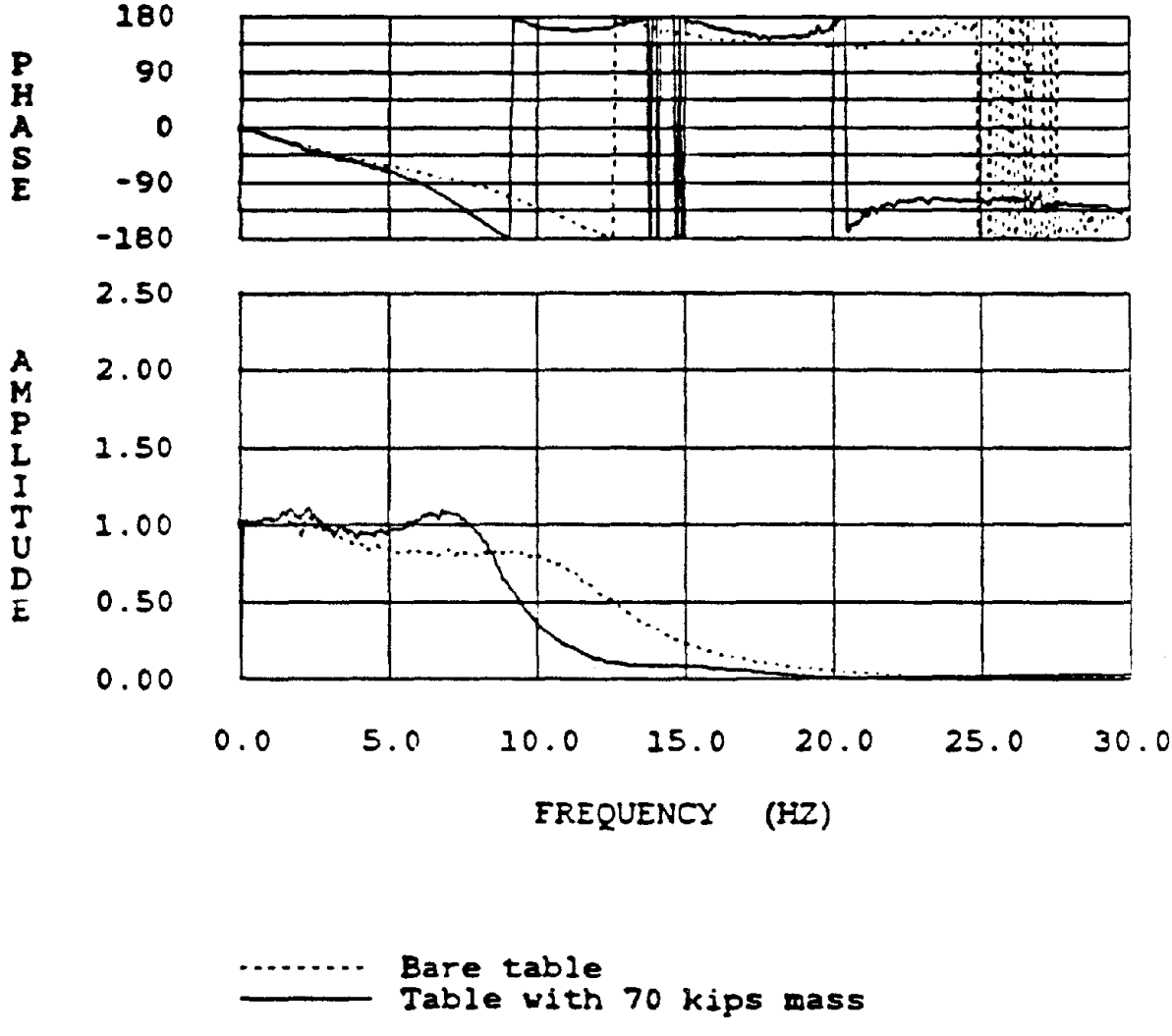

Fig. 3.5: Transfer Functions of Table Horizontal Displacement over Horizontal Command Displacement.

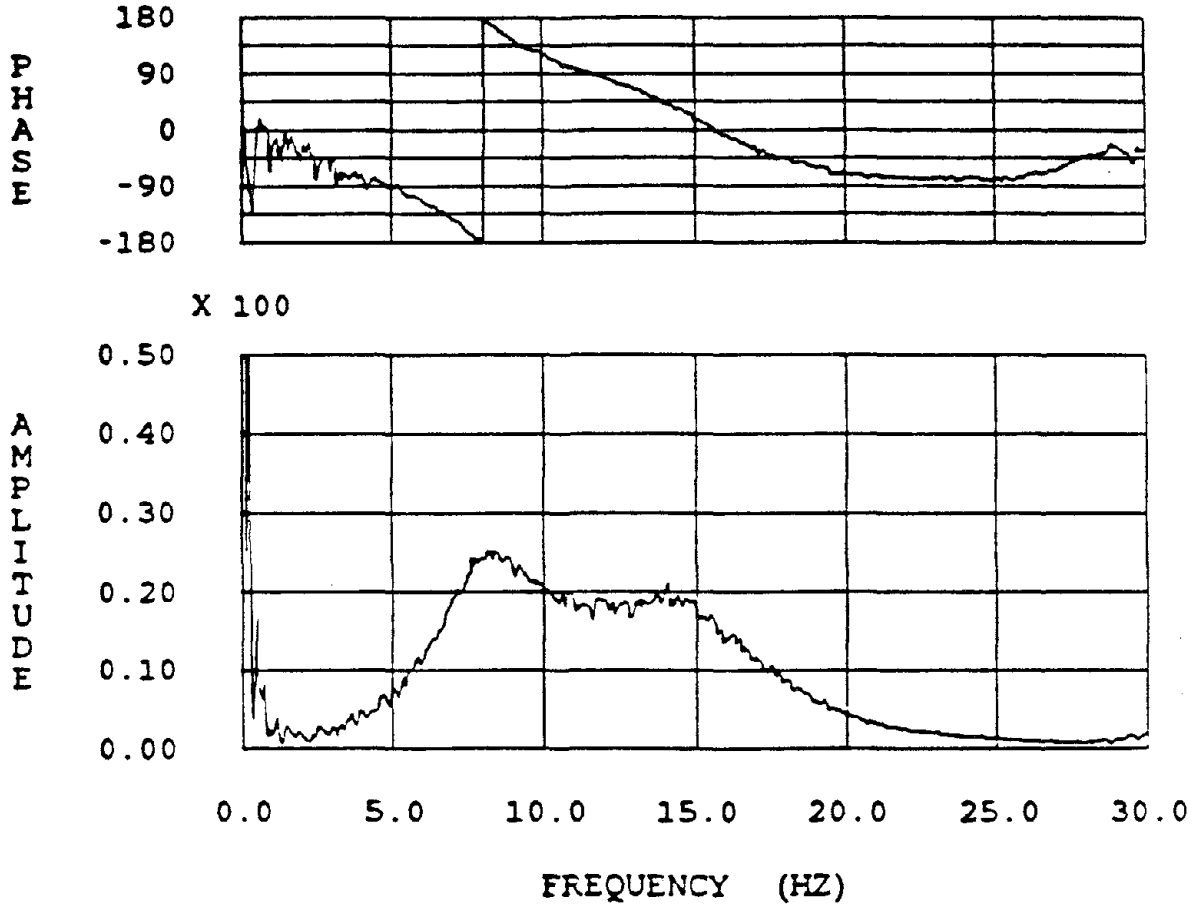

Fig. 3.6: Transfer Function of Table Pitch Displacement over Horizontal Command Displacement (rad/inch).
Table Loaded with 70 kips Mass.

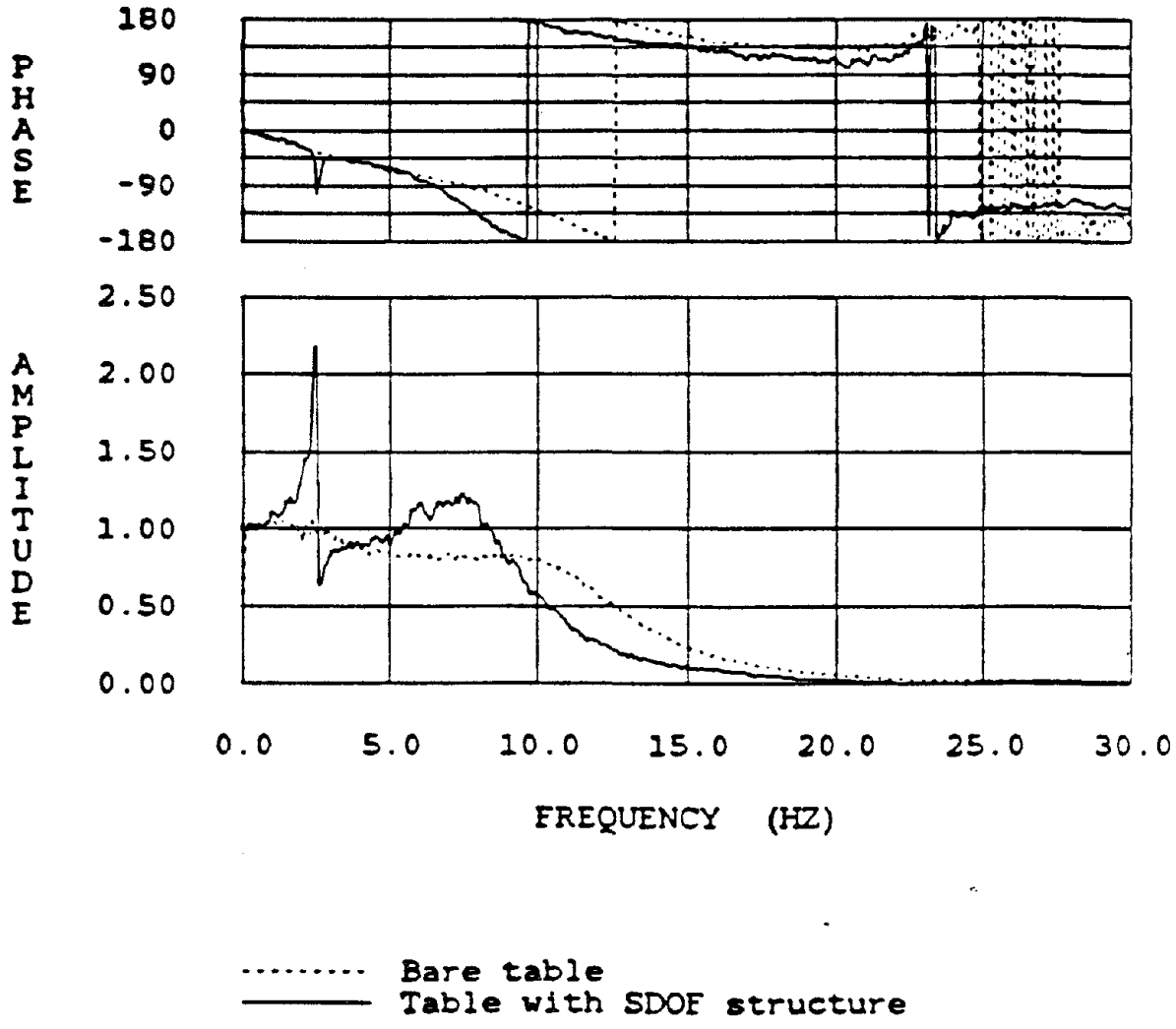

Fig. 3.7: Transfer Functions of Table Horizontal Displacement over Horizontal Command Displacement.

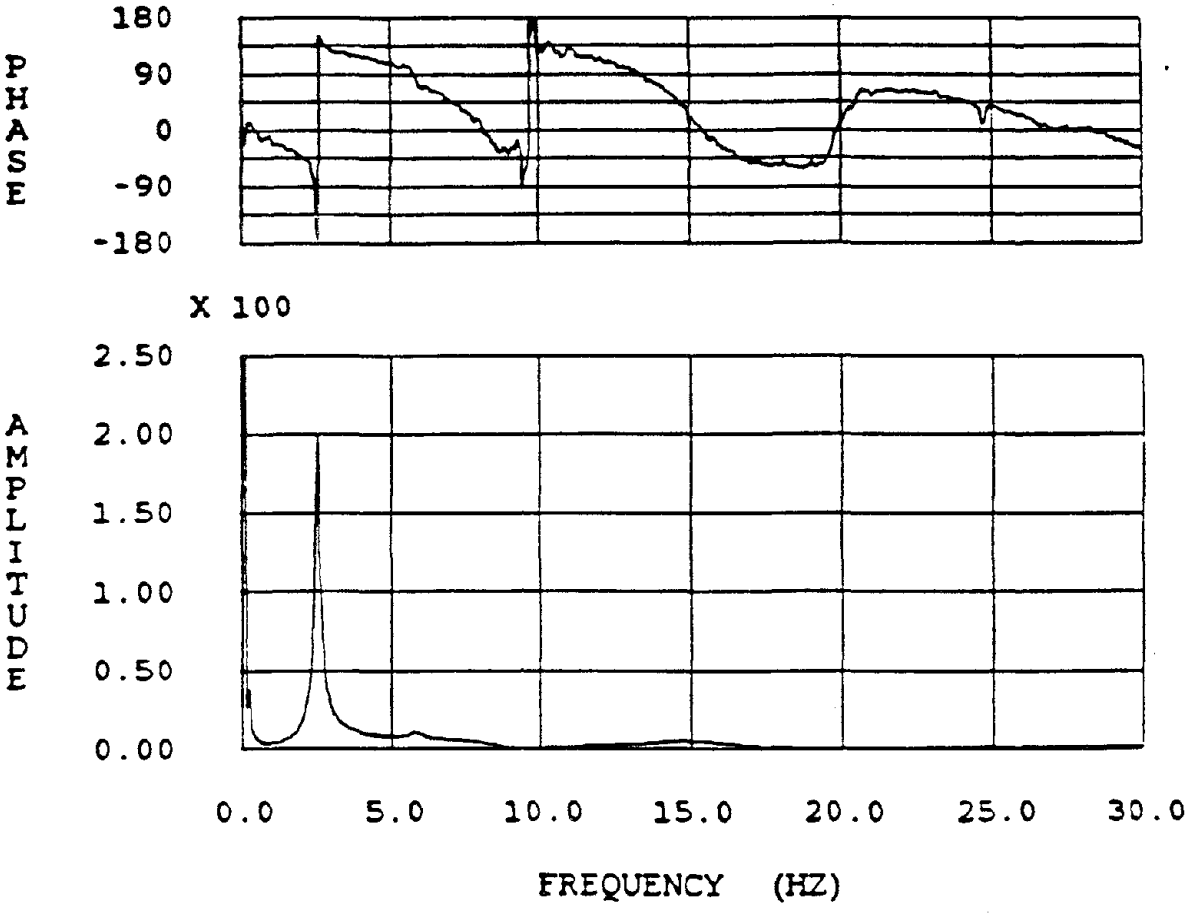

Fig. 3.8: Transfer Function of Table Pitch Displacement over Horizontal Command Displacement (rad/inch).
Table Loaded with SDOF Structure.

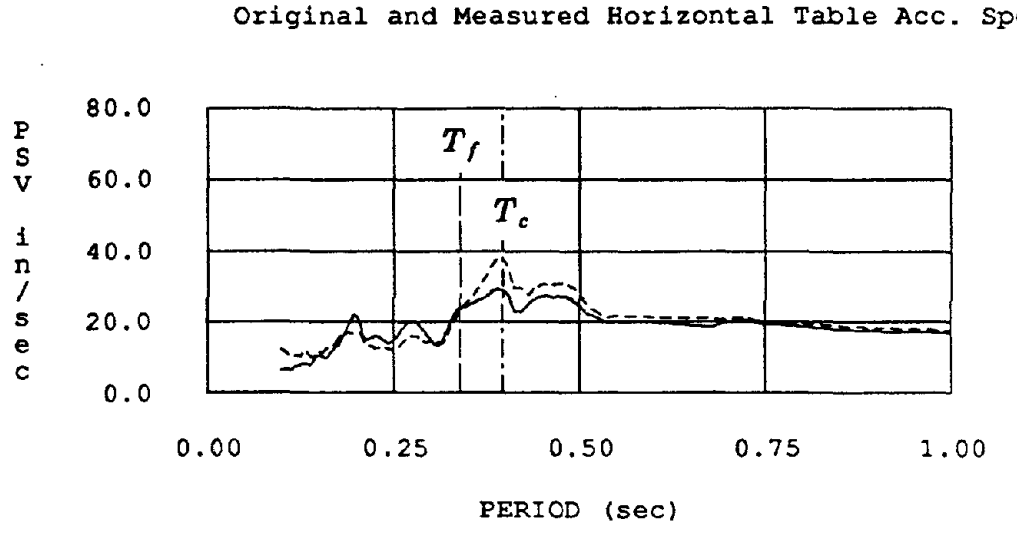

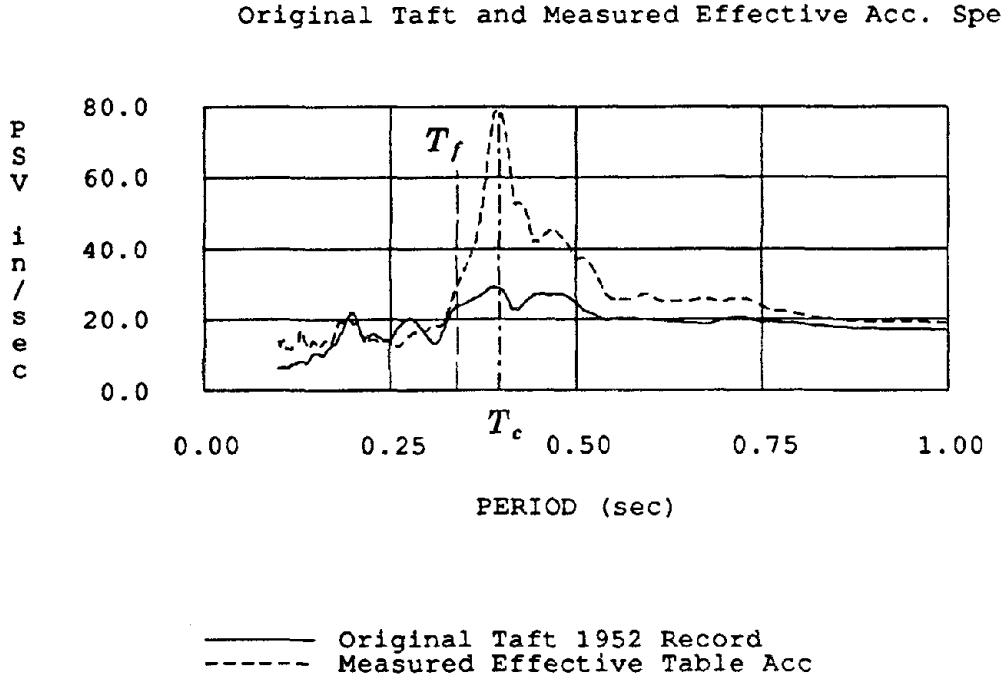

Fig. 3.9: Effect of Shaking Table-Structure Interaction on Pseudo Velocity Response Spectra.

Chapter Four

MODELS FOR ANALYSIS INCLUDING SHAKING TABLE-STRUCTURE INTERACTION

4.1 INTRODUCTION

This chapter serves as an introduction to the rest of this report. It describes ways of avoiding complicated interaction analysis techniques when analyzing and correlating test results with analytical models. It also describes a mechanical model that may be used to approximate interaction effects. In addition, control system models and hybrid models are described briefly.

4.2 AVOIDING INTERACTION ANALYSIS

Two ways of avoiding table-structure interaction effects in calculating the dynamic response are discussed in this section. Both methods require the measurement of the table horizontal and rocking motions. The first method is an exact method and requires an analysis program to account for both horizontal and rocking ground motions as earthquake input. The second method is an approximation and requires an analysis tool to account for the horizontal ground motion input only.

4.2.1 Two Directional Base Input

The shaking table can be considered rigid within the usual frequency range of operation [0-12 Hz]. The structure supported on this rigid platform will undergo a base movement equal to that of the platform, the motion of which includes a horizontal as well as a rocking component. All other table motions are assumed negligible, but they could be accounted for similarly if they were found to be significant.

The analysis of structural response to multi-component ground motion is a common problem in structural dynamics [11]. The necessary information for analyzing a structure for a two-component ground motion will be

summarized in this section.

Consider a multi-degree-of-freedom building structure as shown in Fig. 4.1. The governing equation for a horizontal and rocking base motion can be written as

$$\mathbf{M_s}\ddot{\mathbf{x}}_\mathbf{s}^\mathbf{t} + \mathbf{C_s}\dot{\mathbf{x}}_\mathbf{s} + \mathbf{K_s}\mathbf{x_s} = 0 \tag{4.1}$$

and the total structural displacement can be written as

$$\mathbf{x}_\mathbf{s}^\mathbf{t} = \mathbf{x_s} + \mathbf{r_t}x_t + \mathbf{r_\theta}\theta \tag{4.2}$$

where

$\mathbf{M_s}$,$\mathbf{C_s}$,$\mathbf{K_s}$ are structural mass, damping and stiffness matrices defined with respect to the displacement vector $\mathbf{x_s}$

$\mathbf{x_s}$ Vector of horizontal story displacements relative to a fixed-base

$\mathbf{x}_\mathbf{s}^\mathbf{t}$ Vector of total horizontal story displacements

$\mathbf{r_t}$,$\mathbf{r_\theta}$ Vectors of story displacements due to unit horizontal base displacement x_t and base rotation θ

For a building where the story displacements are the only degrees of freedom, the influence coefficient vectors, $\mathbf{r_t}$ and $\mathbf{r_\theta}$ are given by

$$\mathbf{r_t} = [\ 1\ 1\ 1\ \ldots\ 1\ ]^T \tag{4.3}$$

$$\mathbf{r_\theta} = [\ h_1\ h_2\ h_3\ \ldots\ h_n\ ]^T \tag{4.4}$$

Note that the height h of a given story should be measured from the level at which the table horizontal displacement is measured. For the EERC shaking table this corresponds to the location of the horizontal actuators. Differentiating Eq. (4.2) twice and substituting the result in Eq. (4.1), the equation of motion can be written as

$$\mathbf{M_s}\ddot{\mathbf{x}}_\mathbf{s} + \mathbf{C_s}\dot{\mathbf{x}}_\mathbf{s} + \mathbf{K_s}\mathbf{x_s} = -\mathbf{M_s}\mathbf{r_t}\ddot{x}_t - \mathbf{M_s}\mathbf{r_\theta}\ddot{\theta} \tag{4.5}$$

Up to this point the solution is exact, and some linear dynamic response analysis programs are available to handle such two component input motion.

4.2.2 One-Directional Base Input: Effective Base Motion

Some available nonlinear analysis programs cannot handle both horizontal and rocking input motions concurrently. One obvious way of getting around this problem is to modify the program to account for such an extended input requirement, but if that is not feasible the effect of the table pitching can be accounted for approximately by defining an equivalent "effective horizontal table acceleration" $\ddot{x}_{eff}$ (Section 3.3.2.1) to substitute for the two directional input motions, and using it as an excitation.

4.2.2.1 Single Degree of Freedom Structure Case: Equations (4.3) and (4.4) can be simplified for a single mass system as

$$\mathbf{r_t} = \left\{ 1 \right\} \tag{4.6}$$

$$\mathbf{r_\theta} = \left\{ h \right\} \tag{4.7}$$

The equation of motion (Eq. 4.5) can then be rewritten as

$$m_s\ddot{x}_s + c_s\dot{x}_s + k_s x_s = -m_s(\ddot{x}_t + \ddot{\theta}h) \tag{4.8}$$

If the base of the structure were prevented from pitching, the equation of motion for a single direction input would be

$$m_s\ddot{x}_s + c_s\dot{x}_s + k_s x_s = -m_s(\ddot{x}_t) \tag{4.9}$$

Note that the equation of motion for the two types of input motion are very similar, in fact Eq. (4.8) can be written in terms of an equivalent one directional motion or "effective horizontal acceleration" as

$$m_s\ddot{x}_s + c_s\dot{x}_s + k_s x_s = -m_s(\ddot{x}_{eff}) \tag{4.10}$$

where the "effective horizontal acceleration" is given by

$$\ddot{x}_{eff} = \ddot{x}_t + \ddot{\theta}h \tag{4.11}$$

This definition is useful since the problem of finding the response due to two-directional base input can be reduced into that of finding the response to a single direction base motion. This equivalence between the two systems is shown in Fig. 4.2. The "effective" motion is very useful in identifying the

fixed-base structural frequency and damping as was shown in Section 3.3.1.2.

The effective acceleration analysis procedure is exact for a SDOF system; the effective motion to be used for multi-degree-of-freedom systems is derived in the next section.

4.2.2.2 Multi-Degree-of-Freedom Structure Case The effective acceleration concept described earlier in Section 4.2.2.1 for a single-degree-of-freedom system cannot be exactly extended to multi-degree-of-freedom systems as we will see in this section. However approximate methods are available and can be applied effectively to multi-degree-of-freedom systems [12].

For a multi-degree-of-freedom system subjected to both translational as well as pitching motion, the equation of motion (Eq. 4.5) was derived in Section 4.2.1; this equation can be used to solve for the structural responses once the two motions, x_t and θ are known. However, as noted in Section 4.2.2.1, many analysis softwares deal only with the single base-input motion. In this section an approximate single base input solution is provided to account for the two input time histories.

Equation (4.5) can be rewritten using this equivalent "effective acceleration" as in the following

$$\mathbf{M_s}\ddot{\mathbf{x}}_\mathbf{s} + \mathbf{C_s}\dot{\mathbf{x}}_\mathbf{s} + \mathbf{K_s}\mathbf{x_s} = -\mathbf{M_s}\mathbf{r_t}(\ddot{x}_t)_{eff} \tag{4.12}$$

where the effective table acceleration can be expressed in the form

$$(\ddot{x}_t)_{eff} = \ddot{x}_t + h_e\ddot{\theta} \tag{4.13}$$

in which h_e is the effective height of the structure.

Equating the right hand sides of Eqs. (4.5) and (4.12) we get

$$\mathbf{M_s}\mathbf{r_t}h_e = \mathbf{M_s}\mathbf{r_\theta} \tag{4.14}$$

where h_e represents the first estimate of the effective height of the structure.

The above equation consists of n equations for an n DOF system and has only one unknown; hence it cannot be solved exactly for h_e. Nevertheless,

an approximate least squares solution can be obtained by premultiplying each side of the above equation by $\mathbf{r}_t^T\mathbf{M}_s$ as

$$h_e \approx \frac{\mathbf{r}_t^T\mathbf{M}_s^2\mathbf{r}_\theta}{\mathbf{r}_t^T\mathbf{M}_s^2\mathbf{r}_t} \tag{4.15}$$

For an idealized shear building with diagonal mass matrix and where $\mathbf{r}_t$ and $\mathbf{r}_\theta$ are given by Eqs. (4.3-4.4), the above equation simplifies to

$$h_e \approx \frac{\sum_{j=1}^{n} m_j^2 h_j}{\sum_{j=1}^{n} m_j^2} \tag{4.16}$$

where h_j is the height of the j'th story from the ground or the table level and m_j is the mass of the j'th story.

Uang [12] decoupled the linear system in 4.5 into modal coordinates as

$$\ddot{Y}_i + 2\xi_i\omega_i\dot{Y}_i + \omega_i^2 Y_i = -L_{ti}\ddot{x}_t + L_{\theta i}\ddot{\theta} \tag{4.17}$$

where

$$\mathbf{x}_s = \sum_{i=1}^{n} \boldsymbol{\phi}_i Y_i \tag{4.18}$$

$\boldsymbol{\phi}_i$ = i'th mode shape of the structure.

and

$$L_{ti} = \frac{\boldsymbol{\phi}_i^T\mathbf{M}_s\mathbf{r}_t}{\boldsymbol{\phi}_i^T\mathbf{M}_s\boldsymbol{\phi}_i} = \text{participation factor for base horizontal excitation in i'th mode} \tag{4.19}$$

$$L_{\theta i} = \frac{\boldsymbol{\phi}_i^T\mathbf{M}_s\mathbf{r}_\theta}{\boldsymbol{\phi}_i^T\mathbf{M}_s\boldsymbol{\phi}_i} = \text{participation factor for base pitching excitation in i'th mode} \tag{4.20}$$

The pitching motion will contribute mainly to the first mode for two reasons

(1) The pitching motion frequency spectrum consists mainly of a dominant single peak near the first coupled table-structure frequency.

(2) The first mode shape of the structure is very similar to $\mathbf{r}_\theta$, i.e $\boldsymbol{\phi}_1 \approx \mathbf{r}_\theta$, so that the first pitch participation factor $L_{\theta 1}$ will be dominant.

For that reason it may be more accurate to calculate the effective height of the structure (h_e) from the first modal coordinates equation in (4.17) as

$$\boldsymbol{\phi}_1^T \mathbf{M}_s \mathbf{r}_\theta = \boldsymbol{\phi}_1^T \mathbf{M}_s \mathbf{r}_t \, h_{e_1} \tag{4.21}$$

from which h_{e_1} can be evaluated as

$$h_{e_1} = \frac{\boldsymbol{\phi}_1^T \mathbf{M}_s \mathbf{r}_\theta}{\boldsymbol{\phi}_1^T \mathbf{M}_s \mathbf{r}_t} \tag{4.22}$$

In the absence of the first mode shape, the approximation $\boldsymbol{\phi}_1 \approx \mathbf{r}_\theta$, can be used so that

$$h_{e_1} \approx \frac{\mathbf{r}_\theta^T \mathbf{M}_s \mathbf{r}_\theta}{\mathbf{r}_\theta^T \mathbf{M}_s \mathbf{r}_t} \tag{4.23}$$

Again if $\mathbf{r}_\theta$ and $\mathbf{r}_t$ are given by Eqs. (4.3) - (4.4), the above equation can be simplified to

$$h_{e_1} \approx \frac{\sum_{j=1}^{n} m_j h_j^2}{\sum_{j=1}^{n} m_j h_j} \tag{4.24}$$

In fact h_{e_1} can also be called the effective height of the first modal mass. Similarly the effective height of the second modal mass h_{e_2} could be evaluated using the second mode shape but that would lead to a different input history for each mode and may not be handled easily for nonlinear systems, since the method of superposition does not apply.

For equal story heights and masses the effective height h_{e_1} is about 2/3 of the total height of the structure, and the effective height h_e is about 1/2 of

the total height. Depending on whether or not the contribution of the higher modes is significant, an appropriate value for the effective height can be determined.

4.3 SIMPLIFIED INTERACTION ANALYSES: MECHANICAL MODELS

In this section simplified methods for dealing with the interaction effects will be described. These methods consist mainly of adding springs and dampers to the base of the structure to account for shaking table flexibilities.

4.3.1 Rocking Flexibility Model

On some occasions, as was the case for several tests on the EERC table, the table pitching motion was not recorded. In this situation, the interaction effects can be approximated by using the measured table horizontal displacement as the test input and adding a rotational spring and a rotational dash-pot to the model of the structure being tested as shown in Fig. 4.3. The characteristics of the pitching spring and damper to be added to the model may be evaluated by system identification or by a trial and error analysis such that the measured coupled frequency matches that of the model with the spring. This procedure has been used by many U.C. researchers in the past [2,3,4,5,6]. Alternatively, values of the parameters for the spring and damper may be determined by other methods as is explained in Chapter 5.

4.3.2 Rocking and Horizontal Flexibility Model

Mechanical models of this type have been used successfully in soil structure interaction analysis for many years [13,14,15,16,17,18]. In such interaction analyses, it is customary to provide an additional spring and damper to represent the horizontal soil flexibility as shown in Fig. 4.4. In this case it is important to note that the earthquake input is applied through the supports of this spring and dash-pot; however for shaking table tests, the

command signal represents the earthquake input. The measured horizontal table acceleration should not be used as the horizontal spring support input as in the previous section. The reason is that the measured horizontal acceleration already includes the effect of the flexibility in the horizontal direction, approximated in this case by the horizontal spring and damper.

The required characteristics of the springs and dampers can be determined using the methods described in Chapter 5.

4.4 CONTROL SYSTEM MODELS

The shaking table system task is to reproduce a certain displacement input history. To achieve this goal, the system continually compares the command signal with the table displacement and applies a correction proportional to the difference between the two signals. This feedback mechanism cannot be represented exactly with a spring-damper model. A control system model intended to represent the shaking table horizontal interaction will be discussed in Chapters 6 and 7 and Appendices B and C. A more complicated system that accounts for the pitching control system will be discussed in Chapter 8.

4.5 HYBRID MODELS

As will be shown in Chapter 8, when the command pitch displacement is zero, (which is normally the case), the pitching feedback mechanism can be represented by a frequency dependent spring and a dashpot. The hybrid model approach then consists of combining these frequency dependent spring and damper components with a horizontal feedback mechanism. This will significantly simplify the model for the total system. The hybrid model will be dealt with in more detail in Chapter 8.

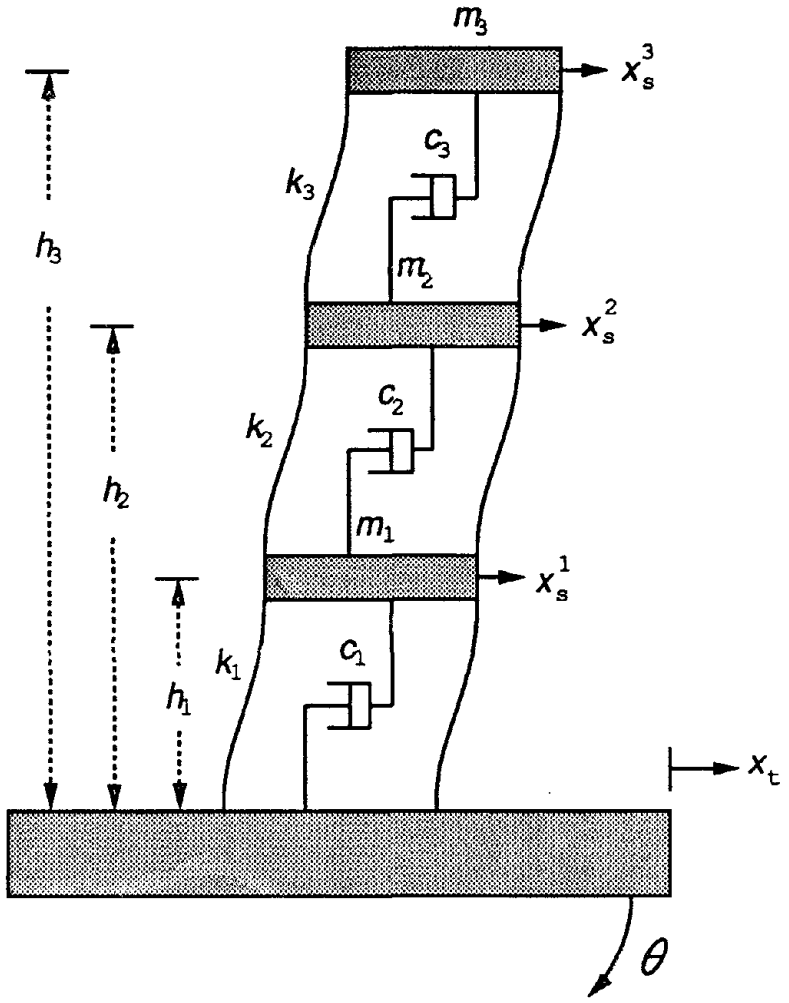

Fig. 4.1: Multi-Degree-of-Freedom Structural Model with Base Translation and Rotation.

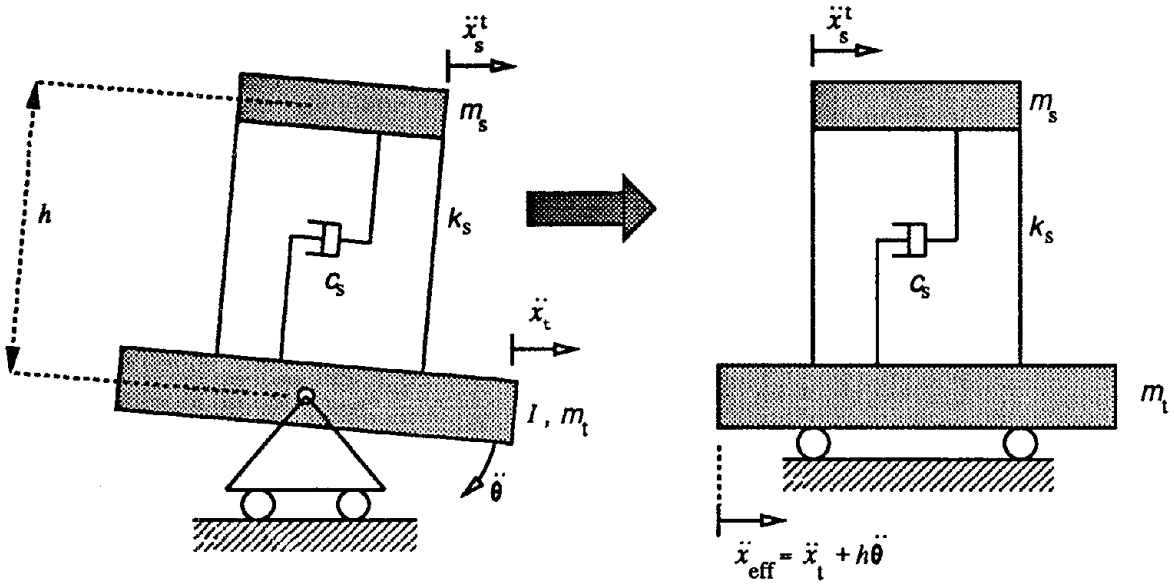

Fig. 4.2: Equivalence of two-directional base input
and "effective" uni-directional base input

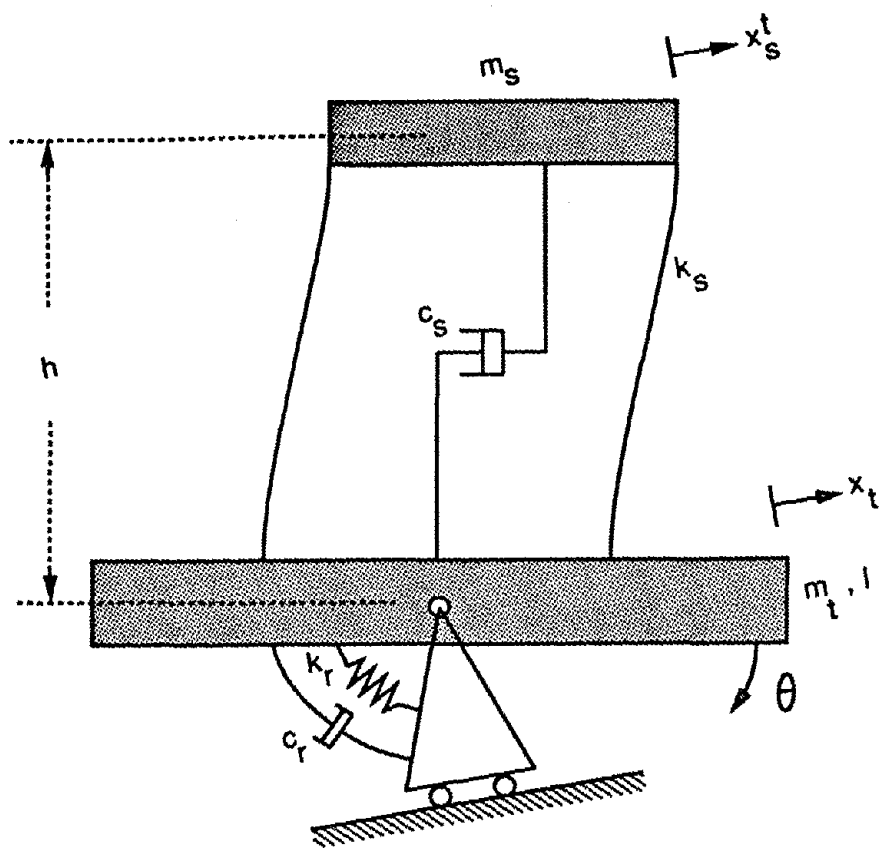

Fig. 4.3: Rocking Flexibility Model.

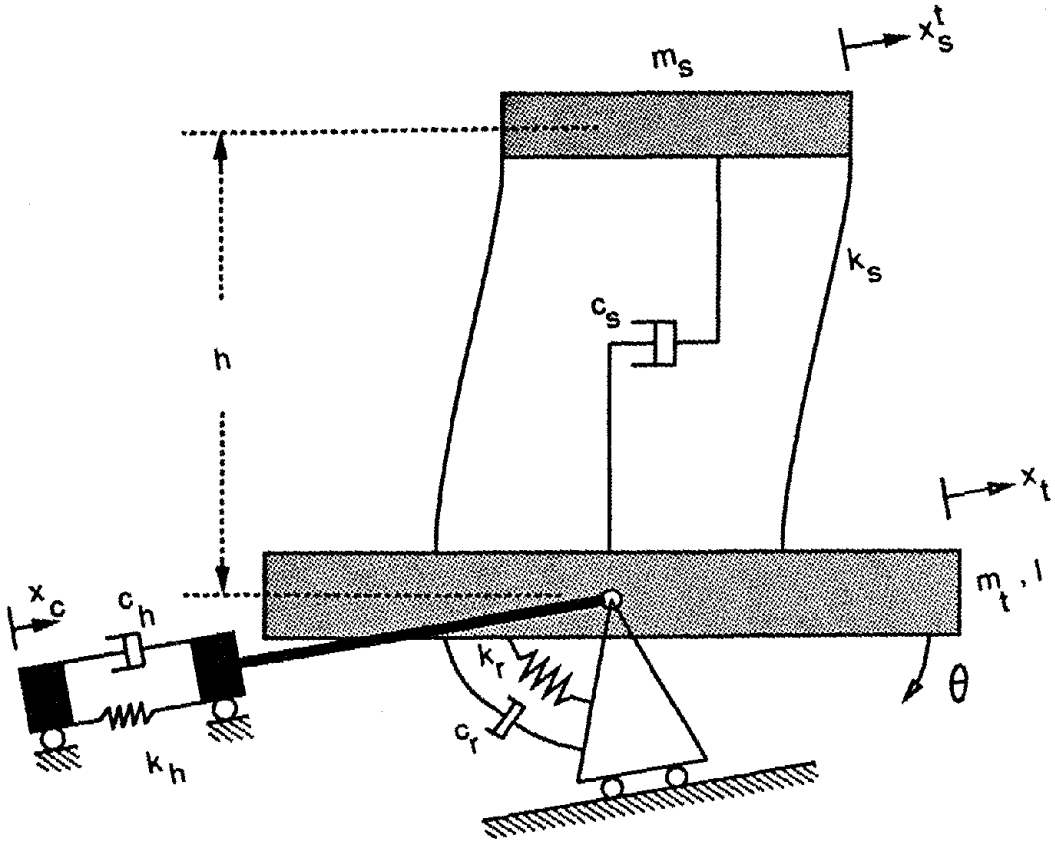

Fig. 4.4: Rocking and Horizontal Flexibility Model.

Chapter Five
EVALUATION OF MECHANICAL MODEL PARAMETERS

5.1 INTRODUCTION

This chapter describes the mechanical model which was initially introduced in the previous chapter and is shown in Fig. 5.1. It also presents methods for evaluating the necessary parameters in the analysis. Mechanical models are known for their simplicity and were frequently used in the past. Most researchers applied a trial and error approach of parameter evaluation for the springs. They frequently used different parameters for different tests of the same model because of shaking table system nonlinearities. Frequently the analyst used the parameters that gave the best correlation between the experimental and analytical results; however, this approach should be used with caution as it can mask errors in the analytical modeling of the test structure. In this chapter, ways of estimating the parameters from the coupled and fixed-base frequencies will be discussed. In addition, methods for estimating the damping and stiffness using frequency domain as well as time domain methods will be described. A comparison is made between the mechanical model transfer function and the actual shaking table transfer function in order to show the limitations of the mechanical model compared with control system models.

5.2 DESCRIPTION OF THE MECHANICAL MODEL

The mechanical model used in this study to represent shaking table interaction is shown in Fig. 5.1. It consists of a rigid base constrained by horizontal and rotation springs and dash-pots. Several researchers in the past ignored the flexibility in the horizontal degree of freedom because its effects are less evident in the response than is the rotational flexibility.

5.3 PARAMETER EVALUATION FROM COUPLED AND FIXED-BASE FREQUENCIES

This section describes a method for estimating the stiffnesses in the mechanical model using only the values of the coupled and fixed-base frequencies. This method can be applied to individual tests and different parameters can be justified as the frequencies of the test structure change from one test to another.

5.3.1 Estimation of Coupled and Fixed-Base Frequencies

Certainly the coupled and fixed-base frequencies can be obtained from simple standard tests of the test structure. Typically the tools include the use of a pull test, and a rotating mass shaker or a small shaker driving a small mass along a fixed axis. Normally these tests are conducted only a few times during the course of many more shaking table earthquake runs applied to the specimen. Since the frequencies and damping of the system can depend on the amplitude of shaking [24], the results of the tests may not be very useful since the magnitude of shaking during these tests is relatively small. A more useful approach is to use the transfer function method of estimation from the measured test channels. The transfer function method will be introduced in the following paragraphs.

Normally if one applies a displacement signal x_c to the horizontal spring support, as shown in Fig 5.1, the response of the structure would reflect the coupling in the horizontal as well as the rocking degrees of freedom. On the other hand if a displacement signal x_t is applied to the rigid table directly, rather than to the spring support, the horizontal spring will have no significance and the response will only reflect the coupling in the rocking degree of freedom (as in Fig. 5.2). If two displacements are specified for the rigid table, a horizontal, x_t, and a rocking, θ, then the response will reflect only the fixed-base characteristics (as in Fig. 5.3).

In order to evaluate the fixed-base characteristics of any SDOF test structure, one can estimate the transfer function obtained by dividing the Fourier transform of the relative mass movement by that of the effective horizontal

acceleration at the mass level of height h: $\ddot{x}_t + h\ddot{\theta}$. The theoretical foundation of this procedure is discussed in Section 3.3.1.2. One can estimate from the peak and bandwidth of the transfer function H_f , the fixed-base frequency and fixed-base damping of the system [11]. In mathematical form the transfer function can be written as

$$H_f(\omega) = \frac{x_s(\omega)}{x_t(\omega)+h\,\theta(\omega)} \tag{5.1}$$

Here H_f stands for the fixed-base transfer function, x_s is the measured relative structural displacement which excludes the rigid body contributions of the horizontal, x_t, and the rocking, $h\,\theta$, motions of the shaking table and can be expressed as

$$x_s = x_s^t - x_t - h\,\theta \tag{5.1a}$$

where x_s^t is the measured total structural displacement with respect to a stationary reference point. The resulting estimated fixed-base frequency and damping can be denoted by ω_f and ξ_f, respectively. The use of the relative structural motion in evaluating the fixed-base characteristics is emphasized by Beliveau [19] in the analysis of uni-directional base excitation. A least squares method of estimation of the damping and frequency is outlined in Appendix D.

Similarly the transfer function representing coupling in the rocking degree of freedom can be denoted by H_r and can be calculated from (refer to Fig. 5.3)

$$H_r(\omega) = \frac{x_s(\omega)}{x_t(\omega)} \tag{5.2}$$

The frequency and damping associated with this transfer function can be denoted by ω_r and ξ_r, respectively.

The transfer function representing the relation between the command signal and the relative structural movement is denoted by H_{hr}. It represents the coupling in the horizontal and rocking degrees of freedom, and is defined as

$$H_{hr}(\omega) = \frac{x_s(\omega)}{x_c(\omega)} \tag{5.3}$$

where x_c is the command or spring support displacement as shown in Fig. 5.1. The coupled frequency and damping for this function are denoted by ω_{hr} and ξ_{hr}, respectively.

Table 3.1 lists the spring and damping parameters for the tested SDOF structure using the above mentioned procedure.

This procedure applies only to a SDOF system. For multi-degree of freedom systems, the above procedure can still lead to good results if the height h is replaced by the "effective height" corresponding to the first mode response as described in Section 4.2.2.

Figure 5.4 shows the transfer functions H_f , H_r and H_{hr} for a Taft 1952 earthquake test applied to the SDOF test structure. Note that the fixed-base peak frequency is the highest and that the peak frequency is reduced as more coupling is introduced.

5.3.2 Estimation of Horizontal and Pitching Spring Stiffnesses

Relations between the coupled and fixed-base frequencies of a SDOF system can be derived for a rigid **massless** table as is explained in [13], leading to the following result

$$\omega_r^2 = \frac{\omega_f^2}{1+\dfrac{m_s \omega_f^2 h^2}{k_r}} \tag{5.4}$$

Having obtained ω_f, ω_r as explained in the previous section, the structural mass m_s in Eq. (5.4) can be used to compute the rocking spring stiffness.

Another equation that relates ω_{hr} to ω_f is given in the same reference as follows

$$\omega_{hr}^2 = \frac{\omega_f^2}{1+\dfrac{m_s \omega_f^2}{k_h}+\dfrac{m_s \omega_f^2 h^2}{k_r}} \tag{5.5}$$

This equation may be used to estimate the horizontal spring stiffness, k_h. For a MDOF system, m_s becomes the modal mass of the first mode. A good estimate of the modal mass can be obtained from

$$m_1 = \phi_1^T \mathbf{M} \phi_1 \tag{5.6}$$

In this expression, the mode shape ϕ_1 for a shear building with height for each story above the basement, h_i, can be approximated by

$$\phi_1^T = [\, h_1 \, h_2 \, h_3 \ldots h_n] \tag{5.7}$$

where **M** is the (nxn) diagonal mass matrix of the MDOF system.

5.4 EVALUATION OF PARAMETERS FROM ACTUATOR TRANSFER FUNCTIONS

In the mechanical model, the resistance of the system in the pitching mode is represented by a rotational spring and a damper. Then the total moment acting on the rigid table, which will be denoted here by M, can be written in terms of the pitching angle θ as

$$M = k_r \theta + c_r \dot{\theta} \tag{5.8}$$

in which k_r and c_r are the parameters of the spring and damper in the rocking degree of freedom. In the frequency domain, Eq. (5.8) can be written as

$$G_r(\omega) = \frac{M(\omega)}{\Theta(\omega)} = k_r(\omega) + i\,\omega c_r(\omega) \tag{5.9}$$

where i is the complex equivalent of $\sqrt{-1}$. The moment acting on the table $M(\omega)$ can be evaluated either from the measured forces of the vertical actuators supporting the table or from the measured structural inertias. The transfer function $G_r(\omega)$ can be evaluated easily using Eq. (5.9). This transfer function has the following important properties

$$Real\,[G_r(\omega)] = k_r(\omega) \tag{5.10}$$

$$Imag\,[G_r(\omega)] = \omega c_r(\omega) \tag{5.11}$$

From the above equations, the frequency dependent stiffness and damping

parameters can be determined. Figure 5.5a shows the real and imaginary parts of the transfer function $G_r(\omega)$ as defined by Eq. (5.9) that was obtained from the response of the SDOF test structure to the Taft 1952 earthquake where the control system was set to a span of 200. Figures 5.5b and 5.5c show the individual contributions of the active and passive actuators to the total pitch resistance. As can be seen from Fig. 5.5d, most of the pitch response is concentrated around the coupled table-structure frequency ω_{hr}; for this reason reasonable results can be expected by ignoring the frequency dependence of the stiffness and damping parameters and using the values evaluated at the coupled table-structure frequency.

It is important to note at this stage that both the vertical actuators and stabilizers work to reduce the pitching by applying forces proportional to the pitching motion. This is in direct agreement with the assumed rotational spring property. The same concept, however, does not apply to the horizontal actuators. The forces applied by the horizontal actuators are intended primarily for producing a prescribed table displacement. Obviously they do not serve to maintain a zero displacement of the table.

5.5 IDENTIFICATION OF PARAMETERS FROM HYSTERESIS LOOPS

In the above procedure a frequency domain method is used to estimate the system properties. Similar results can also be obtained using a time domain method, namely from evaluation of the hysteresis loops of the applied moment-rocking displacement relationship during horizontal excitation. Figure 5.6 shows the hysteresis loops measured from the Taft 1952 test. An average value of the system stiffness can be obtained from the slope of the regression line shown in Fig. 5.6 which was derived by a regression analysis of the measured data during the test. In addition a damping estimate can be made from the area inside the loops as follows

$$\xi_v = \frac{W_D}{4\pi W_s} \tag{5.12}$$

where ξ_v is the viscous damping ratio and W_D and W_s are the areas as shown in Fig. 5.7. The damping coefficient C can be estimated from

$$C = \frac{W_D}{\pi\omega\theta_{max}^2} \tag{5.13}$$

Here ω represents the excitation frequency and in this case it represents the coupled table-structure frequency. θ_{max} is the amplitude of the measured pitching displacement as shown in Fig. 5.7.

Note that while the frequency domain method allows us to see the variation of the stiffness and damping with frequency, the time domain method can show the variation of those quantities with time and amplitude of shaking.

Alternatively, one may estimate the table pitching flexibility from the force-displacement curves of the individual vertical actuators and passive stabilizers shown in Figs. 5.8 and 5.9 as follows

$$k_r = \sum_{i=1}^{i=4} (k_{v_i} d_{v_i}^2 + k_{p_i} d_{p_i}^2) \tag{5.14}$$

where k_{v_i} and k_{p_i} are the stiffnesses of the i'th individual vertical actuator and passive stabilizer located respectively at distances d_{v_i} and d_{p_i} from the center of symmetry of the table. The layout of the actuators and stabilizers is shown in Fig. 2.1.

5.6 EVALUATION OF HORIZONTAL SPRING AND DAMPER PARAMETERS FROM A BARE TABLE TRANSFER FUNCTION

Figure 3.3 shows the transfer function of the shaking table horizontal displacement over the command displacement. When an analytical model including the feedback loops is derived for the uni-directional shaking table as described in Chapter 6, system identification could then be used to identify the parameters of the model from fitting the transfer function to the analytical model using a nonlinear least squares algorithm [30,31,32,33]. The fitted model is displayed in Fig. 6.4 together with the experimental curve. The parameters for this case were: the open loop frequency $f_o = 2\pi\omega_o$ = 12.6 Hz, the open loop damping ξ_o = 47.7 percent and the open loop gain

k_o = 25.07. As will be seen in Chapter 7 these parameters change when the table is loaded with a SDOF structure. The corresponding parameters for the table with a SDOF structure are f_o = 9.6 Hz, ξ_o = 60.6 percent and k_o = 29.54 (Table 7.2).

Section 8.5 shows a simplified model of the pitch actuator when the pitch command displacement is set at zero. This same model approach could be used to evaluate the shaking table flexibility in the horizontal degree of freedom. It should be noted that, in general, the assumption of zero command signal is not realistic. However it does occur in some cases. For example, before testing most structures on the shaking table, the structure is tested in a fixed-base condition by the blocking the table from movement. The structure is also tested in the coupled case by having the table operational with a zero horizontal and rotational command signal.

The horizontal spring stiffness k_h and the damping constant c_h can be evaluated by a method analogous to that in Section 8.5 as

$$k_h(\omega) = \frac{m_t \omega_o^2(\omega^2+2\xi_o \omega_o k_o)}{\omega^2+4\xi_o^2\omega_o^2} \tag{5.15}$$

$$c_h(\omega) = \frac{m_t \omega_o^2(2\xi_o \omega_o - k_o)}{\omega^2+4\xi_o^2\omega_o^2} \tag{5.16}$$

And for the numerical model parameters listed above the frequency dependent stiffness and damping can be plotted as shown in Fig. 5.10a and 5.10b. Two cases are shown in Fig. 5.10, the bare table case and the case when the table is loaded with SDOF test structure. Figure 5.10a shows that the equivalent horizontal spring stiffness $k_h(\omega)$ increases with frequency and that the stiffness for the loaded table case is always lower than the bare table case. Figure 5.10b indicates that the horizontal damping constant $c_h(\omega)$ decreases with frequency and that the loaded table has a higher damping constant.

5.7 HOW WELL DOES A MECHANICAL MODEL REPRESENT THE ACTUAL SYSTEM?

Figure 5.11 shows a transfer function obtained by dividing the measured shaking table horizontal displacement by the command displacement. The transfer function obtained similarly from the calculated response of the mechanical model due to the command displacement is shown by the dashed line on the figure. The analytical model parameters are listed in Table 5.1. Appendix A shows the derivation of the transfer function for the mechanical model. It is clear that the mechanical model overestimates the response at frequencies above the structure's resonance frequency. The mechanical model predicts very well the peak and notch frequencies as can be seen from Fig. 5.11.

Figure 5.12 similarly shows the transfer function obtained by dividing the measured pitching displacement by the command horizontal displacement, together with the corresponding mechanical model transfer function.

As mentioned in Section 5.3, the pitching flexibility can be satisfactorily represented by a pitching spring and damper. Horizontal flexibility on the other hand cannot be completely represented by springs and dampers because of the feedback mechanism.

Mechanical models can be used effectively for analysis if the horizontal interaction is eliminated through the use of the measured horizontal table acceleration as the control signal; in this case the model includes only the rotational parameters.

In Chapter 8, a control system model for the horizontal degree of freedom is combined with the rotational springs and dampers to account more accurately for horizontal interaction.

As was seen in Section 5.6, the characteristics of the model for the loaded table are different from that for the bare table. This suggests that the mechanical model parameters should be identified whenever the loading conditions are changed because of system nonlinearities.

Structural Mass (kips)	m_s	68.4
Structural Stiffness (kips/in)	k_s	57.9
Structural Damping (lb-sec/in)	c_s	64.2
Table Mass (kips)	m_t	100.0
Table Horizontal Stiffness (kips/in)	k_h	401.0
Table Horizontal Damping (lb-sec/in)	c_h	6126.0
Table Inertia (kips-in^2)	I	1251.0
Table Rocking Stiffness (kips/rad)	k_r	2.22E+07
Table Rocking Damping (lb-sec/in)	c_r	3.70E+05
Height of Structure (inches)	h	219.0

Table 5.1

Mechanical Model Parameters For Analytical Curves in Fig. 5.10.

* Model equations are derived in appendix A.

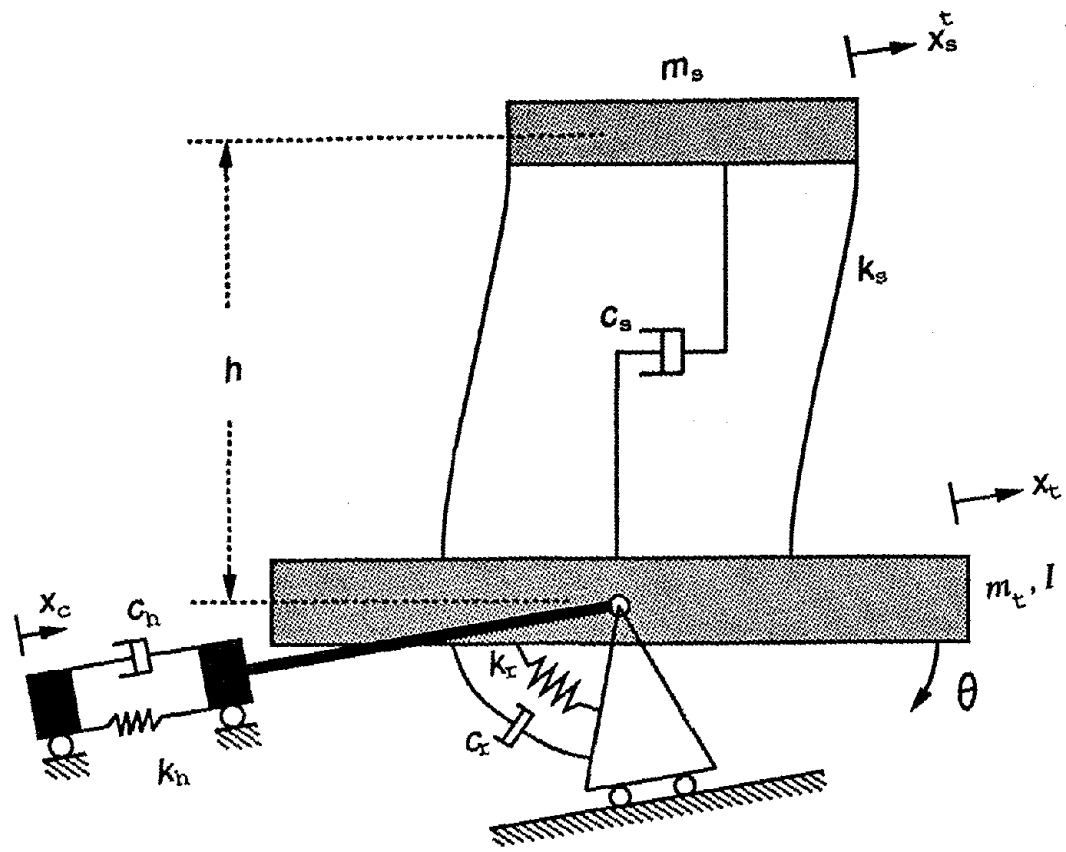

Fig. 5.1: Mechanical model of table-structure system.

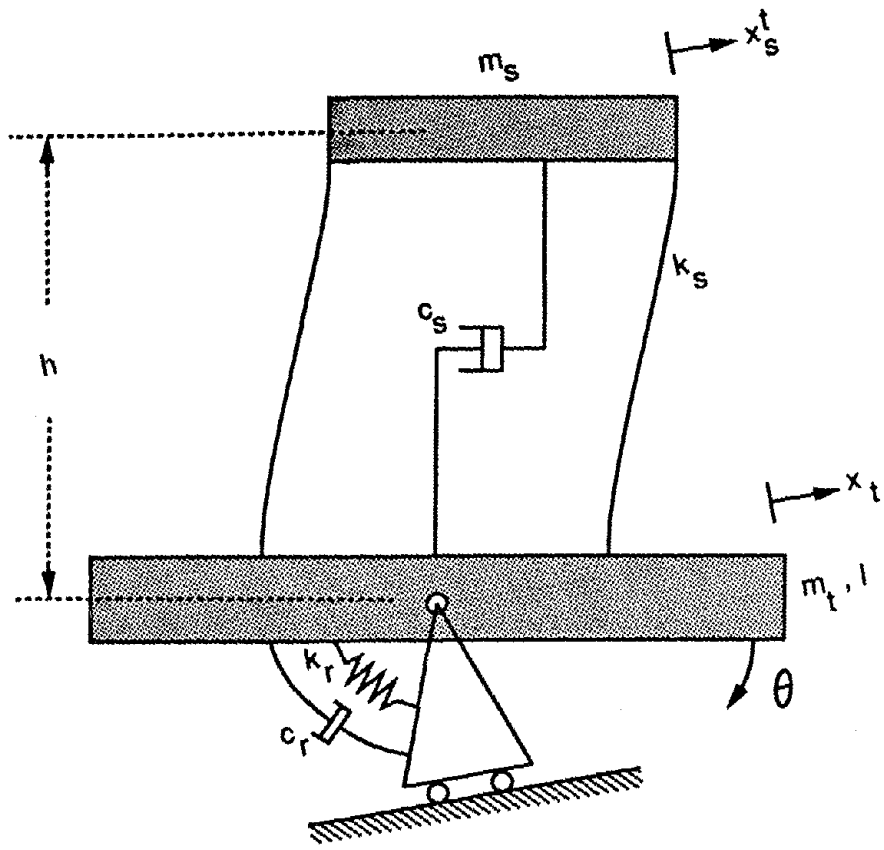

Fig. 5.2: Mechanical model for rocking coupling.

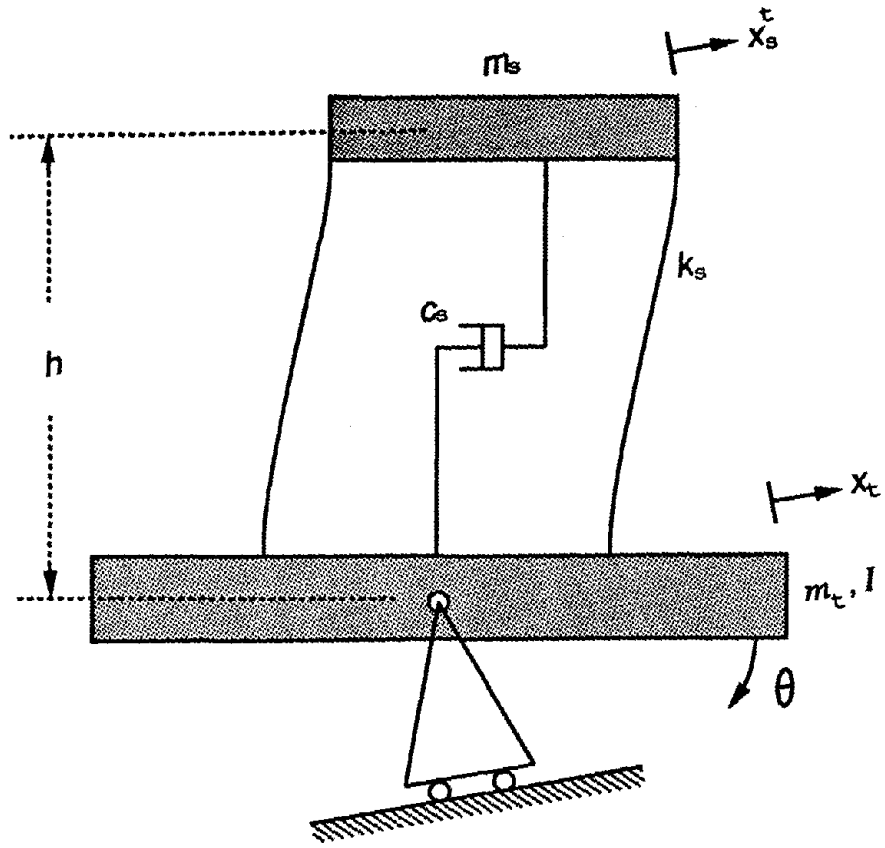

Fig. 5.3: Mechanical model with no coupling.

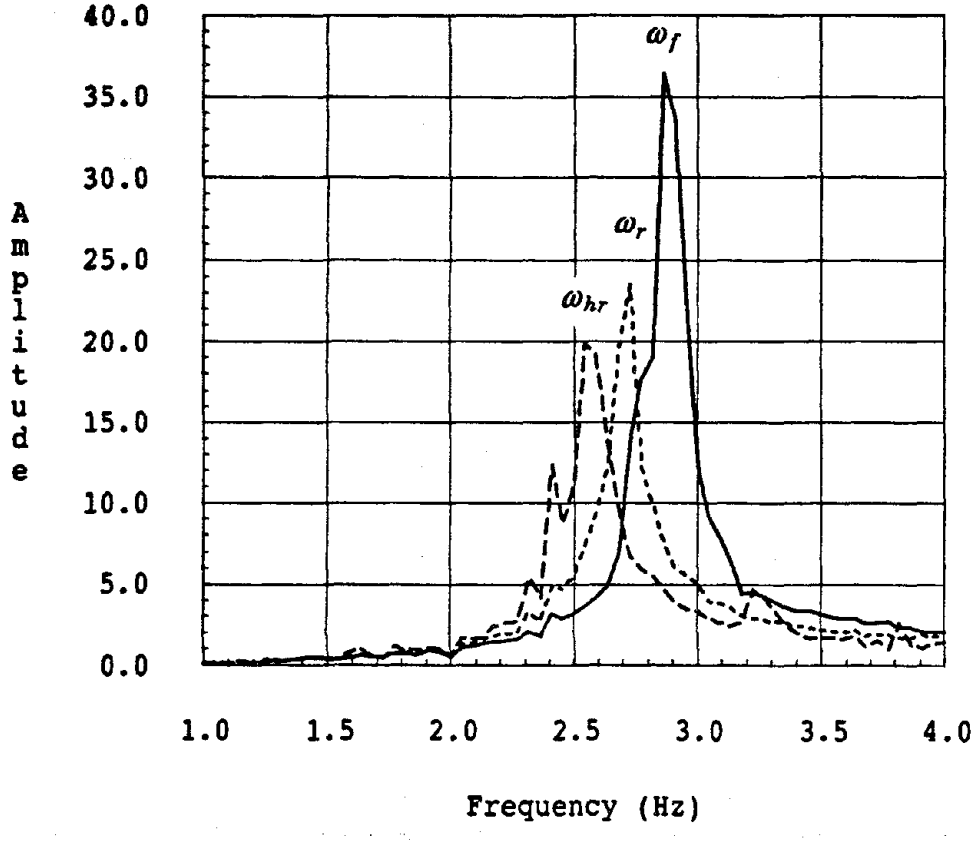

Fig. 5.4: Transfer Functions x_s/x_{eff}, x_s/x_t and x_s/x_c

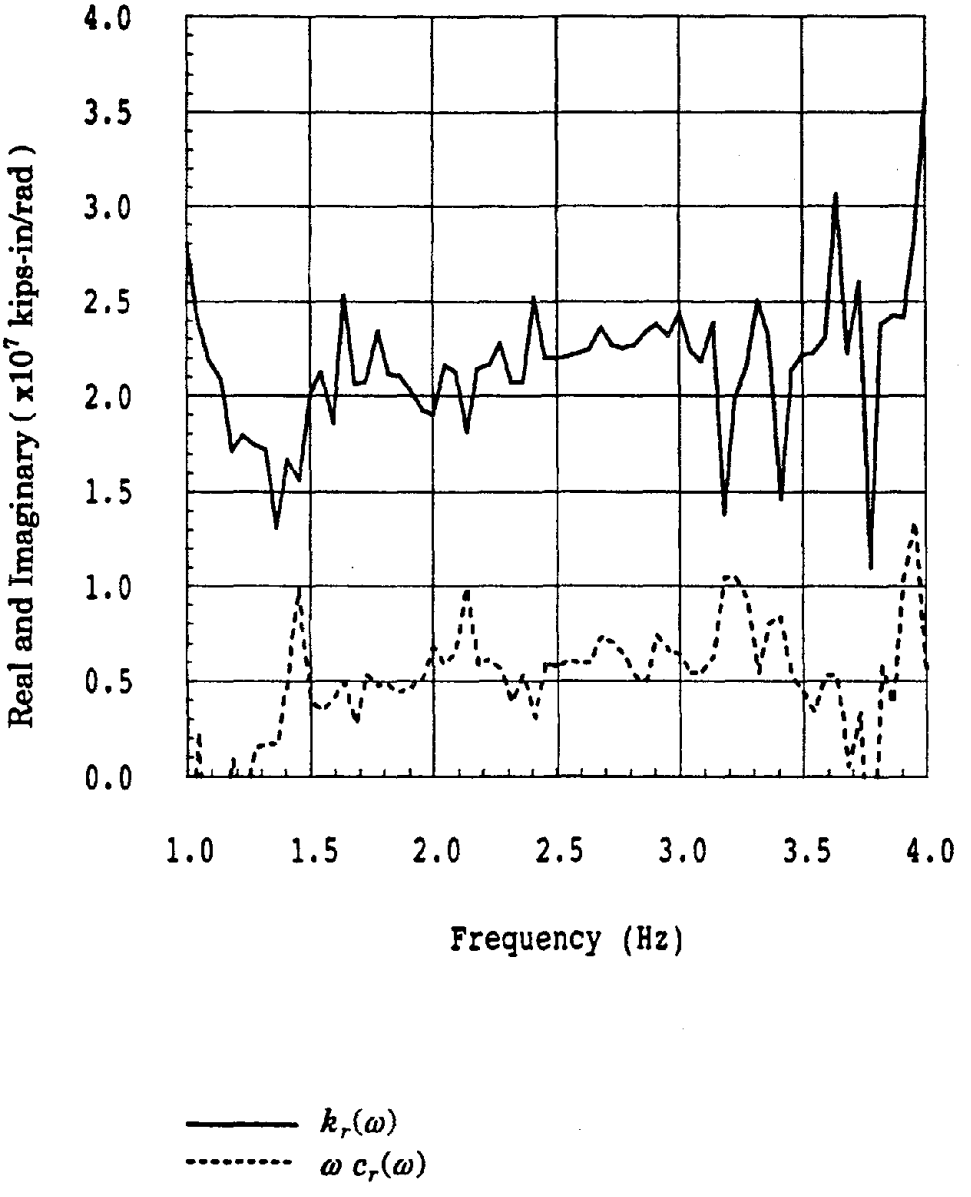

Fig. 5.5a: Transfer Function of Pitch Moment over Pitch Rotation

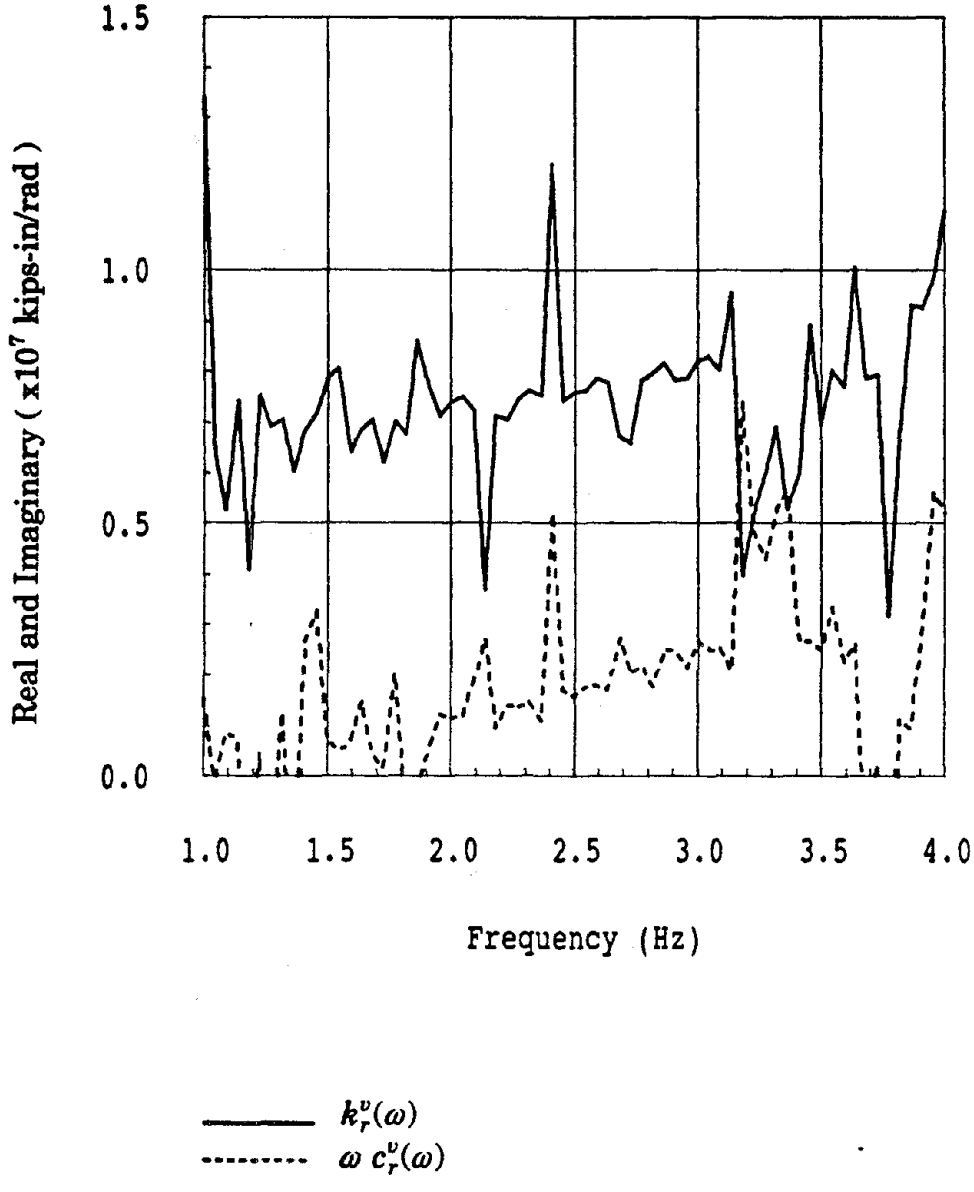

Fig. 5.5b: Transfer Function of Vertical Actuators Moment over Pitch Rotation

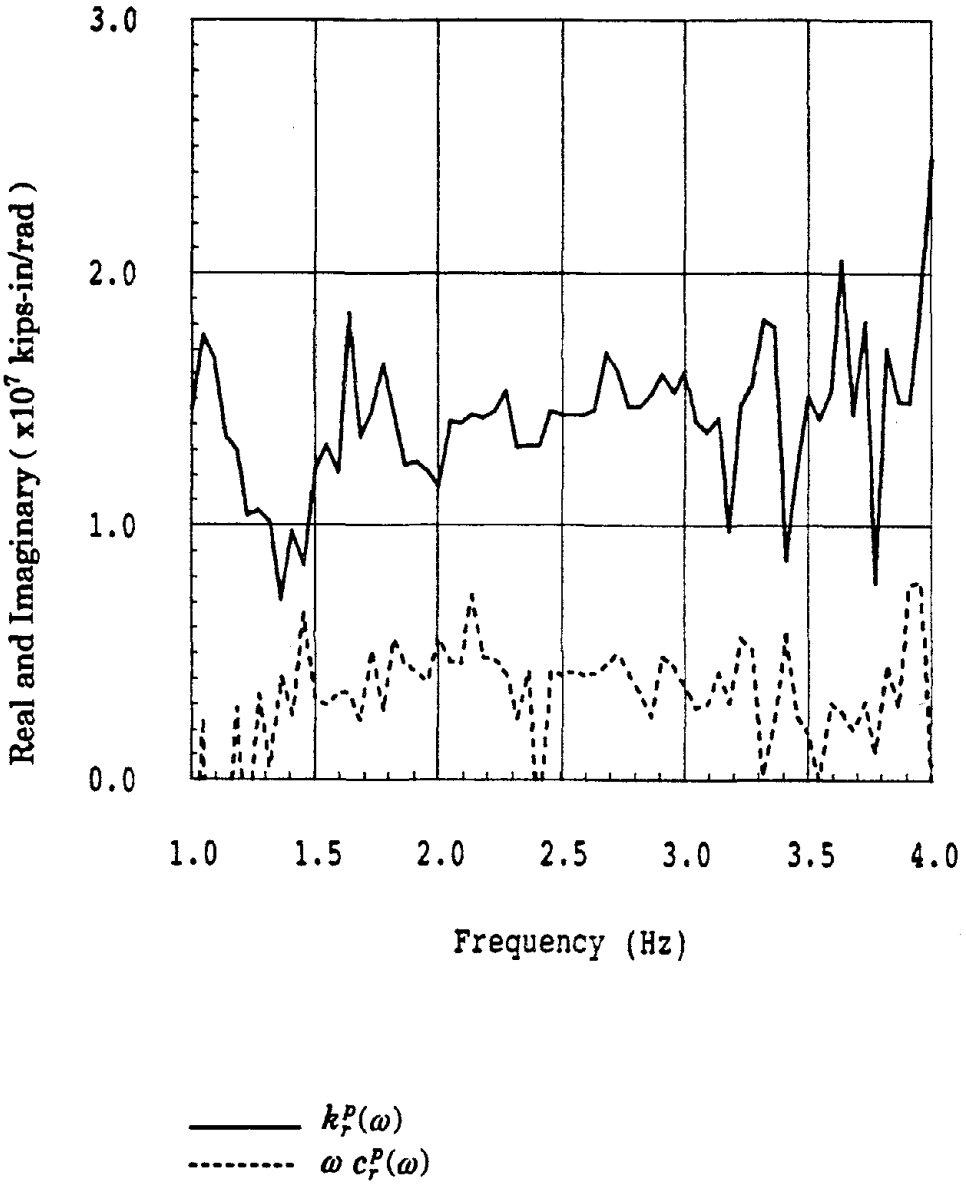

Fig. 5.5c: Transfer Function of Passive Stabilizers Moment over Pitch Rotation

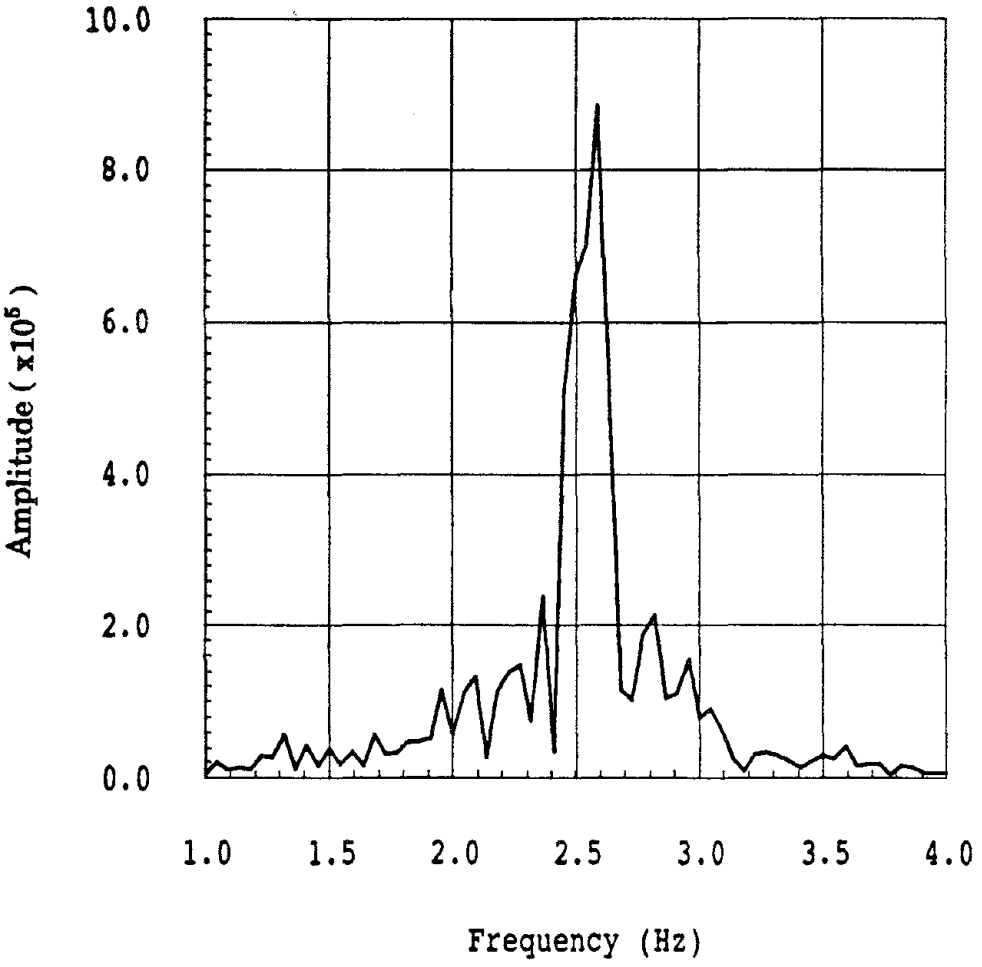

Fig. 5.5d: Fourier Amplitude Spectrum of Pitch Displacement

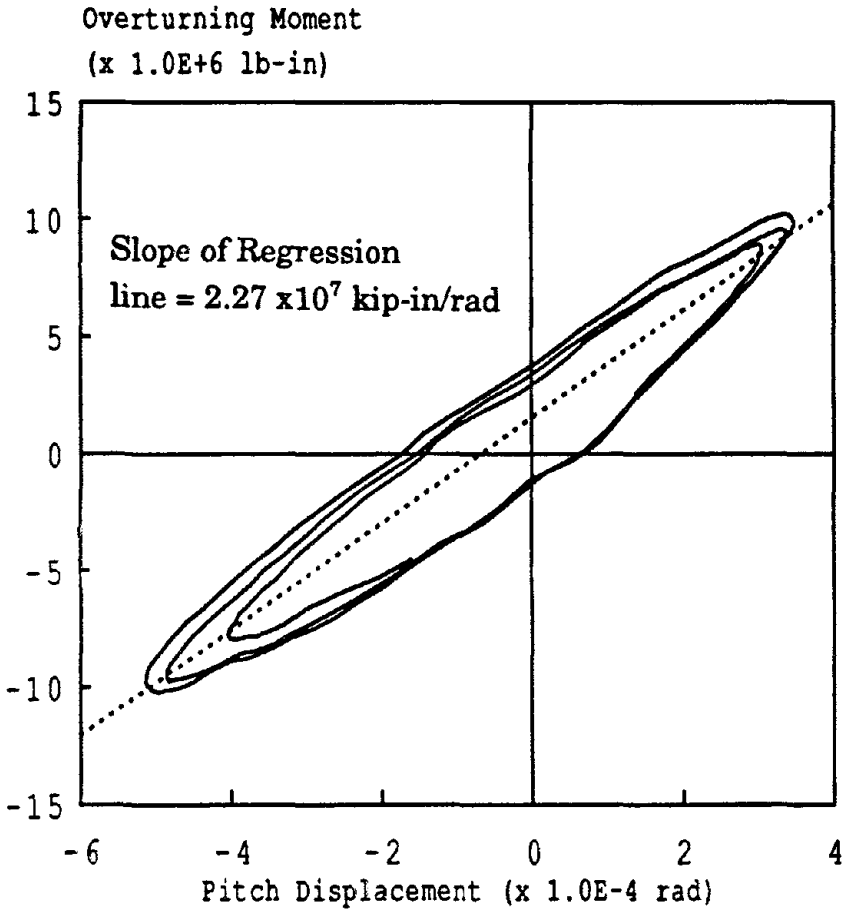

Fig. 5.6: Hysteresis Loops of Overturning Moment-Pitch Rotation
Run 850819.26 Taft Span=200

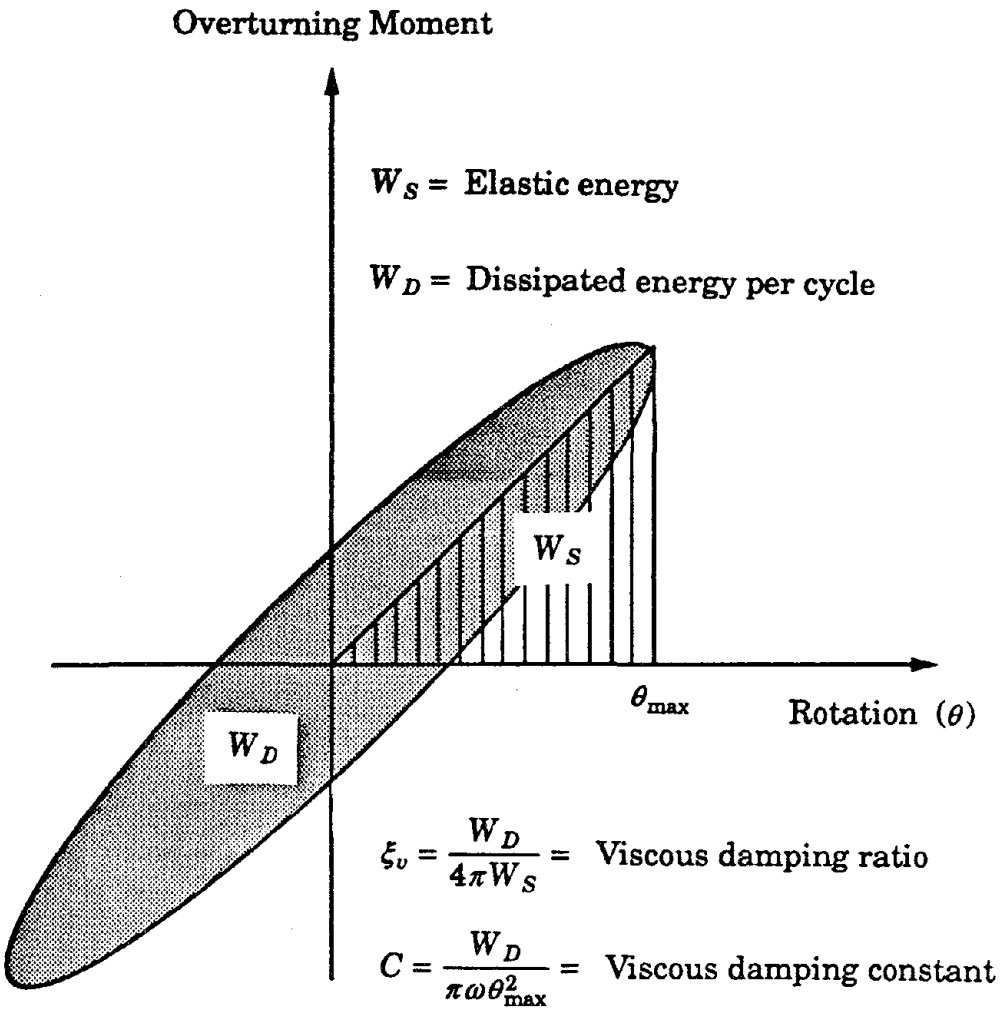

Fig. 5.7: Estimation of Damping Properties from Hysteresis loops.

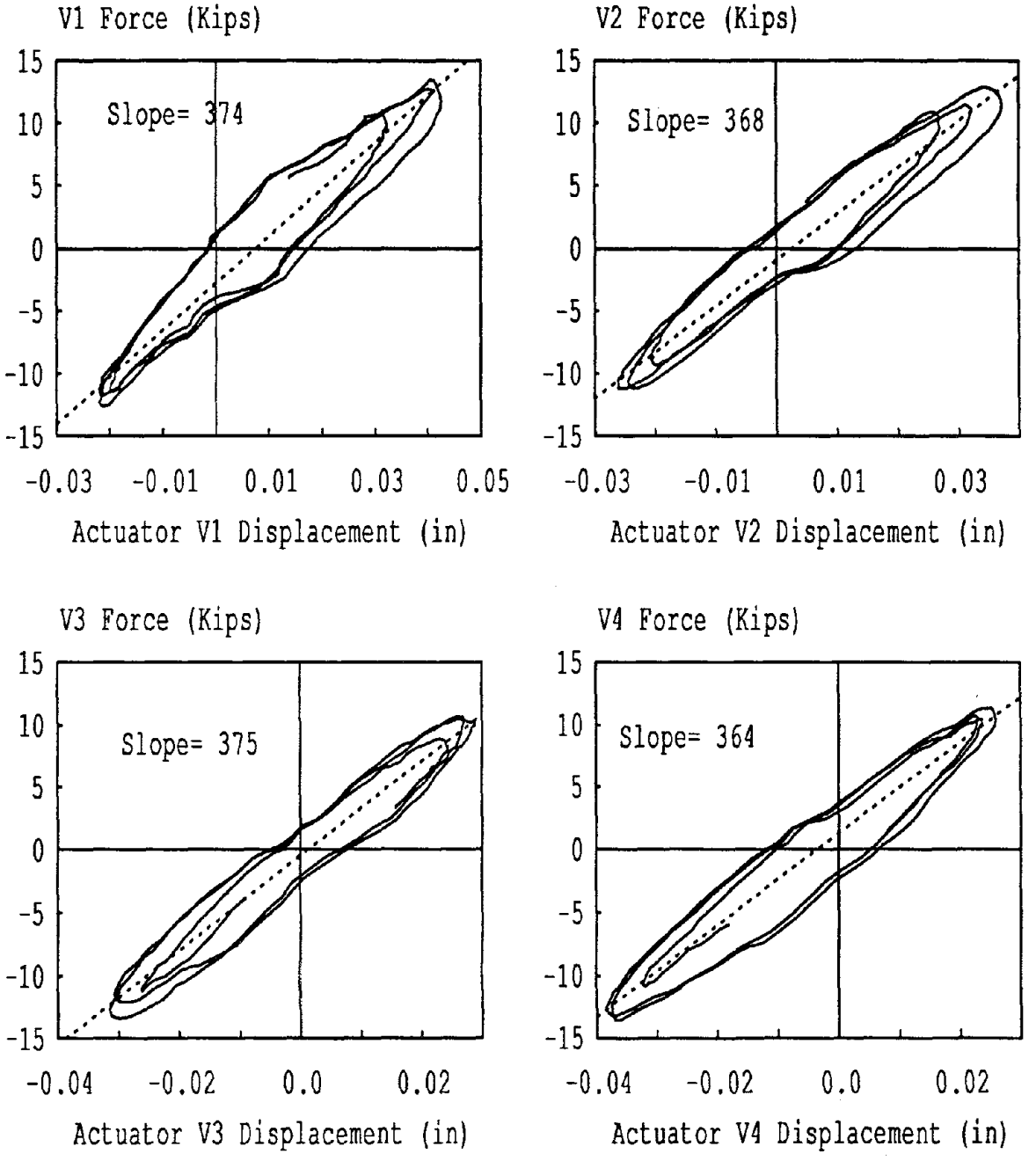

Fig. 5.8: Hysteresis Loops of Actuator Forces versus Displacement
Run 850819.26 Taft Span=200, Time=9.3-10.4 seconds.

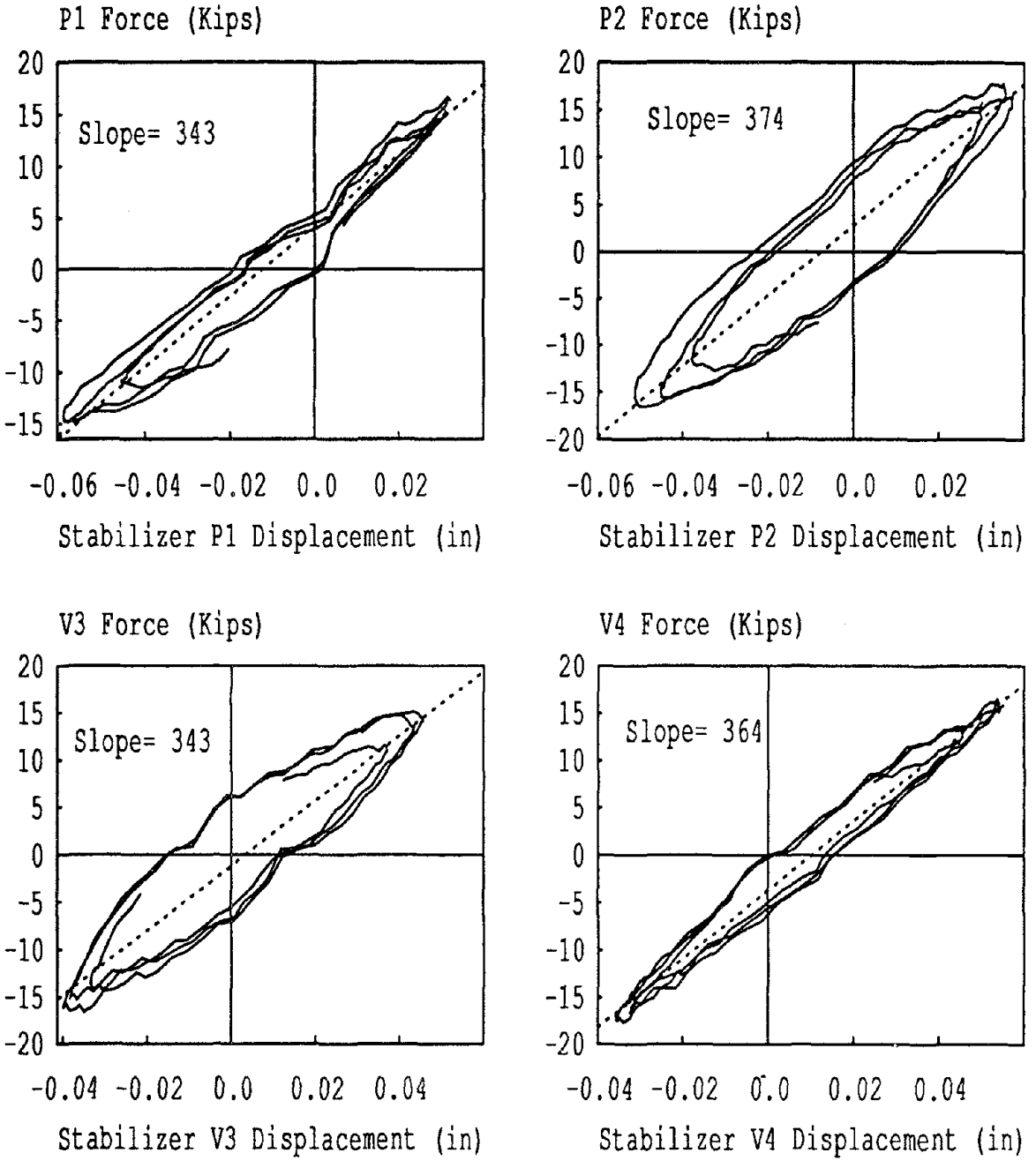

Fig. 5.9: Hysteresis Loops of Stabilizer Forces versus Displacement
Run 850819.26 Taft Span=200, Time=9.3-10.4 seconds.

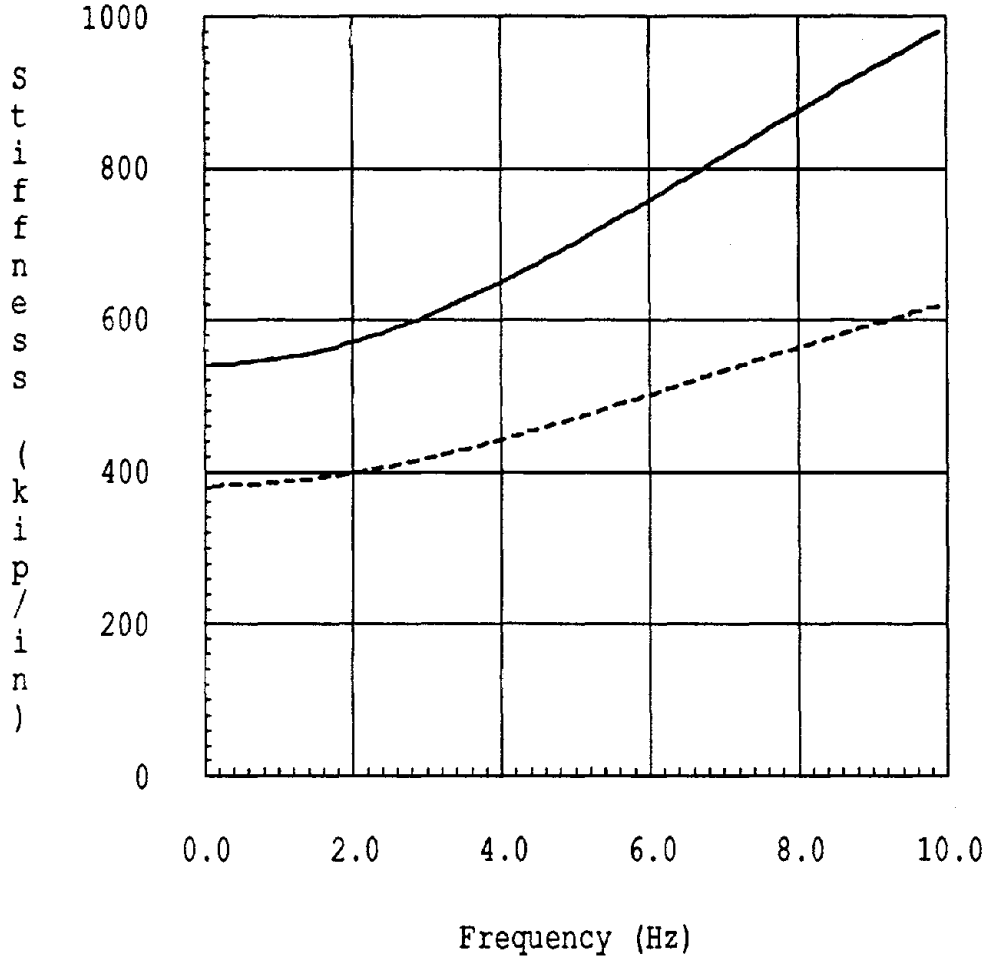

Fig. 5.10a: Equivalent Stiffness for Horizontal Actuator

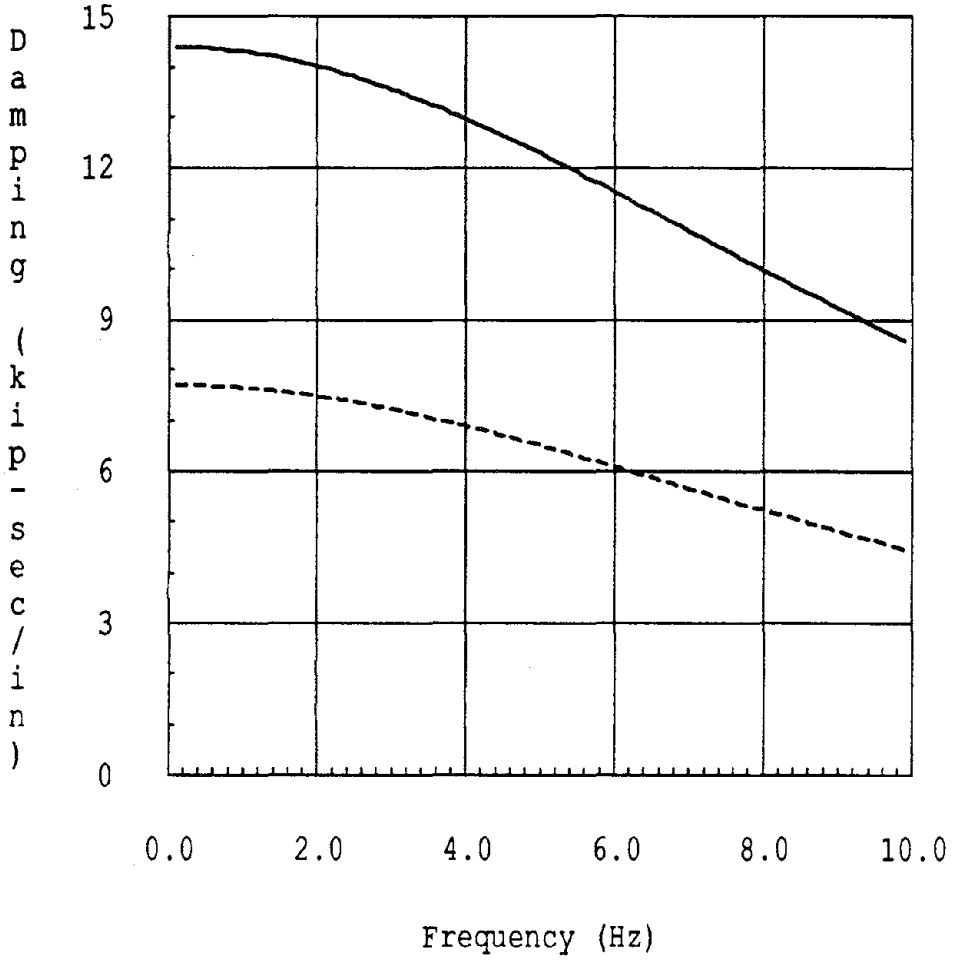

Fig. 5.10b: Equivalent Damping for Horizontal Actuator

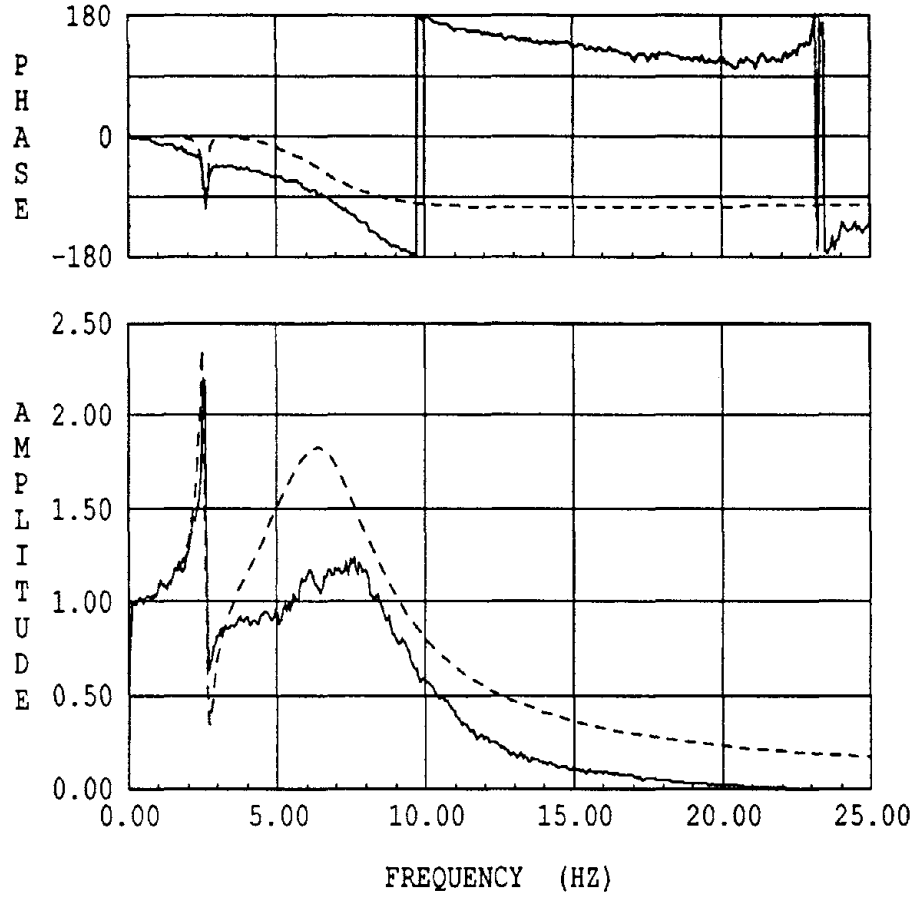

Fig. 5.11: Transfer Function of Table Horizontal Displacement over Command Displacement

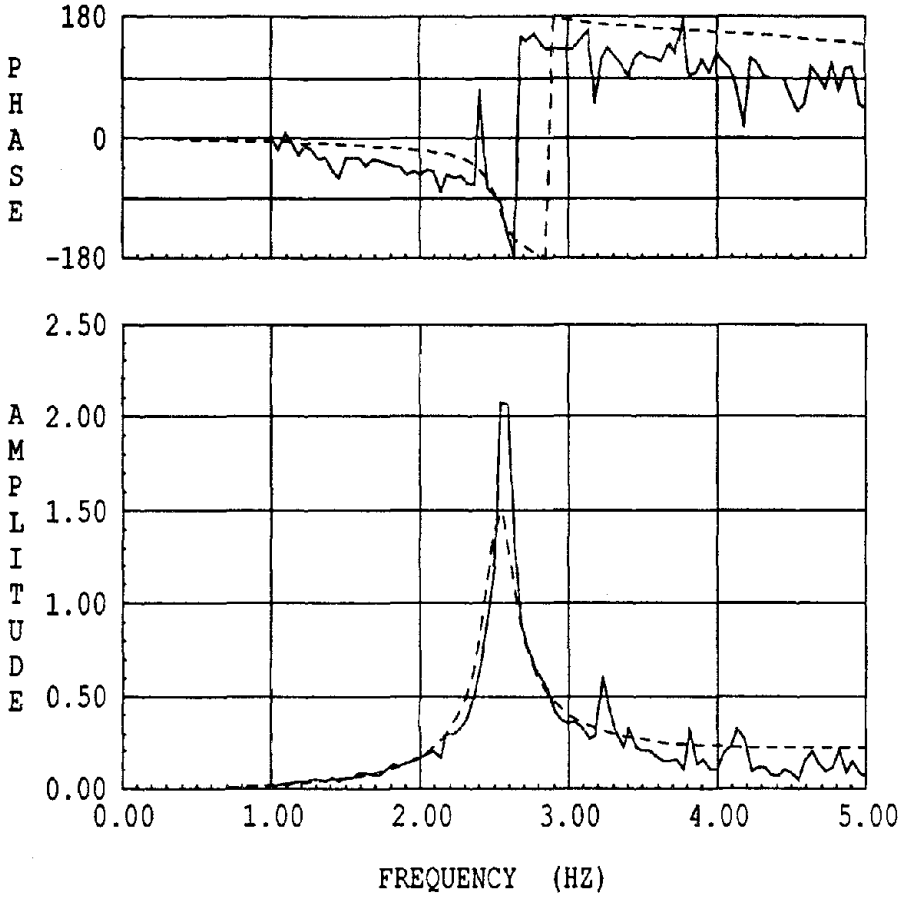

Fig. 5.12: Transfer Function of Table Pitch Displacement*h over Command Displacement

Chapter Six
ANALYSIS OF UNI-DIRECTIONAL EARTHQUAKE SIMULATORS

6.1 INTRODUCTION

Electrohydraulic shaking tables are driven by actuators that are controlled by an electrohydraulic servomechanism. Several books have dealt with the analysis of electrohydraulic servomechanisms [20,21,22,23]. Analysis and performance of unidirectional shaking tables have been the subject of numerous researchers [7,8,24,25,26,27,28]. This chapter presents the development of an analytical model for unidirectional earthquake simulators. Both time and frequency domain analyses are included, and stability conditions are derived.

6.2 TIME DOMAIN SOLUTION

A sketch of the main components of a typical table-actuator system is shown in Fig. 6.1 [7]. It consists of a rigid table mass driven by an actuator which is controlled by a two stage servovalve. The servovalve consists of a pilot stage spool to which input forces are applied and a slave spool that is driven by the pilot spool. In two stage servovalves, the feedback loops tend to linearize the input force-slave spool displacement relationship so that (following Rea's [7] assumptions)

$$x_{sp} = k_1 F_i \tag{6.1}$$

where

F_i is external force applied to the pilot spool

x_{sp} is slave spool displacement

k_1 is gain factor

The oil flow induced to the slave spool is usually a nonlinear function of the spool displacement x_{sp} and the force in the actuator F_a [20]. However, for spool position near the equilibrium position, the relationship can be

linearized by a Taylor's series expansion to get

$$q = k_q x_{sp} - k_c F_a \tag{6.2}$$

In this equation, q is the slave stage load flow, while k_q and k_c are, respectively the flow-gain and flow-force coefficients. The first term on the right hand side is the flow induced by the spool valve displacement, and the second term represents the flow due to leakage, assumed to be proportional to the force in the actuator.

The differential equation governing the actuator piston can be expressed by the formula [7]

$$q = \dot{x}_t A + (V/4\beta A)\dot{F}_a \tag{6.3}$$

where

A *is* Actuator piston area.

V *is* Volume of oil in the actuator.

β *is* Bulk modulus of fluid.

x_t *is* Table horizontal displacement.

F_a *is* Actuator force applied to the table.

The above equation indicates that the flow provided by the slave valve can be decomposed into two components: a flow generated by the displacement of the piston and a flow induced by the compression of the oil in the actuator chamber.

Normally earthquake simulators employ a displacement feedback, a velocity or rate feedback and a force or differential pressure feedback. The displacement feedback is used in order to improve the accuracy of reproducing the command signal, while the force and velocity feedback are usually employed to increase system stability [29].

The input force F_i applied to the pilot stage of the servovalve is proportional to the difference between the command displacement and the sum of the different feedback signals, as is given by

$$F_i = k_2(x_c - k_f F_a - k_d x_t - k_v \dot{x}_t) \tag{6.4}$$

where

x_c *is* displacement command signal

k_f, k_d, k_v *is* gains of force,displacement and velocity feedback

Figure 6.2 represents, in block diagram form, the dynamic response of the earthquake simulator system as described by Eqs. (6.1)-(6.4). Equation (6.4) is valid as long as the displacement, velocity and acceleration limits of the system are not exceeded. These limits were shown in Fig. 2.3 for the bare table system.

Eliminating q from Eqs. (6.2) and (6.3) and substituting Equations (6.1) and (6.4) into the resulting equation we get

$$(V/4\beta A)\dot{F}_a + (k_t k_f + k_c)F_a + (k_t k_v + A)\dot{x}_t + (k_t k_d)x_t = k_t x_c \tag{6.5a}$$

where

$$k_t = k_q k_1 k_2 \tag{6.5b}$$

The actuator force-table acceleration relationship, neglecting the damping effects, is expressed by

$$F_a = m_t \ddot{x}_t \tag{6.6}$$

where m_t is the table mass.

The differential equation of the system relating the command displacement to the output table displacement is obtained by substituting Eq. (6.6) into (6.5a)

$$(Vm/4\beta A)\frac{d^3x_t}{dt} + m(k_t k_f + k_c)\frac{d^2x_t}{dt} + (k_t k_v + A)\frac{dx_t}{dt} + (k_t k_d)x_t = k_t x_c \tag{6.7a}$$

which is of the form

$$a_3 \frac{d^3x_t}{dt} + a_2 \frac{d^2x_t}{dt} + a_1 \frac{dx_t}{dt} + a_o x_t = b_o x_c \tag{6.7b}$$

This equation is a third order linear differential equation with constant coefficients, and can be solved numerically by writing it in the state equation form

$$\dot{\mathbf{X}} = \mathbf{AX} + \mathbf{F} \tag{6.8a}$$

or

$$\frac{d}{dt}\begin{Bmatrix} x_t \\ \dot{x}_t \\ \ddot{x}_t \end{Bmatrix} = \begin{bmatrix} 0 & 1 & 0 \\ 0 & 0 & 1 \\ -a_o/a_3 & -a_1/a_3 & -a_2/a_3 \end{bmatrix}\begin{Bmatrix} x_t \\ \dot{x}_t \\ \ddot{x}_t \end{Bmatrix} + \begin{Bmatrix} 0 \\ 0 \\ b_o/a_3 \end{Bmatrix} x_c \tag{6.8b}$$

where

$$\mathbf{X} = [\, x_t \;\; \dot{x}_t \;\; \ddot{x}_t \,]^T$$

and **A** and **F** are the square matrix and vector on the right hand side of Eq. (6.8b). Equation (6.8b) can be solved in the time domain by the Runga-Kutta method to determine the table displacement, velocity and acceleration responses.

6.3 FREQUENCY DOMAIN SOLUTION

As an alternative, Eq. (6.7b) can be transformed to the Laplace domain to obtain the transfer function as follows

$$H(s) = \frac{x_t(s)}{x_c(s)} = \frac{b_o}{a_3 s^3 + a_2 s^2 + a_1 s + a_o} \tag{6.9a}$$

or using Eq. (6.7a)

$$H(s) = \frac{k_t}{(Vm/4\beta A)s^3 + m(k_t k_f + k_c)s^2 + (k_t k_v + A)s + k_t k_d} \tag{6.9b}$$

In order to reproduce the command displacement, a unity displacement feedback (k_d=1) is required. This results in (b_o=a_o=k_t). Rewriting the transfer function in terms of the original constants leads to

$$H(s) = \frac{x_t(s)}{x_c(s)} = \frac{k_t}{(Vm/4\beta A)s^3 + m(k_t k_f + k_c)s^2 + (k_t k_v + A)s + k_t} \tag{6.10}$$

The amplitude and phase of the transfer function may be obtained by substituting ($i\,\omega$) for (s) in the above equation and separating it into real and

imaginary parts. The table motion resulting from a given input signal x_c may then be obtained by

$$x_t(i\omega)=H(i\omega)\,x_c(i\omega) \tag{6.10a}$$

where $x_t(i\omega)$ and $x_c(i\omega)$ are, respectively, the Fourier Transforms of the table and command displacements. The table response can then be obtained from the inverse Fast Fourier Transform (FFT) of $x_t(i\omega)$. Equation (6.10a) represents the steady state part of the response which, under the normal circumstance of zero initial conditions, would constitute the total response.

The bare table system is stable as long as the roots of the denominator of (x_t/x_c) have no positive real parts. Positive real parts correspond to negative damping in the case of complex roots, and to a growing exponential response in the case of real roots. To insure that all roots have negative real parts, the Routh-Hurwitz criterion [29] can be applied to give

$$k_t>0 \tag{6.11a}$$

$$k_t k_f+k_c>0 \tag{6.11b}$$

$$(k_t k_f+k_c)(k_t k_v+A)-(k_t V/4\beta A)>0 \tag{6.11c}$$

6.4 OPEN LOOP RESPONSE

Often, it is more convenient to express the transfer function in terms of its open loop parameters, such as the open loop frequency and open loop damping. This leads to simplifications of the above transfer function expressions. The open loop response can be obtained by eliminating the displacement, velocity and force feedback loops in Fig. 6.2. or by substituting $(k_d=k_v=k_f=0)$ in Eq. (6.9b) to get

$$G(s)=\frac{k_t}{s[\,(Vm/4\beta A)s^2+(mk_c)s+A\,]} \tag{6.12}$$

$$=\frac{k_t}{A}\,\frac{1}{s[\,(Vm/4\beta A)s^2+(mk_c)s+1\,]}$$

This may be expressed in a more familiar form as

$$G(s) = \frac{\hat{k}_o}{s\,[\,(1/\hat{\omega}_o^2)s^2 + (2\hat{\xi}_o/\hat{\omega}_o)s + 1\,]} \tag{6.13}$$

where

$$\hat{\omega}_o^2 = \frac{4\beta A^2}{mV} \tag{6.14a}$$

$$\hat{\xi}_o = \frac{mk_c\hat{\omega}_o}{2A} \tag{6.14b}$$

$$\hat{k}_o = \frac{k_t}{A} \tag{6.14c}$$

$\hat{\omega}_o$, $\hat{\xi}_o$ and $\hat{k}_o$ are the open loop frequency, damping and gain, respectively. As is clear from the above expression, the open loop frequency is inversely proportional to the square root of the table mass, and the open loop damping is directly proportional to the square root of the table mass.

6.5 CLOSED LOOP RESPONSE: DISPLACEMENT FEEDBACK

The transfer function with displacement feedback can be obtained from G(s) by the following relationship

$$H(s) = \frac{G(s)}{1 + G(s)} \tag{6.15a}$$

$$= \frac{k_o}{s\,[\,(1/\omega_o^2)s^2 + (2\xi_o/\omega_o)s + 1\,] + k_o} \tag{6.15b}$$

The above equation corresponds exactly to Eq. (6.10) when ($k_v = k_f = 0$) is substituted.

6.6 EFFECT OF FORCE AND VELOCITY FEEDBACK

It is evident that the equation would still hold the same form when the force and velocity feedback are added. The new system parameters can be easily found by equating Eqs. (6.10) and (6.15) to get

$$k_o = \frac{k}{kk_v + A} \tag{6.16a}$$

$$\omega_o^2 = \frac{4\beta A(kk_v + A)}{mV} \tag{6.16b}$$

$$\xi_o = \frac{m\omega_o(kk_f + k_c)}{2(kk_v + A)} \tag{6.16c}$$

Therefore, the effect of the force or pressure feedback is to increase the open loop damping in the system. On the other hand, velocity feedback has the effect of decreasing the open loop gain and damping while simultaneously increasing the open loop frequency of the system. Rea et al. [7] suggested that velocity feedback has very little effect on the response of shaking tables.

In terms of these parameters, the stability requirement in (6.11) can be expressed as

$$2\xi_o \omega_o > k_o \tag{6.17b}$$

Also, the state equation [Eq. (6.8)] can be written as

$$\frac{d}{dt}\begin{Bmatrix} x_t \\ \dot{x}_t \\ \ddot{x}_t \end{Bmatrix} = \begin{bmatrix} 0 & 1 & 0 \\ 0 & 0 & 1 \\ -\omega_o^2 k_o & -\omega_o^2 & -2\xi_o \omega_o \end{bmatrix} \begin{Bmatrix} x_t \\ \dot{x}_t \\ \ddot{x}_t \end{Bmatrix} + \begin{Bmatrix} 0 \\ 0 \\ \omega_o^2 k_o \end{Bmatrix} x_c \tag{6.18}$$

6.7 PARAMETER IDENTIFICATION

Tests were performed on the EERC shaking table to determine the bare table system parameters. For this purpose it was fed with a band limited random signal (0-32 Hz) from the GenRad 2515 data acquisition and analysis system. The noise level was set to 0.12 volt on the GenRad, and a span of 400 was selected for the table control system.

Data acquisition was done using two systems: First, time history measurements of 32 channels were made using the VAX computer running under the Unix 4.2 operating system; a sampling rate of 250 samples per second

was chosen to avoid aliasing in the signal after it passed through a 100 Hz analog filter.

Second, transfer function measurements were made between 4 of the above 32 channels using the RTA 2.0 program running under the RT-11 operating system of the GenRad 2515. The GenRad system has a built in anti-aliasing filter. The frequency band was set to 0-32 Hz, and consisted of 512 frequency lines. In the time domain, each frame of 16 seconds consisted of 2048 points. A Hanning window was used to minimize the leakage by eliminating the abrupt ends of the frame discontinuities. Leakage causes the amplitude spectrum at a certain frequency to decrease by transferring some of the energy at that frequency to the adjacent frequencies. The Hanning function also reduces the total energy in the frame but this can be corrected by a factor such that the total energy is the same as that of the original input frame. Overlapping data segments were used in order to minimize the time needed to obtain the 40 averages used to smooth the data. When overlapping segments are used, the system does not wait until a completely new frame is obtained, it simply uses part of the old frame to complete the number of points needed for the FFT.

Estimation of the transfer function from the measured data was described in Section 3.2.1.

System parameters (equivalent open loop frequency, damping and gain) were estimated by performing a nonlinear least squares fit on the experimentally obtained transfer functions. The Levenberg- Marquardt algorithm [30,31] implemented in IMSL [32], and NL2SOL [33] were used for solving the nonlinear least squares problem. NL2SOL is especially convenient as it allows bounds on the optimum parameters. These algorithms are relatively fast when good initial estimates are provided. Good initial estimates for the open loop frequency can be obtained by recognizing a useful characteristic of the closed loop transfer function in (6.15)

$$H(i\omega_o) = \frac{k_o}{k_o - 2\xi_o \omega_o} \tag{6.19}$$

From the stability requirement in (6.19), $H(i\omega_o)$ is real and negative. Hence a good estimate of ω_o is the frequency at which the phase is 180 degrees. Figure 6.3 shows a least squares fit on the experimentally obtained transfer function [bare table displacement/command displacement]. This transfer function corresponds to the standard setting of the EERC shaking table control system that is normally used for testing structures on the table. Figures 6.4-6.5 show the system transfer function when the differential pressure (Delta-P) stabilization is changed from its standard value of 1.5 to 0 and 5 respectively. Figures 6.6-6.7 present the effects of changing the Horizontal Gain from the standard value of 9 to 8 and 10 respectively. Figure 6.8 demonstrates the effect of adding a 70 kips mass to the original table mass of 100 kips. Table 6.1 shows the least squares estimate of the open loop frequency, damping and gain obtained for the different settings mentioned.

As predicted by Eq. (6.14), the added mass caused a decrease in the frequency while increasing the open loop damping. An increase of horizontal gain mainly caused the open loop gain to increase. Increasing the Delta-P however caused an unexpected decrease in the open loop frequency.

6.8 STABILITY STUDY

To study the effect of the various parameters on the bare table system stability, the Nyquist plot of the open loop transfer function was used. The Nyquist plot represents a plot of the real versus imaginary part of the open loop transfer function. This plot can be used in conjunction with the Nyquist Stability Theorem [29] to establish whether the closed loop system is stable. It is also useful for establishing the relative stability of different systems based on the evaluation of the gain and phase margins from this plot. In control theory a system is said to be more stable if it has larger gain and phase margins. The phase margin is defined as the phase angle at which the amplitude is unity. Gain margin on the other hand is the inverse of the

amplitude at which the phase is 180 degrees. Phase and gain margins can be easily obtained from a Nyquist plot of the open loop transfer function $G(s)$ as shown in Fig. 6.9, which also shows their values for the PUC shaking table [8]. For the bare table system, the gain margin can be easily derived from Eq. (6.13) by substituting ($i\omega$) for s and equating the imaginary part to zero. This would yield the frequency at which the Nyquist plot crosses the real axis. The inverse of the amplitude at that frequency would give the gain margin as

$$G_m = \frac{2\xi_o \omega_o}{k_o} \tag{6.20}$$

where $\omega_o = 2\pi f_o$. The equivalent open loop transfer function $G(s)$ can be obtained from the measured closed loop $H(s)$ from Eq. (6.15) as follows

$$G(s) = \frac{H(s)}{1 - H(s)} \tag{6.21}$$

Since the higher the gain margin G_m the more stable is the system, Eq. (6.20) shows that increasing the open loop frequency and damping tends to stabilize the system, however, increasing the gain renders the system less stable. The gain and phase margins obtained from the fitted curves are presented in Table 6.1.

Figures 6.10-6.11 show the effects of varying the Delta-P stabilization and the horizontal gain on the stability of the EERC system. From Figure 6.10 it can be seen that the Delta-P stabilization control knob on the EERC table works in reverse order, so that a smaller Delta-P tends to improve stability. This behavior of the Delta-P gain may be attributed to the highpass filter on the force feedback loop [Appendix B]. On the other hand, Fig. 6.11 shows that an increase in the horizontal gain tends to destabilize the system.

6.9 ANALYTICAL STUDY: EFFECT OF SYSTEM PARAMETERS

The effect of changing the open loop frequency f_o can be seen in Fig. 6.12. The lower the value of f_o the lower the bandwidth of the system.

Frequencies near f_o are more amplified for lower f_o. Equation (6.20) suggests a more stable system for higher f_o.

The effect of changing the equivalent open loop damping is shown in Fig. 6.13. Low damping values cause a significant peak near f_o, and a trough just before that, so that higher gain is attained for frequencies higher than f_o, and lower gain for lower frequencies. Equation (6.20) suggests a more stable system for higher ξ_o.

When k_o is increased, amplification or gain is higher for all frequencies as can be seen in Fig. 6.14. The absolute phase angle tends to be higher for lower k_o and for frequencies less than f_o. For higher frequencies the phase is not affected. Equation (6.20) suggests a more stable system for lower k_o.

SETTING	FREQ (Hz) f_o	DAMPING (percent) ξ_o	LOOP GAIN k_o	GAIN MARGIN G_m	PHASE MARGIN ϕ_m
STANDARD	12.60	47.7	25.07	3.01	70.1
Delta-P=0	13.70	43.4	22.84	3.26	75.4
Delta-P=5	9.00	52.8	23.60	2.53	59.3
Horizontal Gain= 8	12.60	51.2	17.60	4.61	76.1
Horizontal Gain=10	12.00	48.6	28.56	2.56	64.4
Added Mass of 70 kips	9.40	59.4	25.07	2.80	56.8

* Standard Settings: Delta-P=1.5 Gain=9

Table 6.1 : System parameters for different control settings

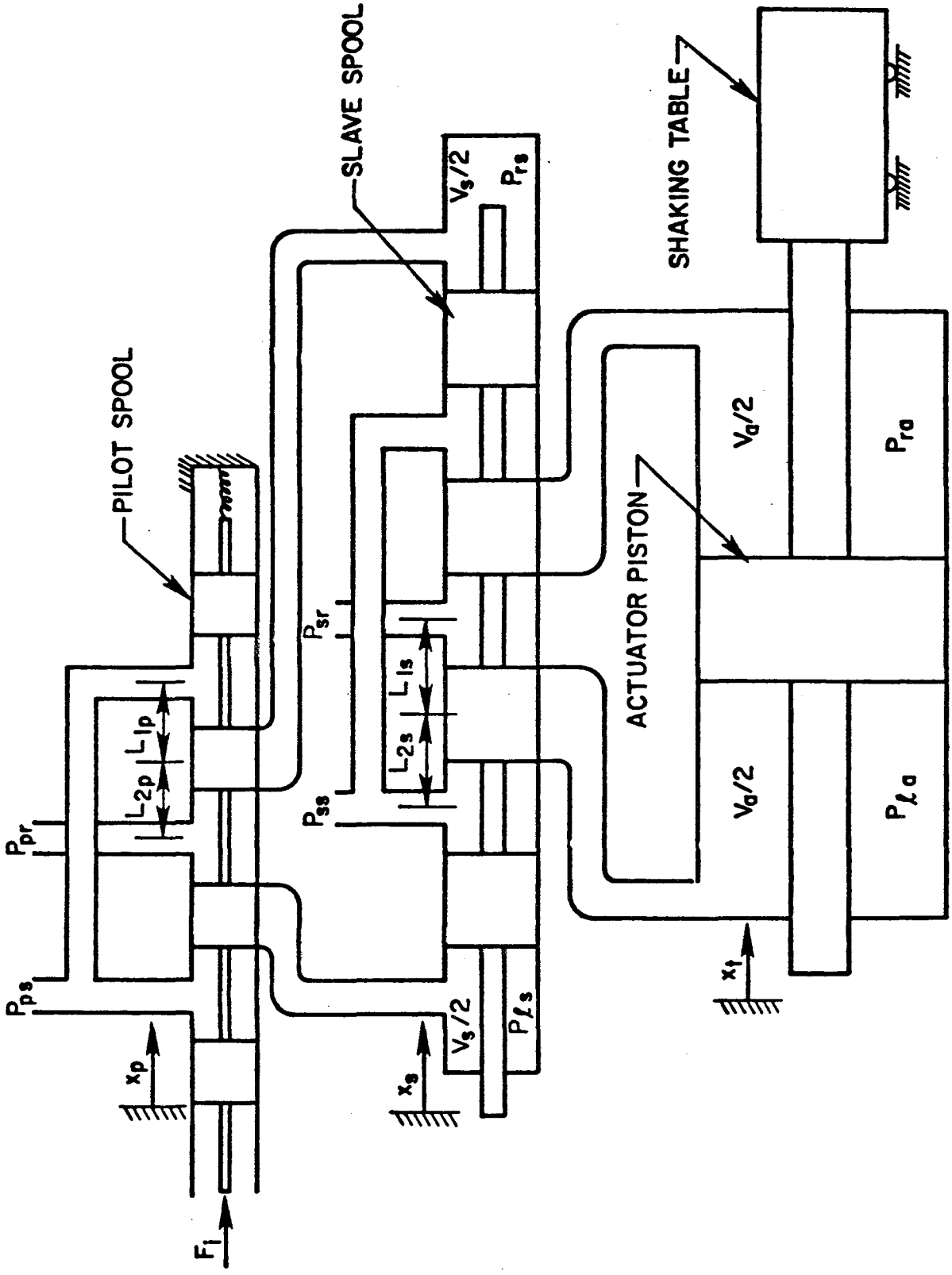

Fig. 6.1: SERVOVALVE-ACTUATOR HYDRAULIC SYSTEM

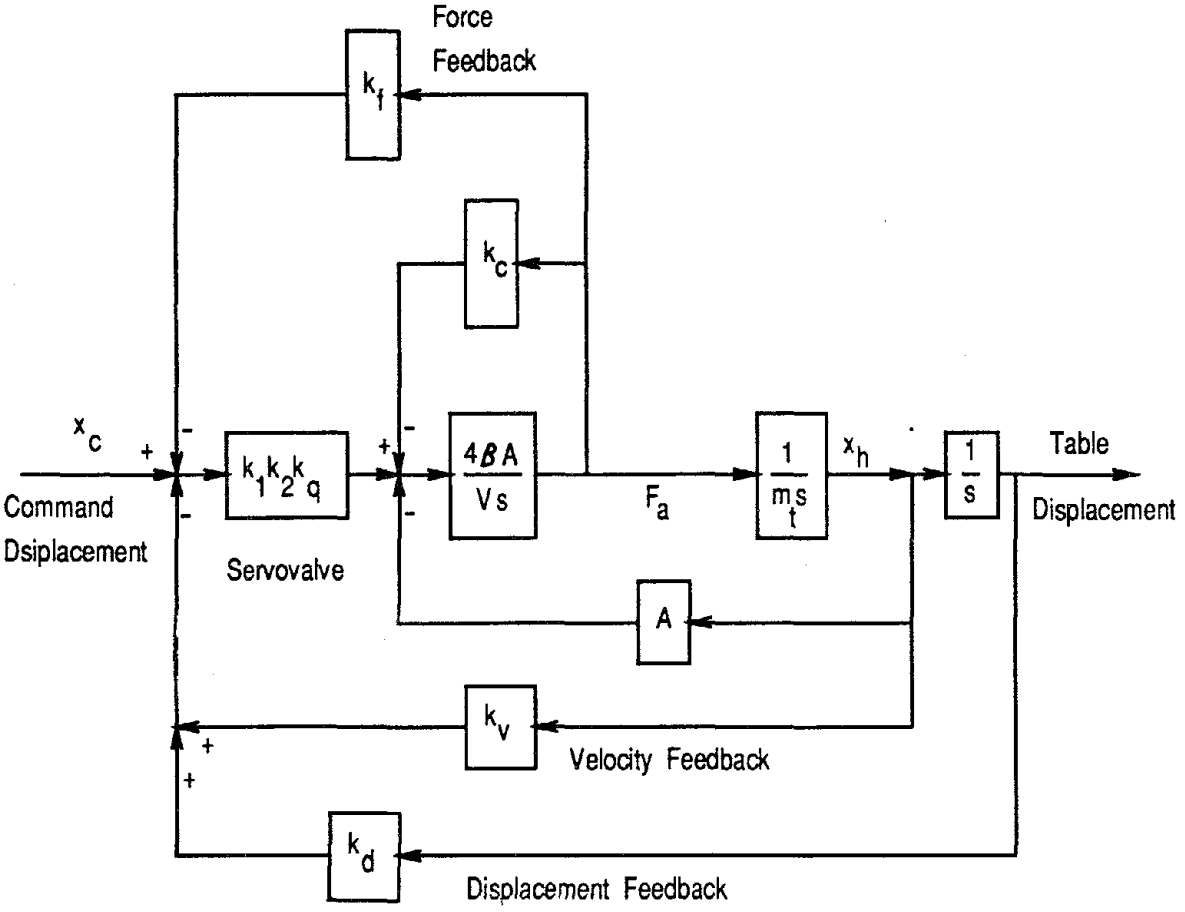

Fig. 6.2: Block diagram of bare uni-directional earthquake simulator.

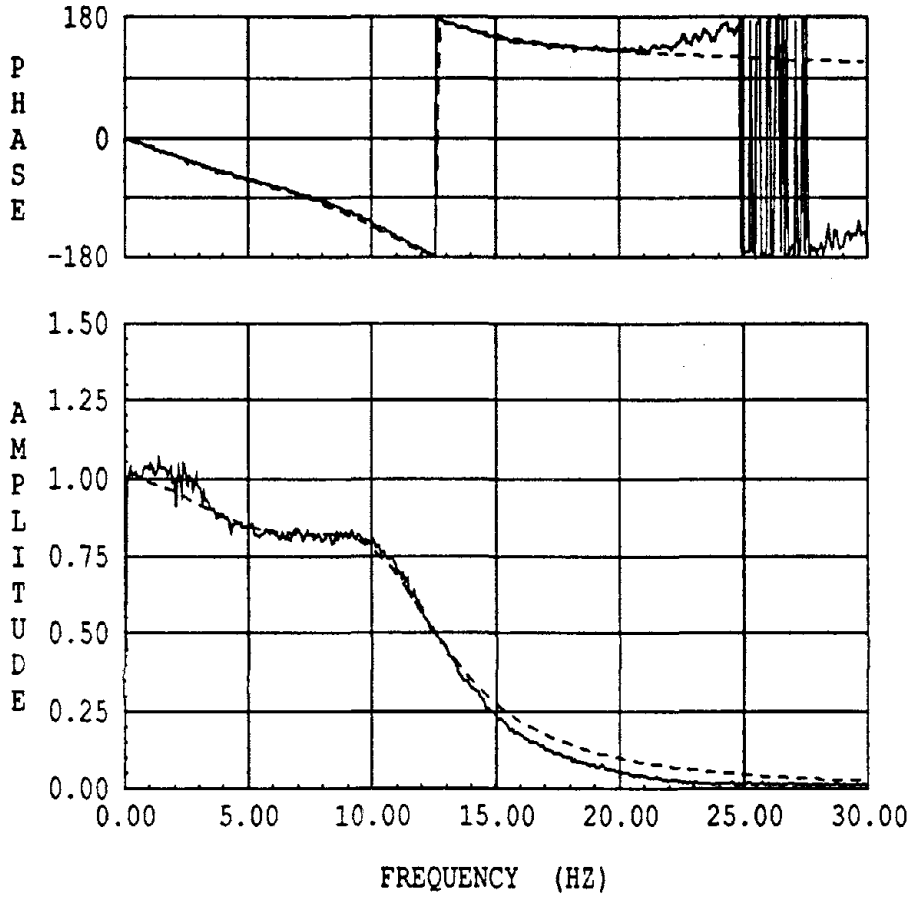

Fig. 6.3: Transfer Function of Bare Table Displacement over Command Displacement (Standard Settings)

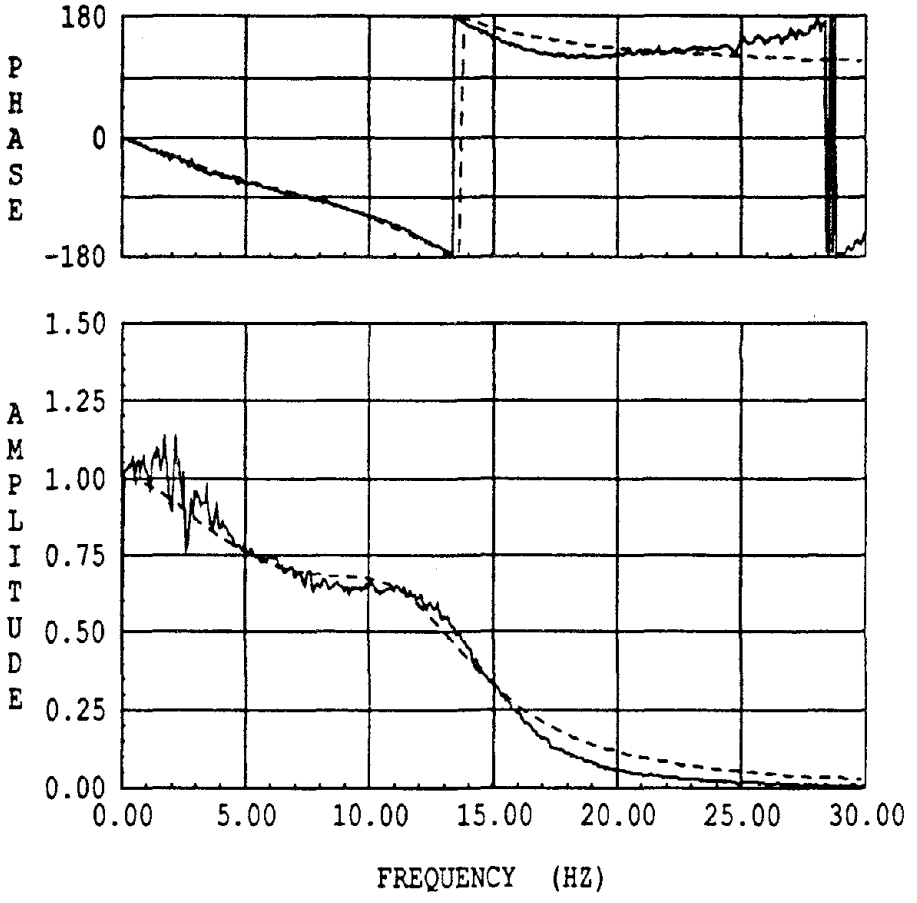

Fig. 6.4: Transfer Function of Bare Table Displacement over Command Displacement (Delta-P=0)

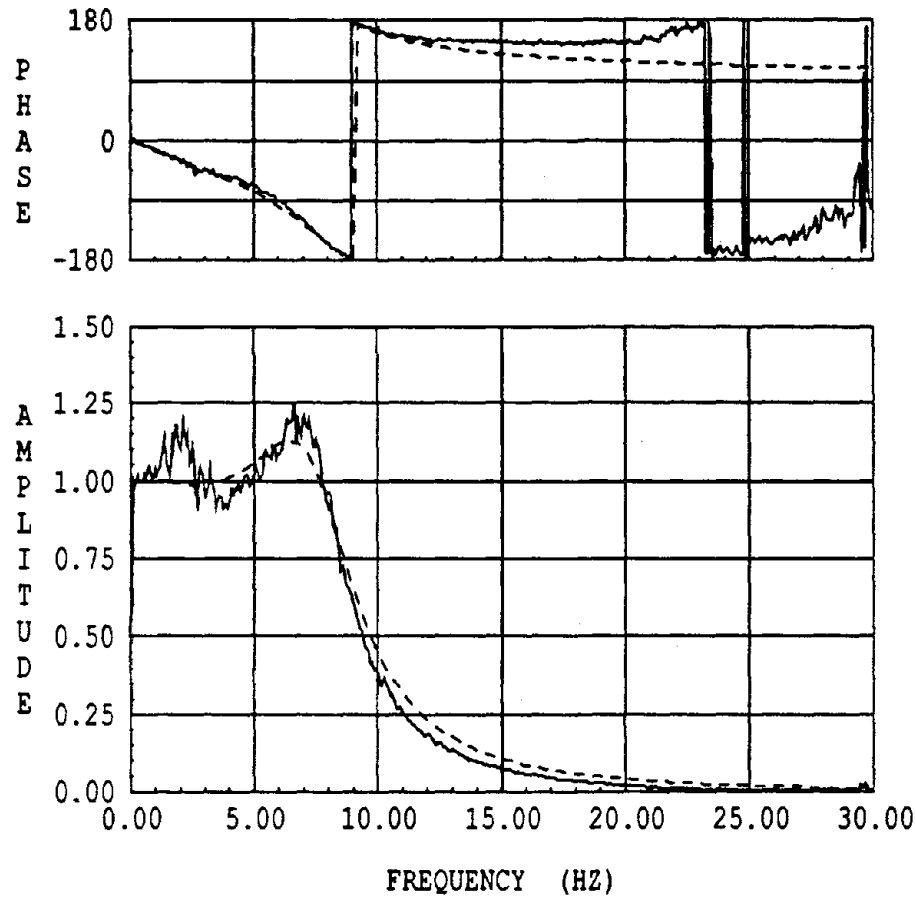

—— Experimental
---- Analytical: Table 6.1

Fig. 6.5: Transfer Function of Bare Table Displacement over Command Displacement (Delta-P=5)

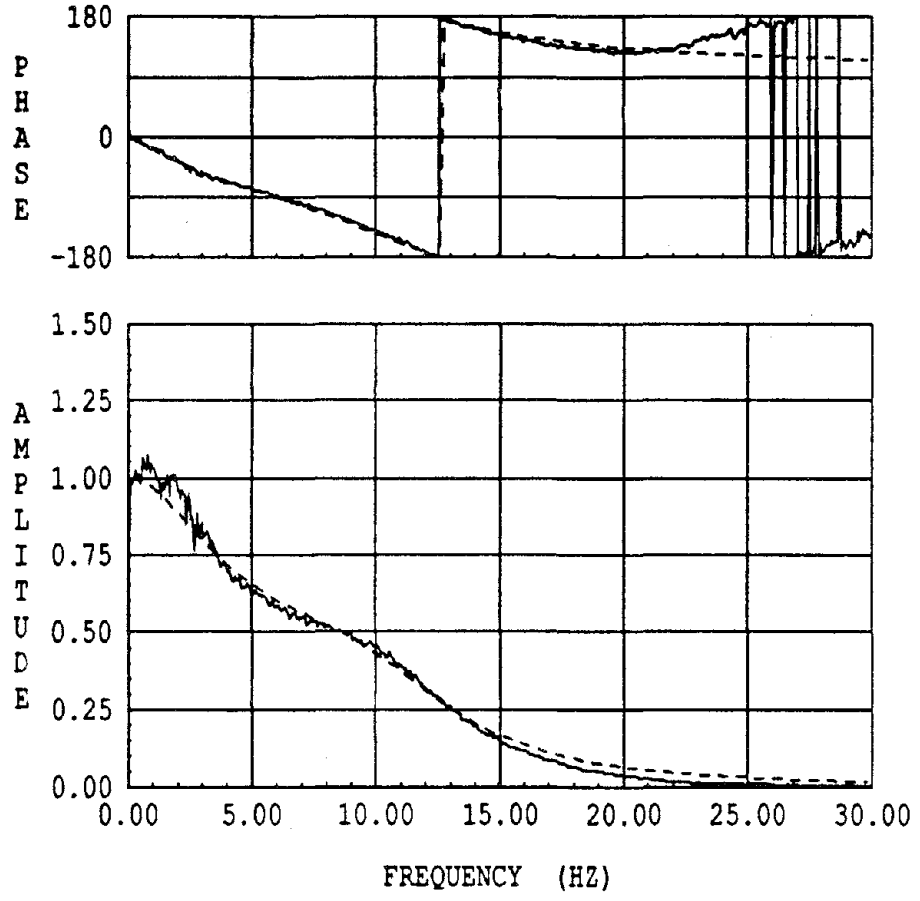

—— Experimental
---- Analytical: Table 6.1

Fig. 6.6: Transfer Function of Bare Table Displacement over Command Displacement (Gain=8)

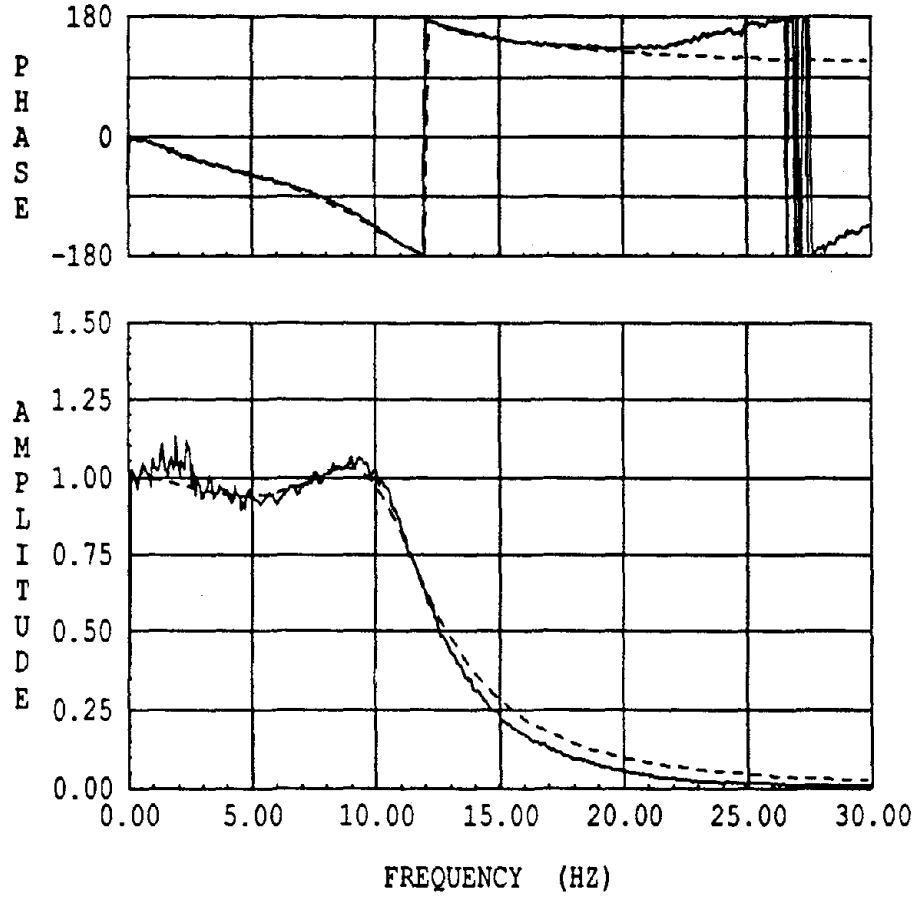

Fig. 6.7: Transfer Function of Bare Table Displacement over Command Displacement (Gain=10)

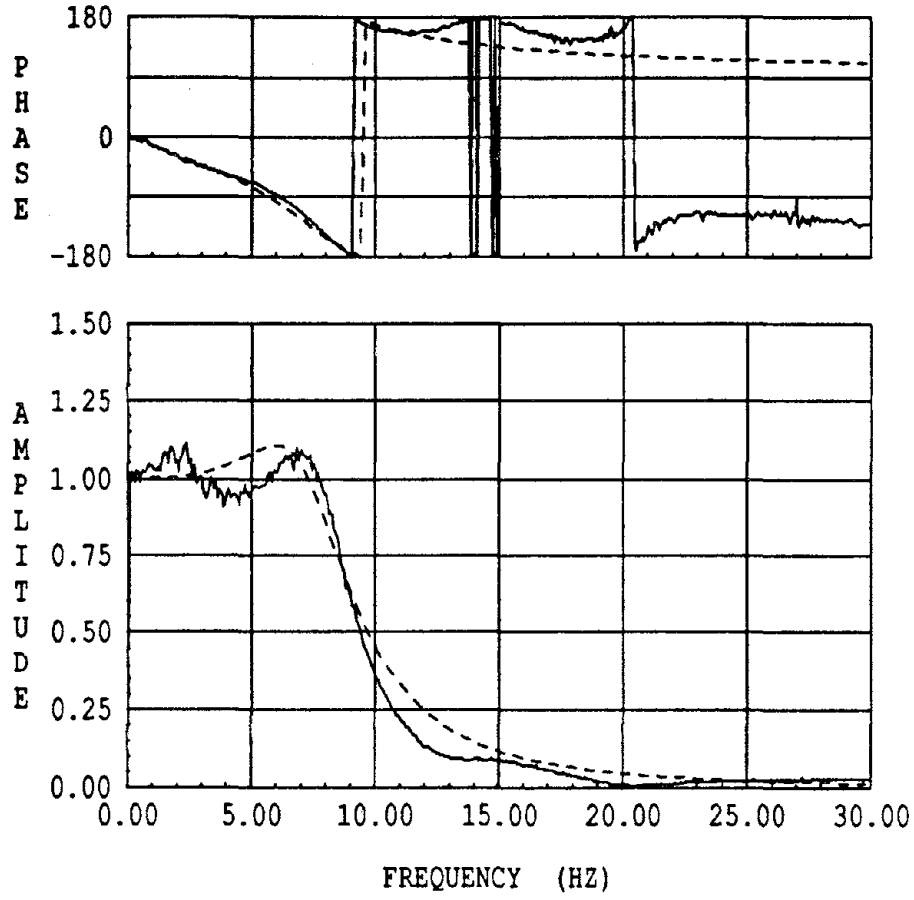

Fig. 6.8: Transfer Function of Table Displacement over Command Displacement (Table with 70 kips Mass)

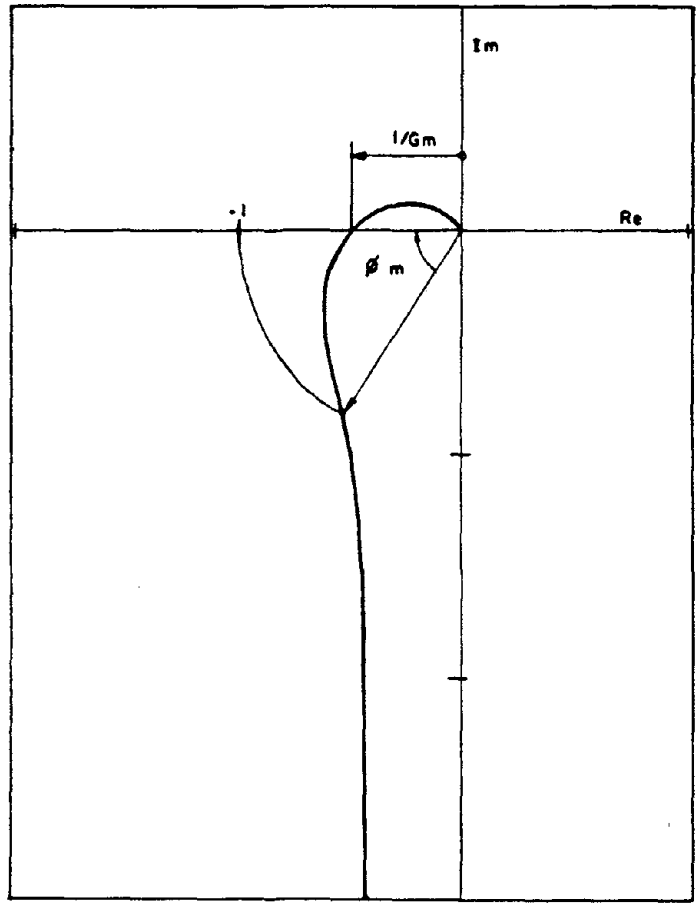

Fig. 6.9 Nyquist Plot of PUC Shaking Table (analytical). Stability Margins: G_m = Gain Margin = 2.06, ϕ_m = Phase Margin = 59 Degrees. From Ref. [8].

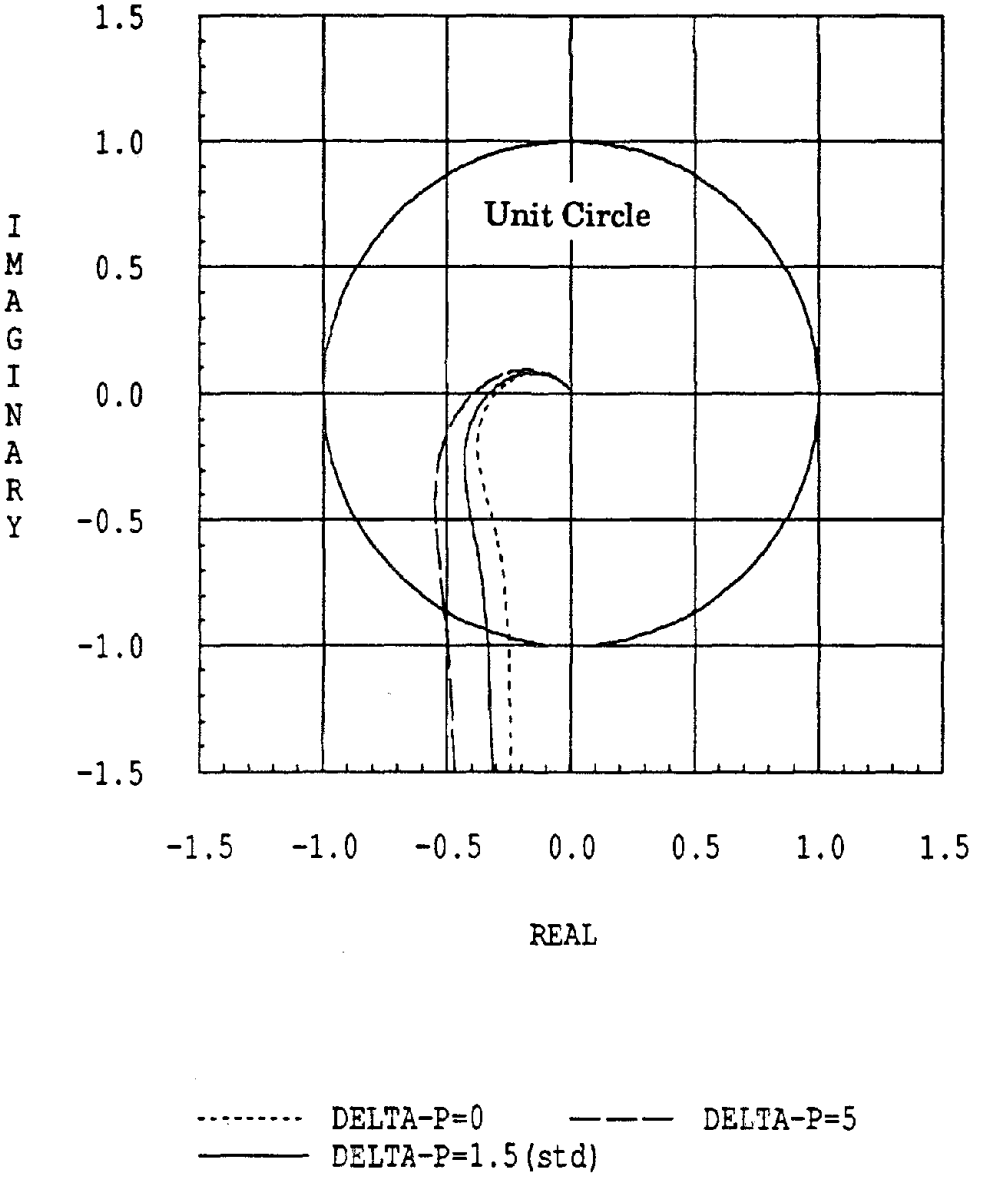

Fig. 6.10: Effect of Delta-P on Bare Table Stability: Nyquist Plot

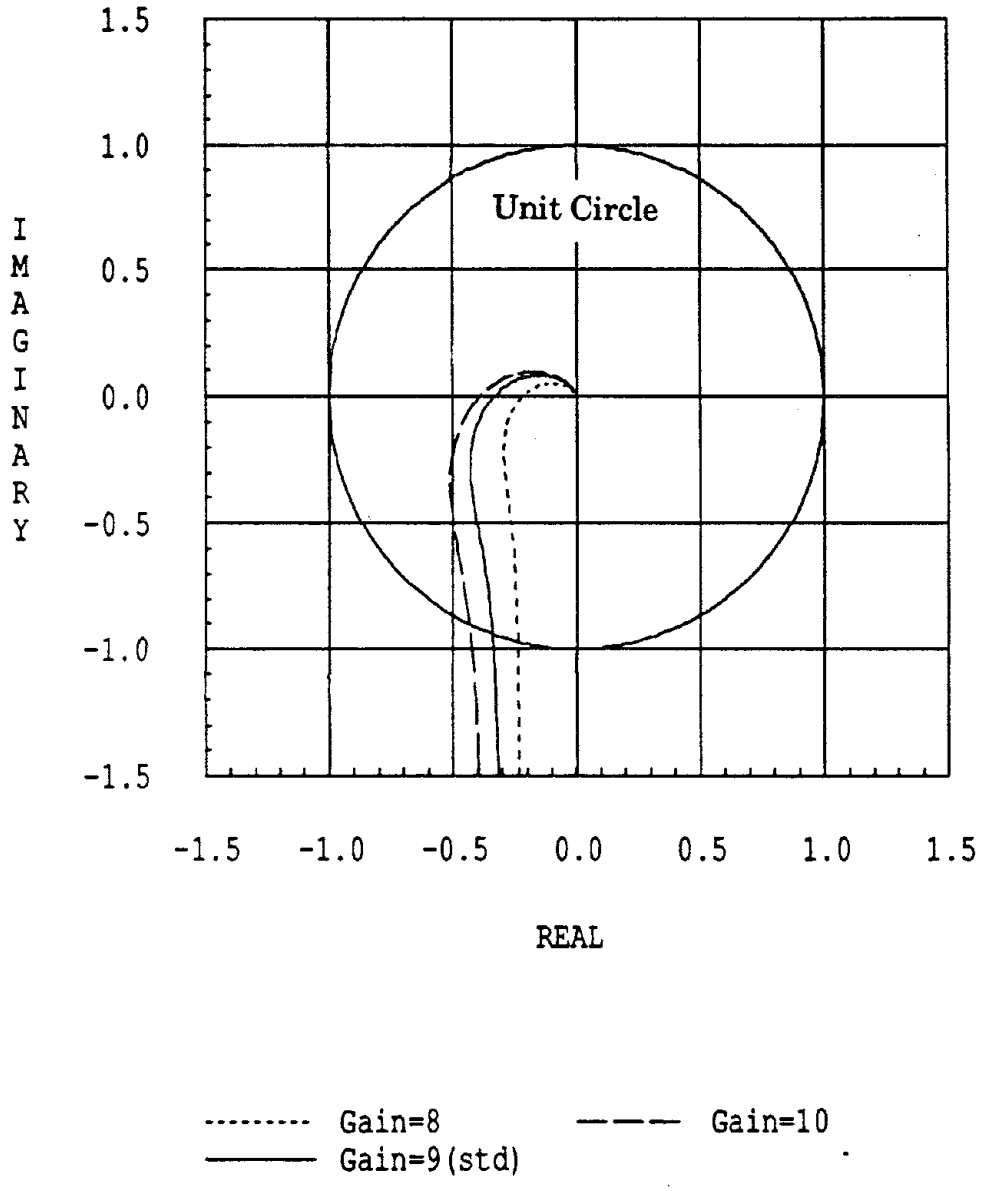

Fig. 6.11: Effect of Gain on Bare Table Stability: Nyquist Plot

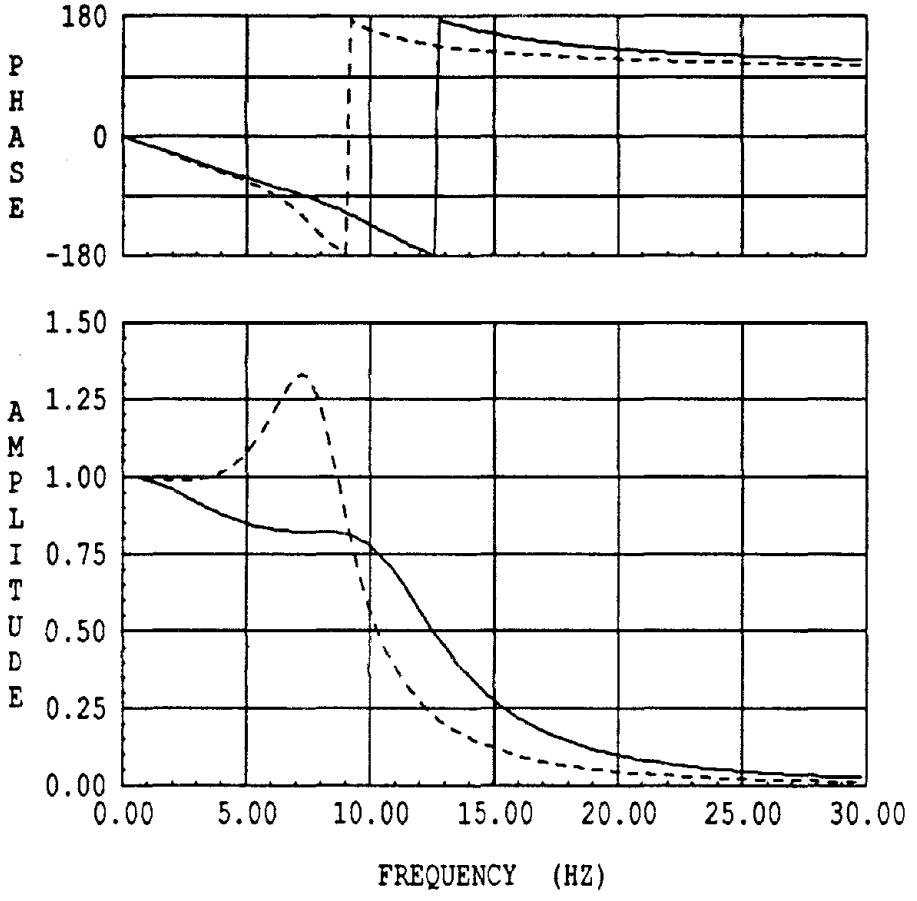

—— f_o = 12.6 Hz (Standard Settings)
---- f_o = 9.0 Hz

Fig. 6.12: Effect of Changing Open Loop Frequency on Bare Table Transfer Function.

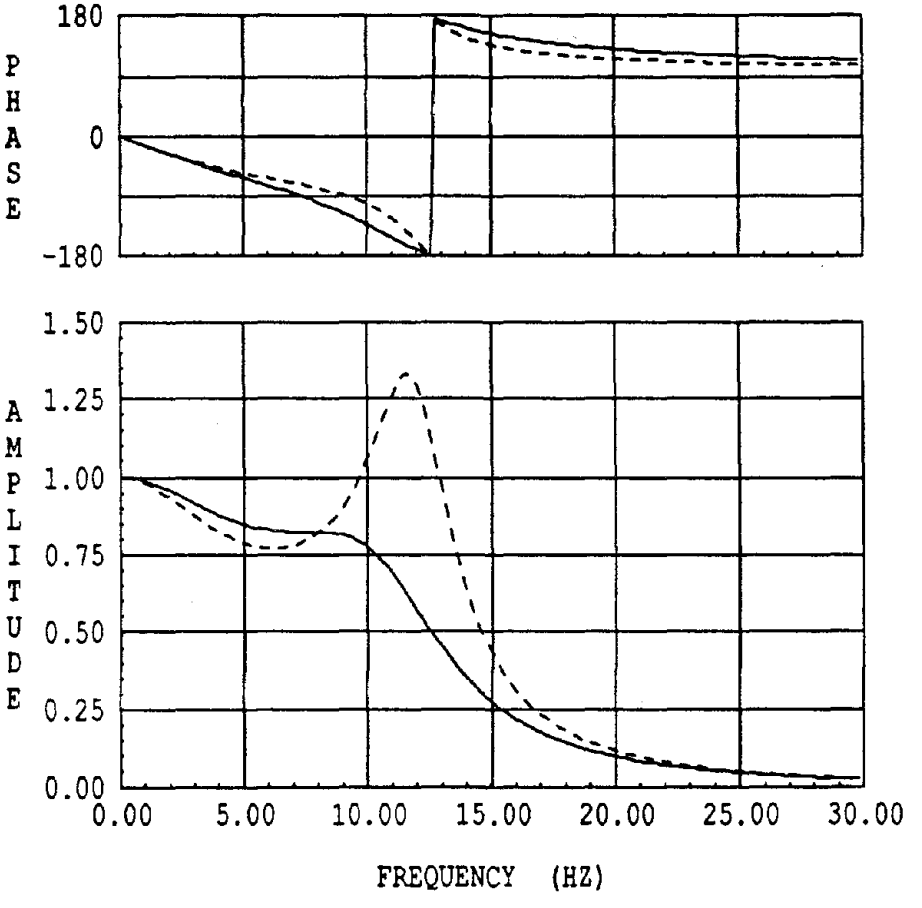

—— ξ_o = 47.7 % (Standard Settings)
---- ξ_o = 30.0 %

Fig. 6.13: Effect of Changing Open Loop Damping on Bare Table Transfer Function.

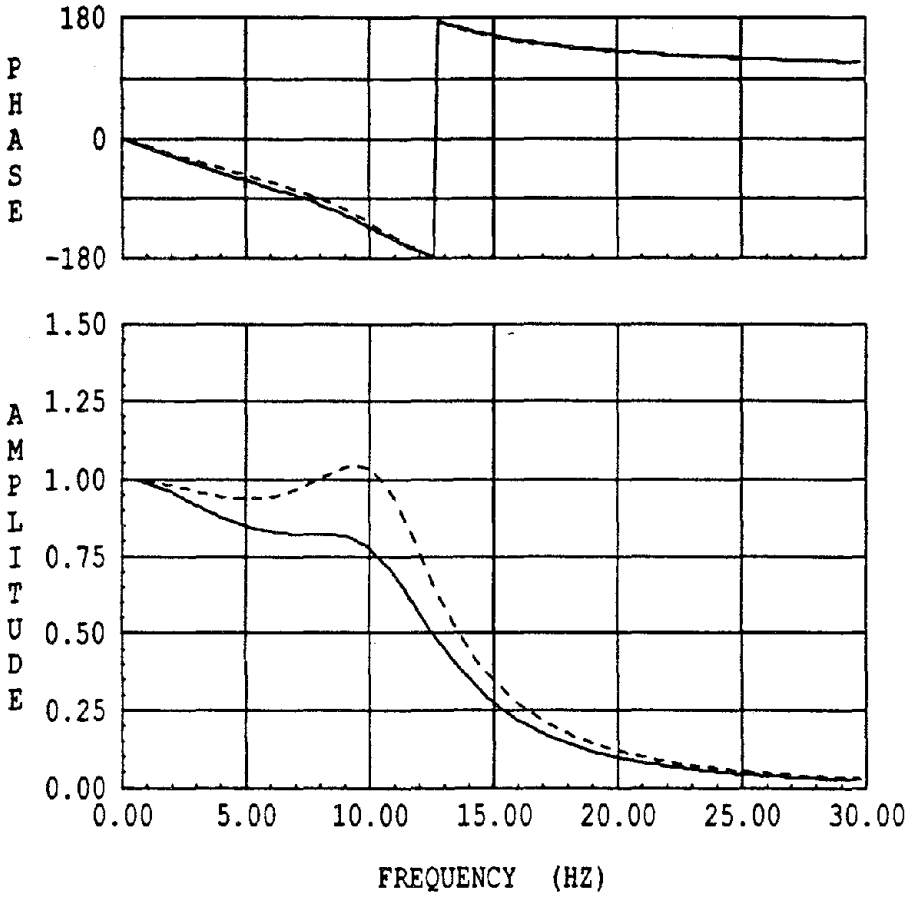

—— $k_o = 25.07$ (Standard Settings)
---- $k_o = 30.0$

Fig. 6.14: Effect of Changing Open Loop Gain on Bare Table Transfer Function.

Chapter Seven
UNIDIRECTIONAL EARTHQUAKE SIMULATOR WITH SDOF STRUCTURE

7.1 INTRODUCTION

The effects of a viscoelastic SDOF structure on the response and stability of the earthquake simulator system are discussed in this chapter.

Figure 7.1a shows the 2DOF combined system. The table of mass m_t is loaded with a SDOF structure of mass m_s, stiffness k_s and damping c_s. The table is driven by a horizontal actuator using a a displacement and force feedback mechanism. Table pitching is neglected here, but will be treated in later chapters. A block diagram of the system is shown in Fig. 7.2.

7.2 TIME DOMAIN SOLUTION

When a structure is added to the shaking table, the actuator force F_a shown in Fig. 7.1b is acting on the table-structure system, instead of acting on the table mass alone as in the case of the bare table. Equilibrating the forces results in

$$m_t \ddot{x}_t + c_s(\dot{x}_t - \dot{x}_s^t) + k_s(x_t - x_s^t) = F_a \tag{7.1}$$

$$m_t \ddot{x}_s^t - c_s(\dot{x}_t - \dot{x}_s^t) - k_s(x_t - x_s^t) = 0 \tag{7.2}$$

where

x_s^t *is* total structural displacement.

x_t *is* total table displacement.

x_c *is* Command displacement.

It is more convenient to represent the structure in terms of its frequency ω_s and damping ξ_s, and for this purpose Eqs. (7.1) and (7.2) are rewritten as

$$\ddot{x}_t + 2\xi_s \omega_s u(\dot{x}_t - \dot{x}_s^t) + \omega_s^2 u(x_t - x_s^t) = \frac{F_a}{m_t} \tag{7.3}$$

$$\ddot{x}_s^t + 2\xi_s \omega_s (\dot{x}_s^t - \dot{x}_t) + \omega_s^2 (x_s^t - x_t) = 0 \tag{7.4}$$

where

$$u = \frac{m_s}{m_t} \tag{7.5}$$

The response of the electro hydraulic actuator and control system is described by Eqs. (6.1) to (6.5). These equations will still hold when the structure is attached to the table platform. In particular, Eq. (6.5a) which expresses the actuator force in terms of the table and command displacements, can be rewritten as

$$\frac{1}{m_t \omega_o^2} \dot{F}_a + \frac{2\xi_o}{m_t \omega_o} F_a + \dot{x}_t + k_o x_t = k_o x_c \tag{7.6}$$

The above Eqs. (7.3) to (7.6) represent the table-structure system, and can be written in the state equation form

$$\dot{\mathbf{X}} = \mathbf{A}\mathbf{X} + \mathbf{F} \tag{7.7a}$$

$$\frac{d}{dt}\begin{Bmatrix} x_t \\ \dot{x}_t \\ F_a/m_t \\ x_s^t \\ \dot{x}_s^t \end{Bmatrix} = \begin{bmatrix} 0 & 1 & 0 & 0 & 0 \\ -\omega_o^2 u & -2\xi_s \omega_s u & 1 & \omega_s^2 u & 2\xi_s \omega_s u \\ -\omega_o^2 k_o & -\omega_o^2 & -2\xi_o \omega_o & 0 & 0 \\ 0 & 0 & 0 & 0 & 1 \\ \omega_s^2 & 2\xi_s \omega_s & 0 & -\omega_s^2 & -2\xi_s \omega_s \end{bmatrix} \begin{Bmatrix} x_t \\ \dot{x}_t \\ F_a/m_t \\ x_s^t \\ \dot{x}_s^t \end{Bmatrix} + \begin{Bmatrix} 0 \\ 0 \\ \omega_o^2 k_o \\ 0 \\ 0 \end{Bmatrix} x_c \tag{7.7b}$$

The above system can be easily solved in the time domain using suitable numerical methods (such as Runga-Kutta) to obtain the structure and table responses due to any command displacement x_c.

7.3 FREQUENCY DOMAIN SOLUTION

Equation (7.5) can be transformed into the Laplace domain to give

$$H_{st} = \frac{x_s^t(s)}{x_t(s)} = \frac{2\xi_s \omega_s s + \omega_s^2}{s^2 + 2\xi_s \omega_s s + \omega_s^2} \tag{7.8}$$

x_s^t from Eq. (7.8) can be substituted into Eq. (7.3) to give F_a as a function of x_t. Inserting that in Eq. (7.6) results in the system transfer function

$$H_{tc} = \frac{x_t(s)}{x_c(s)} = \frac{k_o(s^2 + 2\xi_s \omega_s s + \omega_s^2)}{a_5 s^5 + a_4 s^4 + a_3 s^3 + a_2 s^2 + a_1 s + a_o} \tag{7.9}$$

The denominator coefficients are given by

$$a_o = k_o \omega_s^2$$

$$a_1 = \omega_s^2 + 2\omega_s \xi_s k_o$$

$$a_2 = 2(1+u)\omega_s^2 \xi_s/\omega_o + 2\xi_s \omega_s + k_o$$

$$a_3 = (\omega_s/\omega_o)^2(1+u) + 4(\omega_s/\omega_o)\xi_o \xi_s (1+u) + 1$$

$$a_4 = 2[(1+u)(\omega_s/\omega_o)\xi_s + \xi_o]/\omega_o$$

$$a_5 = 1/\omega_o^2$$

The conditions for absolute stability can be obtained by applying the Hurwitz criterion [29] as follows

$$c_1 = a_3 a_4 - a_2 a_5 > 0$$

$$c_2 = a_1 c_1 - a_4(a_1 a_4 - a_o a_5) > 0 \tag{7.10}$$

$$c_3 = -a_o a_3 c_1 + a_o a_5(a_1 a_4 - a_o a_5) + a_1 c_2 > 0$$

Once the command displacement is known, the table displacement can be computed from

$$x_t(\omega) = H_{tc}(\omega)\, x_c(\omega) \tag{7.11}$$

and

$$x_t(t) = \mathbf{INVFFT}(x_t(\omega)) \tag{7.12}$$

where $x_c(\omega)$ and $x_t(\omega)$ represent the Fast Fourier Transform (FFT) of the command and table displacement signals. The time history of table displacement can then be evaluated using the Inverse Fast Fourier Transform (INVFFT). Similarly, the structural response can be evaluated from

$$x_s^t(\omega) = H_{st}(\omega)\, x_t(\omega) \tag{7.13}$$

and

$$x_s^t(t) = \mathbf{INVFFT}(x_s^t(\omega)) \tag{7.14}$$

The transfer function H_{tc} , given by Eq. (7.9), can be written in a more familiar form [7] as

$$\frac{x_t(s)}{x_c(s)} = \frac{k_t}{(Vm_e/4\beta A)s^3+m_e(k_t k_f+k_c)s^2+(k_t k_v+A)s+k_t} \tag{7.15}$$

where

$$m_e = m_t\left(1 + \frac{m_s}{m_t}\frac{x_s^t}{x_t}\right) \tag{7.16}$$

$$= \frac{s^2 + 2\xi_s\omega_s(1+u)s + \omega_s^2(1+u)}{s^2 + 2\xi_s\omega_s s + \omega_s^2}m_t$$

Equation (7.15) is similar to that of the bare table [Eq. (6.10)]; the only difference here is that the bare table mass m_t is replaced by the effective mass m_e given by Eq. (7.16).

This effective mass is mainly influenced by the transmissibility function x_s^t/x_t, relating structural displacement response to the table displacement. This transmissibility was derived earlier in Eq. (7.8). Fig. 7.3 shows a typical transmissibility function for different amounts of structural damping.

As is clear from Fig. 7.3, the transmissibility function (x_s^t/x_t) is nearly unity for frequencies up to 70 percent of the natural frequency of the structure, and it is nearly zero for frequencies greater than two times the natural frequency.

Adjacent to the natural frequency of the structure the transmissibility function (x_s^t/x_t) shows a significant peak that can be approximated by $1/(2\xi_s)$ (the dynamic amplification factor [11]).

Figures 7.4 to 7.5 show the influence of structural damping and mass ratio on the effective mass.

As is clear from Fig. 7.4, at the lower frequencies the effective table mass is given by

$$m_e = m_t + m_s \tag{7.17}$$

and at the higher frequencies it becomes

$$m_e = m_t \tag{7.18}$$

Noting the abrupt change of phase of the transmissibility function near the natural frequency of the structure, the effective mass just below the natural frequency is

$$m_e = m_t + \frac{m_s}{2\xi_s} \tag{7.19}$$

and at frequencies just above the natural frequency the effective mass becomes

$$m_e = m_t - \frac{m_s}{2\xi_s} \tag{7.20}$$

For structures with a small amount of damping, the term $\frac{m_s}{2\xi_s}$ can be comparable to the table mass and hence, a significant peak and notch is expected in the frequency response curve of the table near the natural frequency of the structure.

7.4 ANALYTICAL SIMULATION

The bare system parameters were determined in the preceding chapter. These parameters consist of the open loop frequency $f_o = 2\pi\omega_o = 12.6$ Hz, the open loop damping $\xi_o = 0.477$ and the open loop gain $k_o = 25.07$. The uncoupled structural frequency and damping were chosen as 2.90 Hz and 0.4 percent, respectively. The transfer function of the table horizontal displacement over the command displacement $x_s^t(\omega)/x_t(\omega)$ is shown by the solid line in Fig. 7.6. Figure 7.6 also shows the effect of varying the structural frequency on the transfer function of the table-structure system. It is clear from this figure that a significant peak and notch are present. The notch, or attenuation of the frequencies, occurs at and around the uncoupled structural frequency. The peak, or amplification of the frequencies, occurs at frequencies lower than the uncoupled structural frequency. For structural frequencies higher than the open loop frequency of the table, a second peak is observed

at frequencies larger than the uncoupled structural frequency. The frequency interval between the peak and notch is increased for higher structural frequencies. The notch implies that the input energy near structural resonance is seriously reduced near the uncoupled structural frequency. This seems like a serious problem for shaking table testing as it may lead to lower damage potential for the actual table displacement in comparison with the command displacement. It will be shown in Chapter 9 that this effect is not as serious as it appears here; the reason is that the structural frequency varies due to the coupling effect.

Figure 7.7 presents the effect of structural damping on the system transfer function. It shows a clear advantage in having higher structural damping. The peak and notch effect are significantly reduced for higher amounts of structural damping. Table response is slightly lower at higher frequencies for higher amounts of damping.

Figure 7.8 shows the effect of the structural mass m_s on the system transfer function. It shows clearly an increase in peak and notch effects for heavier structures. It also shows a decrease in the peak and notch frequency.

The effect of changing the open loop frequency $\omega_o = 2\pi f_o$ can be seen in Fig. 7.9. The higher the open loop frequency, the lower the peak value, although the notch amplitude is not influenced significantly. In addition, the amplitude at corner frequency is greatly influenced. The lower the open loop frequency, the higher the amplification of frequencies near that frequency, at the same time higher frequencies are rapidly attenuated.

Open loop damping does not seem to have a significant effect on the peak and notch amplitudes, as may be seen in Fig. 7.10. However the range of the peak and notch seems to be widened when ξ_o is increased. In addition a higher amount of damping tends to attenuate the higher frequencies much faster. At $\xi_o = 30$ percent a significant peak is developed near ω_o, as shown in Fig. 7.10.

Figure 7.10 also shows how the phase angle changes with ξ_o. Higher ξ_o causes a larger phase difference between the command displacement and the table displacement for frequencies lower than ω_o, and a lower phase

difference for frequencies higher than ω_o.

The effect of changing the open loop gain k_o can be seen in Fig. 7.11. Higher gain values tend to amplify the peak amplitude. No significant effect was noticed with the notch. The abrupt phase change near the peak and notch was only slightly affected. Lower k_o values tend to attenuate the higher frequencies much faster.

7.5 EXPERIMENTAL RESULTS

Tests were performed on the shaking table at EERC to verify the validity of analytical model. Note that this analytical model does not take into account the table rocking effects.

The test structure and its instrumentation were described in Chapter 2. Figure 2.4 is a photograph of the test structure on the shaking table. Structural vibration characteristics were determined in Section 3.3. Some transfer function results were shown in Section 3.4.2. For a random command displacement, the transfer function of the table displacement over the command displacement was instantaneously calculated using the GenRad system. The transfer function for the standard EERC table settings, is shown in Fig. 7.12. Also shown (dotted) is the transfer function corresponding to the bare table.

As is clear from Fig. 7.12 the transfer function shows a significant peak (amplitude=2.2) and notch (amplitude=0.7), as Eq. (7.9) predicts. It also shows a significant phase lag near the peak and notch frequencies.

Compared with the bare table transfer function, the SDOFS transfer function in addition to the peak and notch effects, shows amplification at frequencies between 5 and 8 Hz, and attenuation at frequencies higher than 8 Hz. In addition the out-of-phase frequency (frequency at which the phase is 180 degrees) was significantly lower. All that contributed to producing a lower bandwidth.

In order to study the effect of the control settings, tests were performed by varying the horizontal control settings on the EERC shaking table. The effect of increasing the horizontal gain from 9 to 10 can be seen from the

transfer function in Fig. 7.13. It caused an amplification in the frequencies higher than 7 Hz. The effect of increasing the Delta-P setting from 1.5 to 5 can be seen in Fig. 7.14. In addition to amplifying the peak and notch effects, the increase in Delta-P caused a lower bandwidth and corner frequency and a much faster phase lag as the frequency increases.

7.6 CORRELATION WITH ANALYTICAL MODEL

To predict the table-structure system response (standard settings), the parameters obtained in chapter 6 for the bare table system were used here in Eq. (7.9). Those parameters were the equivalent open loop frequency ($f_o = 2\pi\omega_o$ = 12.6 Hz), the equivalent open loop damping (ξ_o = 47.7 percent), and the equivalent open loop gain (k_o = 25.07). The structure's lateral frequency ($f_s = 2\pi\omega_s$ = 2.87 Hz) and damping (ξ_s = 0.4 percent) and mass ratio of 0.60 also were considered (60 kips/100 kips).

The resulting computed transfer function is shown in Fig. 7.15 together with the experimentally obtained transfer function. The analytical function differs from the experimental function in two respects:

First, the peak and notch frequency is slightly lower for the experimental function. That can be attributed to the fact that the pitch effect was not included in the analytical model.

Second, the equivalent open loop frequency has decreased significantly; that can be attributed to the nonlinear system behavior [Appendix C] as can the increase in equivalent open loop gain.

Appendix C shows that the system parameters can change with loading conditions on the table. It also states that the system can be considered linear at a given operating point, so that the linear system would have different characteristics for different system configurations or inputs. Because of the change in the loading condition in this case (bare table versus table with SDOF structure) new parameters had to be determined. In order to find the best analytical representation of the experimental transfer functions, the nonlinear least squares algorithm used in Section 6.4 was again used here to fit the data to the analytical transfer function given by Eq. (7.9). In

this case the algorithm needed to find five parameters, rather than three as in the bare table case, which required more iterations. This means that values for structural damping and frequency and bare table parameters will be different than those measured. The damping and frequency variation should be attributed in this case to the coupling in the pitch degree of freedom, so that a lower frequency and a higher damping were obtained.

It was found that the algorithm failed to converge in most cases when the amplitude of the complex error was minimized. On the other hand, if the difference between the amplitudes of the analytical and experimental functions was minimized, convergence was much faster and more stable. As for the phase, it was found that fixing the frequency $f_o = 2\pi\omega_o$ to a value slightly lower than the frequency at which the phase in the experimental function is 180 degrees, yielded a very nice fit to both the amplitude and phase functions.

Figure 7.16 presents a fit to the transfer function obtained using the standard setting of the EERC shaking table. Another set of experimental transfer functions corresponding to different control settings was also fitted. Figure 7.17 shows the fitted curve and parameters when the horizontal gain was raised to 10 from the standard value of 9. In this case only the equivalent open loop gain parameter was different than that of the standard setting. It was higher, as expected.

Figure 7.18 demonstrates the effect of decreasing the Delta-P setting to zero, as compared with the standard value of 1.5. In this case the decrease in Delta-P had the effect of decreasing the equivalent open loop gain (k_o) and equivalent open loop damping (ξ_o). Similar effects were noticed for the bare table.

Figure 7.19 illustrates the effect of increasing the Delta-P to the value of 5. As in the case of the bare table, this resulted in lower open loop gain k_o, but higher open loop damping ξ_o. In addition it led to a significant decrease in the open loop frequency $f_o = 2\pi\omega_o$, which also was noticed in the case of the bare table.

The variation of the open loop gain k_o with Delta-P is clearly nonlinear. Decreasing or increasing the Delta-P setting led in both cases to a lower open loop gain k_o.

7.7 STABILITY STUDY

7.7.1 Introduction

In this section the effect of the various parameters on the stability of the shaking table system is studied. For this purpose the parameters obtained using least squares fit in the last section were used as a reference. The fitted parameters for the different table settings are listed in Table 7.1, together with the corresponding gain and phase margins obtained from the fitted parameters.

7.7.2 Effect of Control Settings

As is clear from Table 7.1, the decrease in the Delta-P setting led to both higher gain and phase margins, and hence to higher stability. This also can be seen from Fig. 7.20. The effect of the Delta-P could have been influenced by the high-pass filter on the force feedback loop.

The increase in the horizontal gain on the other hand, led to smaller gain and phase margins as shown in Fig. 7.21.

7.7.3 Effect of Shaking Table Parameters (Analytical Model)

In order to study the effect of the system parameters on the system stability, the bare table parameters were chosen as reference. The different parameters used are shown in Table 7.2.

When the equivalent open loop gain was decreased from 29.5 to 25.0, the gain and the phase margins were both increased. Increasing k_o on the other hand to 35 led to a smaller gain margin but to a slightly higher phase margin. It can be said here that near this point, the larger the k_o value the less stable the system will be.

A decrease in $f_o = 2\pi\omega_o$ led to much lower gain and phase margins. An increase in f_o resulted in higher gain and phase margins. System stability is greatly affected by the oil column resonance frequency.

The effect of the increase in ξ_o is to raise the gain margin while decreasing the phase margin. Stability is improved since the gain margin is more important.

7.7.4 Effect of Structure

The slight change in the structure frequency did not seem to produce a significant change in the stability margins. The decrease in the structure damping however has the effect of significantly reducing the phase margin. The gain margin is slightly reduced.

The mass ratio u has a significant effect on the phase margin. Increasing u leads to a lower phase margin, but a slightly higher gain margin on the other hand.

7.8 EFFECT OF PITCH COUPLING

In order to get a feel of how the pitch flexibility might have affected the system transfer function, the coupled structural frequencies that include only the coupling due to the pitching degree of freedom can be estimated and are listed in Table 3.1. Assuming the values corresponding to the Taft record with span of 200, these coupled frequencies are $f_s = 2\pi\omega_s = 2.70$ Hz and $\xi_s = 1.0$ percent.

Figure 7.22 shows the analytical transfer function using bare table system parameters evaluated in Chapter 6. The peak and notch frequencies match very well with the experimental curve (shown as a solid line in the figure). However the overall quality of fit is not good. Figure 7.23 shows the same transfer function using the loaded system parameters evaluated in this chapter. The analytical curve shows an excellent match with the experimental transfer function for the new system parameters.

7.9 CONCLUSIONS

The table parameters derived for the bare table in Chapter 6 were not the same for the loaded shaking table. The main effect of the table load is a decrease in its open loop frequency from 12.6 Hz to 9.6 Hz. This confirms Merritt's [20] statement about the change of system frequency response with different loading conditions on the table.

SETTING	OPEN LOOP GAIN k_o	TABLE FREQ (Hz) f_o	TABLE DAMP (%) ξ_o	structure FREQ (Hz) f_s	structure DAMP (%) ξ_s	Mass Ratio $\frac{m_s}{m_t}$	GAIN MARGIN G_m	PHASE MARGIN ϕ_m
STANDARD*	29.54	9.60	60.6	2.76	3.33	0.60	2.54	34.5
Delta-P=0	22.66	9.60	50.3	2.76	3.33	0.60	2.75	41.1
Delta-P=5	26.85	7.67	64.2	2.76	3.33	0.60	2.39	29.2
Gain=10	32.79	9.60	60.6	2.76	3.33	0.60	2.29	34.4

* STANDARD SETTING: Delta-P=1.5 Horizontal Gain=9

Table 7.1 : System parameters for different settings

CASE	OPEN LOOP GAIN k_o	TABLE FREQ (Hz) f_o	TABLE DAMP (%) ξ_o	structure FREQ (Hz) f_s	structure DAMP (%) ξ_s	Mass Ratio $\frac{m_s}{m_t}$	GAIN MARGIN G_m	PHASE MARGIN (Deg.) ϕ_m
Standard*	29.54	9.60	60.6	2.76	3.33	0.60	2.54	34.5
$k_o = 25$	25.07	9.60	60.6	2.76	3.33	0.60	2.99	37.3
$k_o = 35$	35.00	9.60	60.6	2.76	3.33	0.60	2.14	34.6
$f_o = 6Hz$	29.54	6.00	60.6	2.76	3.33	0.60	1.63	19.8
$f_o = 15Hz$	29.54	15.0	60.6	2.76	3.33	0.60	3.94	47.7
$\xi_o = 0.406$	29.54	9.60	40.6	2.76	3.33	0.60	1.71	39.4
$\xi_o = 0.806$	29.54	9.60	80.6	2.76	3.33	0.60	3.40	31.9
$f_s = 2.50Hz$	29.54	9.60	60.6	2.50	3.33	0.60	2.54	37.7
$f_s = 2.90Hz$	29.54	9.60	60.6	2.90	3.33	0.60	2.55	34.1
$\xi_s = 0.004$	29.54	9.60	60.6	2.76	0.40	0.60	2.49	21.8
$\xi_s = 0.060$	29.54	9.60	60.6	2.76	6.00	0.60	2.61	43.6
$\xi_s = 0.100$	29.54	9.60	60.6	2.76	10.0	0.60	2.69	53.6
$\frac{m_s}{m_t} = 0$	29.54	9.60	60.6	2.76	3.33	0.	2.48	50.3
$\frac{m_s}{m_t} = 0.10$	29.54	9.60	60.6	2.76	3.33	0.10	2.48	52.2
$\frac{m_s}{m_t} = 2.00$	29.54	9.60	60.6	2.76	3.33	2.00	2.71	22.3

*Standard Settings: Delta-p=1.5 Horizontal Gain=9

Table 7.2 : Stability Margins for Different System Parameters

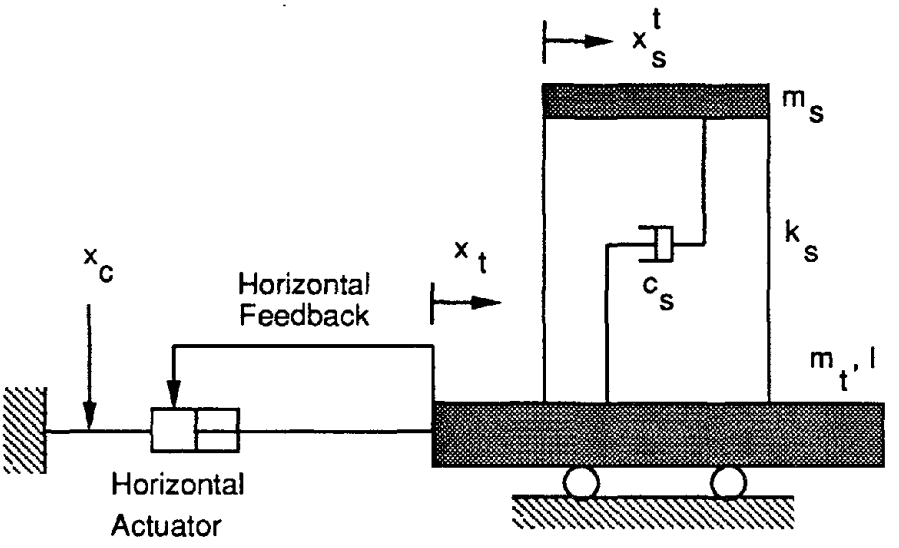

Fig. 7.1a: Model of a uni–directional earthquake simulator loaded with a SDOF structure.

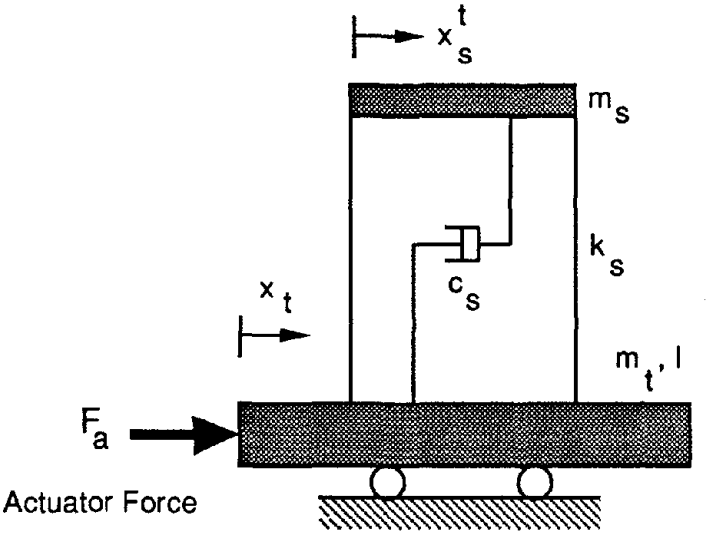

Fig. 7.1b: Simplified diagram of a uni–directional earthquake simulator.

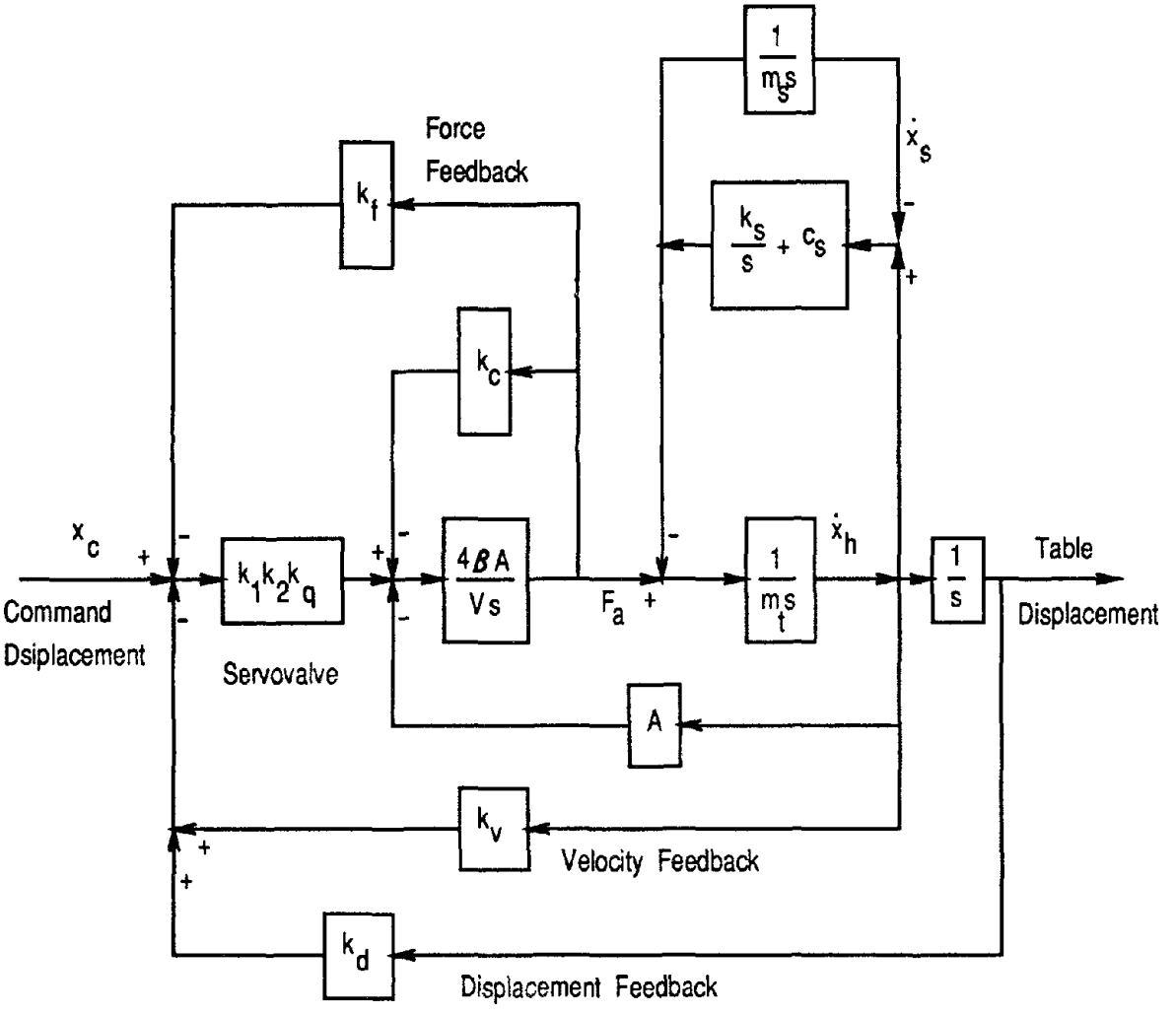

Fig. 7.2: Block diagram of a uni-directional earthquake simulator loaded with a SDOF structure.

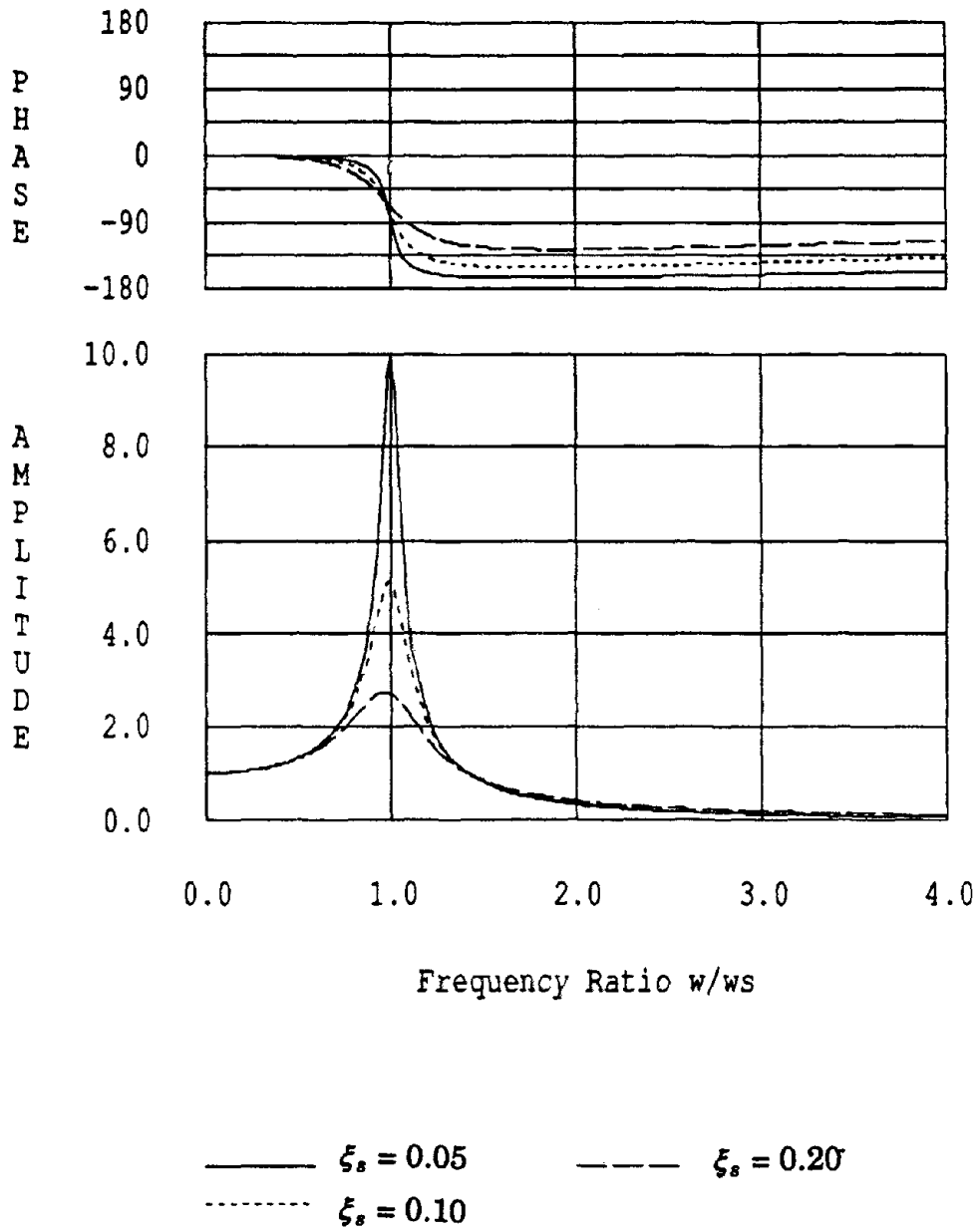

Fig. 7.3: Transmissibility function x_s'/x_t for different values of damping.

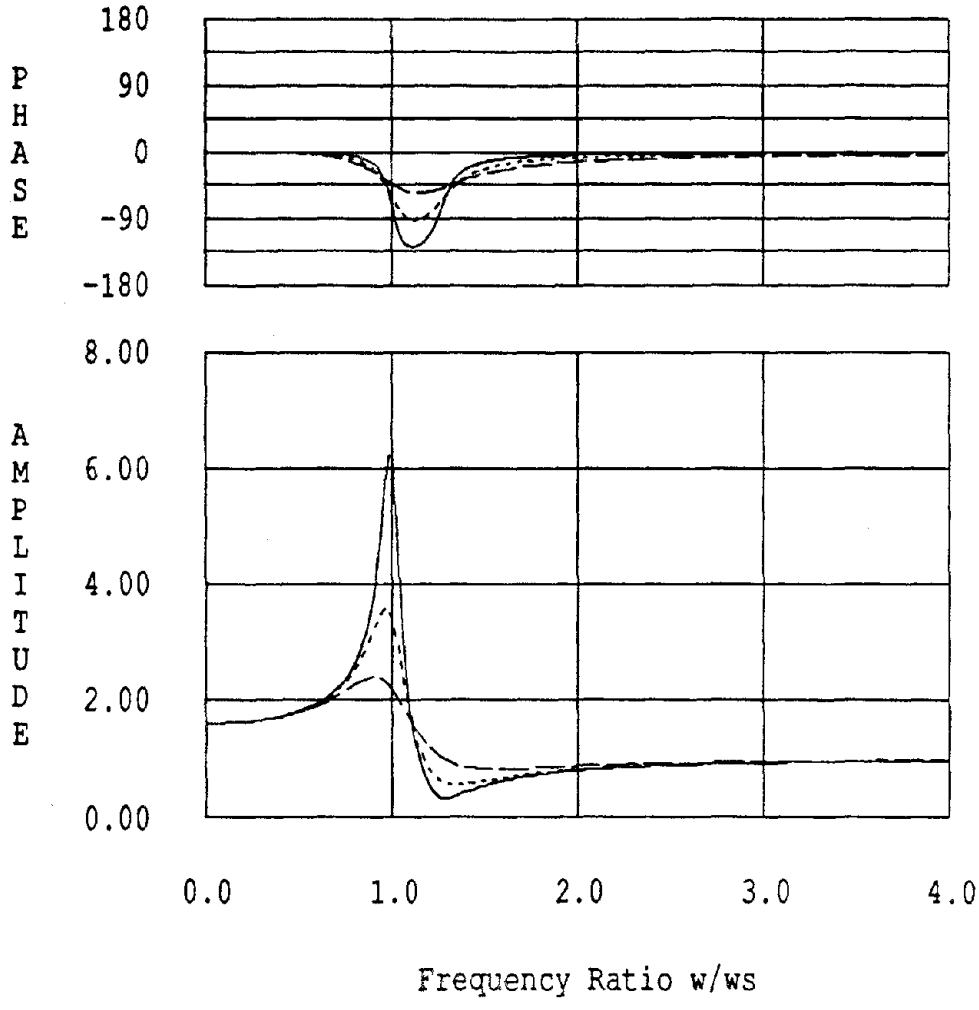

Fig. 7.4: Effective mass ratio $\frac{m_e}{m_t}$ for different values of damping.

(u = m_e/m_t = 0.6)

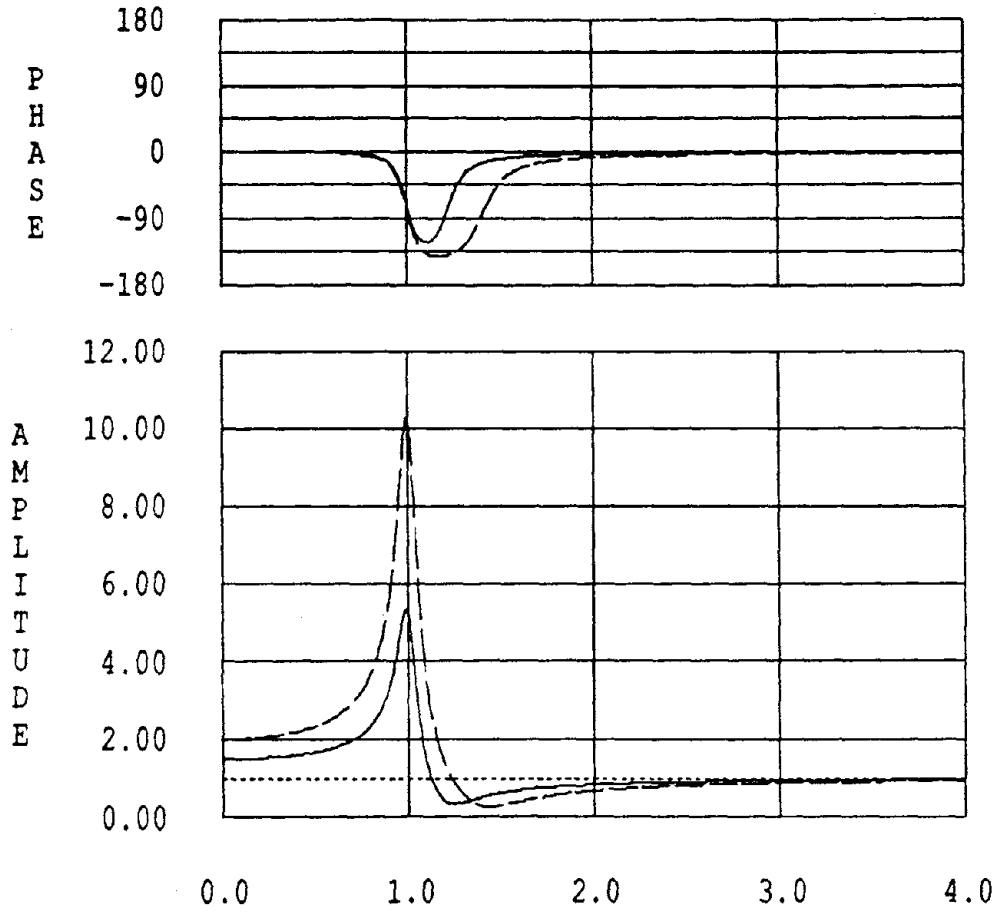

Fig. 7.5: Effective mass ratio $\frac{m_e}{m_t}$ for different values of mass ratio $u = m_s/m_t$.

(Damping = 5 %)

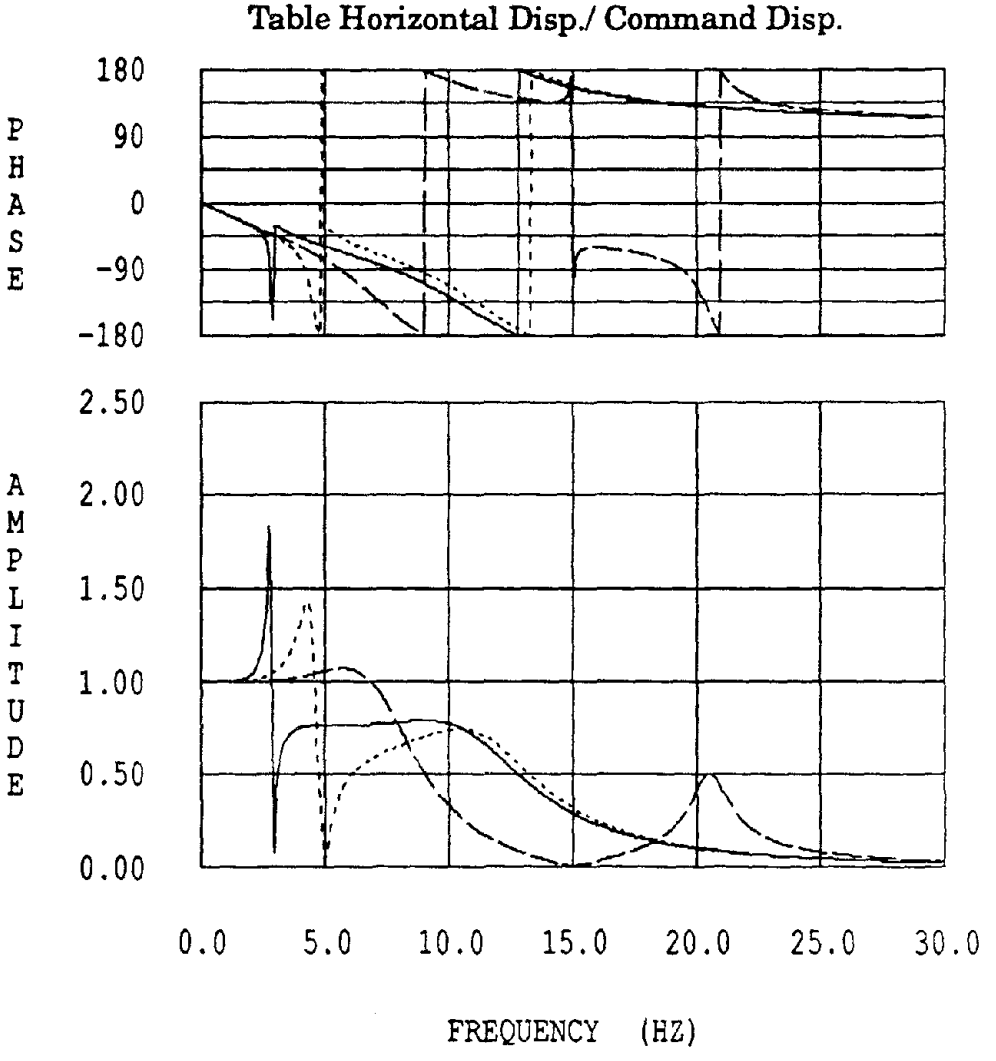

Fig. 7.6: Effect of changing structural frequency on system transfer function.

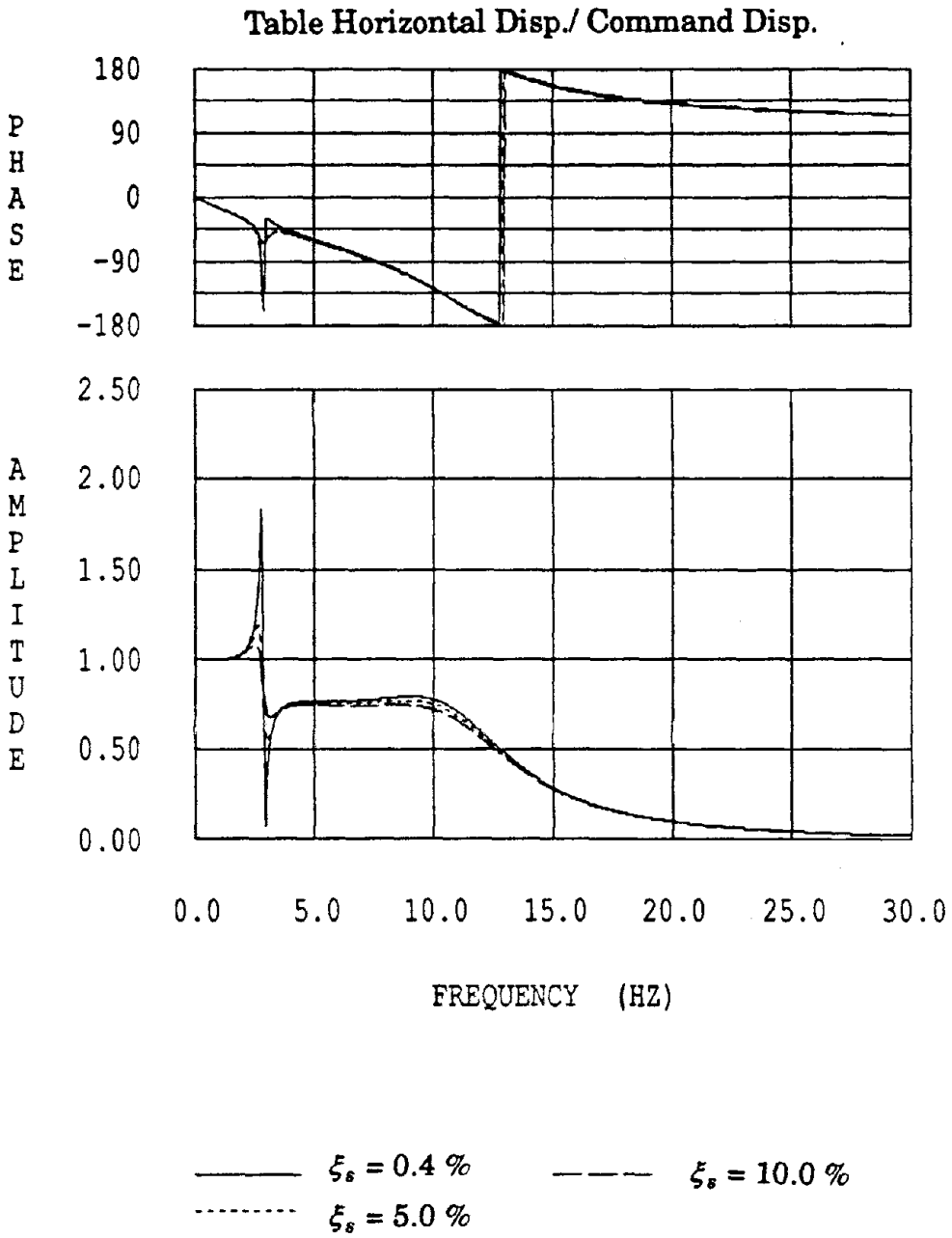

Fig. 7.7: Effect of changing structural damping on system transfer function.

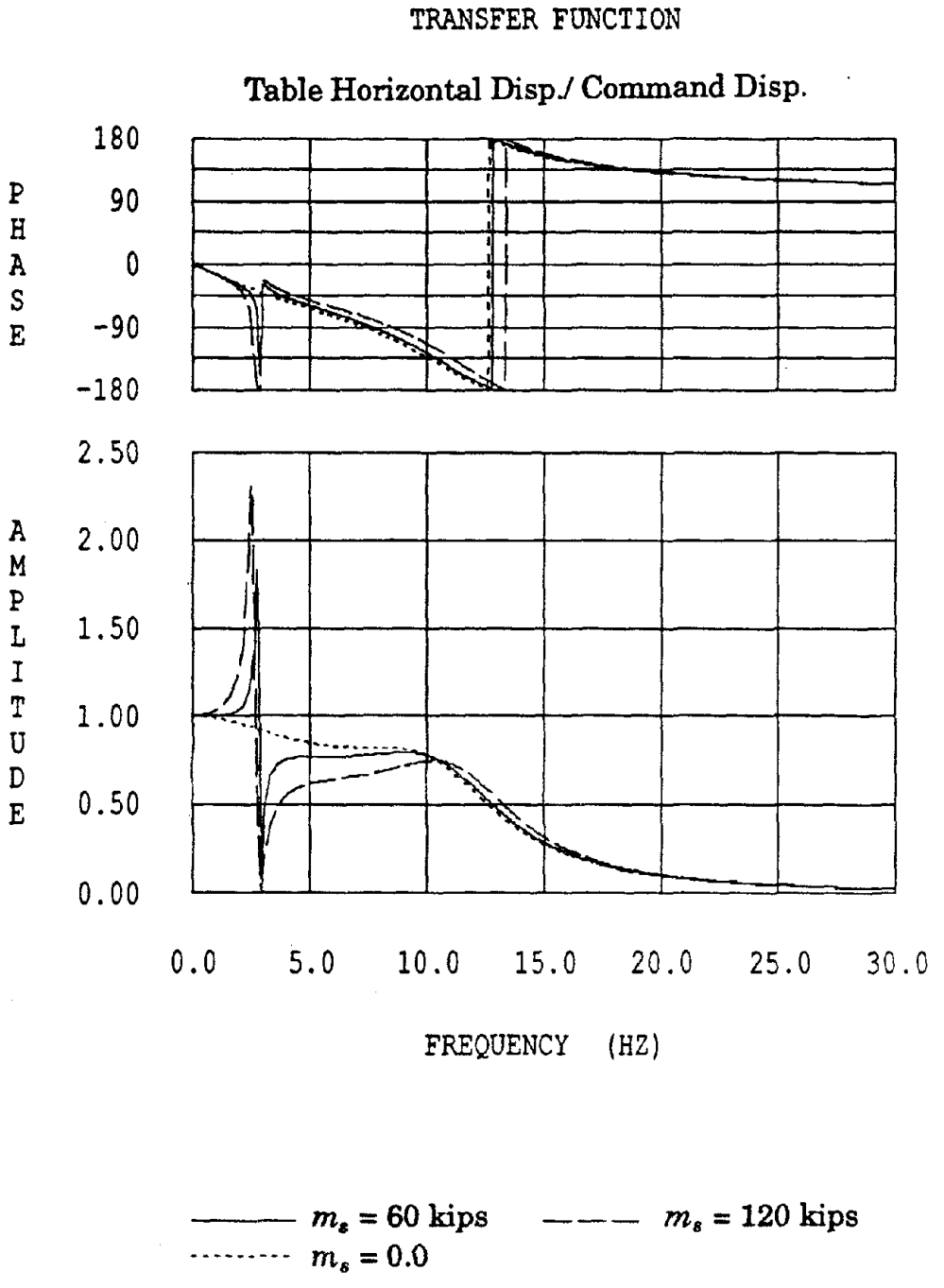

Fig. 7.8: Effect of changing structural mass on system transfer function.

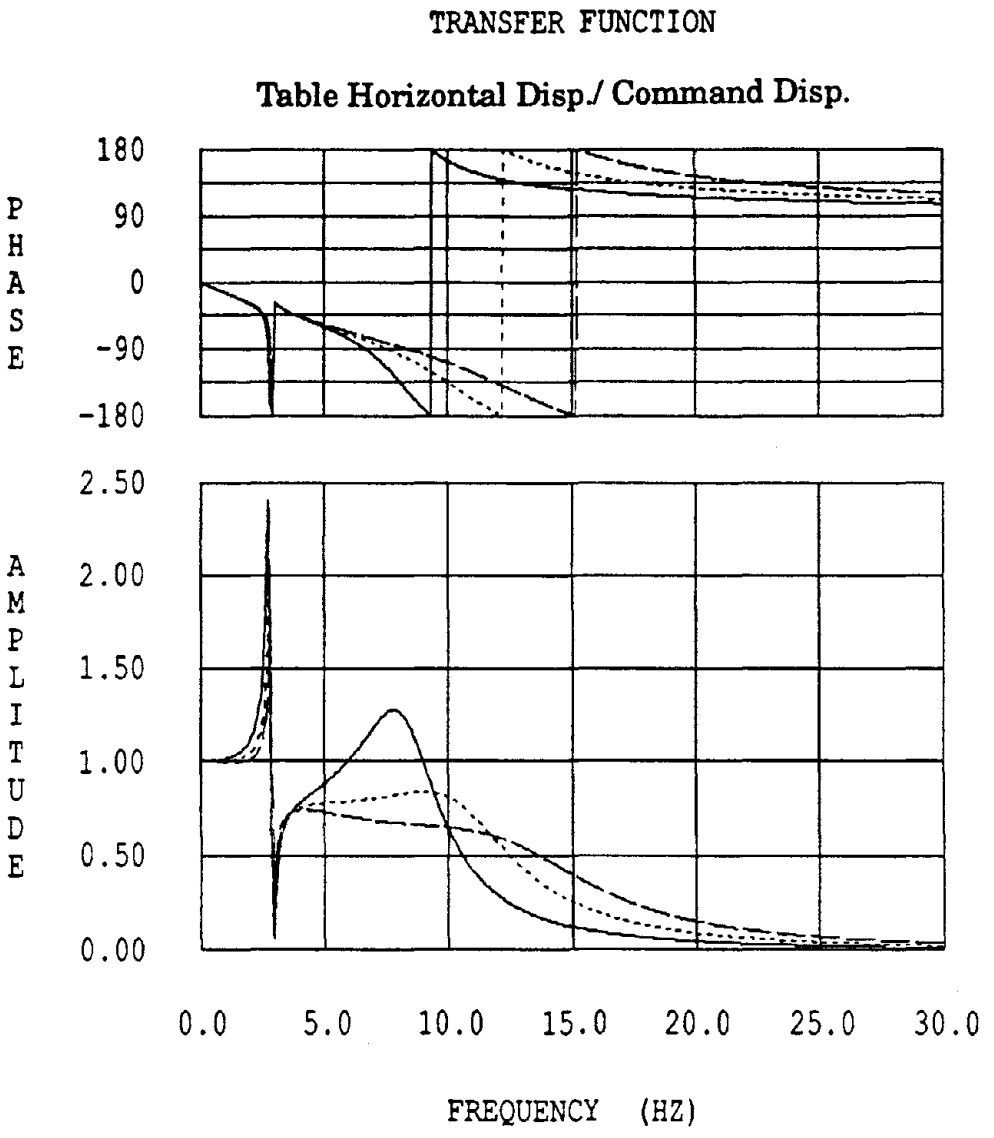

Fig. 7.9: Effect of changing $\omega_o = 2\pi f_o$ on system transfer function.

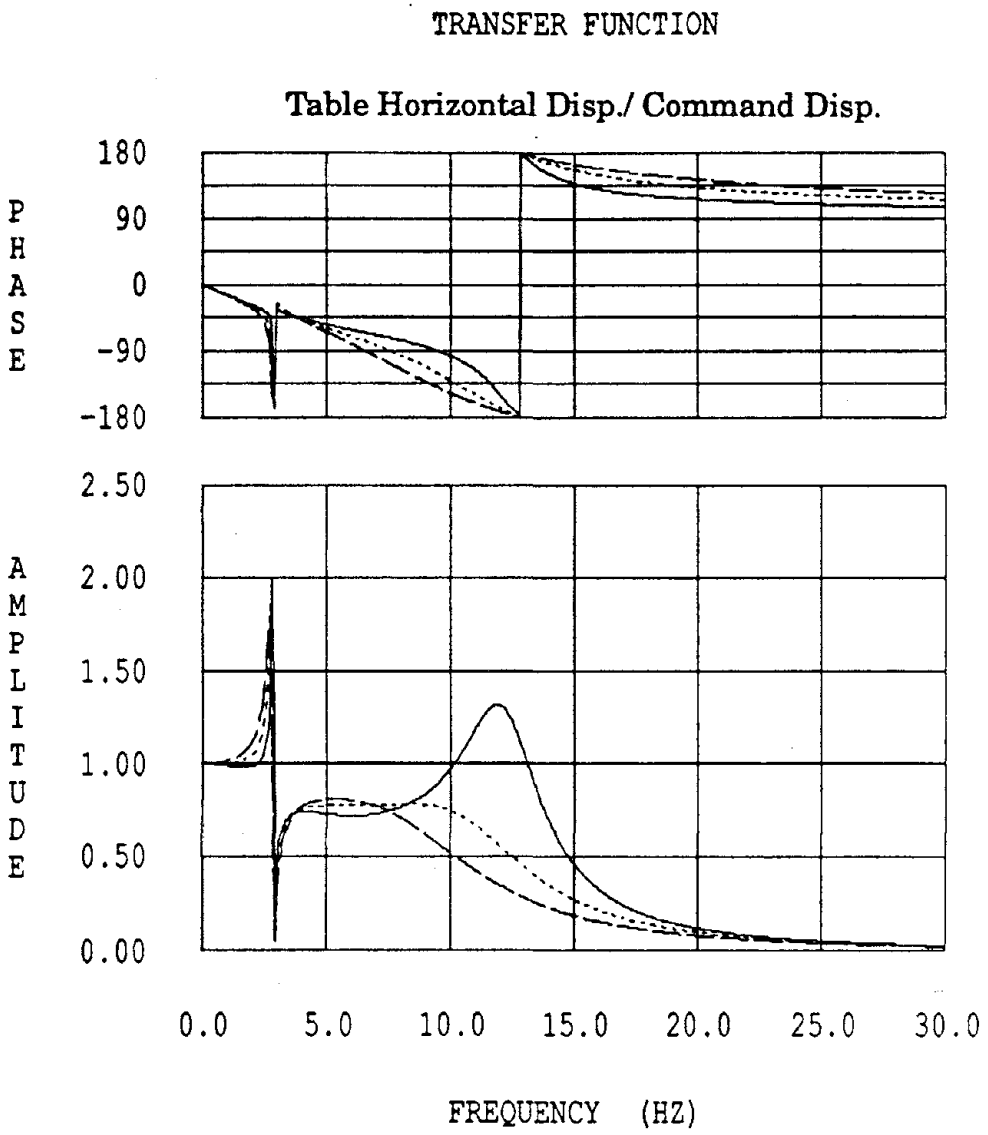

Fig. 7.10: Effect of changing ξ_o on system transfer function.

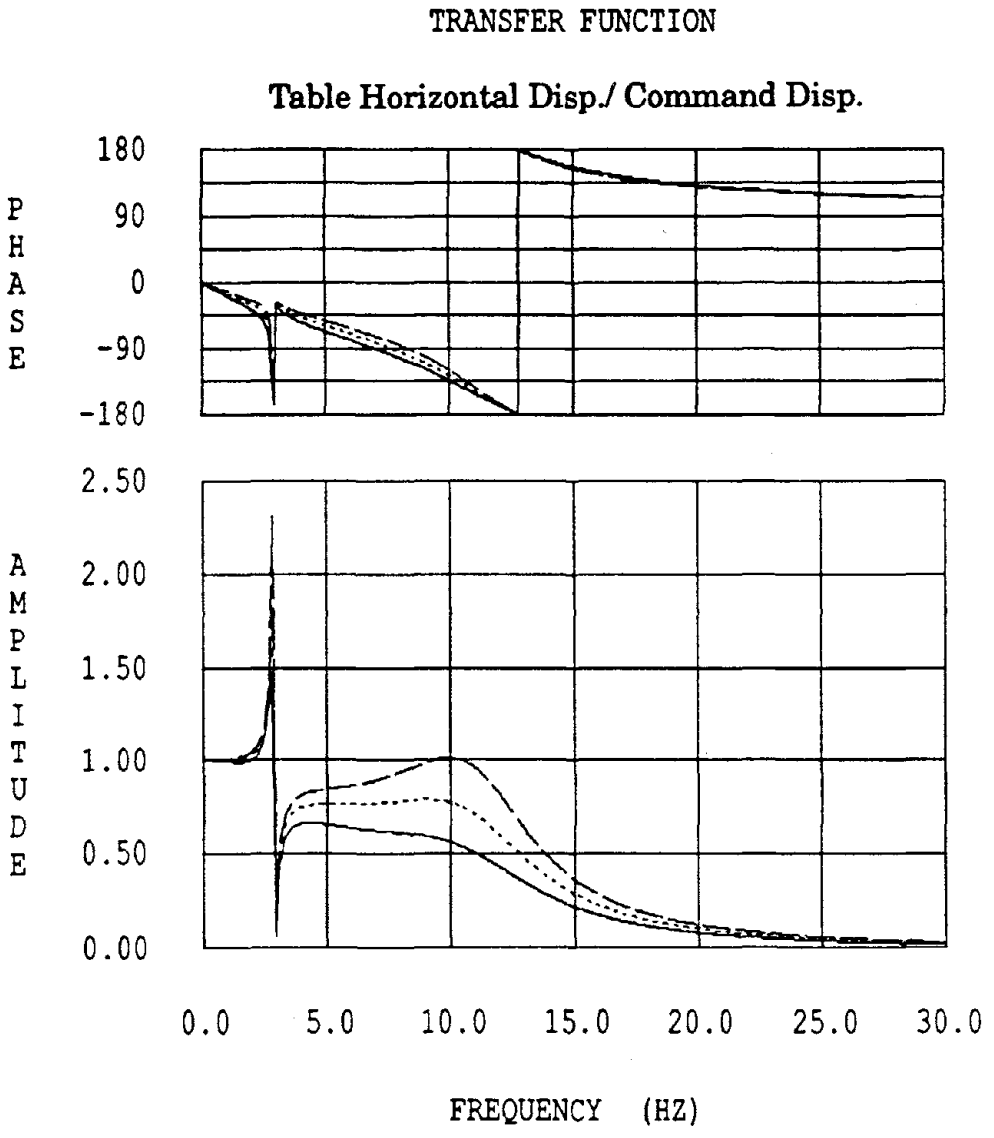

Fig. 7.11: Effect of changing k_o on system transfer function.

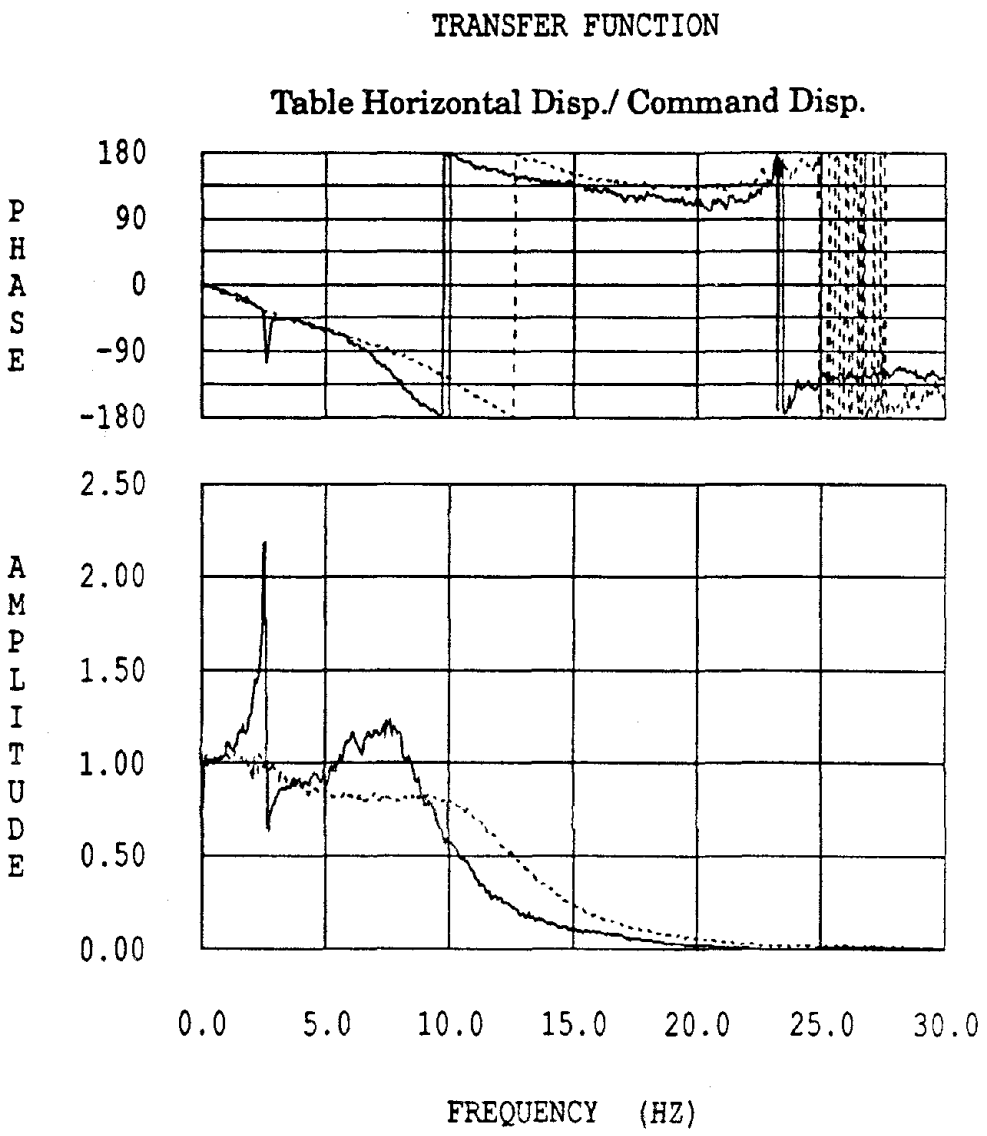

Fig. 7.12 Experimental transfer functions for the standard settings of EERC shaking table.

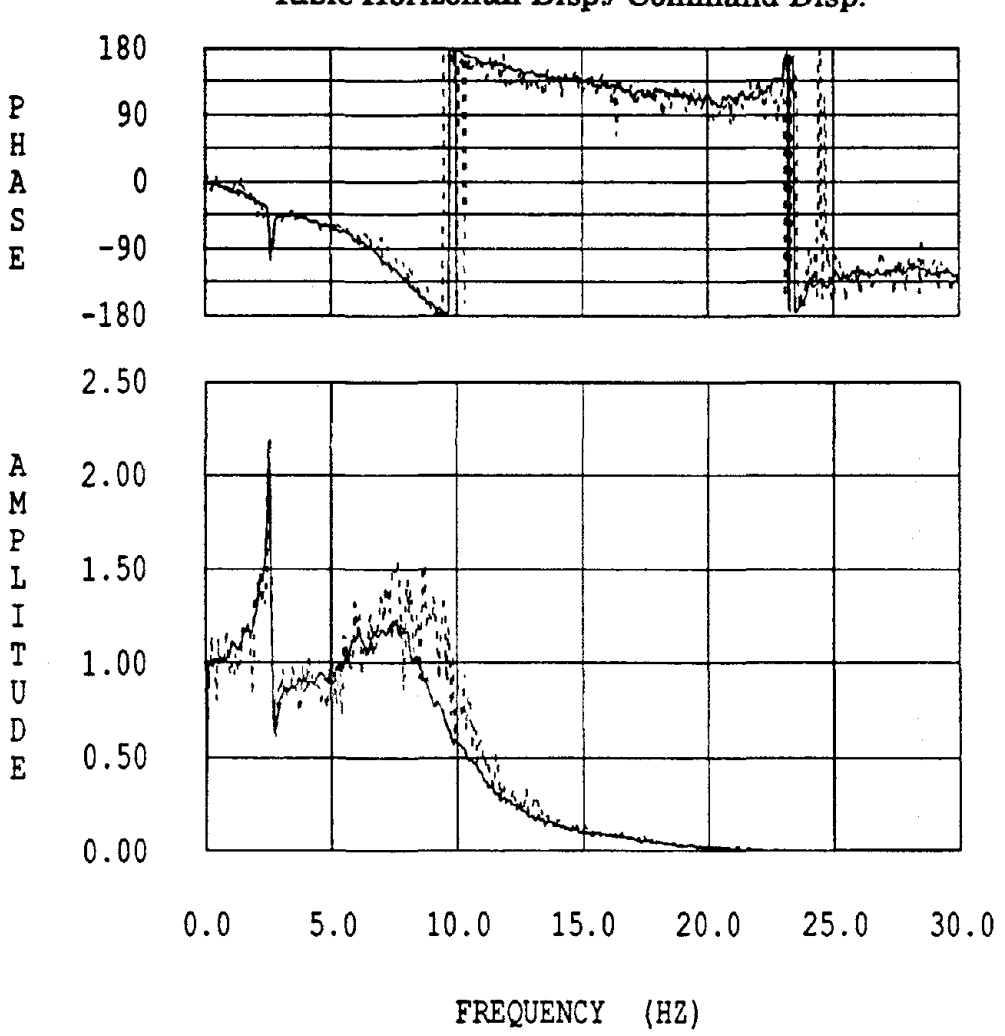

Fig. 7.13: Effect of changing Horizontal Gain setting on system transfer function.

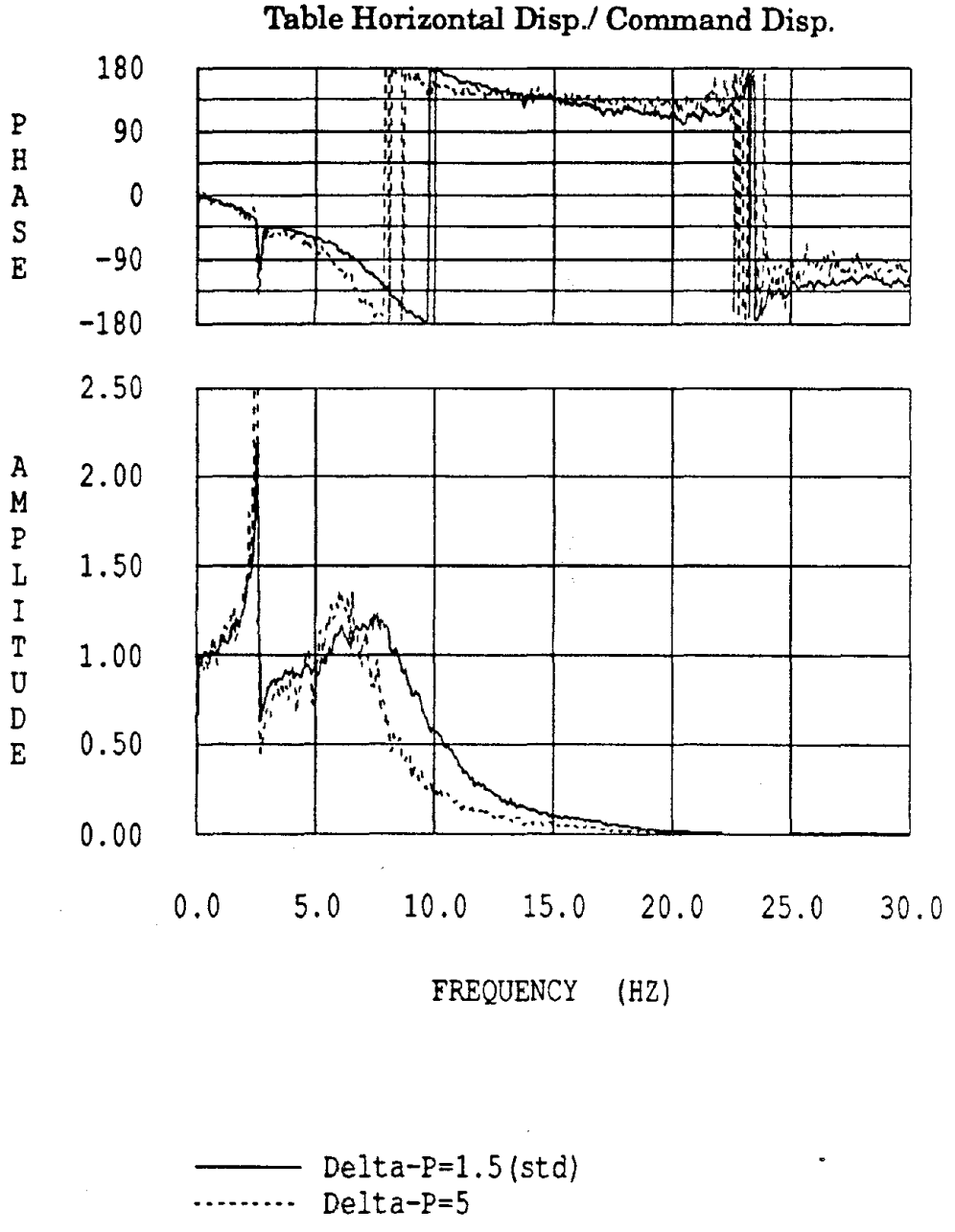

Fig. 7.14: Effect of changing horizontal Delta-P setting on system transfer function.

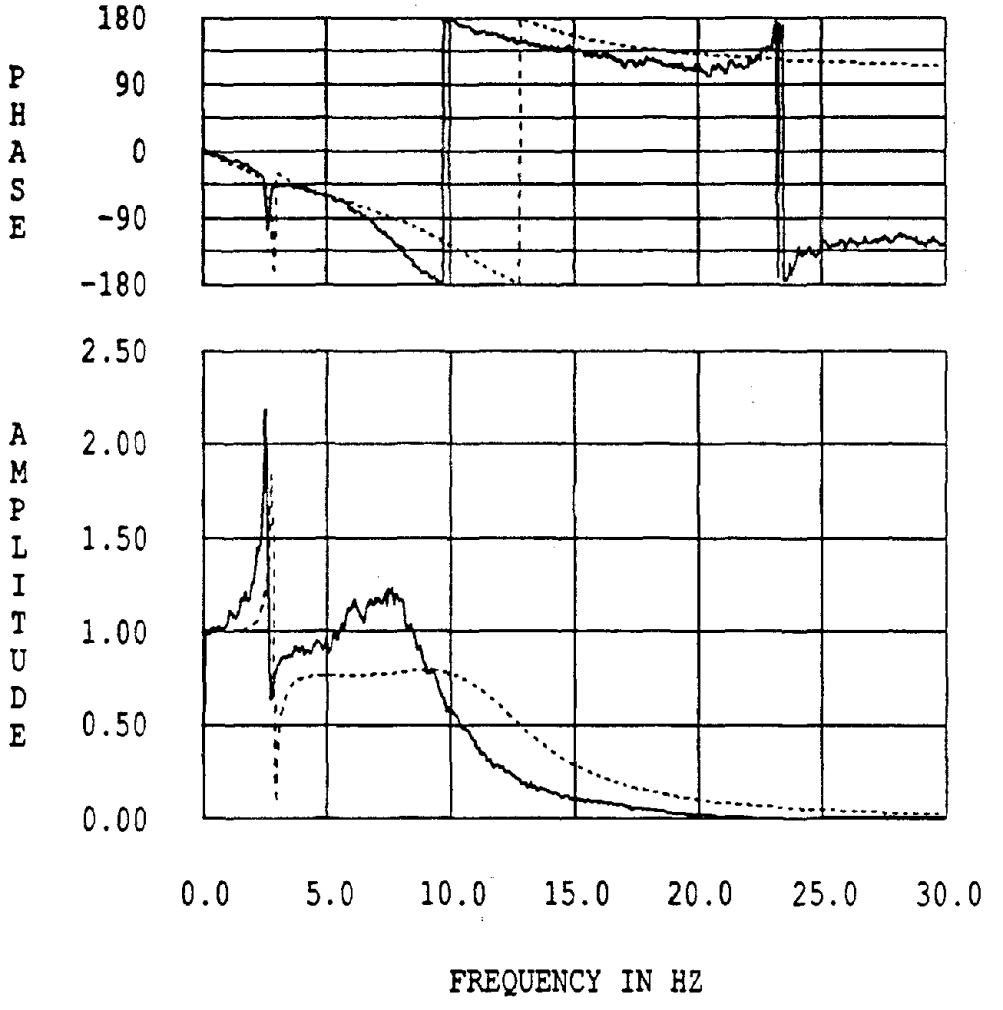

Fig. 7.15: Experimental and analytical transfer functions for the standard settings of EERC shaking table.

Analytical model parameters:

f_o= 12.60 Hz $\quad \xi_o$= 0.477 $\quad k_o$= 25.07

f_s= 2.87 Hz $\quad \xi_s$= 0.004 $\quad \frac{m_s}{m_t}$= 0.60

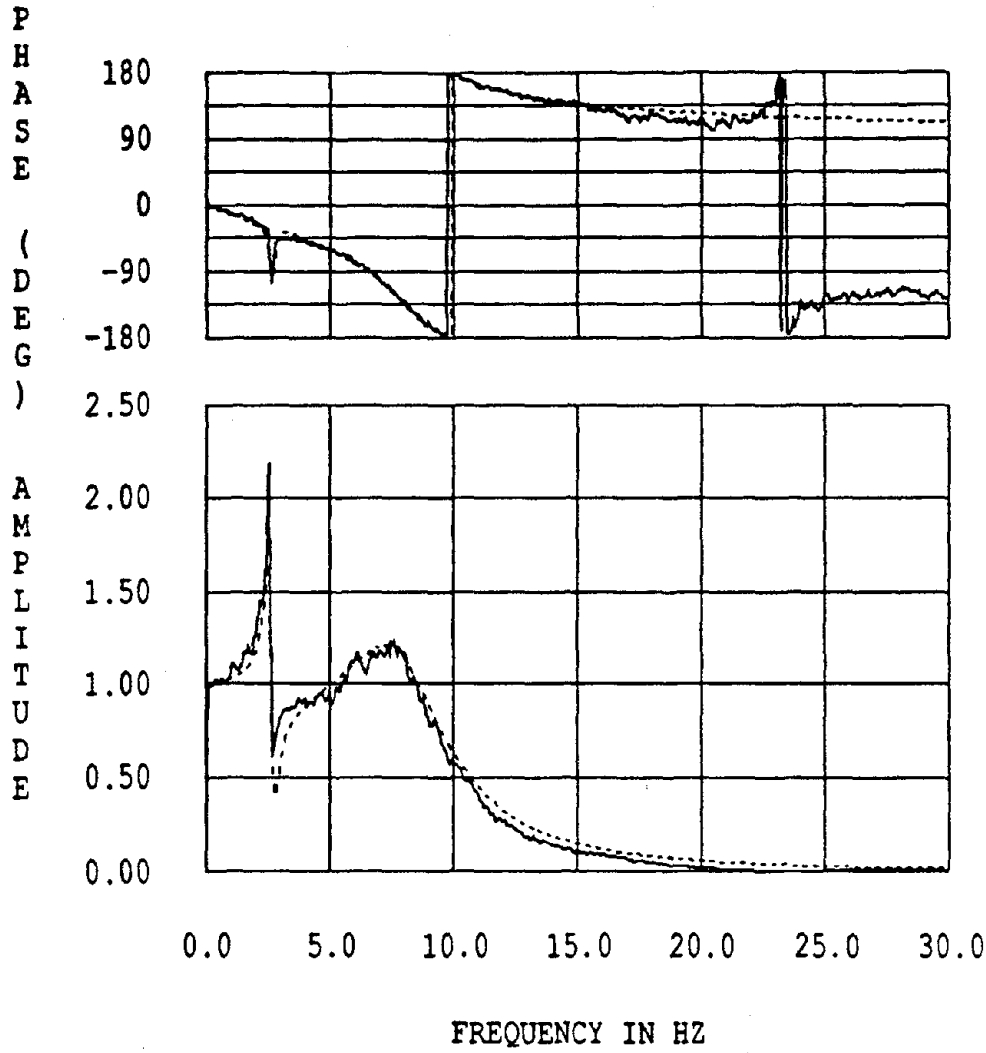

Fig. 7.16: Experimental and best fit analytical transfer functions for the standard settings of EERC shaking table.

Analytical model parameters:

f_o= 9.60 Hz $\quad \xi_o$= 0.606 $\quad k_o$= 29.54

f_s= 2.76 Hz $\quad \xi_s$= 0.033 $\quad \frac{m_s}{m_t}$= 0.60

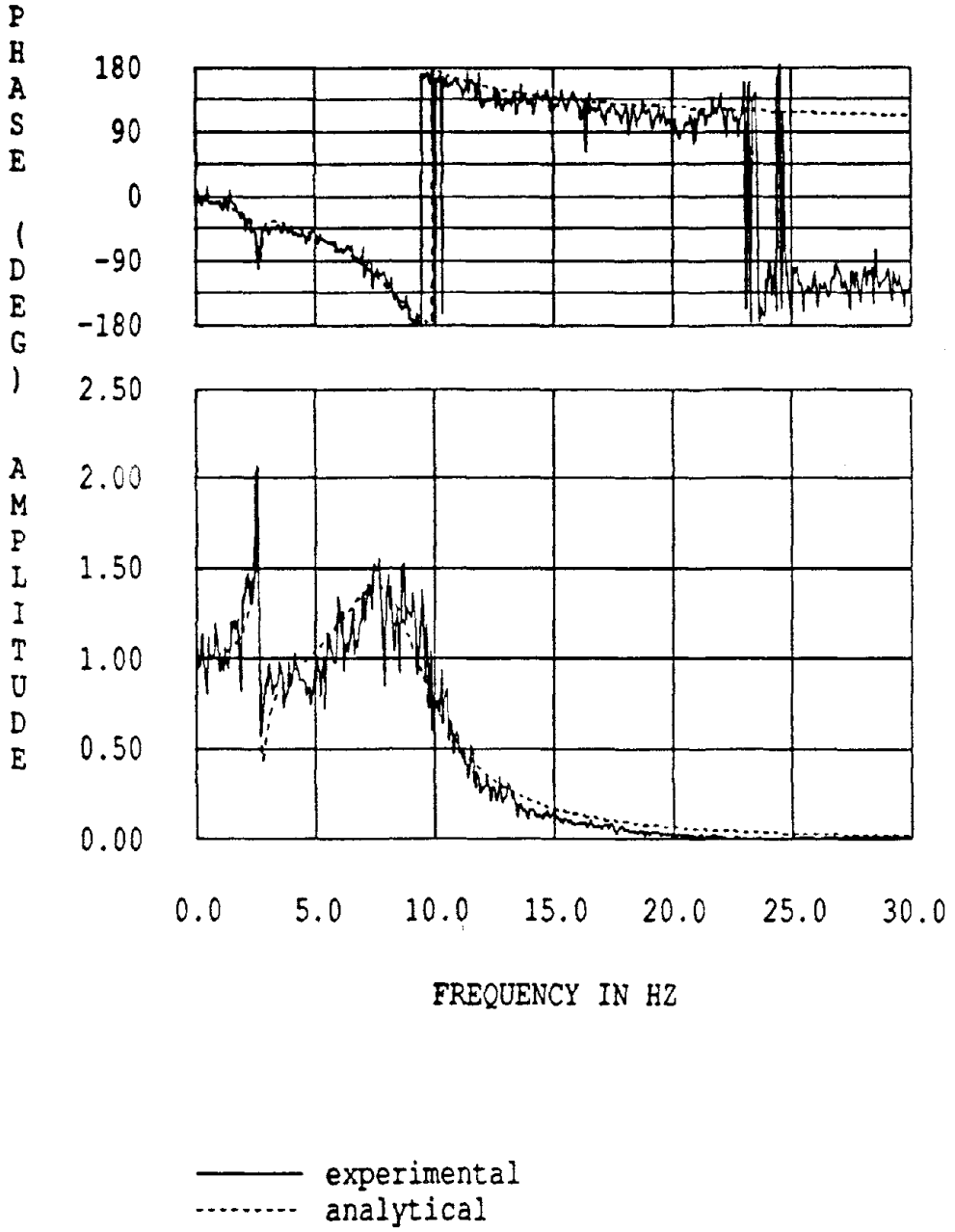

Fig. 7.17: Experimental and best fit analytical transfer functions for the standard settings with Horizontal Gain =10 of EERC Shaking Table.

Analytical model parameters:

f_o= 9.60 Hz $\quad \xi_o$= 0.606 $\quad k_o$= 32.79

f_s= 2.76 Hz $\quad \xi_s$= 0.033 $\quad \frac{m_s}{m_t}$= 0.60

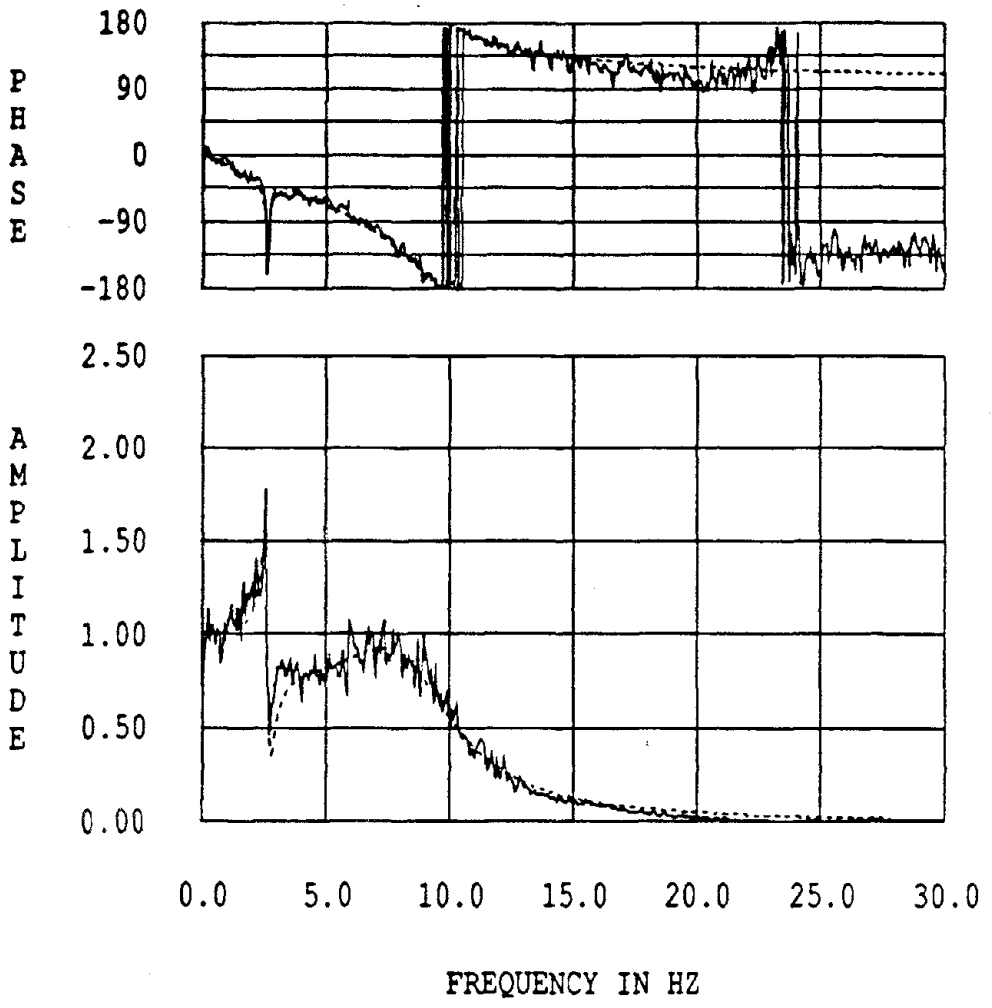

Fig. 7.18: Experimental and best fit analytical transfer functions for the standard settings with Delta-P = 0.

Analytical model parameters:

f_o = 9.60 Hz $\quad \xi_o$ = 0.503 $\quad k_o$ = 22.67

f_s = 2.76 Hz $\quad \xi_s$ = 0.033 $\quad \frac{m_s}{m_t}$ = 0.60

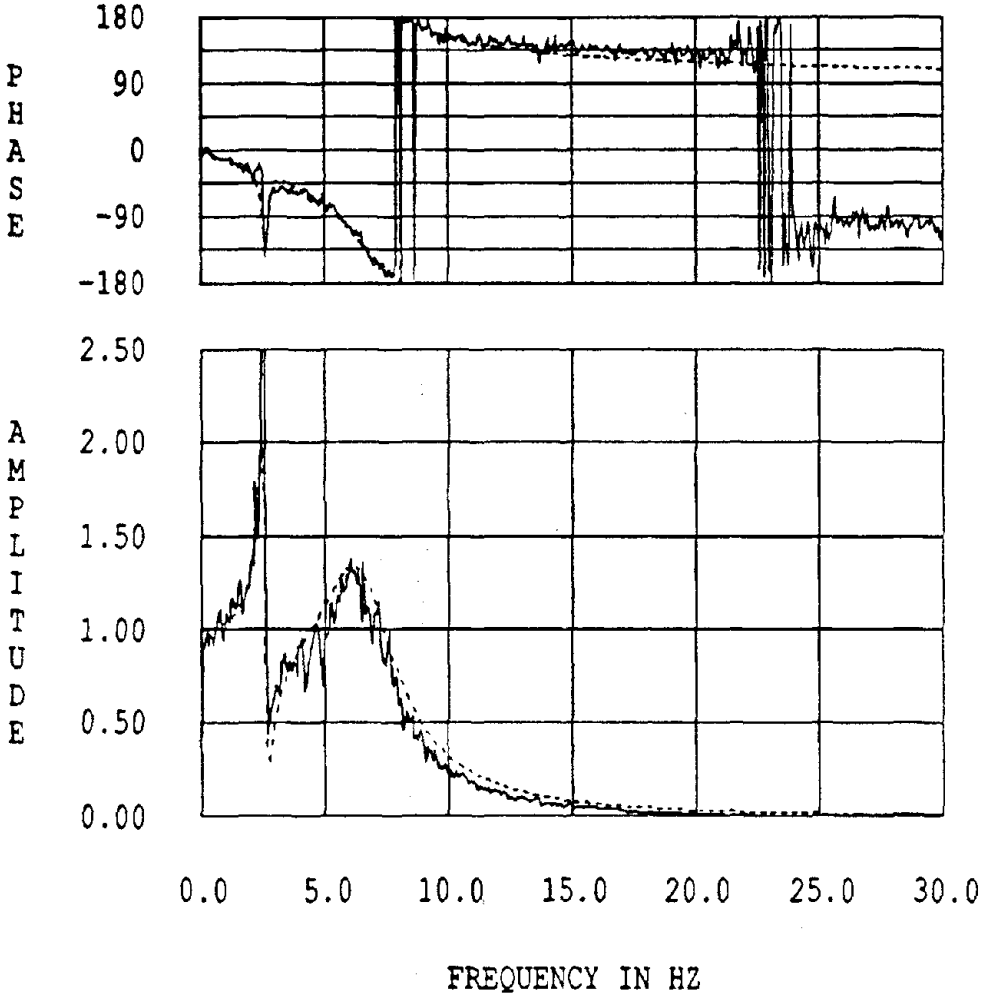

Fig. 7.19: Experimental and best fit analytical transfer functions for the standard settings with Delta-P = 5.

Analytical model parameters:

$f_o = 7.67$ Hz $\quad \xi_o = 0.641 \quad k_o = 26.85$

$f_s = 2.76$ Hz $\quad \xi_s = 0.033 \quad \frac{m_s}{m_t} = 0.60$

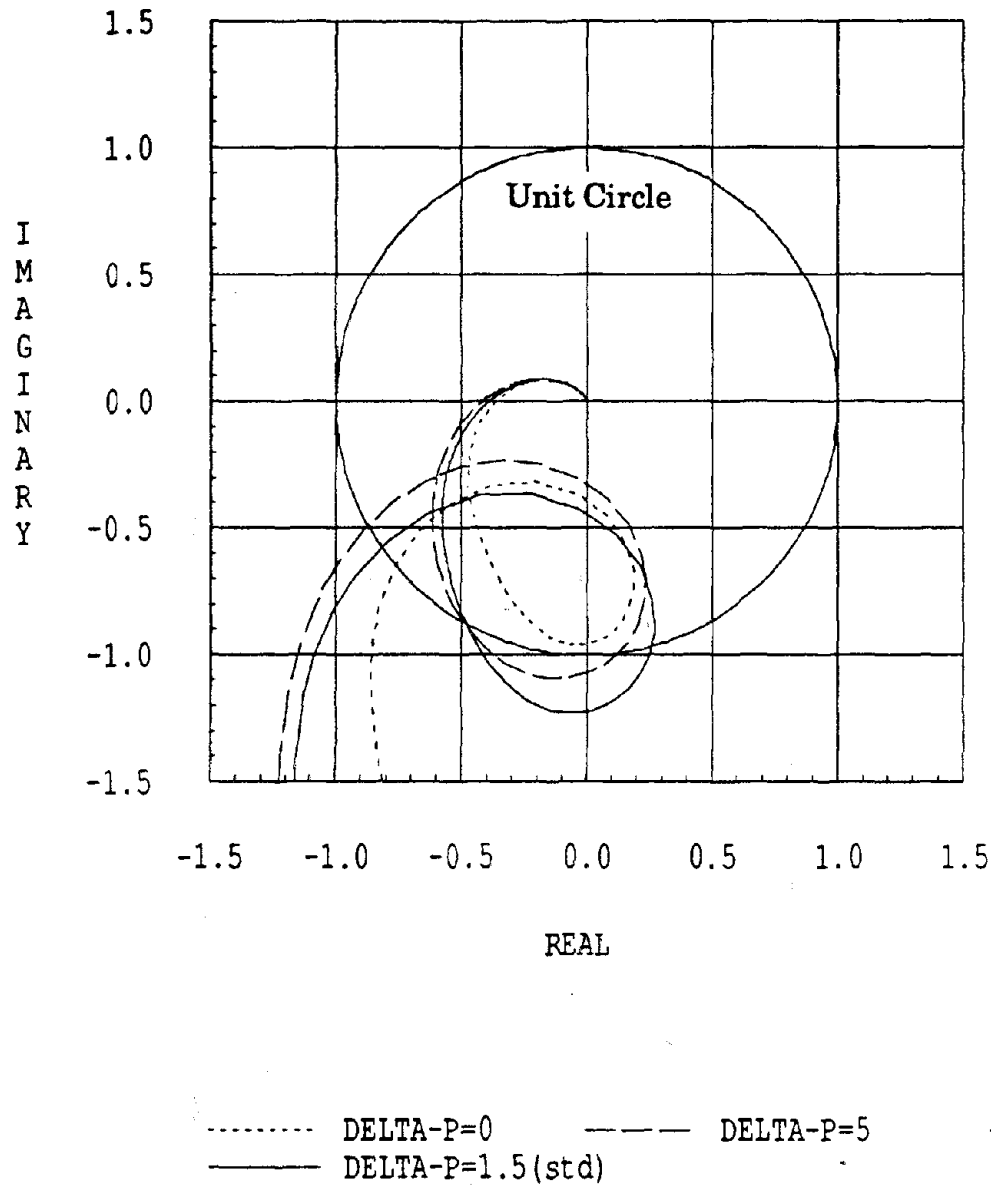

Fig. 7.20: Effect of Delta-P on Table-Structure Stability: Nyquist Plot

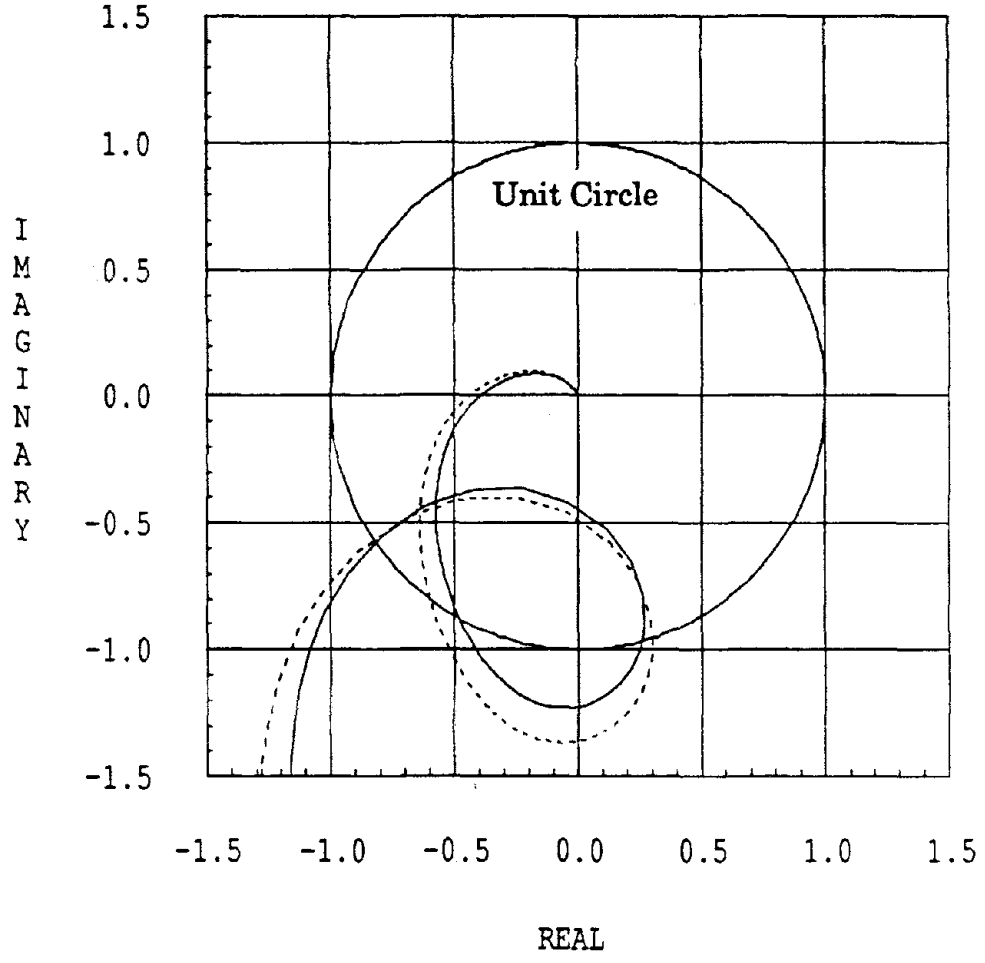

Fig. 7.21: Effect of Gain on Table-Structure Stability: Nyquist Plot

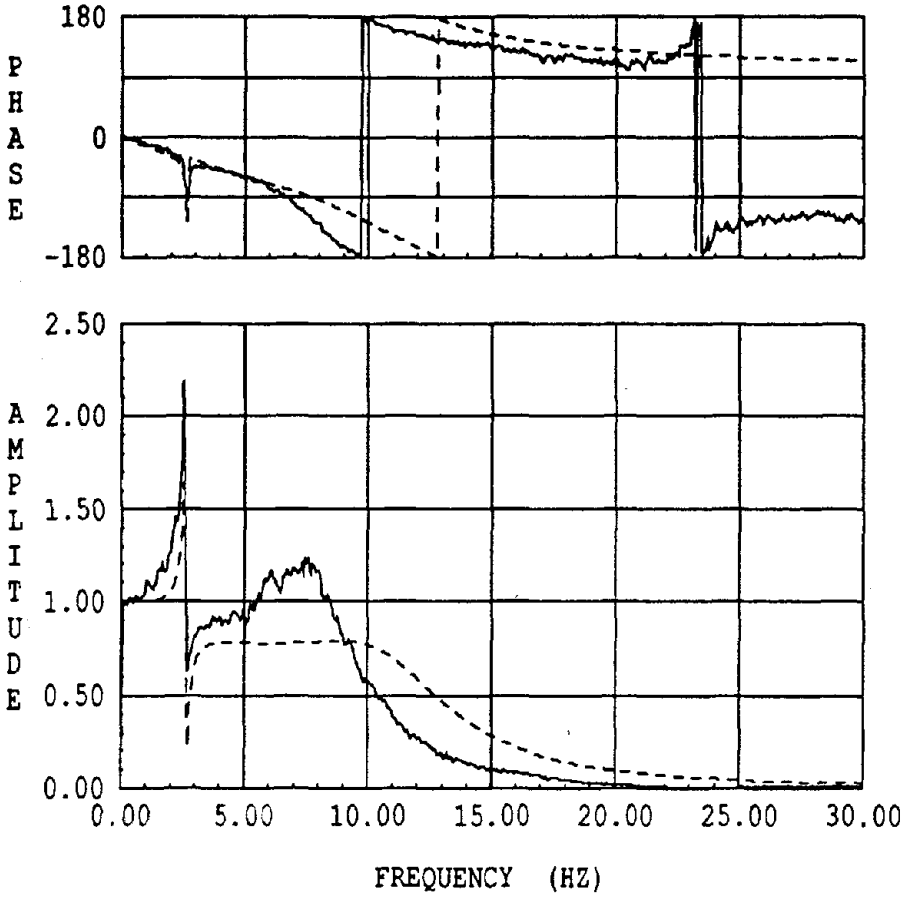

—— Experimental
---- Computed using bare table parameters

Fig. 7.22: Experimental and analytical transfer functions using pitch-coupled table-structure parameters

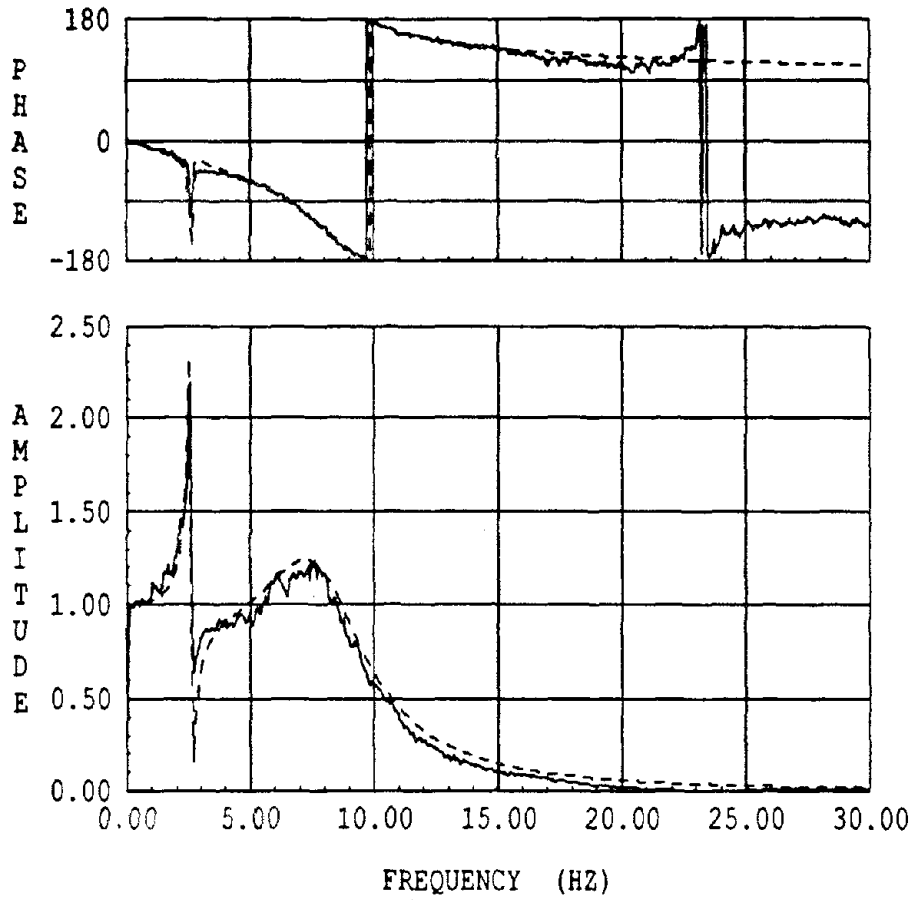

Fig. 7.23: Experimental and analytical transfer functions using pitch-coupled table-structure parameters

Chapter Eight
TWO-DIRECTIONAL EARTHQUAKE SIMULATOR

8.1 INTRODUCTION

In this chapter a model of a two-directional shaking table is presented where both horizontal and pitching degrees of freedom are involved. The system with only a horizontal degree of freedom was treated in chapters 6 and 7 where the equations for the horizontal actuator were derived. In this chapter a model is derived which includes a pitching actuator and a passive stabilizer.

8.2 PITCHING ACTUATORS

In Chapter 7 it was shown that the horizontal actuator force F_a acting in a closed loop shaking-table system is a function of both the table command displacement and the table horizontal displacement as indicated in Eq. (7.6), which is repeated here for convenience:

$$\frac{1}{\omega_o^2}\left(\frac{\dot{F}_a}{m_t}\right) + \frac{2\xi_o}{\omega_o}\left(\frac{F_a}{m_t}\right) + \dot{x}_h + k_o x_t = k_o x_c \qquad (8.1)$$

Here ω_o , ξ_o and k_o represent, respectively, the equivalent open loop frequency, damping and gain for the horizontal actuator-bare table system described in Chapter 6. The vertical actuators employed with the EERC table are similar in character to the horizontal actuators but they have smaller piston area and lower flow capacity. The actuator specifications are listed in Table 2.1. In the absence of a vertical command displacement signal, their action is intended to reproduce the command table pitch record (usually zero). When the table is instructed to move horizontally, the test structure generally will induce overturning moments. These moments need to be resisted by the vertical actuators through the pitch controller in attempting to prevent any pitch movement. Assuming that the pitch actuator moment is a function of the pitch table displacement and the pitch command displacement by analogy with Eq. (8.1) for the horizontal actuator

Preceding page blank

case, the equation for the pitch actuator-bare table system is

$$\frac{1}{\omega_r^2}\left(\frac{\dot{M}_r}{I}\right) + \frac{2\xi_r}{\omega_r}\left(\frac{M_r}{I}\right) + \dot{\theta} + k_r\theta = k_r\theta_c \tag{8.2}$$

where M_r is the moment applied to the shaking table by the pitch actuators; ω_r , ξ_r and k_r are, respectively, the equivalent open loop frequency, damping and gain of the pitch actuator system.

8.3 PASSIVE STABILIZERS

The EERC table was modified in the late seventies by adding four vertical passive stabilizers to provide enhanced control of the table pitch motion. These passive stabilizers act independently of any control system and produce equal and opposite vertical forces to reduce the pitch motion.

A schematic diagram of one set of passive actuators is shown in Fig 2.2. While this system has virtually no resistance to forces applied in the same direction on both pistons, it offers significant resistance to forces applied in opposite directions; this fact makes the system ideal for resisting the pitching motion.

When the forces F are applied in the downward direction, the bottom piston chambers will be in compression and the top ones in tension. This causes the flow of the fluid from the bottom chamber of one actuator to the top of the other. The only resistance offered here is friction and flow resistance adding some damping to the vertical motion, in addition to the inertial resistance of the oil flow which may increase the effective mass of the table in the vertical direction [23].

When the forces F on the actuators act in opposite directions as shown in Fig 2.2, the oil in the bottom chamber of the left piston and the top of the right piston will both be in compression as well as in the oil line connecting them. When ignoring frictional forces, the displacement Δx of each actuator piston can be related to the force F as follows [34]

$$\Delta x = \left(\frac{V}{2\beta_e A^2} + \frac{\pi r_1^3 L}{A^2 t_1 E_1} + \frac{\pi r_2^3 L_c}{A^2 t_2 E_2} + \frac{C_l}{A^2}\right)F \tag{8.3}$$

The four terms in the above expression are due respectively to the oil compression, the expansion in the oil line due to hoop stress caused by pressure, the corresponding expansion of the wall of the actuator chamber, and the leakage of oil across the actuator piston from the high pressure chamber to the lower pressure chamber. The parameters in the above equation are as follows; L, t_1, a and r_1 : oil line length, wall thickness, flow area and pipe radius, respectively; L_c, t_2, A and r_2 : actuator cylinder length, wall thickness, piston area and radius respectively; β_e: the effective bulk modulus of the oil, V: the volume of the compressed oil given by $V=AL_c+aL$; and C_l: a leakage coefficient relating the amount of leaking oil to the pressure difference across the actuator piston. From the above relation the moment rotation stiffness for two sets of passive stabilizers or four actuators can be written as

$$k_p = (\frac{F}{\Delta x})d_p^2 \tag{8.4}$$

where d_p is the horizontal distance between the two passive actuators. Note that the main contribution to the stiffness comes from the first term in Eq. (8.3) which corresponds to oil compressibility. This compressibility or bulk modulus is a function of the amount of entrained air in the oil and the pressure in the compressed cylinder. An increase in the pressure will increase the effective bulk modulus of the oil-gas mixture. An increase in the entrained air will cause a drop in the bulk modulus and hence in the stiffness. This effect can be described by the following equation [20]:

$$\frac{1}{\beta_e} = \frac{1}{\beta} + \frac{r}{1.4P} \tag{8.5}$$

where β_e is the effective bulk modulus of the oil-air mixture and P is the pressure in the compressed cylinder.

It should be noted here that the pressure in the passive stabilizer has two benefits; first it increases the stiffness by increasing the bulk modulus of the oil, and second it helps prevent cavitation of the actuator. Cavitation occurs when pressure in the chamber under tension drops below zero. Having a high initial operating pressure will prevent such a phenomenon and thus

will increase the loading capacity of the stabilizers.

Finally friction in the actuators causes some damping in the system and hence the moment resistance of the passive actuator can be written as

$$M_p = -k_p\,\theta - c_p\,\dot{\theta} \tag{8.6}$$

where M_p is the moment applied by the passive stabilizers, θ is the table pitch displacement, k_p is rocking stiffness contributed by the passive stabilizers and c_p is the coefficient of the viscous damping contribution to the pitching motion. In this report, the terms pitching, rotational and rocking are synonymous and they refer to the direction represented by the angle of rotation θ shown in Fig. 8.1.

8.4 ANALYTICAL MODEL OF THE SYSTEM

Figure 8.1 shows a model of the two-directional shaking table. It includes a horizontal actuator, a pitching actuator, and a rotational spring and damper representing the passive stabilizer system. The actuators have a closed loop feedback mechanism which feeds back the measured displacements and forces into the control system. The system also includes a single-degree-of-freedom structure.

Equilibrium of the forces acting on the mass of the structure mounted on the table requires that

$$m_s\ddot{x}_s^t + c_s(\dot{x}_s^t - \dot{x}_h - \dot{\theta}h) + k_s(x_s^t - x_t - \theta h) = 0 \tag{8.7}$$

Equilibrating the horizontal forces acting on the table gives

$$m_t\ddot{x}_t = F_a + c_s(\dot{x}_s^t - \dot{x}_h - \dot{\theta}h) + k_s(x_s^t - x_t - \theta h) \tag{8.8}$$

and equilibrating the table moments leads to

$$I\ddot{\theta} = M_r + M_p + c_s(\dot{x}_s^t - \dot{x}_h - \dot{\theta}h)h + k_s(x_s^t - x_t - \theta h)h = 0 \tag{8.9}$$

If we let

$$\frac{k_s}{m_s} = \omega_s^2 \qquad \frac{c_s}{m_s} = 2\omega_s \xi_s$$

$$\frac{k_p}{I} = \omega_p^2 \qquad \frac{c_p}{I} = 2\omega_p \xi_p$$

$$x_f = \frac{F_a}{m_t} \qquad x_m = M_r \frac{h}{I} \tag{8.10}$$

$$u = \frac{m_s}{m_t} \qquad v = \frac{m_s h^2}{I}$$

$$x_r = \theta h$$

Equations (8.1,8.2,8.6-8.9) can be rewritten as

$$\dot{x}_f = -2\xi_o \omega_o x_f - \omega_o^2 \dot{x}_h - k_o \omega_o^2 x_t + k_o \omega_o^2 x_c \tag{8.11}$$

$$\dot{x}_m = -2\xi_r \omega_r x_m - \omega_r^2 \dot{x}_r - k_r \omega_r^2 x_r + k_r \omega_r^2 \theta_c h \tag{8.12}$$

$$\ddot{x}_s^t = -2\xi_s \omega_s (\dot{x}_s^t - \dot{x}_h - \dot{x}_r) - \omega_s^2 (x_s^t - x_t - x_r) \tag{8.13}$$

$$\ddot{x}_t = 2\xi_s \omega_s u (\dot{x}_s^t - \dot{x}_h - \dot{x}_r) + \omega_s^2 u (x_s^t - x_t - x_r) + x_f \tag{8.14}$$

$$\ddot{x}_r = 2\xi_s \omega_s v (\dot{x}_s^t - \dot{x}_h - \dot{x}_r) + \omega_s^2 v (x_s^t - x_t - x_r) + x_m - \omega_p^2 x_r - 2\xi_p \omega_p \dot{x}_r \tag{8.15}$$

Or in matrix form

$$\frac{d}{dt}\mathbf{x} = \mathbf{F}\mathbf{x} + \mathbf{G}\mathbf{u} \tag{8.16}$$

where **x** is a vector of system state variables and **u** is the input vector of command horizontal and pitch displacements

$$\mathbf{x} = \begin{Bmatrix} x_t \\ x_r \\ x_s^t \\ \dot{x}_h \\ \dot{x}_r \\ \dot{x}_s^t \\ x_f \\ x_m \end{Bmatrix} \qquad \mathbf{u} = \begin{Bmatrix} x_c \\ \theta_c \end{Bmatrix}$$

and where the matrices **F** and **G** are as follows

$$\mathbf{F} = \begin{bmatrix} 0 & 0 & 0 & 1 & 0 & 0 & 0 & 0 \\ 0 & 0 & 0 & 0 & 1 & 0 & 0 & 0 \\ 0 & 0 & 0 & 0 & 0 & 1 & 0 & 0 \\ -\omega_s^2 u & -\omega_s^2 u & \omega_s^2 u & -a & -a & a & 1 & 0 \\ -\omega_s^2 v & b & \omega_s^2 v & -c & -d & c & 0 & 1 \\ \omega_s^2 & \omega_s^2 & -\omega_s^2 & e & e & -e & 0 & 0 \\ -k_o \omega_o^2 & 0 & 0 & -\omega_o^2 & 0 & 0 & f & 0 \\ 0 & -k_r \omega_r^2 & 0 & 0 & -\omega_r^2 & 0 & 0 & g \end{bmatrix} \quad \mathbf{G} = \begin{bmatrix} 0 & 0 \\ 0 & 0 \\ 0 & 0 \\ 0 & 0 \\ 0 & 0 \\ 0 & 0 \\ k_o \omega_o^2 & 0 \\ 0 & k_r \omega_r^2 h \end{bmatrix}$$

in which

$$\begin{aligned} a &= 2\xi_s \omega_s u & b &= -\omega_s^2 v - \omega_p^2 \\ c &= 2\xi_s \omega_s v & d &= 2\xi_s \omega_s v + 2\xi_p \omega_p \\ e &= 2\xi_s \omega_s & f &= -2\xi_o \omega_o \\ g &= -2\xi_r \omega_r \end{aligned} \tag{8.17}$$

The solution of Eq. (8.16) can be written as

$$\mathbf{x}(t) = e^{\mathbf{F}t}\mathbf{x}_o + \int_0^t e^{\mathbf{F}(t-\tau)}\,\mathbf{G}\mathbf{u}(\tau)\,d\tau \tag{8.18}$$

or in the Laplace domain this becomes

$$\mathbf{x}(s) = [s\,\mathbf{I}-\mathbf{F}]^{-1}\mathbf{x}_o + [s\,\mathbf{I}-\mathbf{F}]^{-1}\mathbf{G}\mathbf{u}(s) \tag{8.19}$$

When the initial conditions are set to zero, the transfer function $\mathbf{H}(s)$ can completely define the system

$$\mathbf{x}(s) = \mathbf{H}(s)\mathbf{u}(s) \tag{8.20}$$

where

$$\mathbf{H}(s) = [s\,\mathbf{I}-\mathbf{F}]^{-1}\mathbf{G} \tag{8.21}$$

In the frequency domain the solution can be obtained by substituting $s = i\,\omega$ as

$$\mathbf{x}(i\,\omega) = \mathbf{H}(i\,\omega)\mathbf{u}(i\,\omega) \tag{8.22}$$

where

$$\mathbf{H}(i\omega) = [i\omega\mathbf{I}-\mathbf{F}]^{-1}\mathbf{G} \tag{8.23}$$

Once the matrices **F** and **G** are known, the transfer matrix $\mathbf{H}(i\omega)$ can be evaluated by solving the system of equations

$$[i\omega\mathbf{I}-\mathbf{F}]\mathbf{H}(i\omega) = \mathbf{G} \tag{8.24}$$

for each frequency. The time history of system responses can then be evaluated by taking the Inverse Fast Fourier Transform **INVFFT** of the state variables vector $\mathbf{x}(i\omega)$.

8.5 SIMPLIFIED MODEL FOR THE PITCH ACTUATOR

If the command pitch displacement θ_c is zero, which normally is the case, Eq. (8.2) can be rewritten in the Laplace domain as

$$M_r(s) = -\frac{I\omega_r^2(s + k_r)}{s + 2\xi_r\omega_r}\ \theta(s) \tag{8.25}$$

and if s is replaced by the frequency parameter $i\omega$, Eq. (8.22) becomes

$$G(i\omega) = \frac{M_r(i\omega)}{\theta(i\omega)} = -\frac{I\omega_r^2(i\omega + k_r)}{i\omega + 2\xi_r\omega_r} \tag{8.26}$$

Equation (8.26) can be rewritten as

$$G(i\omega) = -k_v(\omega) - i\omega c_v(\omega) \tag{8.27}$$

in which k_v and c_v are the parameters for the equivalent frequency dependent rocking stiffness and damper which are expressed as

$$k_v(\omega) = \frac{I\omega_r^2(\omega^2+2\xi_r\omega_r k_r)}{\omega^2+4\xi_r^2\omega_r^2} \tag{8.28}$$

$$c_v(\omega) = \frac{I\omega_r^2(2\xi_r\omega_r-k_r)}{\omega^2+4\xi_r^2\omega_r^2} \tag{8.29}$$

Equation (8.2) can then be rewritten as

$$M_r = -k_v(\omega)\theta - c_v(\omega)\dot{\theta} \tag{8.30}$$

Equation (8.27) suggests that the pitch actuator can be modeled by a rocking spring and a damper as in the case of the passive stabilizers. The difference in this case is that the pitch actuator spring and damper are frequency dependent. Also k_v and c_v are functions of the open loop parameters of the pitch actuator, i.e. ω_r , ξ_r and k_r, which are in turn dependent on the feedback loop gains, or in other words, on the control settings of the pitch controller.

As for the dependence on the control settings, the shaking table is normally set for a standard operation setting and this is unlikely to change unless some instability or other type of poor performance is noticed.

On the other hand, the pitch motion is normally dominated by the coupled table-structure frequency such that the dependence of k_v and c_v on ω is not a major issue; thus these parameters generally can be taken as constants corresponding to their values at the coupled table-structure frequency.

8.6 HYBRID MODEL

Having shown that the pitch actuator can be reasonably represented as a spring and a damper similar to those of the passive stabilizer, these two types of spring and damper constants can be combined to obtain equivalent rocking constants k_θ and c_θ. This in effect eliminates the pitch actuator from the model, and the new model is as shown in Fig. 8.2. This model is termed a hybrid model since it includes a feedback loop on the horizontal displacement but not on the pitch displacement. In contrast to this development, it should be noted that the representation of the horizontal actuator by an equivalent spring and damper cannot be completely justified because the horizontal command signal x_c is not normally zero. The assumption of zero command displacement was the key to deriving the simplified model in Section 8.5; in the next section the equations for the hybrid model are presented.

8.6.1 Mathematical Representation

Equation (8.27) can be combined with Eq. (8.3) as

$$M_t = M_p + M_r = -k_\theta \theta - c_\theta \dot{\theta} \tag{8.31}$$

where

$$k_\theta = k_p + k_v(\omega) \tag{8.32}$$

$$c_\theta = c_p + c_v(\omega) \tag{8.33}$$

Equations (8.8), (8.10) and (8.11) are still applicable. Equation (8.12) can be rewritten as

$$\ddot{x}_r = 2\xi_s \omega_s v (\dot{x}_s^t - \dot{x}_h - \dot{x}_r) + \omega_s^2 v (x_s^t - x_t - x_r) - \omega_\theta^2 x_r - 2\xi_\theta \omega_\theta \dot{x}_r \tag{8.34}$$

where

$$\omega_\theta^2 = \frac{k_\theta}{I} \tag{8.35}$$

$$\xi_\theta = \frac{c_\theta}{2\omega_\theta I} \tag{8.36}$$

Equation (8.16) can then be rewritten as

$$\frac{d}{dt}\hat{\mathbf{x}} = \hat{\mathbf{F}}\hat{\mathbf{x}} + \hat{\mathbf{G}}\hat{\mathbf{u}} \tag{8.37}$$

in which

$$\hat{\mathbf{x}} = \begin{Bmatrix} x_t \\ x_r \\ x_s^t \\ \dot{x}_h \\ \dot{x}_r \\ \dot{x}_s^t \\ x_f \end{Bmatrix} \qquad \hat{\mathbf{u}} = \begin{Bmatrix} x_c \end{Bmatrix}$$

$$\hat{\mathbf{F}} = \begin{bmatrix} 0 & 0 & 0 & 1 & 0 & 0 & 0 \\ 0 & 0 & 0 & 0 & 1 & 0 & 0 \\ 0 & 0 & 0 & 0 & 0 & 1 & 0 \\ -\omega_s^2 u & -\omega_s^2 u & \omega_s^2 u & -a & -a & a & 1 \\ -\omega_s^2 v & \hat{b} & \omega_s^2 v & -c & -\hat{d} & c & 0 \\ \omega_s^2 & \omega_s^2 & -\omega_s^2 & e & e & -e & 0 \\ -k_o \omega_o^2 & 0 & 0 & -\omega_o^2 & 0 & 0 & f \end{bmatrix} \quad \hat{\mathbf{G}} = \begin{Bmatrix} 0 \\ 0 \\ 0 \\ 0 \\ 0 \\ 0 \\ k_o \omega_o^2 \end{Bmatrix}$$

where

$$\begin{aligned} a &= 2\xi_s \omega_s u & \hat{b} &= -\omega_s^2 v - \omega_\theta^2 \\ c &= 2\xi_s \omega_s v & \hat{d} &= 2\xi_s \omega_s v + 2\xi_\theta \omega_\theta \\ e &= 2\xi_s \omega_s & f &= -2\xi_o \omega_o \end{aligned} \tag{8.38}$$

The solution of Eq. (8.37) is then as described by Eqs. (8.18-8.24).

8.6.2 Validation of the Hybrid Model

In order to compare the performance of the two actuator model (Fig. 8.1) to that of the hybrid model (Fig. 8.2), the parameters of the pitching actuator need to be known. However no measurements have been made to estimate those parameters, and in the absence of such experimental data the computed rotational stiffness and damping k_v and c_v of the vertical actuators will be used to evaluate the unknown parameters, using Eqs. (8.28) and (8.29). These equations are not enough, however, to determine the three unknown parameters, namely, the open loop frequency f_r, the open loop damping ξ_r and the open loop gain k_r. To avoid this difficulty, the open loop frequency is assumed and then the other two parameters are evaluated. Considering the computed values of $c_v = 1.04 \times 10^8$ lb-in/(rad/sec) and $k_v = 7.72 \times 10^9$ lb-in/rad, evaluated from Fig. 5.5b at the coupled table-structure frequency, it is found that an open loop frequency of less than 12.5 Hz will lead to negative damping and hence to an unstable system. Two values were considered here which are thought to represent a wide range on the open loop frequency: $f_r = 13\ Hz$ and $f_r = 21\ Hz$. The first of these gave

3.5 percent damping, the second 50 percent damping. The transfer functions of the pitch actuator for these two cases are shown in Fig. 8.3. These functions represent the ratio of the table pitch displacement to the pitch command displacement for a bare table having a pitch actuator only. Note the wide difference in performance for the bare table system, considering these two open loop frequencies. However when both models of the pitching actuator are used to estimate the combined system performance with regard to the horizontal and pitching interaction, they both give virtually the same response as that of the hybrid model as shown by the transfer functions in Figs. 8.4 and 8.5. The results shown in Fig. 8.6 demonstrate that the inclusion of the pitch actuator reduces the pitch response, as expected.

It can be concluded from these studies that the simpler hybrid model can be used with confidence to substitute for the more complicated model derived in Section 8.4. It needs to be noted again, however, that the assumption made here is that the command pitch displacement is zero.

8.6.3 Comparison with Experimental Results

Table 8.1 shows the hybrid model parameters. The bare table mass and inertia are assumed to be 100 kips and 1251 kip-in/sec^2, respectively. The open loop parameters of the loaded table were used which differ from those used for the bare table, as was noted in Chapter 7. The parameters k_θ and c_θ were evaluated from the curves of Fig. 5.5a at the coupled table-structure frequency of 2.58 Hz. f_θ and ξ_θ are evaluated from Eqs. (8.35) and (8.36).

Figure 8.7 shows the comparison of the measured table horizontal transfer function with that predicted using the hybrid model. Equivalent results for the pitch transfer function are shown in Fig. 8.8. The agreement between the experimental and analytic curves representing both transfer functions is considered excellent, thus validating the analytical model. Further discussion of the analytical model is presented in Section 8.6.4. The experimental curve shown by the solid unsmooth curve in Fig. 8.8 was obtained from a transfer function computed from an earthquake type input signal; the earthquake signal did not have high frequencies and a spike would normally

occur when the input energy at a certain frequency is zero while the output energy at the same frequency may not be zero because of the presence of noise in the output signal.

8.6.4 Examination of Analytical Model Response

Figures 8.9 and 8.10 show detailed plots of the analytical transfer functions. Three transfer functions with respect to the table horizontal command displacement x_c are shown. They are the table horizontal x_t displacement, the table pitch displacement scaled by the structural height θh and the effective table displacement which was obtained by adding the first two functions: $x_{eff} = x_t + \theta h$. The latter constitutes a better measure of interaction as it includes the combined effects of the horizontal and rocking interaction. It can be seen from Figs. 8.9 and 8.10 that the pitch motion is concentrated around the coupled table-structure frequency f_c and peaks at f_c. On the other hand the effective motion has maximum attenuation (notch) at the fixed-base frequency f_s of the structure and shows an amplified response near the coupled table-structure frequency. The notch in the transfer function x_t/x_c no longer occurs at the fixed-base frequency of the structure f_s as was the case when pitching was absent (as in Chapter 7), but rather at a lower frequency. At the fixed-base frequency, the pitch and horizontal motion have similar amplitudes and are out of phase, so that they cancel each other; on the other hand, they both peak and add up near the coupled frequency f_c. The method of analytically computing the coupled system parameters is discussed in Chapter 9.

8.6.5 Parametric Study of the Hybrid Model

As noticed in the preceding section, the effective displacement is more relevant when pitching is considered than is the table horizontal displacement. In this section the effect of the various parameters will be studied using the effective and pitch displacement response as a measure. The parameters used in the previous section or those listed in Table 8.1 will be considered as the reference parameters.

8.6.5.1 Rocking stiffness k_θ: Figures 8.11, 8.12 show the effect of doubling the rocking stiffness parameter k_θ. The higher stiffness reduced the rocking motion shown in Fig. 8.12 to about two-thirds of the original value. The effect on the horizontal motion, shown in Fig. 8.11 is not very significant; only a minor increase in the peak frequency is evident.

8.6.5.2 Rocking damping c_θ: Figures 8.13, 8.14 show the effects of varying the damping coefficient c_θ. The dominant effect in this case is an amplification of both the effective and rocking response near the coupled table-structure frequency for lower damping values. Higher damping reduces both the table pitching motion and the overall effective interaction.

8.6.5.3 Open loop frequency f_o: Figures 8.15, 8.16 show the influence of the open loop frequency f_o on the shaking table effective and rocking motion response. The pitching motion was not significantly affected by the increased open loop frequency as can be seen from Fig. 8.16. Also as Fig. 8.15 demonstrates, the peak in the effective motion is reduced and that can be attributed to the horizontal interaction mechanism.

8.6.5.4 Open loop damping ξ_o: Figures 8.17, 8.18 show the effects of varying ξ_o on the system behavior. Lower open loop damping seems to amplify the response near both the coupled table-structure frequency and the open loop bare table system frequency. In addition the table rocking is increased significantly. Table rocking motion now has two peaks, instead of the usual one peak; the second peak is at the open loop bare table frequency f_o. This indicates that open loop damping is very helpful in reducing the pitching and overall interaction.

8.6.5.5 Open loop gain k_o: Figures 8.19, 8.20 show the effects of changing the open loop gain from its value of 29.54 to 40. The higher gain value produced both larger rocking and effective motions.

8.6.5.6 Bare table mass inertia I: Figures 8.21, 8.22 show the effect of the bare table inertia on shaking table performance. An increase of the inertia by a factor of four gave a very minor increase in the table rocking motion and had no effect on the effective motion. Neglecting the table inertia (I=0) virtually produced no change in table performance.

8.6.5.7 Structural height h: Figures 8.23, 8.24 show the effect of reducing the structural height from its value of 219 inches to 110 inches and zero inches, respectively. The reduction of the table height by a factor of two reduced the rocking motion by a factor of four. The rocking motion is eliminated as expected for a zero structural height; the effective motion will then be mainly due to horizontal interaction. Figure 8.23 shows, in a sense, the effect of the rocking motion on system performance.

8.6.5.8 Structural Frequency f_s: Figures 8.25, 8.26 show the effect of varying the structural frequency. Structural frequencies of 1, 3 and 12 Hz were considered. The lower the structural frequency the sharper the peak and notch in the effective transfer function. The peaks are also sharper in the rocking transfer function. The notch occurs at the fixed-base frequency f_s, but the notch phenomenon disappears for the higher frequency f_s=12 Hz. The peak and notch tend to separate more for higher f_s.

8.6.5.9 Structural Damping ξ_s: Figures 8.27, 8.28 show the effect of fixed-base structural damping on system performance. The lower damping produces higher peaks and deeper notches in the effective transfer function; it also introduces more rocking. It can be said that structural damping helps alleviate the interaction effects.

8.6.5.10 Conclusions: Table inertia had a minor influence on table performance and therefore can be neglected. Structural damping, open loop damping and rocking damping are important because they all reduce the system interaction effects. Structural height is an important factor in the rocking interaction but not in the horizontal interaction.

Structural Frequency (Hz)	f_s	2.870
Structural Damping (%)	ξ_s	1.000
Structural Mass (kips)	m_s	68.000
Structural height (inches)	h	219.000
Horizontal Open Loop Frequency (Hz)	f_o	9.600
Horizontal Open Loop Damping (%)	ξ_o	0.606
Horizontal Open Loop Gain	k_o	29.500
Rocking Stiffness (lb-in/rad)	k_θ	2.22E+10
Rocking Damping (lb-in/(rad/sec))	c_θ	3.70E+08
Bare Table Inertia (kip-in-sec2)	I	1251.000
Bare Table Mass (kips)	m_t	100.000

Table 8.1: Hybrid Model Parameters

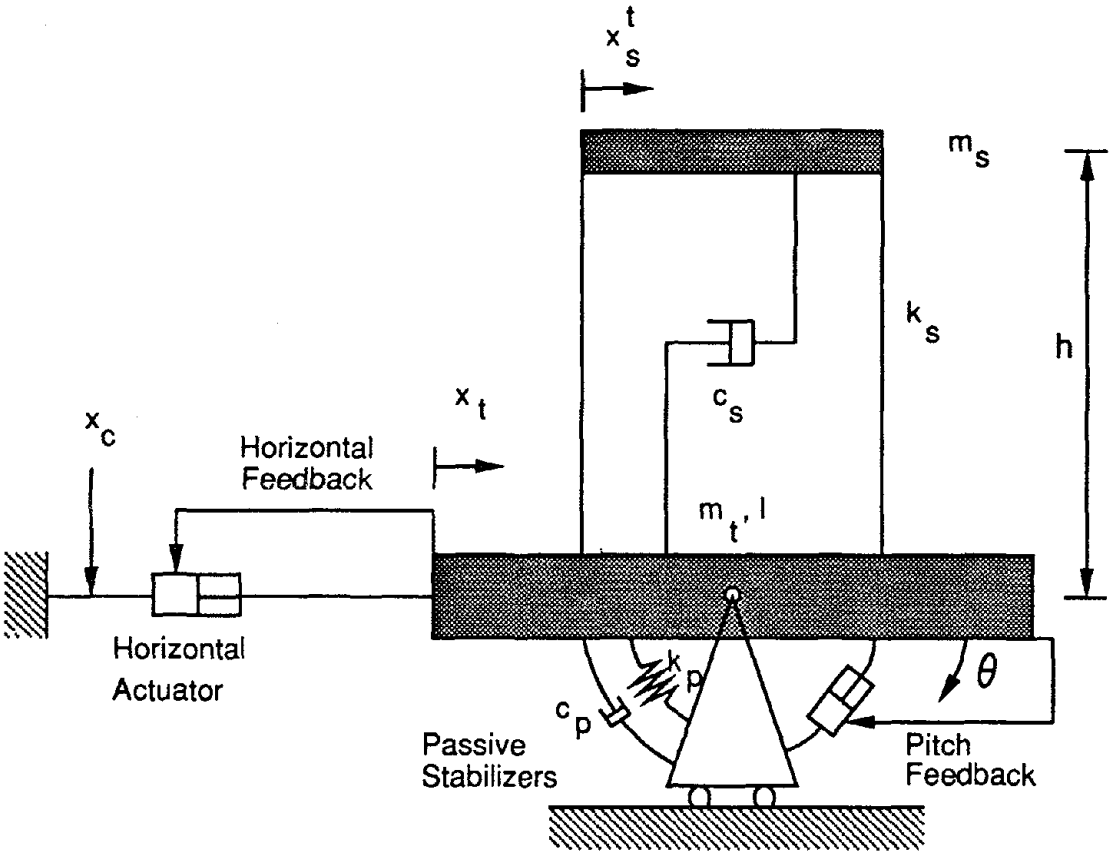

Fig. 8.1: Two-directional earthquake simulator with horizontal and pitch feedback mechanisms.

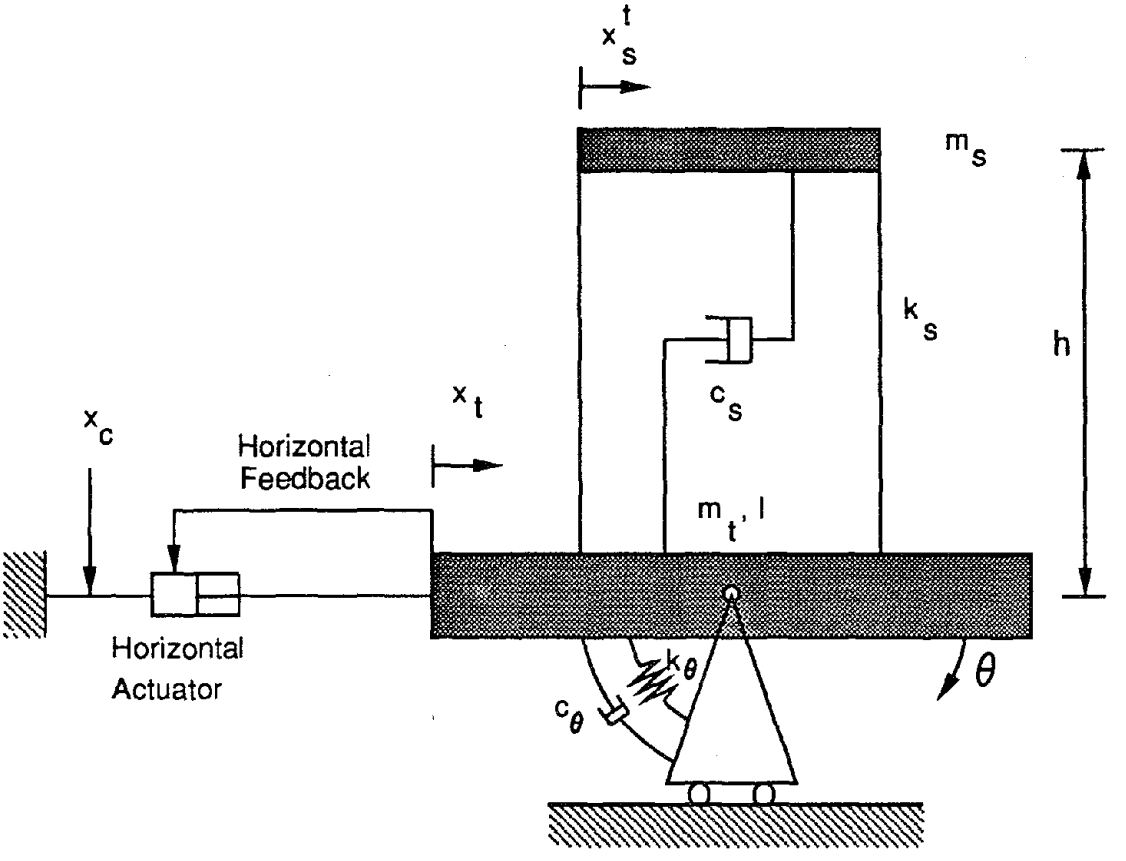

Fig. 8.2: Hybrid model for a two-directional earthquake simulator. The active and passive pitch actuators are modeled as a spring and a dash-pot. The horizontal actuator has a feedback control loop.

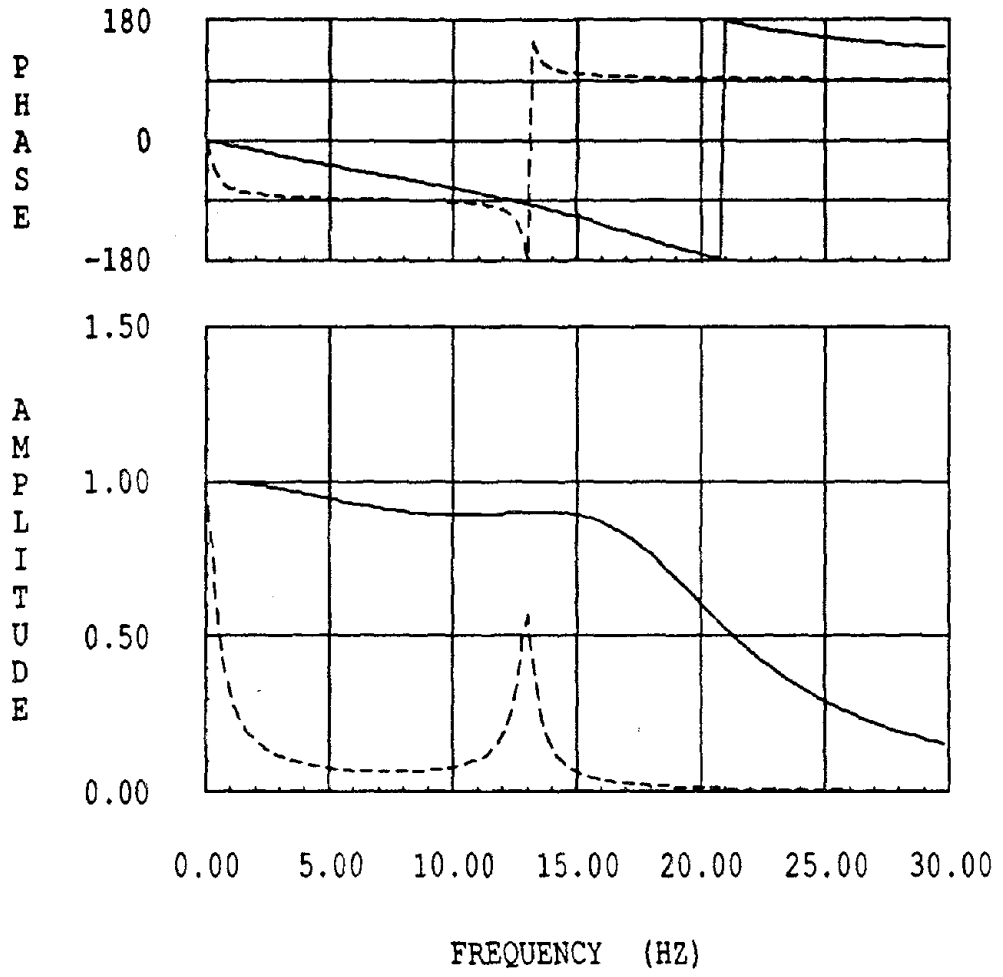

Fig. 8.3: Transfer functions of pitch displacement over command in case of a bare table with only a pitch actuator.

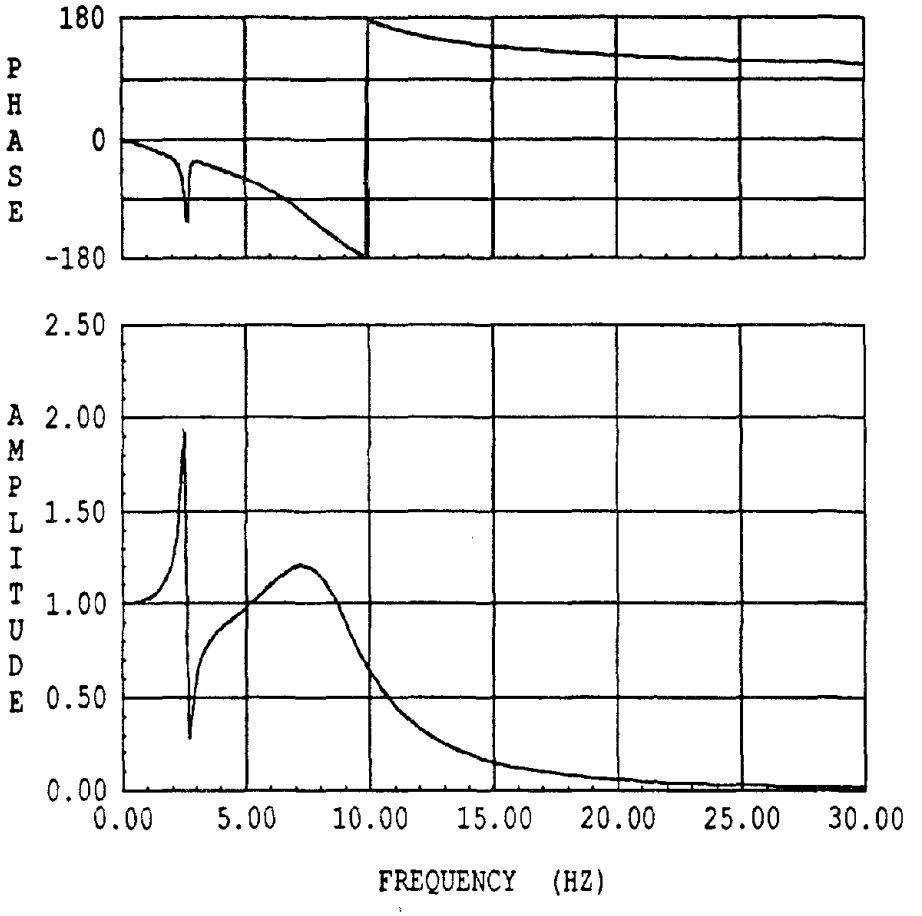

——— f_r = 21 Hz
- - - - f_r = 13 Hz
..... Hybrid Model

Fig. 8.4: Transfer functions of horizontal displacement over command using two pitch actuator frequencies and an equivalent stiffness.

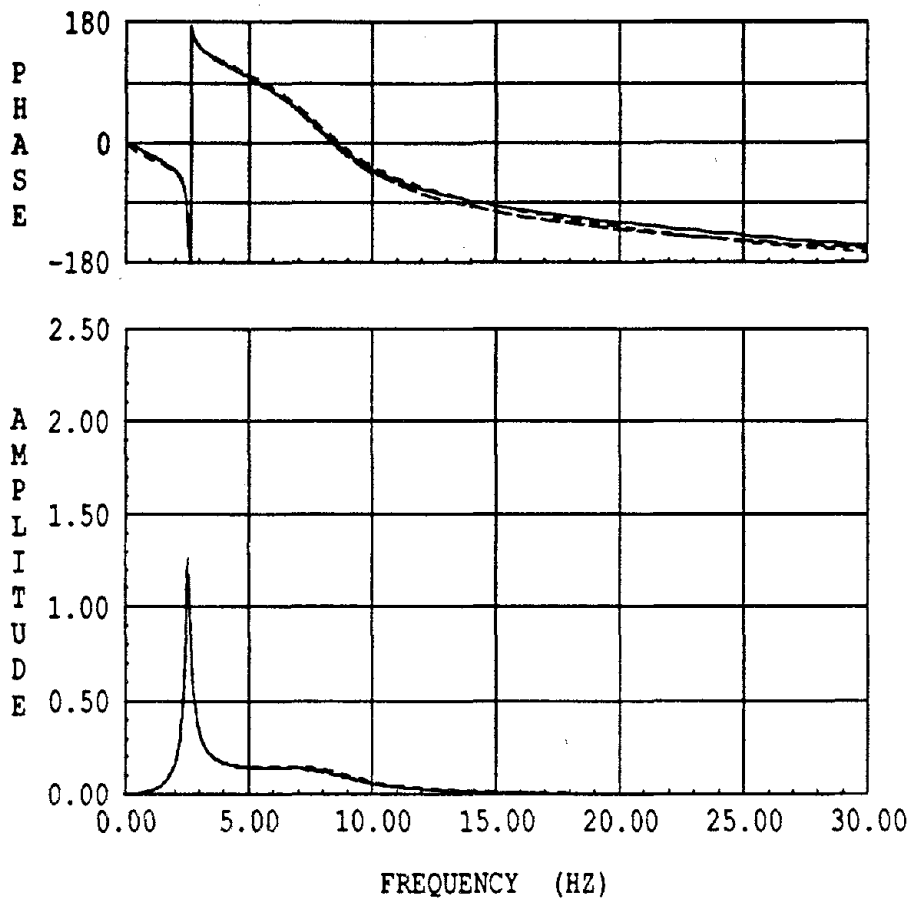

—— f_r = 21 Hz
---- f_r = 13 Hz
..... Hybrid Model

Fig. 8.5: Transfer functions of Theta*h over command using two pitch actuator frequencies and an equivalent stiffness.

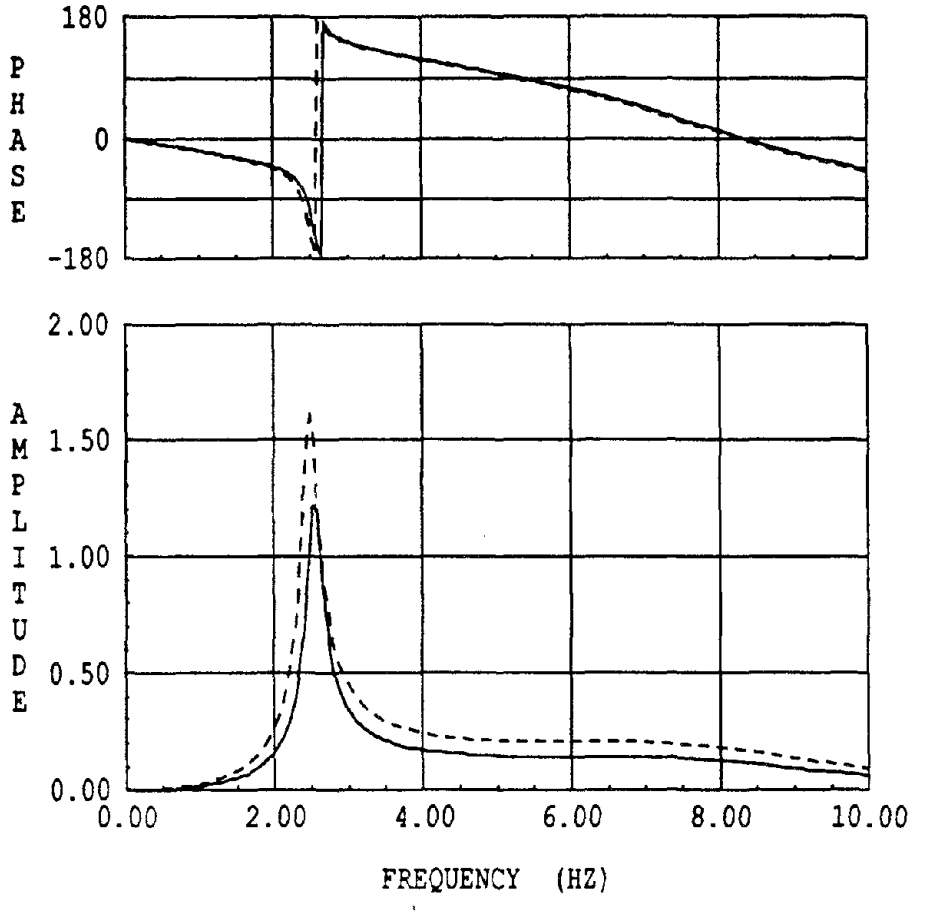

Fig. 8.6: Effect of Active Actuators in Reducing the Pitch Movement. Analytical Prediction Using Hybrid Model.

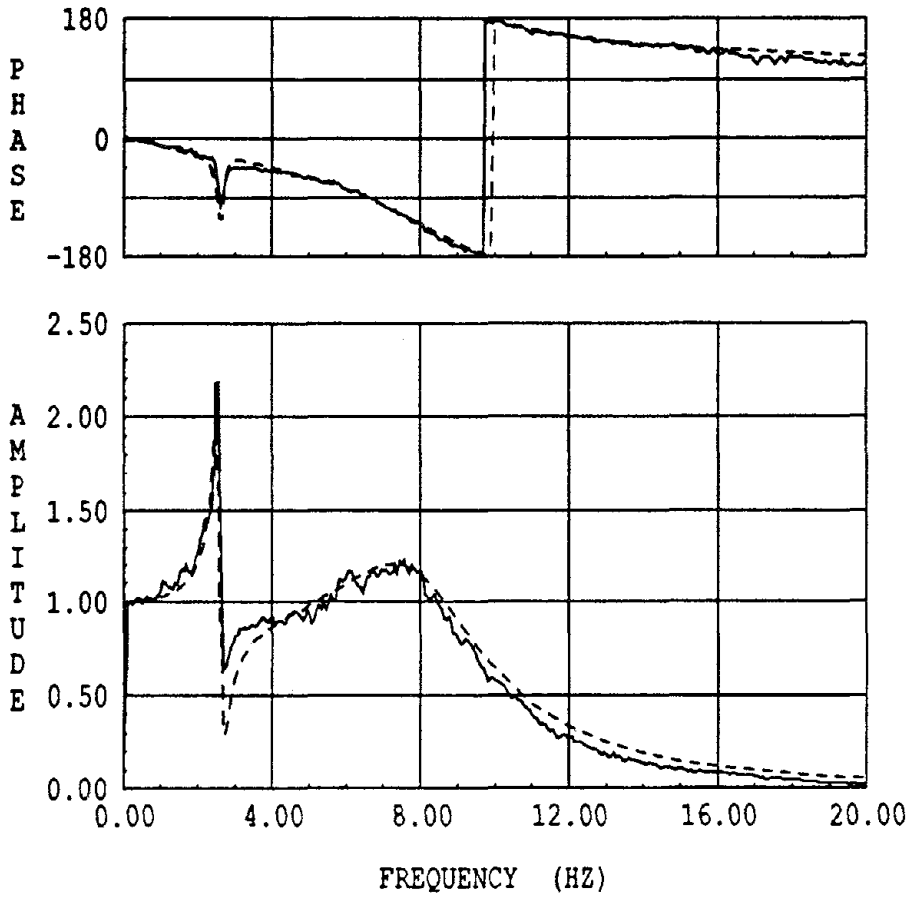

——— Experimental: Random Command Test
---- Hybrid Model

Fig. 8.7: Experimental and Hybrid Model Prediction of the Table Displacement over Command Displacement.

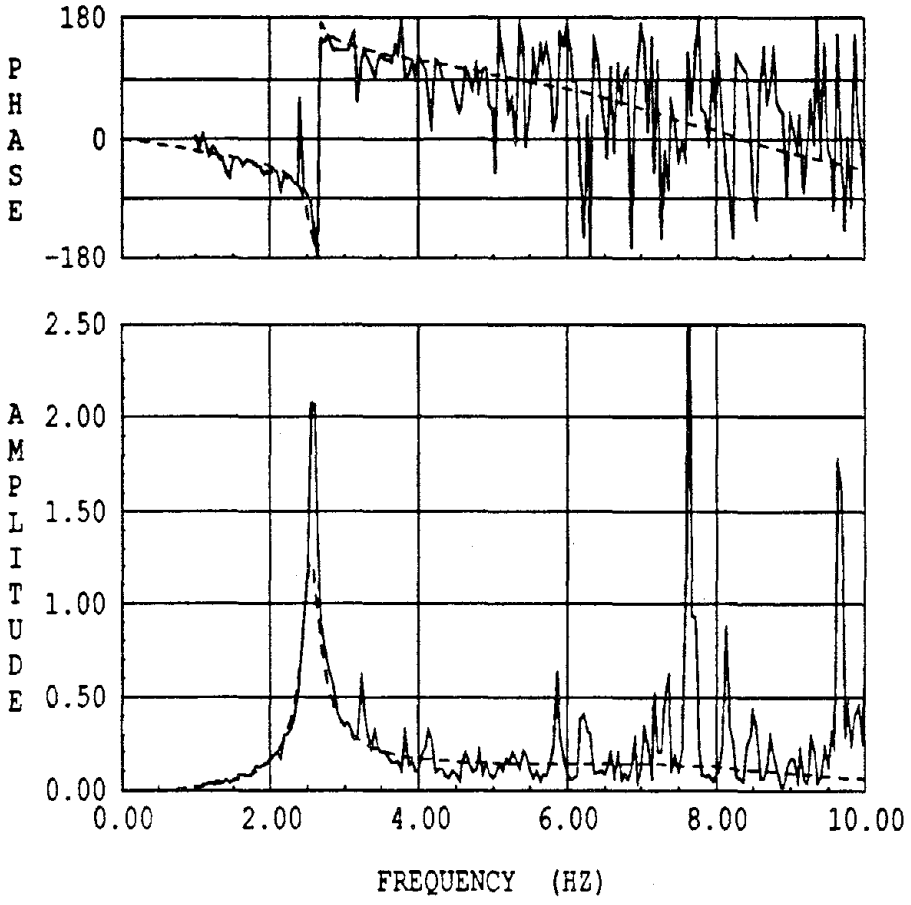

——— Experimental: Taft 200 Test
---- Hybrid Model

Fig. 8.8: Experimental and Hybrid Model Prediction of the Pitch Displacement over Command Displacement.

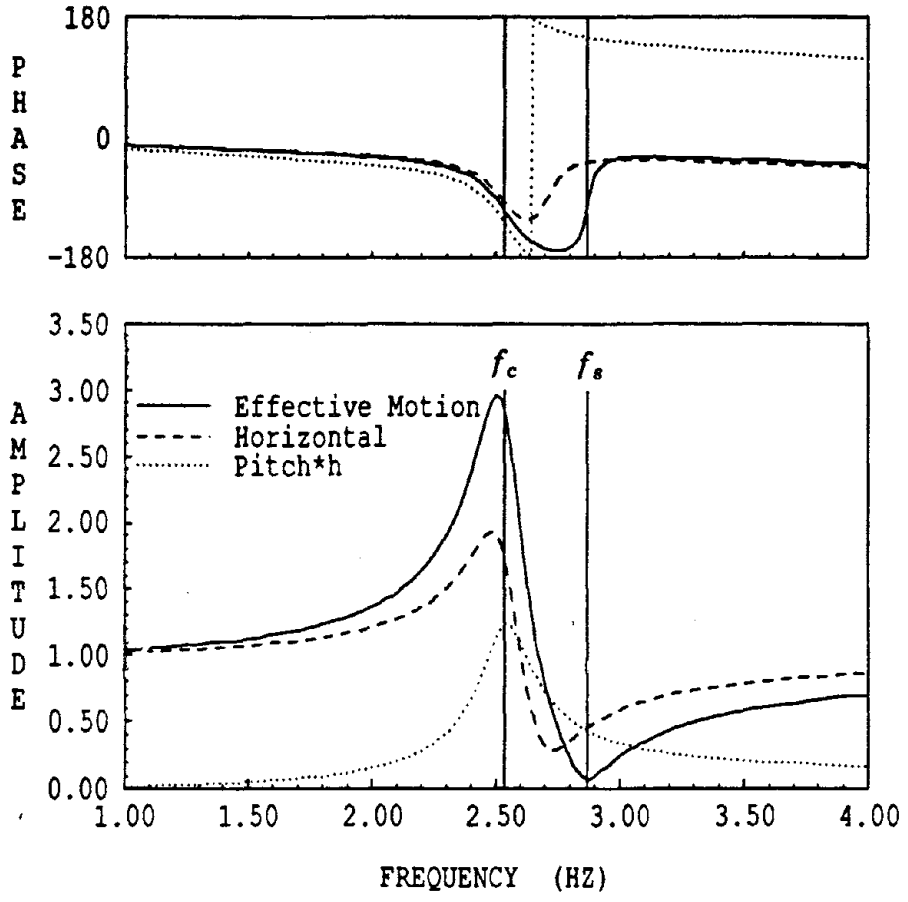

Fig. 8.9: Effective, Horizontal and Pitch Table Displacement over Command Displacement Transfer Functions.

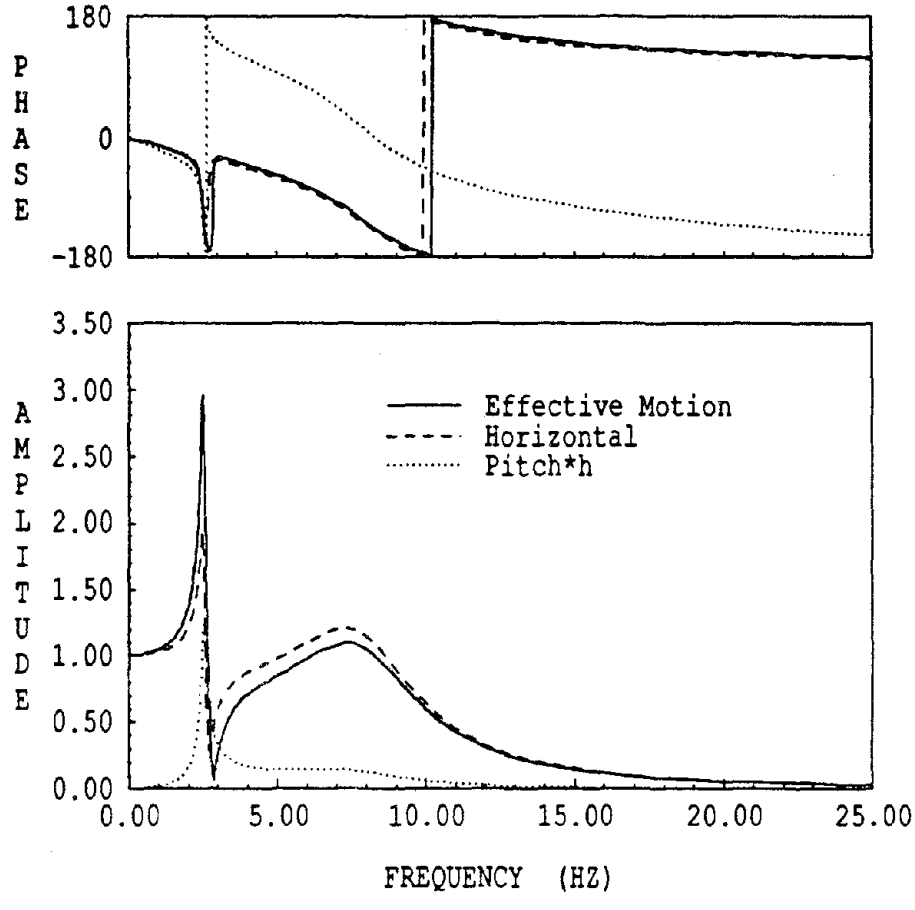

Fig. 8.10: Effective, Horizontal and Pitch Table Displacement over Command Displacement Transfer Functions.

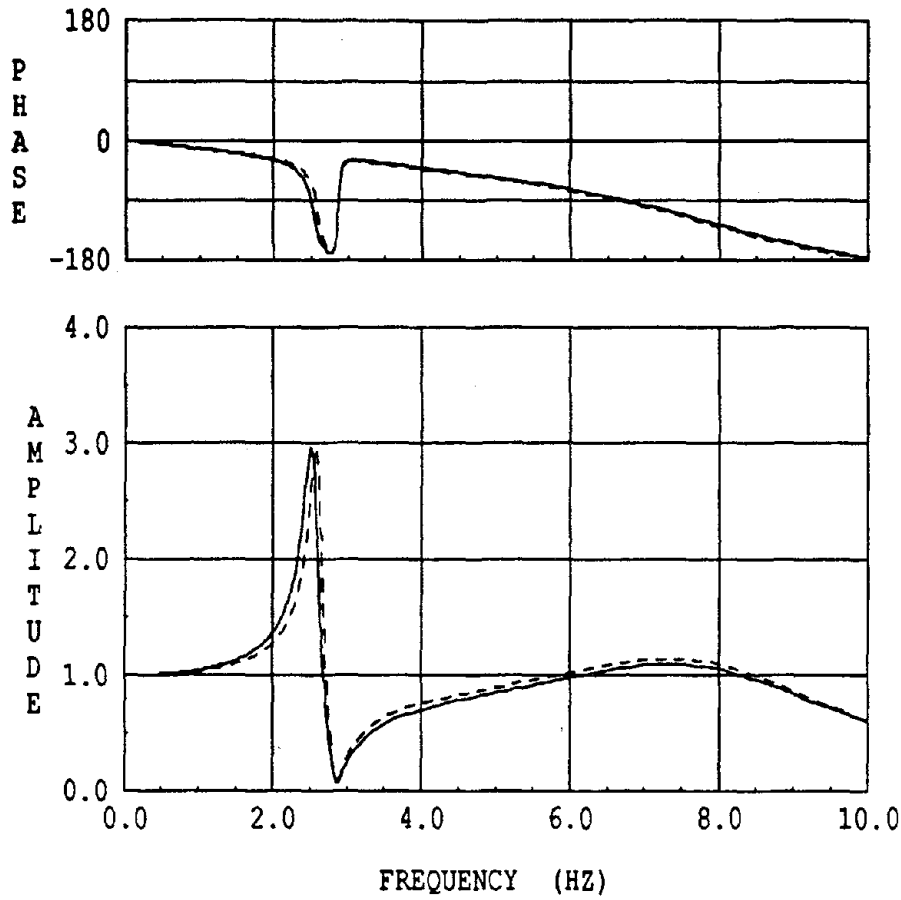

—— $k_\theta = 2.22 \times 10^7$ kip-in/rad

---- $k_\theta = 4.44 \times 10^7$ kip-in/rad

Fig. 8.11: Effect of Rocking Stiffness on the Effective Motion. Table Effective Displacement over Command.

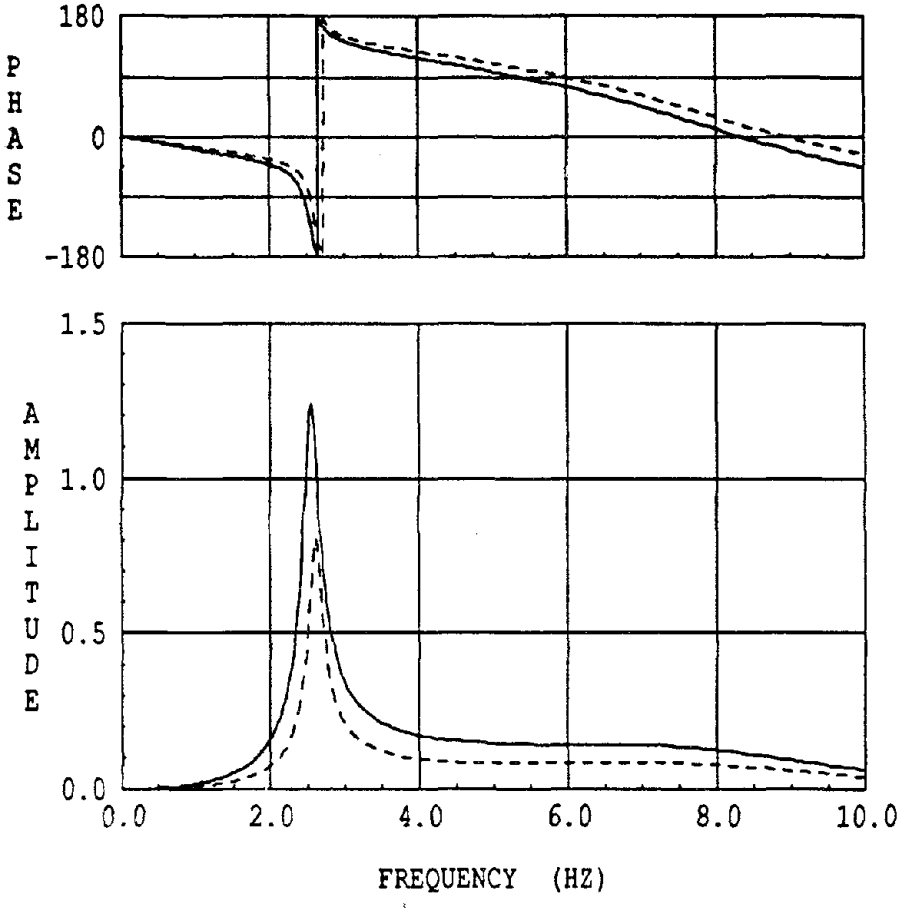

—— $k_\theta = 2.22 \times 10^7$ kip-in/rad

---- $k_\theta = 4.44 \times 10^7$ kip-in/rad

Fig. 8.12: Effect of Rocking Stiffness on the Rocking Motion. Table Pitch*h Displacement over Command.

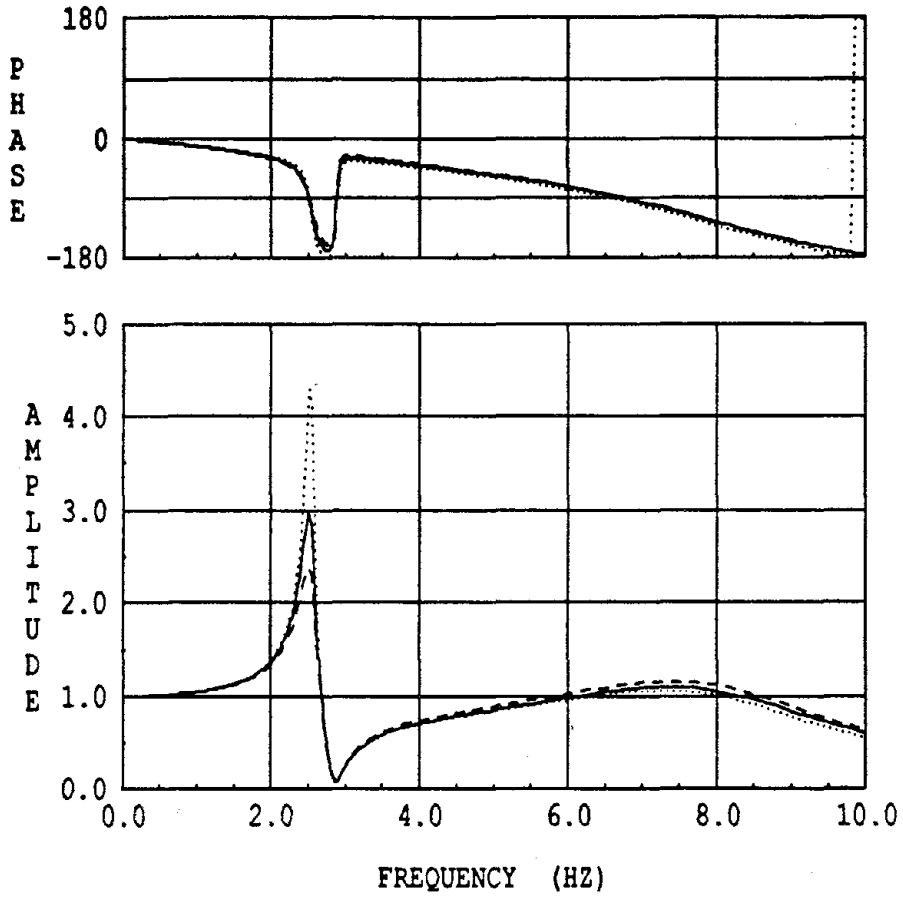

——— $c_\theta = 3.70 \times 10^5$ kip-in/(rad/sec)
- - - - $c_\theta = 7.40 \times 10^5$ kip-in/(rad/sec)
..... $c_\theta = 0.0$

Fig. 8.13: Effect of Rocking Damping on the Effective Motion. Table Effective Displacement over Command.

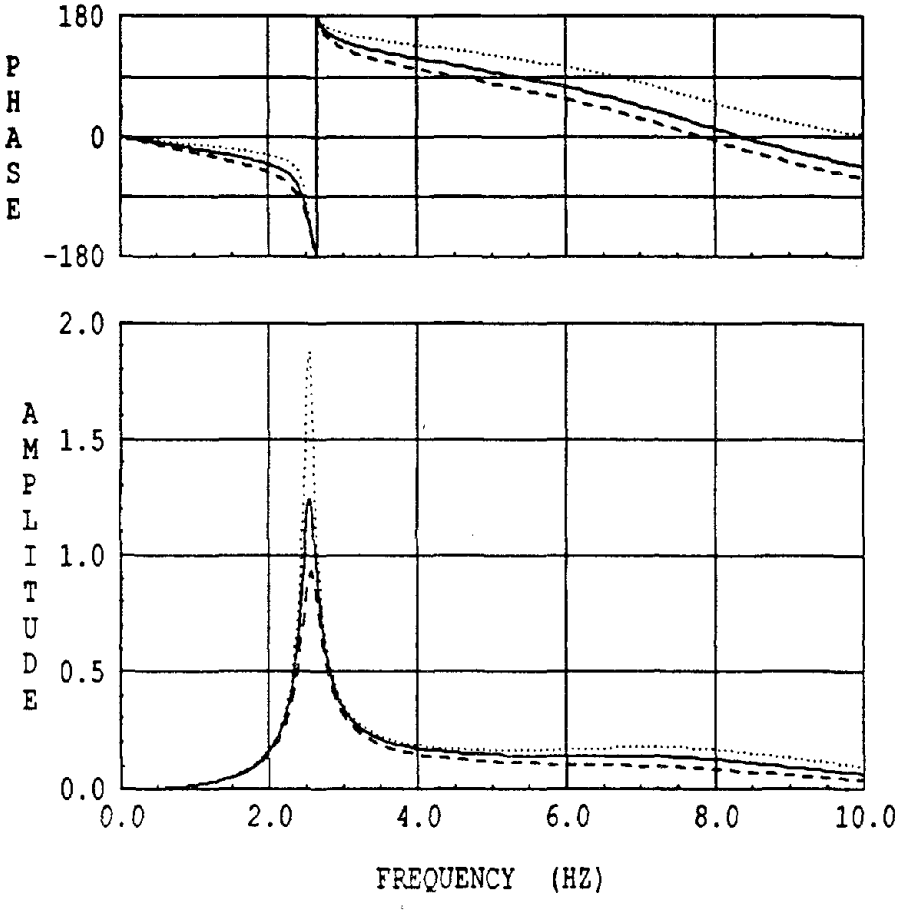

——— c_θ = 3.70 x10^5 kip-in/(rad/sec)
- - - - c_θ = 7.40 x10^5 kip-in/(rad/sec)
..... c_θ = 0.0

Fig. 8.14: Effect of Rocking Damping on the Rocking Motion.
Table Pitch*h Displacement over Command.

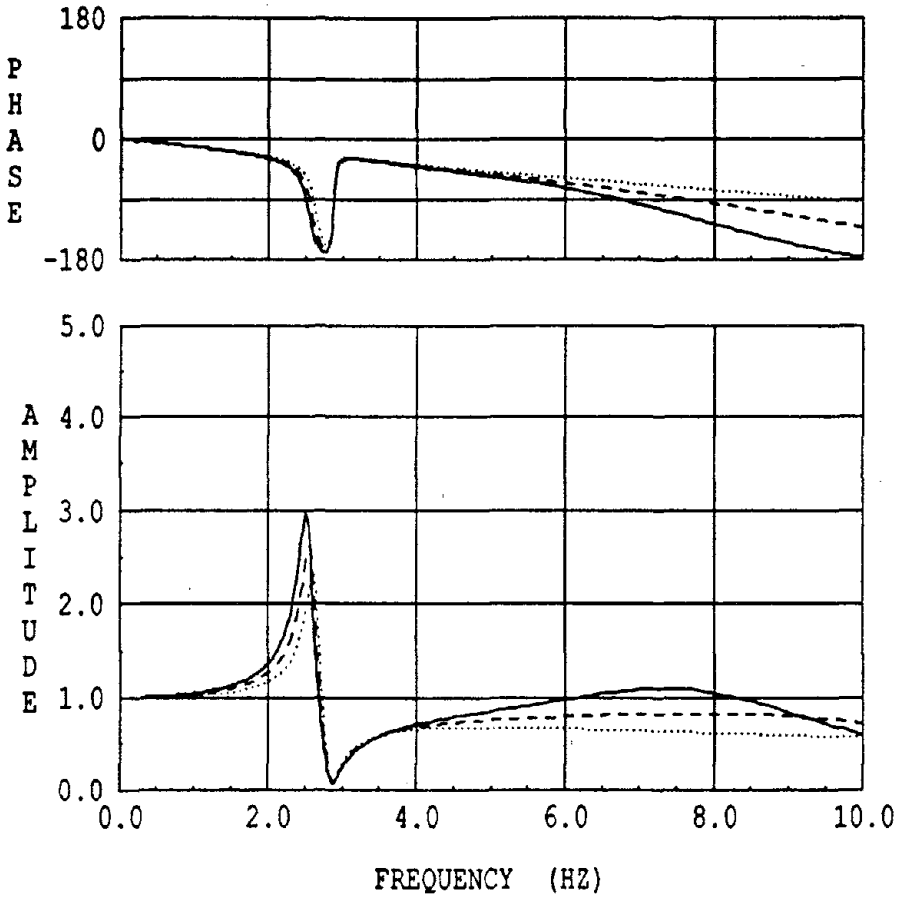

——— f_o = 9.6 Hz
- - - - f_o = 12.6 Hz
..... f_o = 20.0 Hz

Fig. 8.15: Effect of Open Loop Frequency on the Effective Motion. Table Effective Displacement over Command.

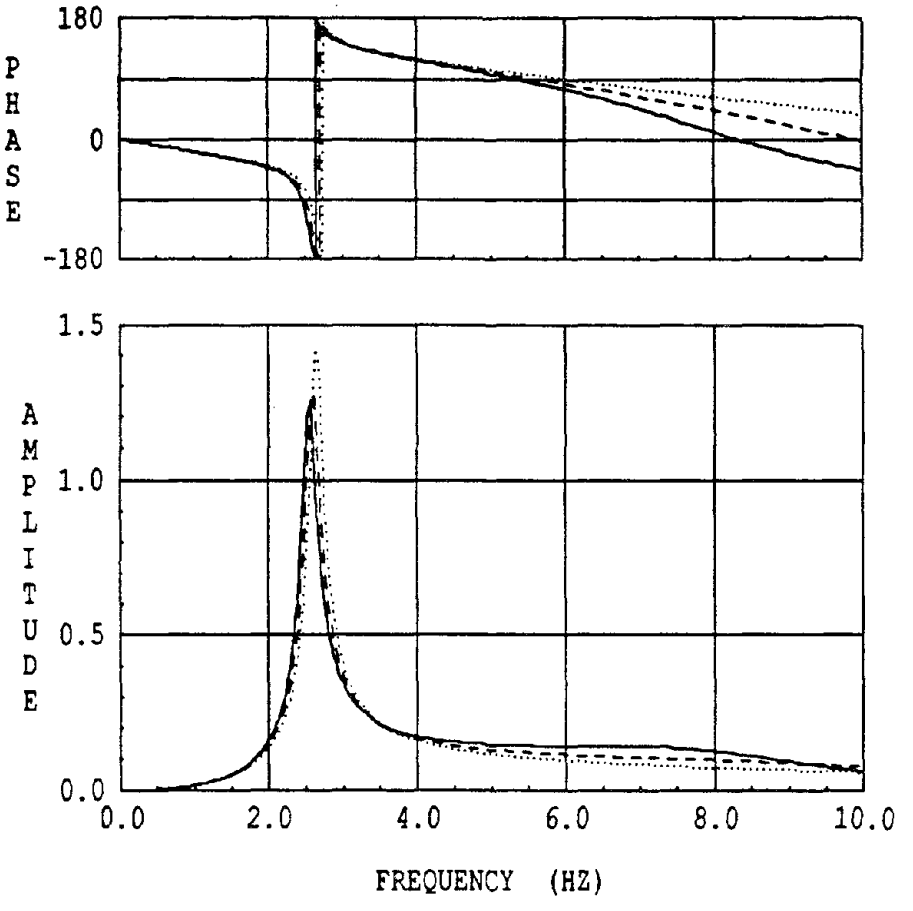

——— f_o = 9.6 Hz
- - - - f_o = 12.6 Hz
..... f_o = 20.0 Hz

Fig. 8.16: Effect of Open Loop Frequency on the Rocking Motion. Table Pitch*h Displacement over Command.

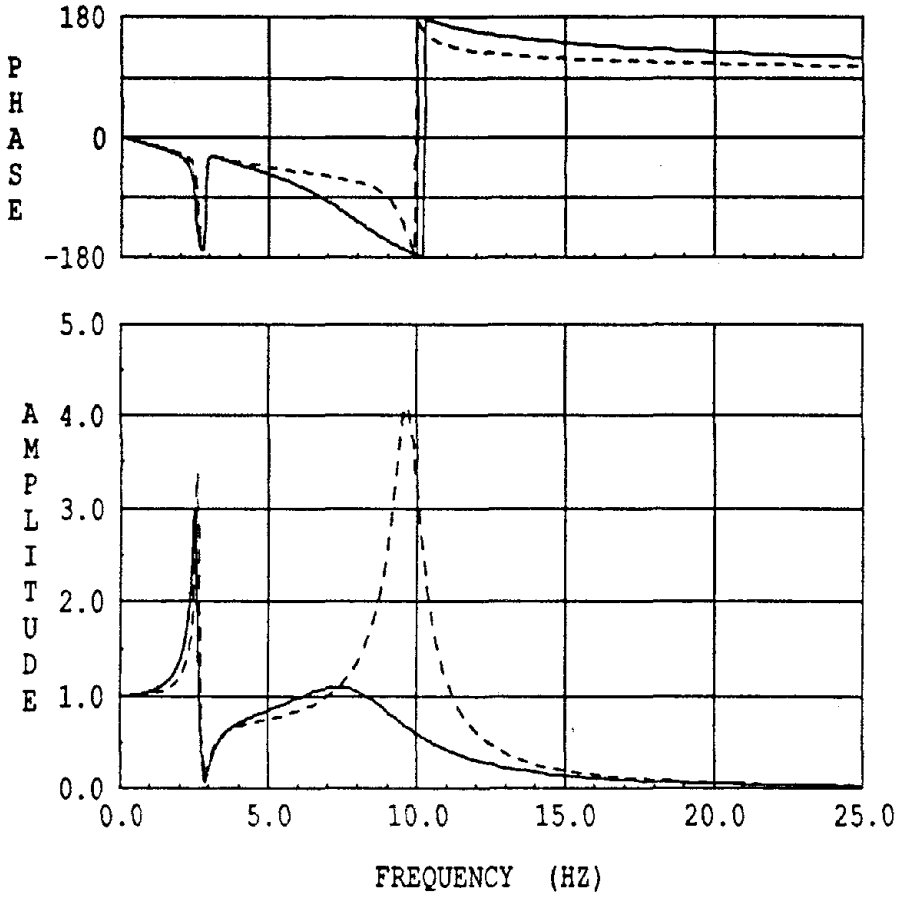

—— $\xi_o = 0.606$
---- $\xi_o = 0.303$

Fig. 8.17: Effect of Open Loop Damping on the Effective Motion. Table Effective Displacement over Command.

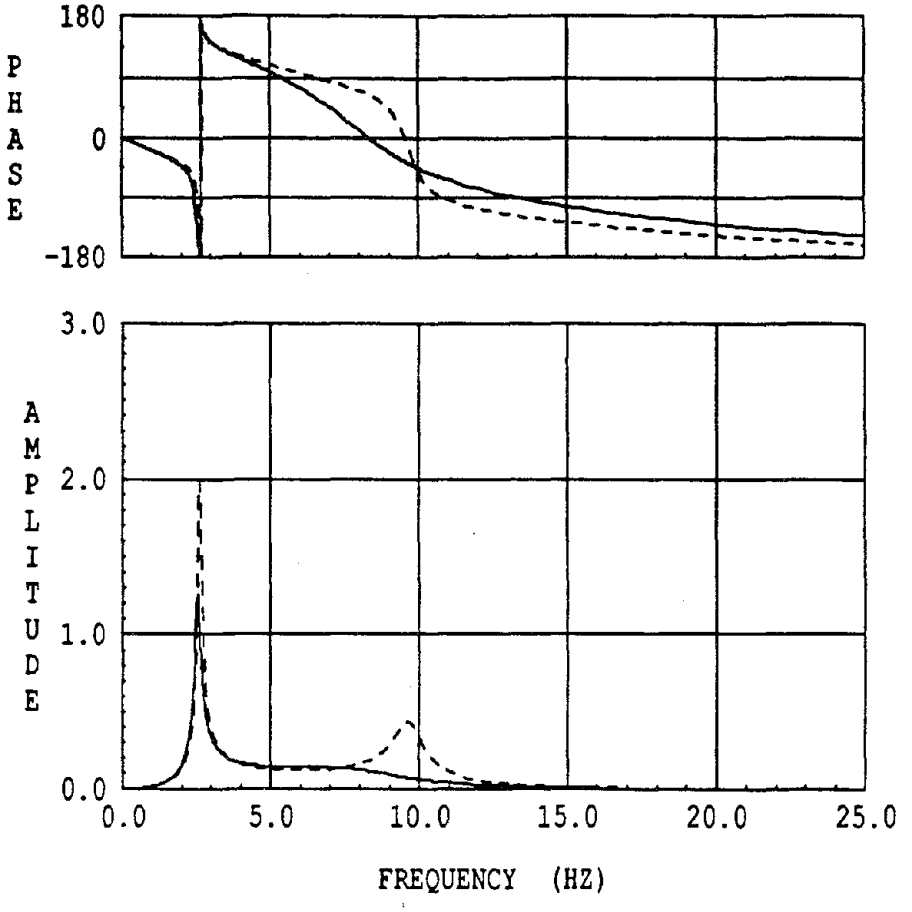

—— $\xi_o = 0.606$
---- $\xi_o = 0.303$

Fig. 8.18: Effect of Open Loop Damping on the Rocking Motion. Table Pitch*h Displacement over Command.

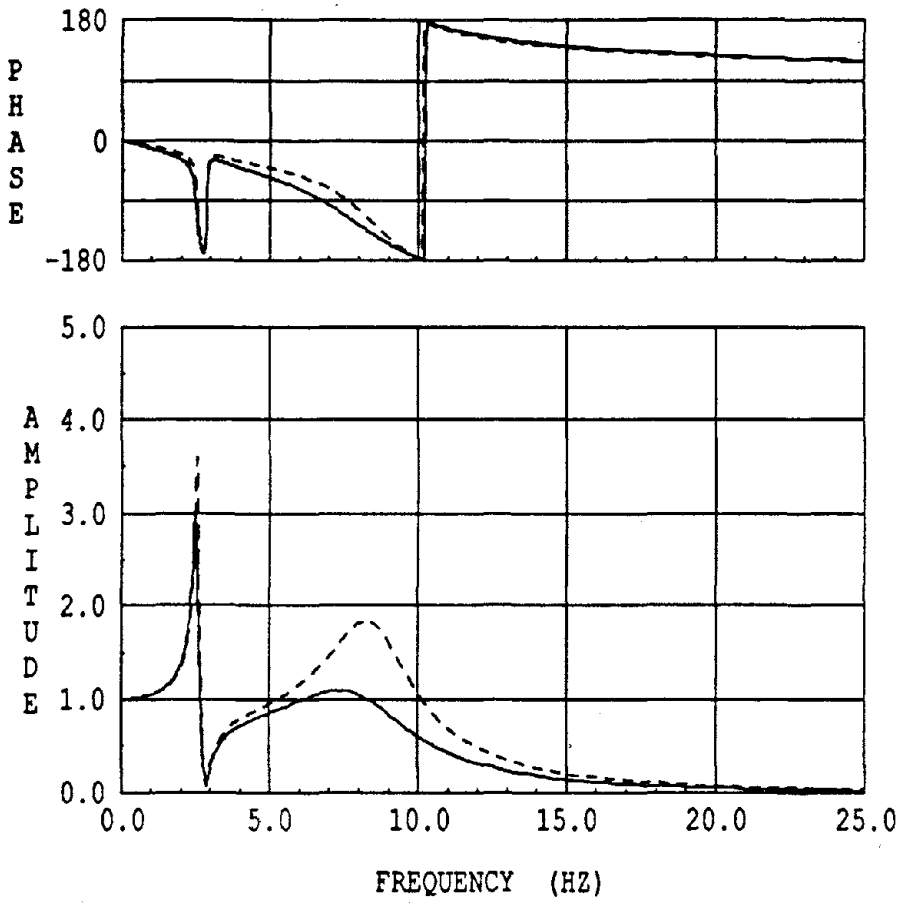

—— $k_o = 29.54$
- - - - $k_o = 40.00$

Fig. 8.19: Effect of Open Loop Gain on the Effective Motion. Table Effective Displacement over Command.

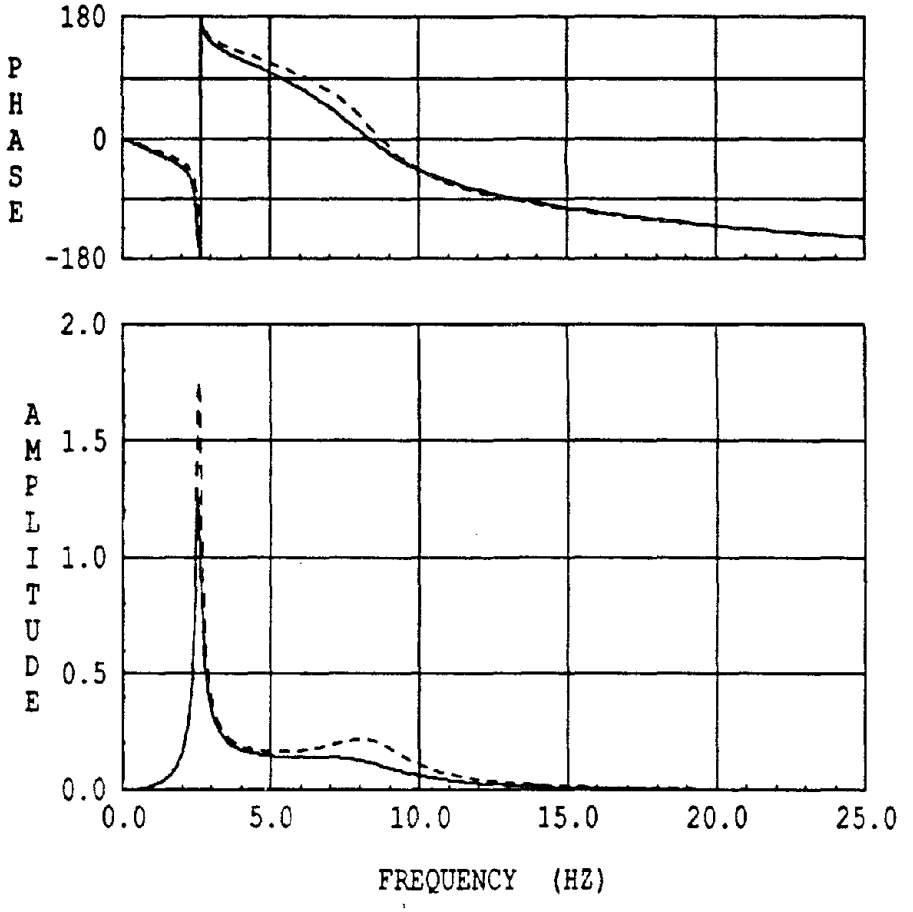

——— $k_o = 29.54$
- - - - $k_o = 40.00$

Fig. 8.20: Effect of Open Loop Gain on the Rocking Motion.
Table Pitch*h Displacement over Command.

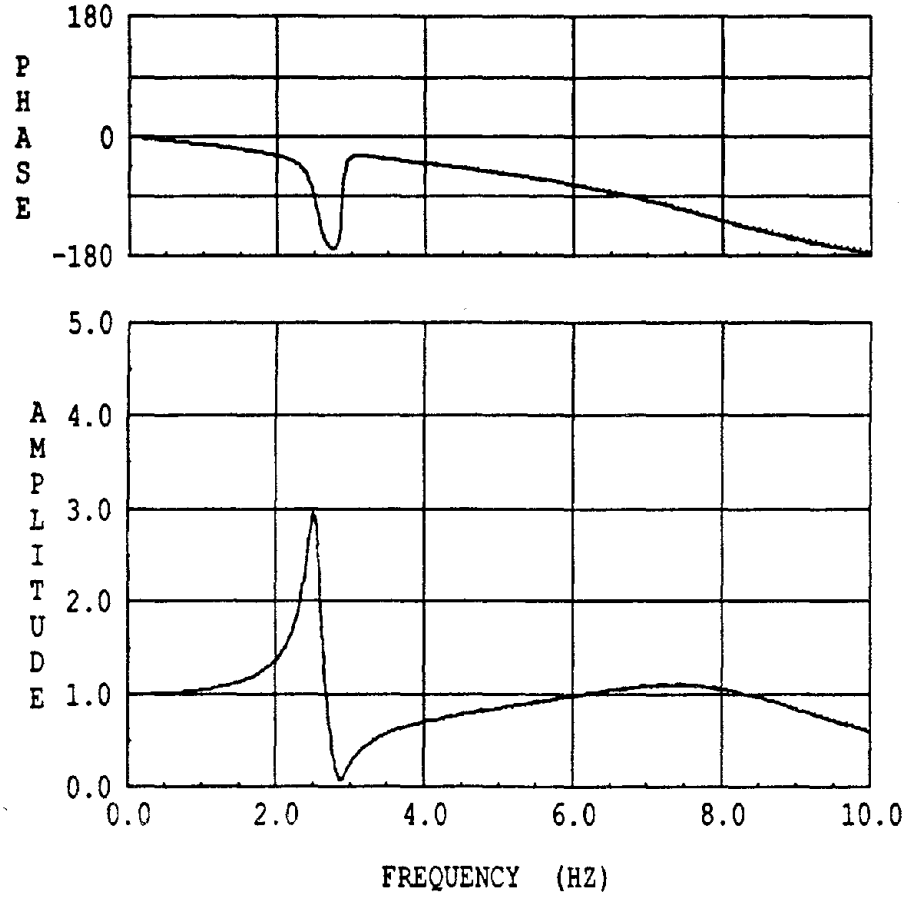

——— I = 1251 kip-in-sec2
---- I = 0
..... I = 5000 kip-in-sec2

Fig. 8.21: Effect of Bare Table Inertia on the Effective Motion. Table Effective Displacement over Command.

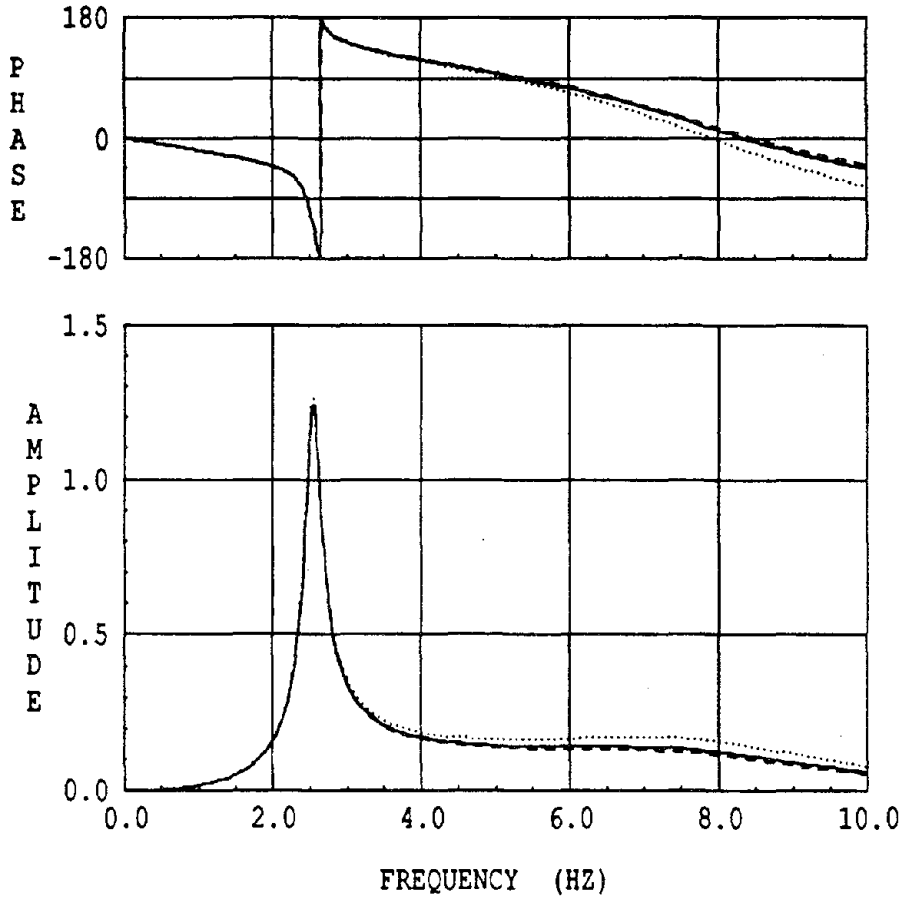

——— I = 1251 kip-in-sec2
---- I = 0
····· I = 5000 kip-in-sec2

Fig. 8.22: Effect of Bare Table Inertia on the Rocking Motion.
Table Pitch*h Displacement over Command.

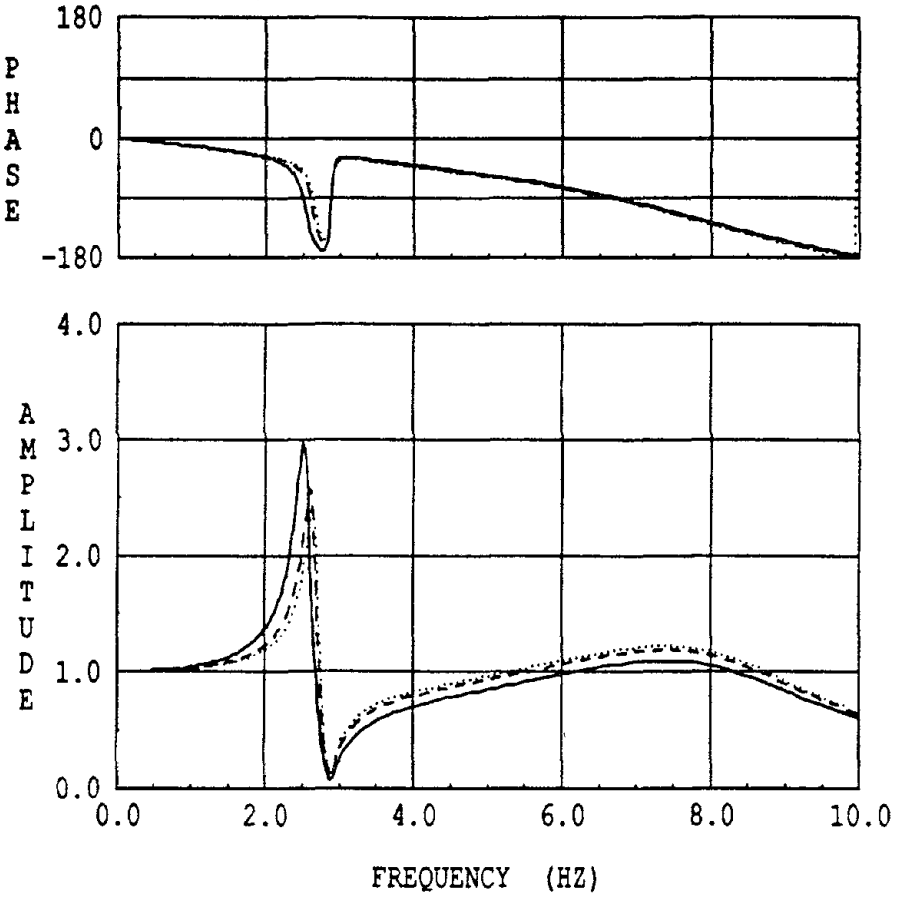

——— h = 219 in
---- h = 110 in
..... h = 0 in

Fig. 8.23: Effect of Structural Height on the Effective Motion. Table Effective Displacement over Command.

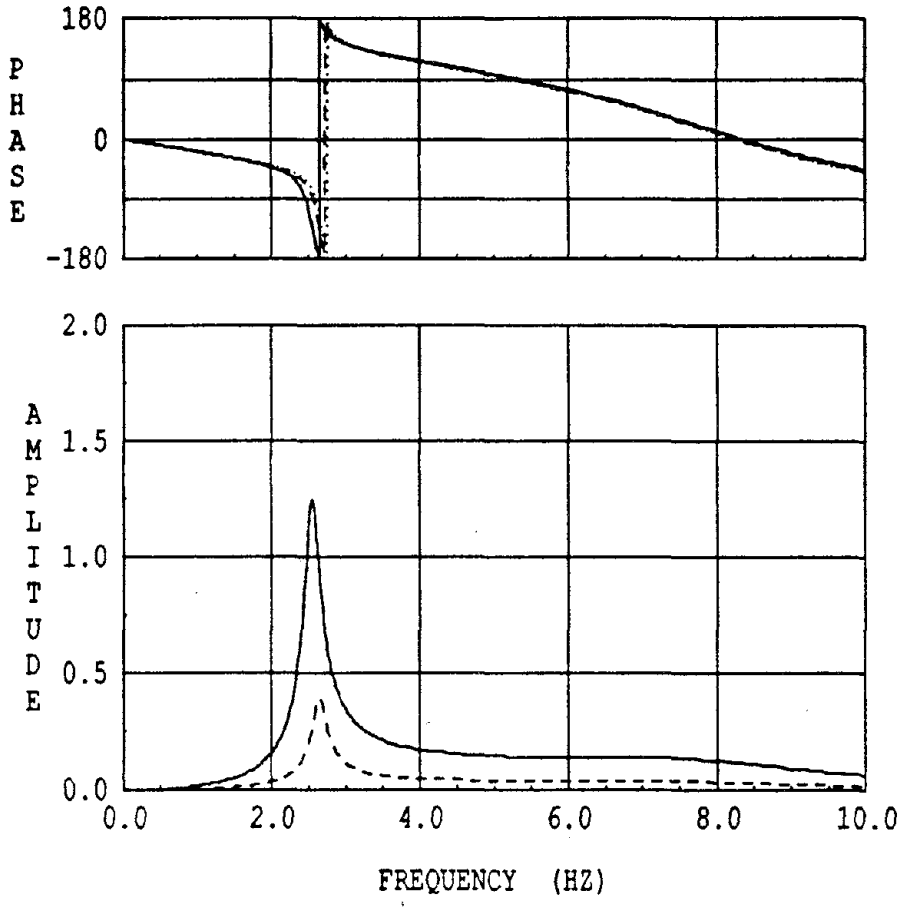

Fig. 8.24: Effect of Structural Height on the Rocking Motion.
Table Pitch*h Displacement over Command.

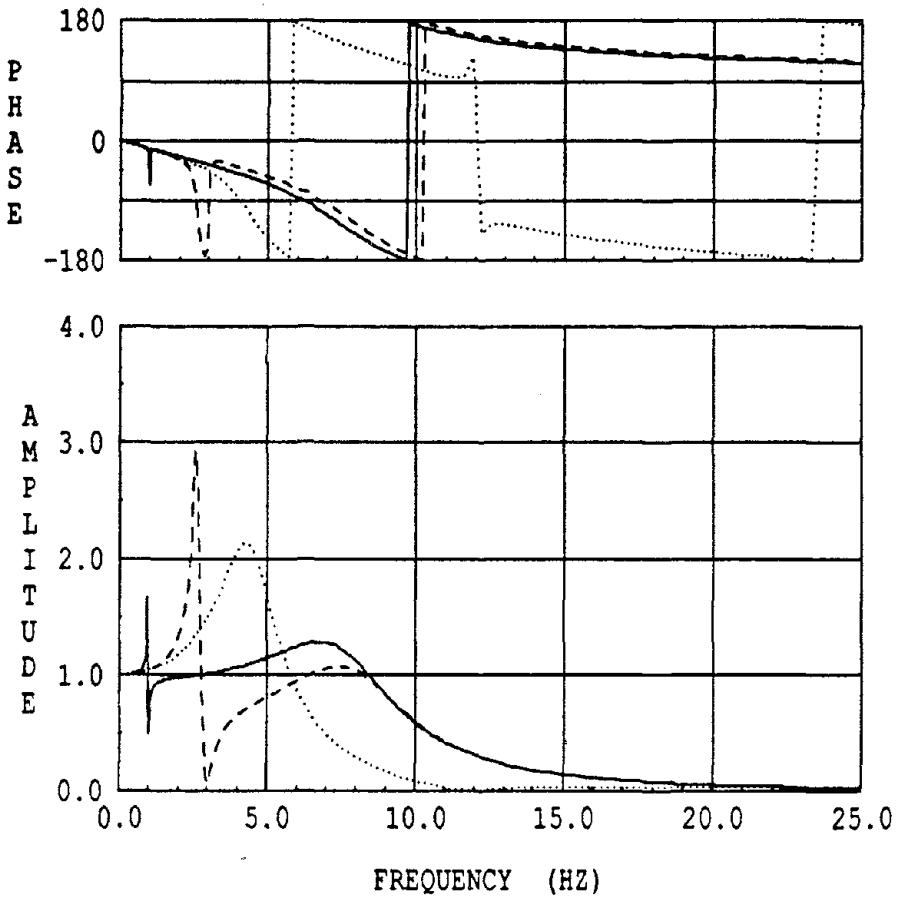

—— f_s = 1 Hz
---- f_s = 3 Hz
..... f_s = 12 Hz

Fig. 8.25: Effect of Structural Frequency on the Effective Motion. Table Effective Displacement over Command.

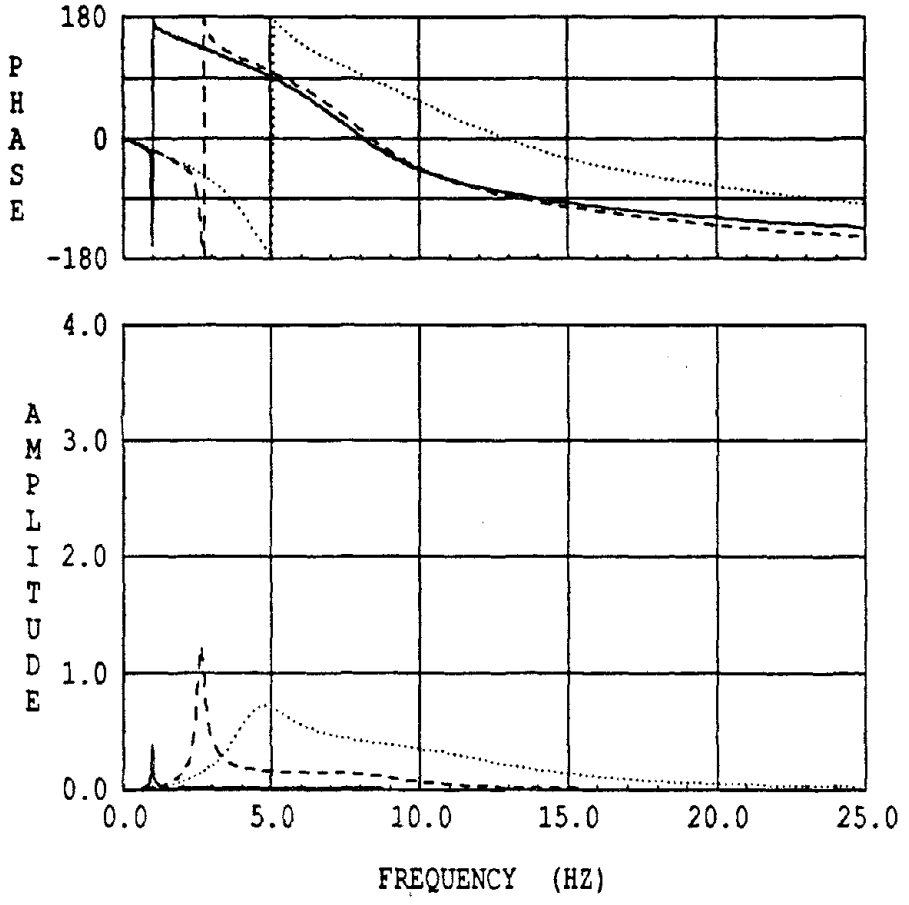

—— f_s = 1 Hz
- - - - f_s = 3 Hz
..... f_s = 12 Hz

Fig. 8.26: Effect of Structural Frequency on the Rocking Motion. Table Pitch*h Displacement over Command.

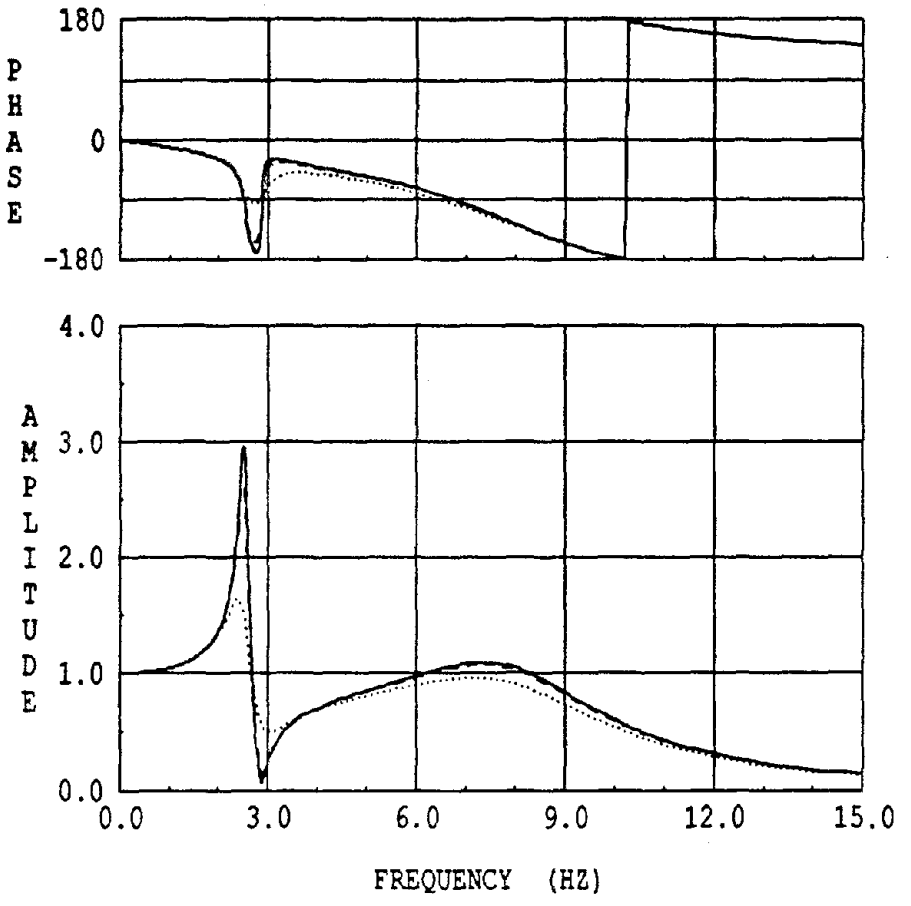

—— ξ_s = 1 %
---- ξ_s = 2 %
..... ξ_s = 10 %

Fig. 8.27 Effect of Structural Damping on the Effective Motion. Table Effective Displacement over Command.

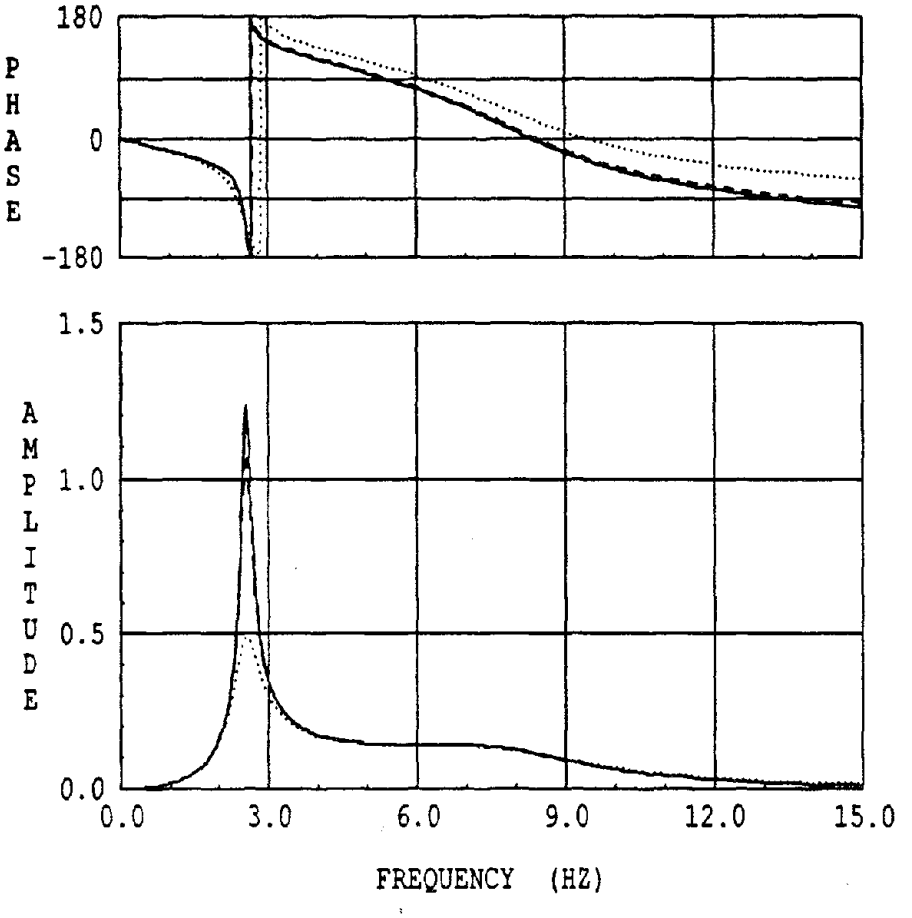

——— ξ_s = 1 %
- - - - ξ_s = 2 %
..... ξ_s = 10 %

Fig. 8.28 Effect of Structural Damping on the Rocking Motion. Table Pitch*Height Displacement over Command.

Chapter Nine
EFFECT OF SHAKING TABLE-STRUCTURE INTERACTION ON THE RESPONSE OF SDOF STRUCTURES

9.1 INTRODUCTION

In Chapter 8, models for the behavior of two-directional shaking table were presented. These models include the interaction in the horizontal as well as the rocking degrees-of-freedom. The hybrid model consists of a feedback control mechanism in the horizontal degree-of-freedom but only a rocking spring and dashpot in the pitching degree-of-freedom. This model was found to be simple and effective for representing the assumed linear system. In this chapter the hybrid model is used for studying the effect of interaction on structures mounted on the shaking table. Other simpler models will also be used as mentioned in Section 9.4 in order to identify the interaction mechanism. The effect of shaking table-structure interaction is studied here by means of response spectra comparisons of three different earthquake records. The interaction effects also are examined through the coupled modes of the table-structure system.

9.2 RESPONSE SPECTRA EVALUATION

A response spectrum represents the maximum structural response of a SDOF system to a given earthquake record for a range (i.e. spectrum) of structural frequencies. For the hybrid model case described in Section 8.6 and for the model parameters listed in Table 9.1, which are equivalent to those shown in Table 8.1, the maximum response can be determined for different structural periods by solving Eq. (8.37) using the fourth order Runga-Kutta integration technique. The command displacement history x_c in Eq. (8.37) was obtained from the corrected accelerogram, by integrating the most intense portion of a given earthquake record. Three different records were used in this study: the 1952 Taft (N21E), the 1957 Miyagi-Ken-Oki and the 1985 Mexico (N90W) earthquake records. All records were

Preceding page blank

scaled so that the range of displacement is 4 inches. The first two records were used in the shaking table tests with a prototype/model length scale factor of 3.2801 corresponding to a time scale factor of 1.811. The Mexico record was used in this analytical study with a length scale factor of 4, i.e. a time scale factor of 2. In the cases of the Taft earthquake, the corrected accelerogram was that distributed by Caltech [35]. The Mexico 1985 record was processed using a trapezoidal bandpass filter with corner frequencies at 0.5, 0.55, 23 and 24 Hz. Some further adjustment was done to the displacement signal to insure the zero initial and final conditions. The corresponding acceleration signal, used as input in the analysis of the SDOF system, was obtained by numerical differentiation of the adjusted displacement record. Two differentiation schemes were used, namely the first order forward difference scheme and the central difference scheme. Results of both schemes were very similar because of the lack of high frequencies in the displacement records.

The displacement signals used in this study are shown in Figs. 9.1a, 9.2a and 9.3a; the corresponding acceleration signals and amplitude spectra are shown in Parts b and c, respectively, of these figures. In this chapter the pseudo velocity response spectrum is used for comparison. It represents the product of the circular fixed-base frequency with the maxima of the displacement responses. The systems considered and the comparisons of the response spectra are described in Sections 9.4 and 9.9, respectively.

9.3 COUPLED SYSTEM PARAMETERS

If a system has a certain fixed-base frequency and damping, when loaded on a shaking table which has flexibilities in the horizontal and rocking degrees-of-freedom it will respond mainly at a lower frequency called the coupled structural frequency and usually, but not always, with higher damping called the coupled damping ratio. In order to understand the interaction mechanism and the difference in the calculated response spectra, the coupled system parameters were computed. There are higher coupled frequencies in the response which correspond to the frequencies associated with the shaking table flexibilities. However, in our case these higher

frequencies do not contribute to the response because of the lack of high frequencies in the earthquake records used.

The coupled frequencies listed in this chapter were computed by solving the eigenvalue problem

$$\mathbf{FV} = \underline{\lambda}\mathbf{V} \tag{9.1}$$

where $\underline{\lambda}$ is a diagonal matrix of eigenvalues λ_k, and **V** is a matrix whose columns constitute the eigenvectors of **F**. For the hybrid model, the matrix **F** was defined in Eq. (8.37). Since **F** is normally unsymmetric, the eigenvalues and eigenvectors are complex valued. A typical eigenvalue can be written as

$$\lambda_k = R_k + jC_k \tag{9.2}$$

where R_k and C_k are the real and imaginary parts, respectively, and $j = \sqrt{-1}$. The frequency and damping can then be computed as

$$\omega_k = \sqrt{R_k^2 + C_k^2} \tag{9.3}$$

$$\xi_k = -\frac{R_k}{\sqrt{R_k^2 + C_k^2}} \tag{9.4}$$

Note that not all λ_k are complex; some are real valued corresponding to non-vibratory decaying exponential response. Note also that any eigenvalue of positive real part (i.e. $R_k > 0$) leads to a negative damping ratio as given by Eq. (9.4). Negative damping ratios indicate a system with infinitely growing exponential response, which implies system instability. Hence, eigenvalue estimation of the system matrix **F** constitutes one way of checking for system stability.

9.4 ANALYTICAL MODELS CONSIDERED

The various analytical models for the shaking table used in this study are as follows:

Hybrid model — The horizontal interaction is modeled by a linear feedback control system, which includes the displacement, velocity and force feedback as described

in Chapter 6. The rocking flexibility is modeled by rotational springs and dashpots as described in Chapter 8. This is considered to be the best linear model used in this study. The characteristics of this model are listed in Table 9.1. These parameters were found to represent the current system configuration as shown in Chapter 8. The main assumption here is that the system is linear. System linearity in shaking tables may be questioned because of many factors as described in Appendix C. However, in general, the system can be considered to be linear about its operation point. The mathematical model is presented in Section 8.6.

One Directional Model — In this model the shaking table is represented by a one degree-of-freedom system and includes the feedback system in the horizontal degree-of-freedom. There is no flexibility in the rocking degree-of-freedom. This model was presented in Chapter 6. The parameters of this model are the same as those of the hybrid model except that no rocking is allowed. This permits study of the influence of the horizontal interaction independently of the rocking interaction.

Rocking Model — The shaking table is modeled in this case by an inertial mass with a rotational spring and a dashpot. The rocking flexibility is the same as was given by the hybrid model. This model is intended to compare the contribution of the rocking interaction to the total system interaction; it is shown in Fig. 5.2.

Mechanical Model — This system was described in detail in Chapter 5. The table is modeled as a rigid mass with

translational as well as rotational inertia, and is connected to horizontal and rocking springs and dashpots. The characteristics of this model are listed in Table 9.3. The system parameters were evaluated using methods described in Chapter 5. A schematic of this model is shown in Fig. 5.1.

9.5 EFFECT OF VARYING STRUCTURAL FREQUENCY ON THE COUPLED SYSTEM PARAMETERS

Since the total structural response is a direct function of the coupled system properties [13], coupled parameters of this type have been used frequently in estimating soil-structure interaction effects [14]. Understanding the variation in coupled system parameters will help in understanding the interaction phenomenon. The effect of varying the structural frequency on the coupled system will be investigated using different shaking table models.

Table 9.1 shows the parameters of the hybrid model including a SDOF structure. The SDOF structure parameters are those identified from the system tested on the shaking table. Table 9.2 shows the coupled system parameters for the above listed model values computed by the procedure described in Section 9.3. The structural response for this system subjected to typical earthquake records in which the major part of the ground motion has frequency content below 5 cycles per second is governed mainly by the first coupled system mode which has a frequency of 2.54 Hz and damping of 4 percent.

By varying the structural frequency f_s from the value of 2.87 shown in Table 9.1 and evaluating the corresponding first coupled frequency and damping, the results shown in Figs. 9.4 and 9.5 for the coupled frequency and damping, respectively, are obtained. For the hybrid model case in these figures it can be clearly seen that for a structural frequency lower than 1 Hz, the coupled system mode is virtually the same as the fixed-base structural mode; hence the interaction effect is negligible for this range of frequencies. For structural frequencies in the range of 1-5 Hz, the ratio of the

coupled structural frequency to the fixed-base frequency varies from 0.98 at 1 Hz to 0.72 at 5 Hz. The ratio between the damping in the fixed-base structure to that of the coupled system varies from 1.14 at 1 Hz to 10.7 at 5 Hz. For the higher frequency range 5-10 Hz, the coupled frequency does not change appreciably and stays around 4 Hz. The coupled damping however varies from 10.7 percent to 20 percent. The general trend in this case is that the coupled system frequency is always lower than the fixed-base system frequency. The damping, on the other hand, is higher in the coupled system. Figures 9.4 and 9.5 show these variations, but it should be emphasized here that these curves were predicted on the basis of the current control system settings of the shaking table and assume a linear system.

Figures 9.4 and 9.5 also show similar results for the case where there is no flexibility in the rocking direction (i.e. horizontal interaction only). This case is equivalent to the unidirectional shaking table treated in Chapter 6. The coupled system parameter variation is remarkably similar to that in the hybrid model case where rocking is considered. The coupled frequencies are consistently slightly larger than in the case with two-directional flexibility. Coupled damping on the other hand is slightly lower at frequencies lower than 6 Hz and higher for frequencies larger than 6 Hz.

Similar results are also seen in Figs. 9.4 and 9.5 for the rocking model which has no horizontal flexibility. Again the phenomenon is remarkably similar, except that the coupled frequencies are slightly larger than those in the pure horizontal case or the hybrid case. The damping is significantly lower than in the two-directional interaction case except for frequencies near 10 Hz. The damping is consistently lower in the horizontal interaction case.

The effect of varying the structural frequency can be looked at from a different perspective by using the transfer function of the effective rigid body translation of the structural mass $x_h + \theta h$ with respect to the command displacement x_c as indicated in Fig. 8.25 of Chapter 8. In this figure the transfer function is evaluated using the hybrid model for frequencies of

1, 3 and 12 Hz. For the low levels of fixed-base damping that pertain to our case, the notches of the transfer function coincide with the fixed-base frequency. The peaks on the other hand occur at frequencies slightly lower than the coupled system frequencies. Note that as the fixed-base frequency increases, the peak and notch tend to depart from each other and also to become broader. The increase in separation means in this case that the difference between the fixed-base and coupled frequencies becomes larger, as Fig. 9.4 indicates. The broader peaks indicate increases in the structural damping for higher frequencies as was seen in Fig. 9.5.

The effect of varying the structural frequency for a SDOF system with a relatively large amount of damping (10 percent) is shown in Fig. 9.6. In this case, the damping in the coupled system is slightly lower than in the fixed-base system for frequencies smaller than 2.5 Hz, but it starts increasing for higher frequencies. It is clear from Fig. 9.6 that structures with already high fixed-base damping would not undergo a large variation of the damping due to interaction.

9.6 EFFECT OF VARYING STRUCTURAL DAMPING ON THE COUPLED SYSTEM PARAMETERS

Figures 9.7 and 9.8 show the effect of varying the fixed-base structural damping for the hybrid system described in Table 9.1. The effect of structural damping on the coupled mode frequency can be seen to be negligible from Fig. 9.7. The coupled damping is shown in Fig. 9.8 to vary linearly with the fixed-base damping. It is important to note that a system with zero fixed-base damping will have 3.33 percent coupled damping, while a system with fixed-base damping of 20 percent will have a coupled damping of 16.8 percent. Thus the coupled damping value is larger if the fixed-base damping is less than 10 percent, but it is lower than ξ_s for higher values of fixed-base damping.

9.7 EFFECT OF VARYING STRUCTURAL MASS ON THE COUPLED SYSTEM PARAMETERS

The effect of varying the structure mass m_s, while keeping the structural frequency, damping and height as those in Table 9.1, is shown in Figs. 9.9 and 9.10. For a larger mass, the difference between the fixed-base frequency and the coupled frequency becomes larger. The coupled damping, on the other hand, is higher for larger mass and low fixed-base frequencies, and it is lower for larger mass and higher fixed-base frequencies.

9.8 EFFECT OF VARYING STRUCTURAL HEIGHT ON THE COUPLED SYSTEM PARAMETERS

The effect of varying the structural height h is shown in Figs. 9.11 and 9.12. For higher h the difference between the fixed-base frequency and coupled frequency becomes larger. The coupled damping, on the other hand is higher for higher h and low fixed-base frequencies and lower for higher h and higher fixed-base frequencies. It is clear that increasing either the mass or the height of the structure causes very similar effects on coupling and interaction.

9.9 RESPONSE SPECTRA COMPARISONS

The pseudo-velocity response spectra of the Taft 1952 Record, the 1957 Miyagi-Ken-Oki Record and the 1985 Mexico Record are shown in Figs. 9.13, 9.14 and 9.15, respectively. The damping assumed in the fixed-base system used in the response analysis is 1 percent. The figures show the effect of the horizontal interaction and the two-directional interaction that includes horizontal and rocking components as compared with the fixed-base response. It is clear that for periods above one second the interaction effects are negligible. This is due to the fact that the coupled system frequency and damping, as shown by Figs. 9.4 and 9.5, are almost the same as those of the fixed-base model. For periods lower than 1 second, the interaction generally, but not always, produced lower responses. That reduction is due mainly to the increase in damping in the coupled system as shown by Fig.

9.5. However, since the coupled systems have higher periods, this reduction is not always achieved as shown by the spectrum of Fig. 9.13.

The horizontal interaction spectrum is not very different from the hybrid model spectrum, for all three earthquakes; however, it is lower than the hybrid model response for periods near 0.1 seconds as a result of the higher damping in the coupled system as shown in Fig. 9.5. The main reason for including the Mexico record was its special frequency characteristics. It was believed that such frequency concentration near 1 Hz would amplify the peak and notch effects and produce some significant interaction. It turned out that this interaction, as shown in Fig. 9.15, was the least in comparison with the response spectra for other earthquakes shown in Figs. 9.13 and 9.14. One reason for this lower interaction is that the coupled mode behavior near 1 Hz is virtually the same as for the fixed-base mode, not to mention that the peak and notch in the transfer function are significantly reduced for structures with frequencies near one Hz (see for example Fig. 8.25).

In order to produce significant interaction, the dominant frequency of the earthquake record should be higher than one Hz. To increase the dominant frequency to 2.5 Hz in the Mexico record would correspond to a length scale factor of 25 or correspondingly a time scale factor of 5. If this scale factor is used and the damping is increased to 10 percent in the fixed-base structure, the response spectra for the Mexico record will be as seen in Fig. 9.18. The response spectra for the Taft and Miyagi-Ken-Oki records also have been calculated for 10 percent structural damping as shown in Figs. 9.16 and 9.17. It is clear by comparison of these figures with Figs. 9.13 and 9.14 that the interaction effect is reduced significantly for a higher amount of structural damping. It can also be seen from the spectra of the Mexico record (Fig. 9.18) that the peak and notch in the transfer function still did not cause the anticipated change in the response for this narrow-banded input signal.

Figures 9.19, 9.20 and 9.21 present the response spectra of the rocking model together with those of the Hybrid and SDOF models. The peak

responses shown in these figures agree very well for high periods. For the lower periods, the rocking model, in general, gives results that lie between those of the two other models. The rocking model coupled period is higher than that of the hybrid model and generally, it has lower damping. This explains the spectrum variation of the rocking model, since an increase in damping causes the response spectrum to decrease in amplitude.

Figures 9.22-9.24 show the rocking interaction effects for higher damping values. It is clear here that the interaction effects are less significant and that all interaction models produce very similar results.

It can be said here that the effect of the horizontal and rocking interactions can be characterized by the variation in the coupled system parameters; that is, by an increase in the period and a change in damping.

9.10 MECHANICAL VERSUS HYBRID MODEL

The mechanical model parameters are listed in Table 9.3. When the structural frequency f_s is varied, the effect on the mechanical coupled system parameters can be evaluated with results as plotted in Figs. 9.25 and 9.26; also shown are the corresponding results for the hybrid model case. It can be seen from these figures that the mechanical model predicts accurately the coupled frequency. Damping errors are relatively less for the higher frequencies than for the lower frequencies.

The pseudo velocity spectra for the mechanical model system are compared with the hybrid system spectra in Figs. 9.27-9.29 for the 1 percent structural damping case, and in Figs. 9.30-9.32 for 10 percent damping. The mechanical model agrees very well with the hybrid model for higher periods, because interaction is not significant for those periods. For the lower periods on the other hand, the mechanical model response is somewhat higher. This increase can be attributed to the lower coupled system damping in the mechanical model, as shown by Fig. 9.26. It is believed that this effect could also be partly due to the contribution of the higher system frequencies. The second coupled mode in the mechanical model is 6.71 Hz while that of the hybrid model is 8.19 Hz.

9.11 CONCLUSIONS

- The effect of the peak and notch behavior on the system response is not as significant as has been previously thought [8]; this conclusion was verified by using the Mexico record which is basically a very narrow-banded input.
- The shaking table interaction effects can be expressed as a lowering in the system frequency and a change in damping, as is frequently the case in soil-structure interaction. For a structure with low fixed-base damping, the effect of interaction is to increase the structural damping significantly; for higher fixed-base damping ratios, the interaction can actually decrease the total damping in the system.
- Interaction effects are negligible for structural systems with periods greater than one second (i.e., frequencies lower than 1 Hz).
- Both the horizontal and rocking interaction mechanisms play an important role in the total system interaction. Figures 9.4 and 9.5 seem to indicate however, that the horizontal interaction is more important for the specific table-structure configuration considered in this study.
- The mechanical model used in this chapter gave a response that is slightly higher than the hybrid model, which in this case was due to the fact that this specific mechanical model has a coupled damping value that is lower than that of the hybrid model. In addition, the second coupled mode is more important in the mechanical model than it is in the hybrid model.
- In general, although not always, shaking table interaction tends to reduce the structural response. This is because the added damping caused by interaction more than compensates for the frequency shift in most cases.

Structural Frequency (Hz)	f_s	2.870
Structural Damping (%)	ξ_s	1.000
Horizontal Open Loop Frequency (Hz)	f_o	9.600
Horizontal Open Loop Damping (%)	ξ_o	0.606
Horizontal Open Loop Gain	k_o	29.500
Rocking Frequency (Hz)	f_θ	21.200
Rocking Damping (%)	ξ_θ	111.500
Mass Ratio	$\frac{m_s}{m_t}$	0.680
Inertia Ratio	$\frac{m_s h^2}{I}$	6.800

Table 9.1
Hybrid Model Parameters.
These parameters are equivalent to those in Table 8.1.

* Note that $f_\theta = 2\pi\omega_\theta$ where ω_θ is given by equation 8.35
All other parameters are defined in section 8.6

Frequency =	2.5391 Hz	Damping =	0.040079
Frequency =	8.1906 Hz	Damping =	0.259045
REAL ROOTS :			
-199.616612			
-99.309331			
-46.343754			

Table 9.2
Coupled System Modes For the SDOF Model Mounted on the Shaking Table

Structural Frequency (Hz)	f_s	2.870
Structural Damping (%)	ξ_s	1.000
Horizontal Frequency (Hz)	f_h	6.250
Horizontal Damping (%)	ξ_h	0.300
Rocking Frequency (Hz)	f_θ	21.200
Rocking Damping (%)	ξ_θ	111.500
Mass Ratio	$\frac{m_s}{m_t}$	0.680
Inertia Ratio	$\frac{m_s h^2}{I}$	6.800

Table 9.3
Mechanical Model Parameters

* Model equations are derived in Appendix A.

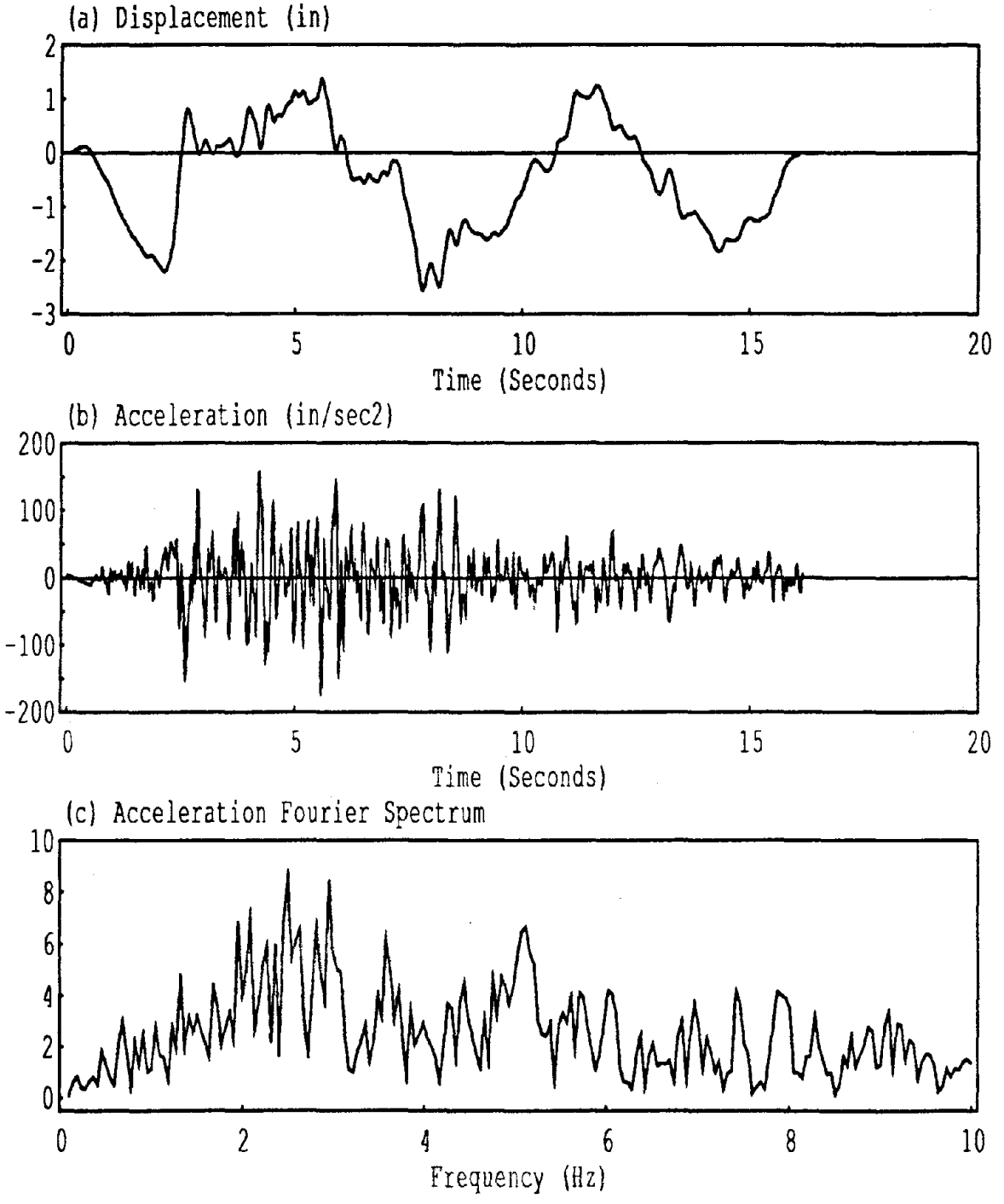

Fig. 9.1: Truncated and Scaled 1952 TAFT N21E Earthquake Record
Time Scale Factor=1.811

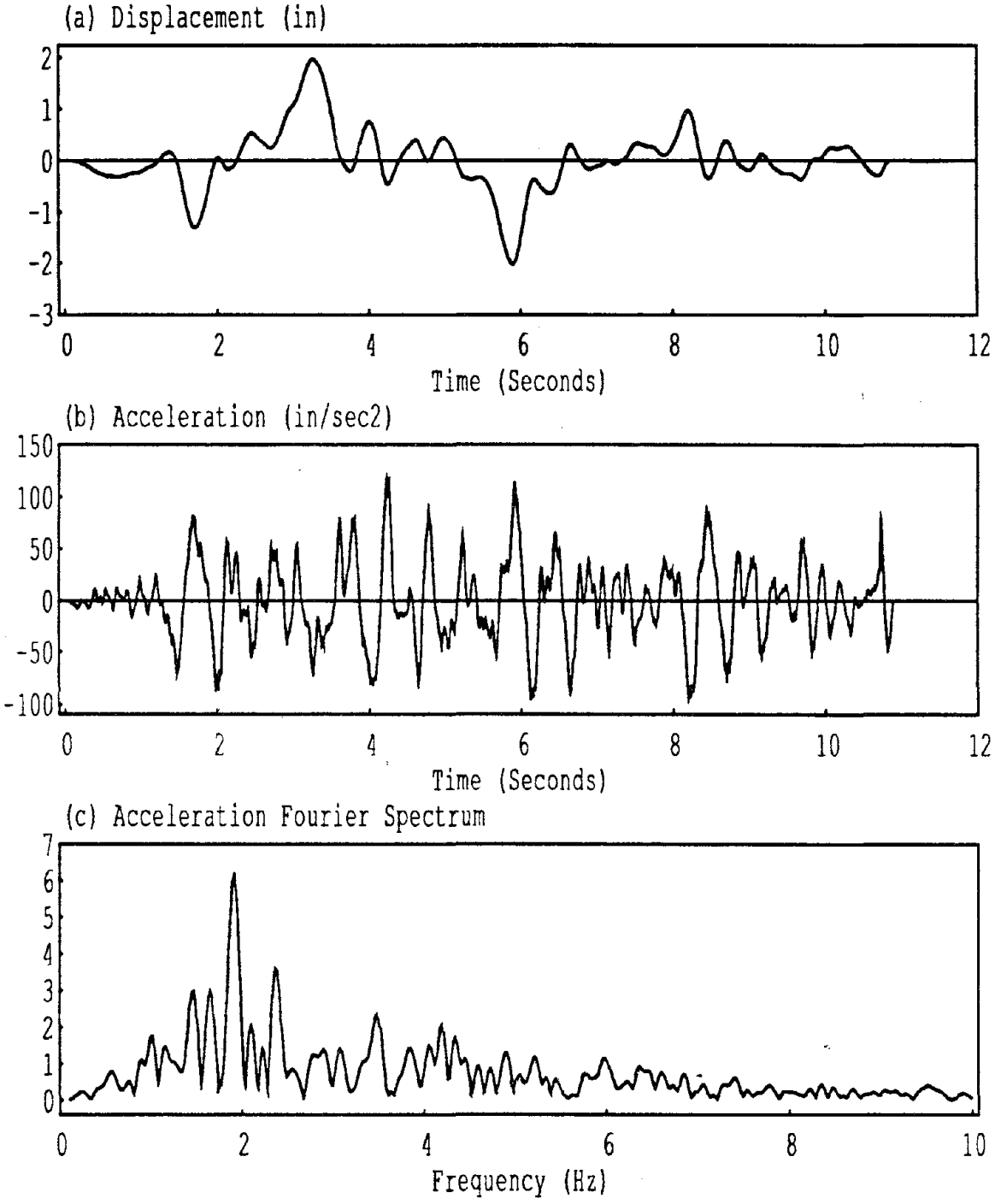

Fig. 9.2: Truncated and Scaled 1957 Miyagi-Ken-Oki Earthquake Record
Time Scale Factor = 1.811

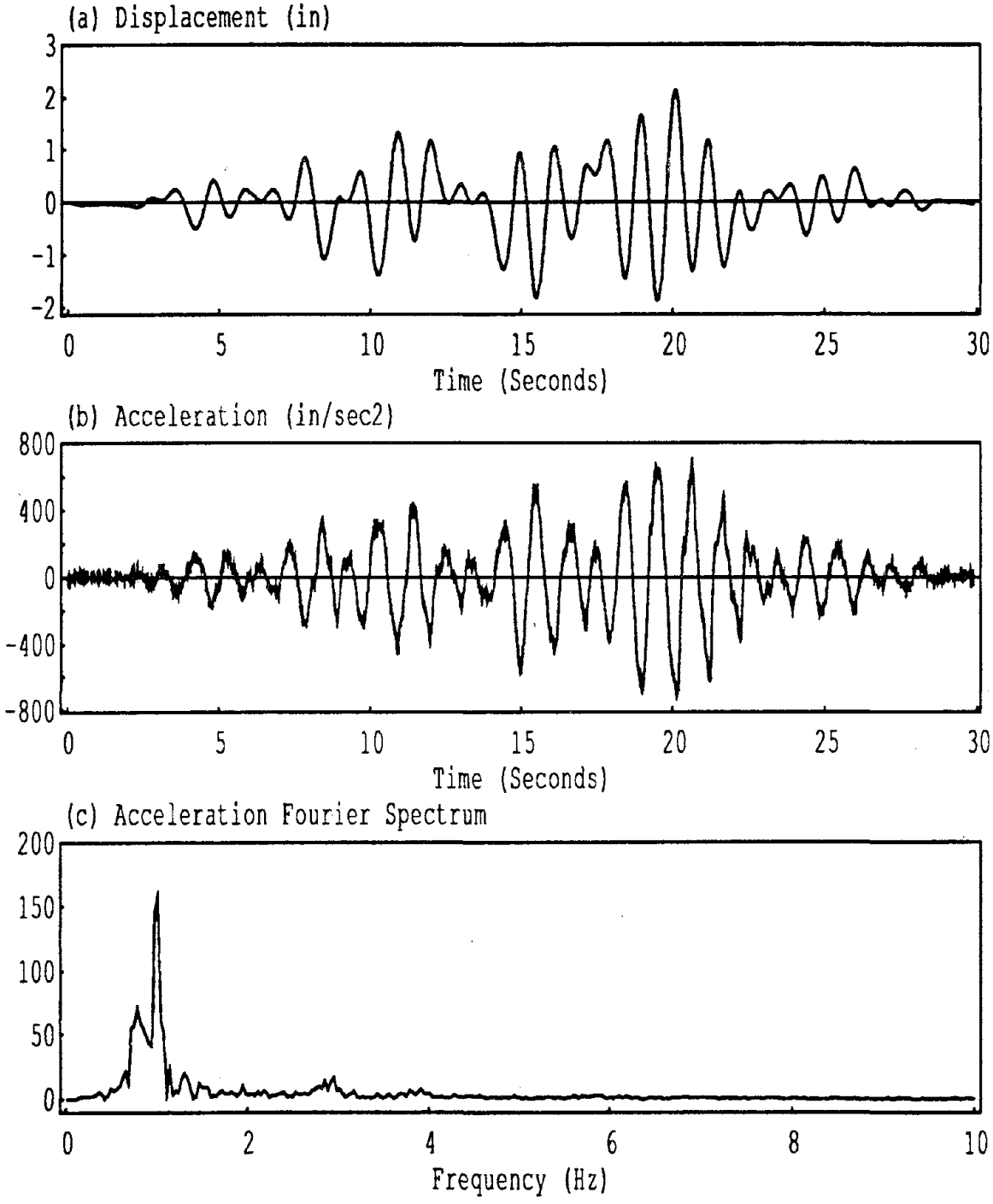

Fig. 9.3: Truncated and Scaled 1985 Mexico N90W Earthquake Record
Time Scale factor = 2

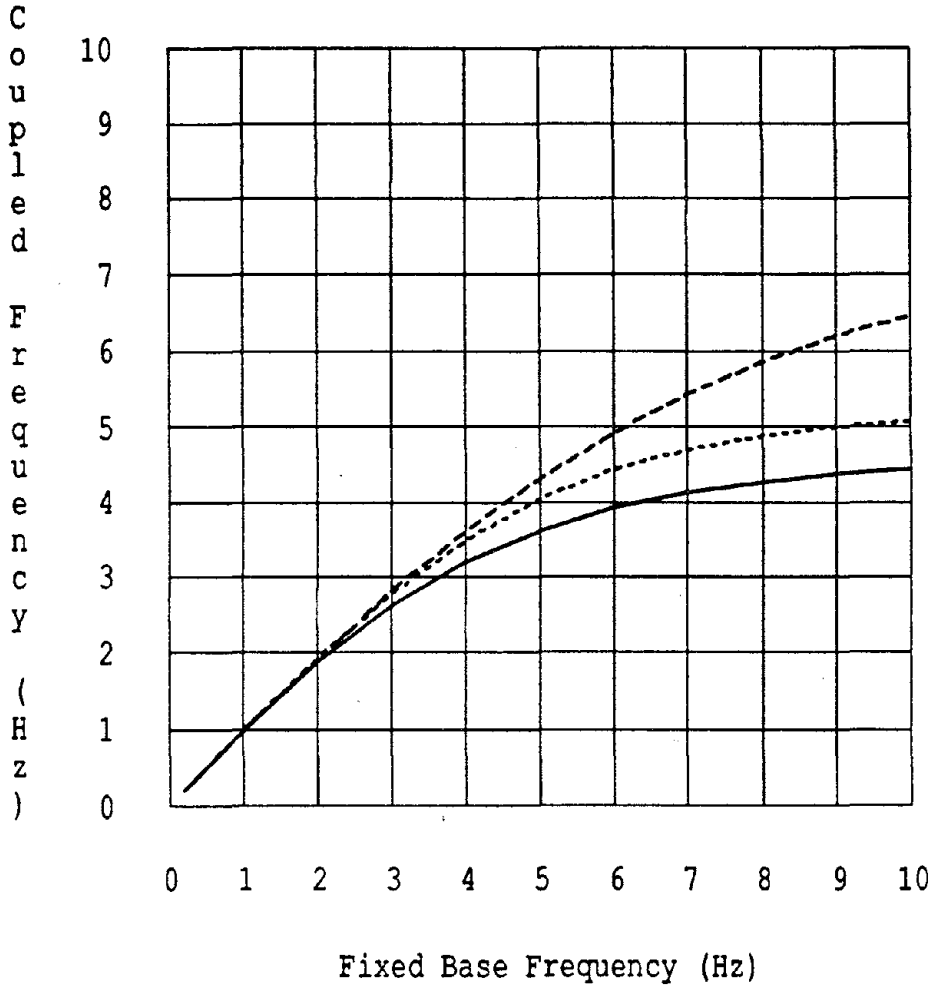

Fig. 9.4: Variation of Coupled System Frequency with Fixed Base Structure Frequency.

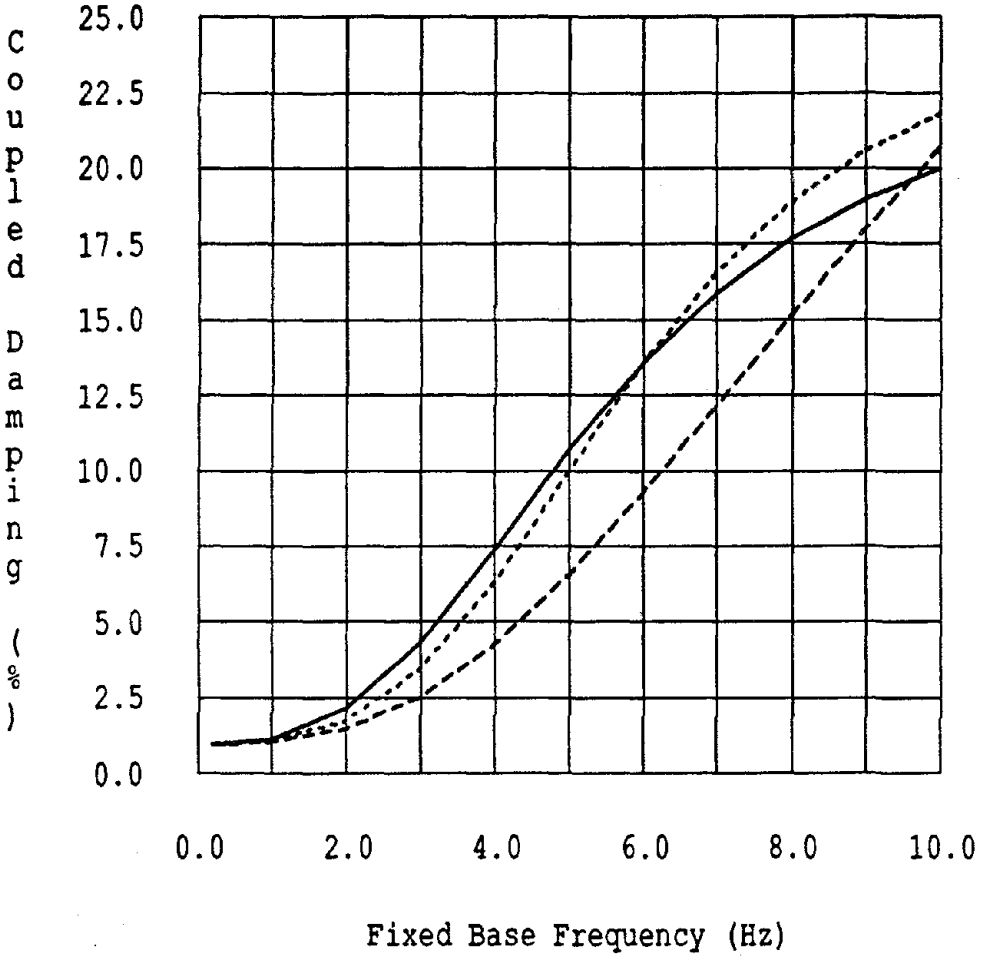

Fig. 9.5: Variation of Coupled System Damping with Fixed Base Structure Frequency.

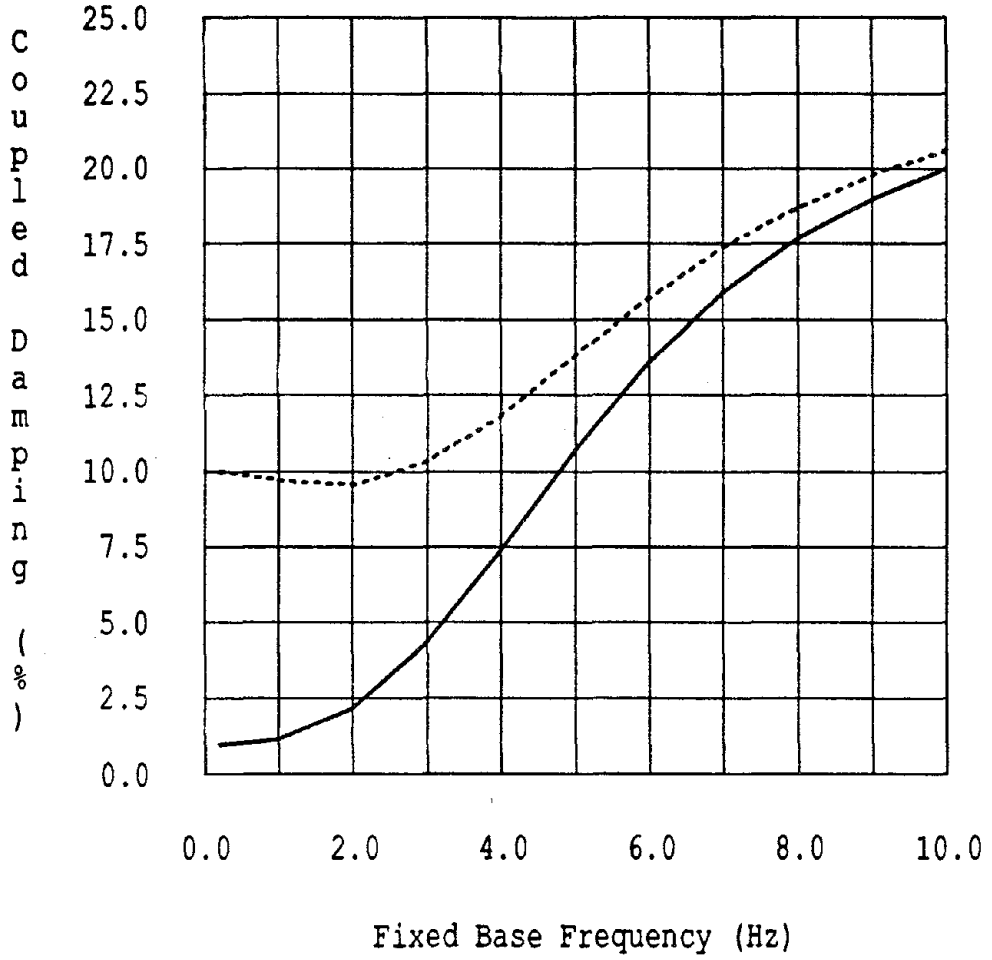

Fig. 9.6: Variation of Coupled System Damping with Frequency for Different Fixed Base Structural Damping: Hybrid Model.

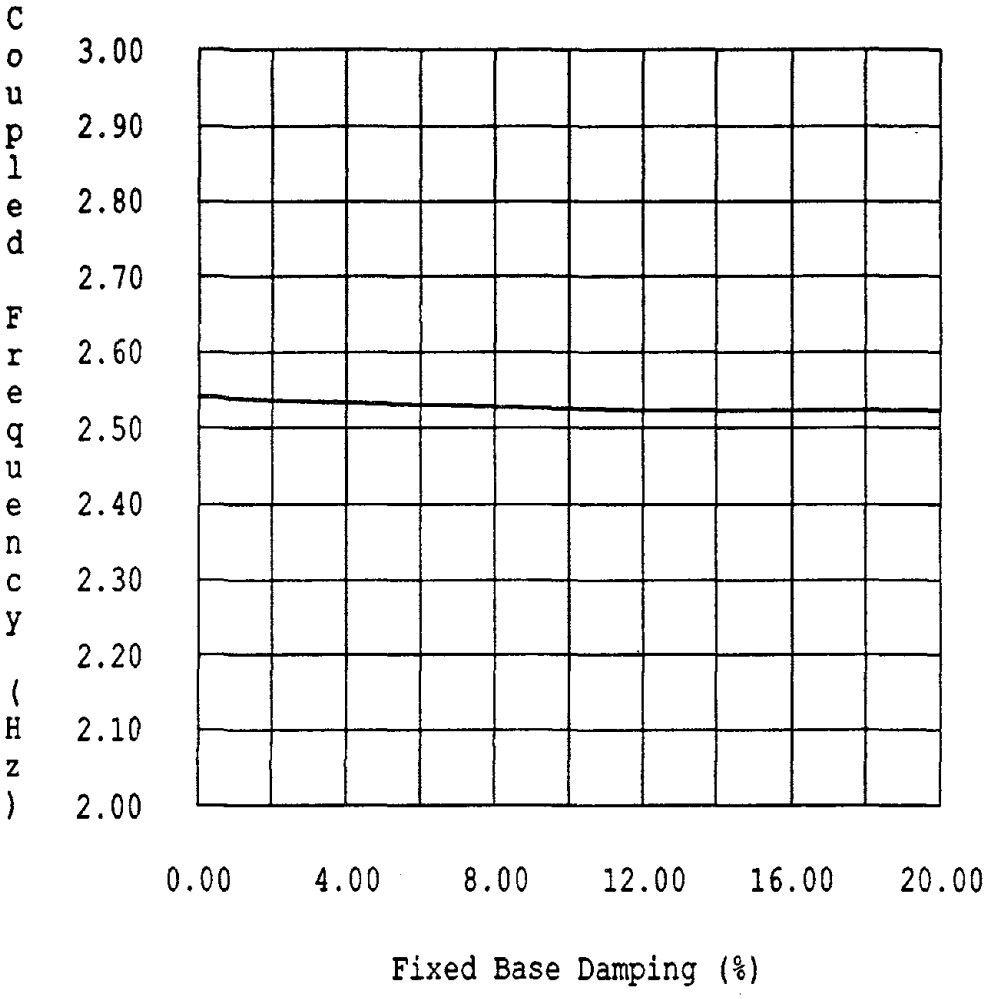

Fig. 9.7: Variation of Coupled System Frequency with Fixed Base Structural Damping: Hybrid Model.

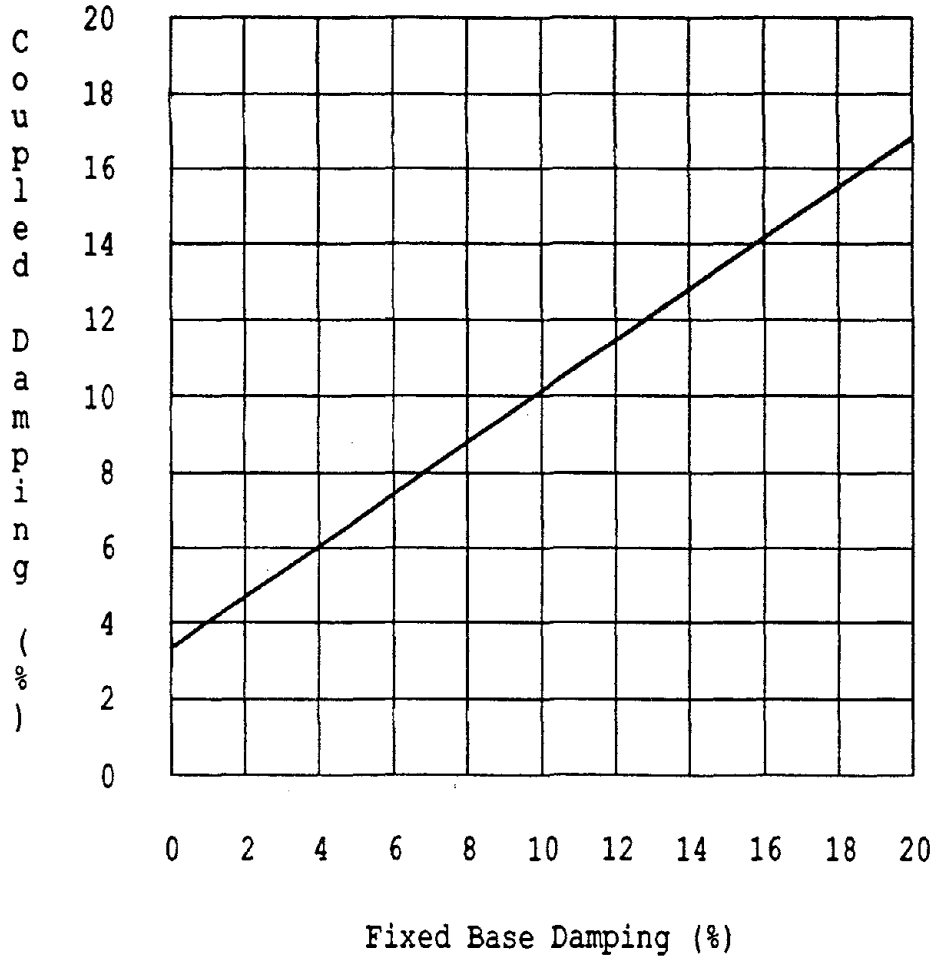

Fig. 9.8: Variation of Coupled System Damping with Fixed Base Structural Damping: Hybrid Model.

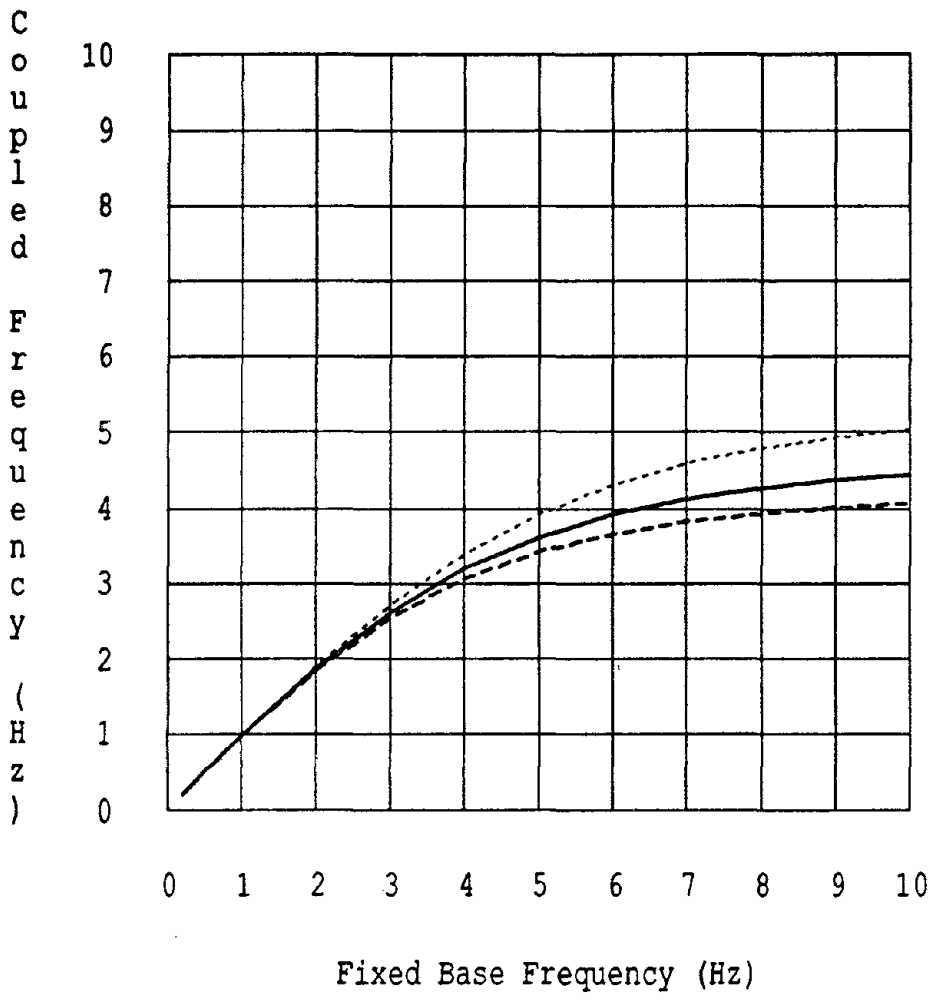

Fig. 9.9: Variation of Coupled System Frequency with Fixed Base Frequency and Structural Mass : Hybrid Model.

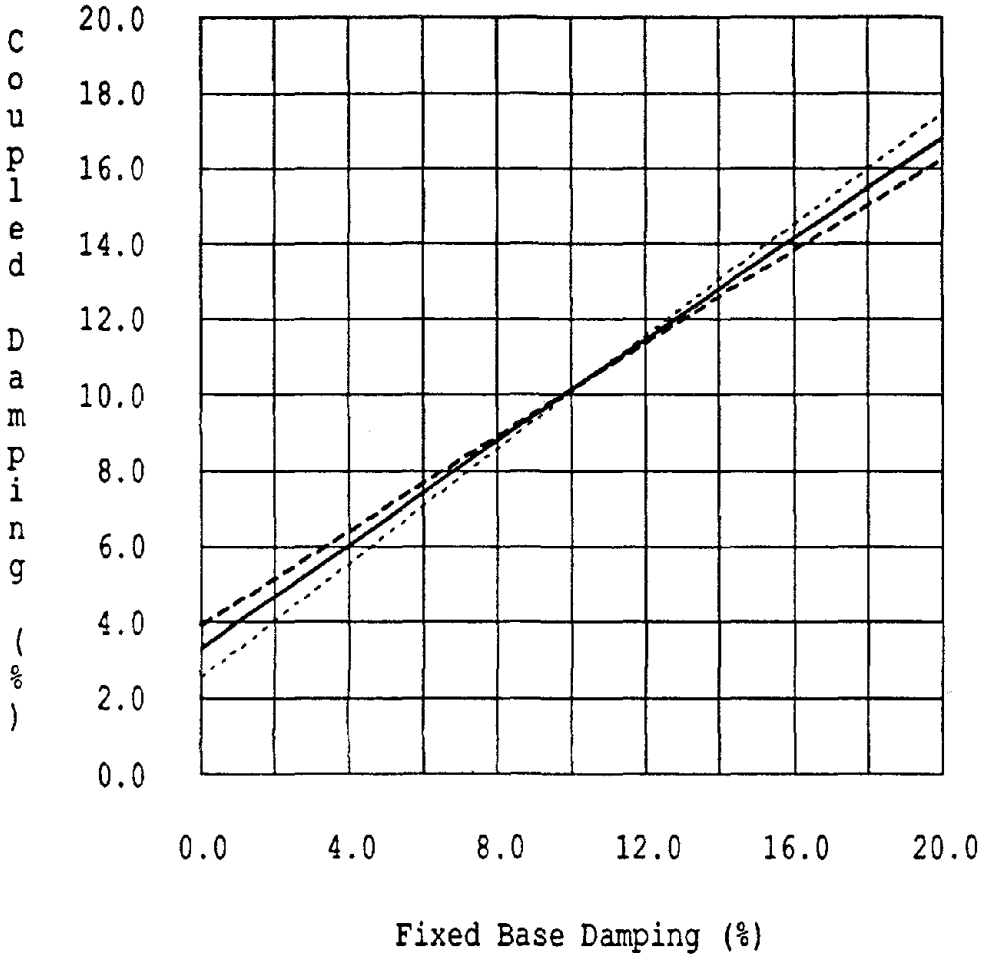

Fig. 9.10: Variation of Coupled System Damping with Fixed Base Damping and Structural Mass : Hybrid Model.

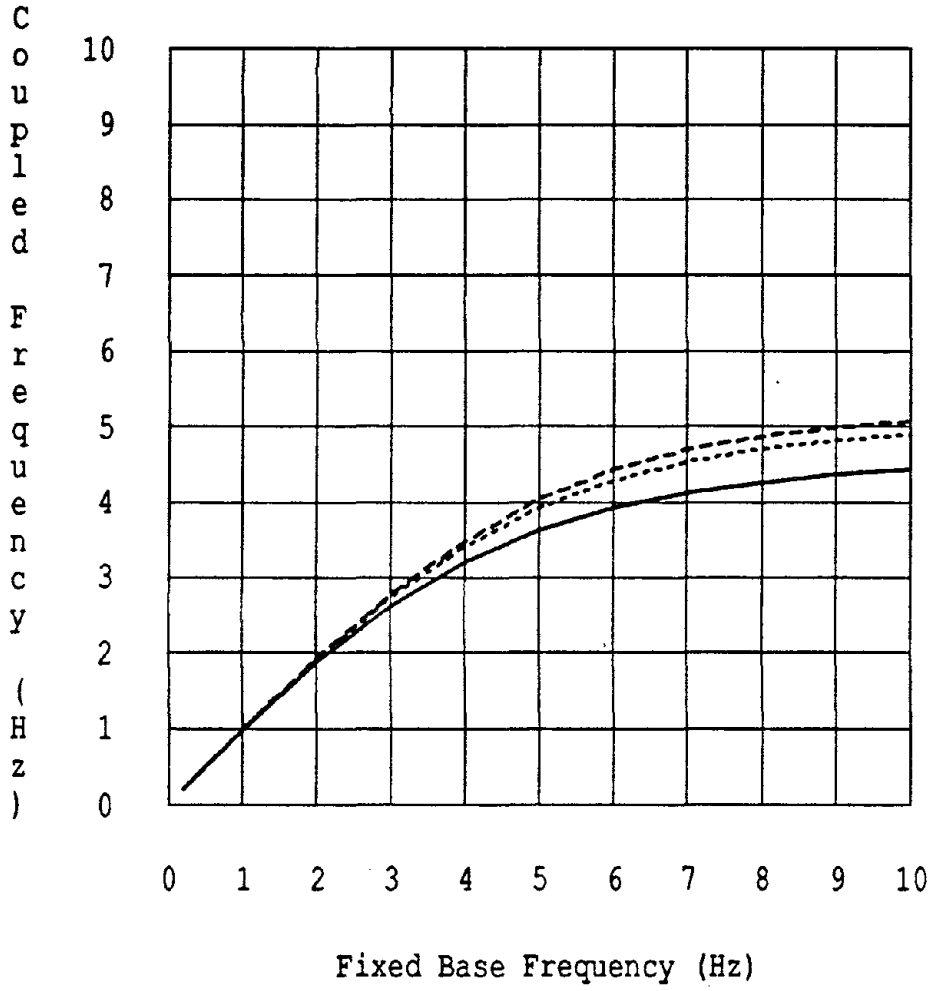

Fig. 9.11: Variation of Coupled System Frequency with Fixed Base Frequency and Structural Height: Hybrid Model.

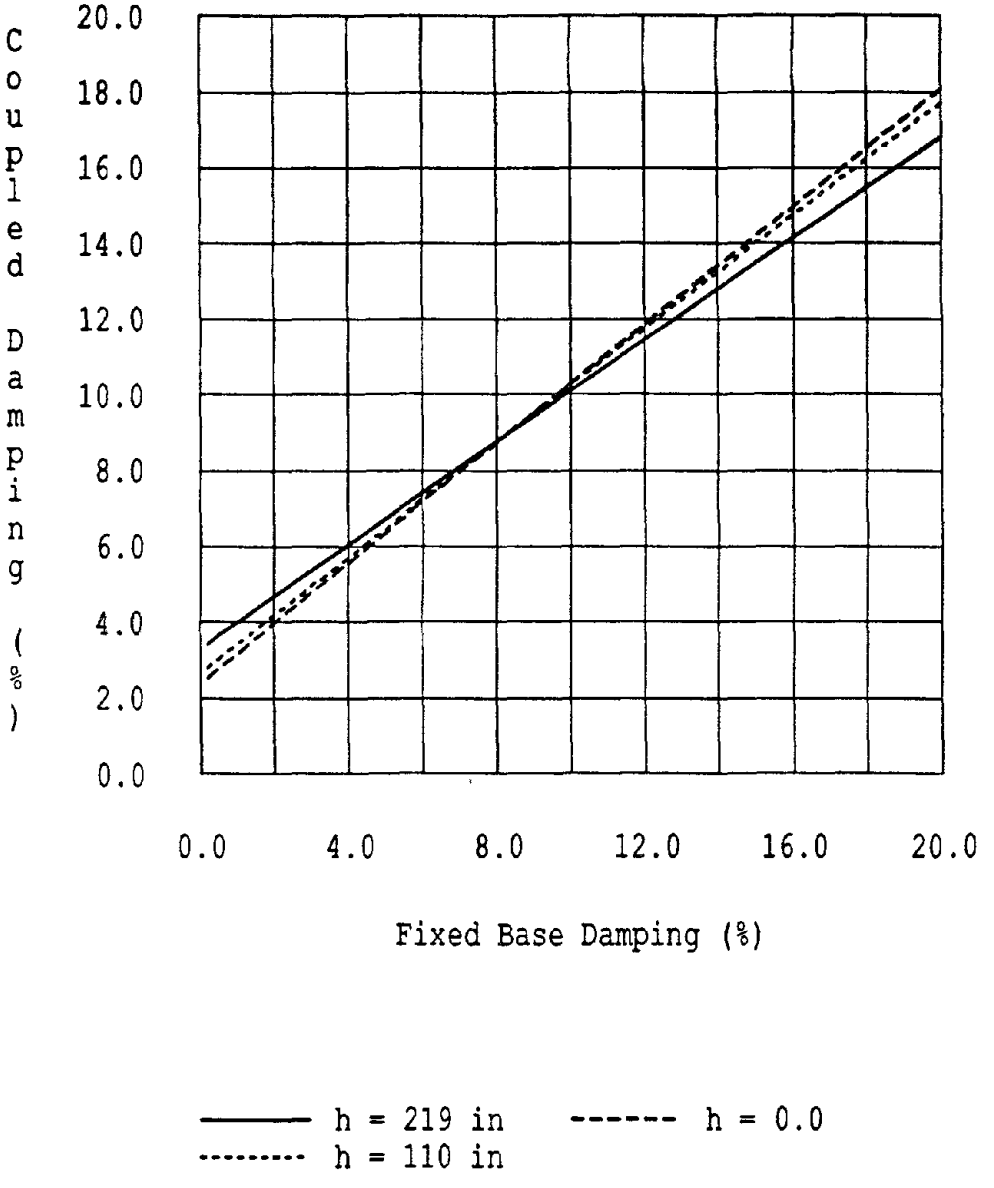

Fig. 9.12: Variation of Coupled System Damping with Fixed Base Damping and Structural Height: Hybrid Model.

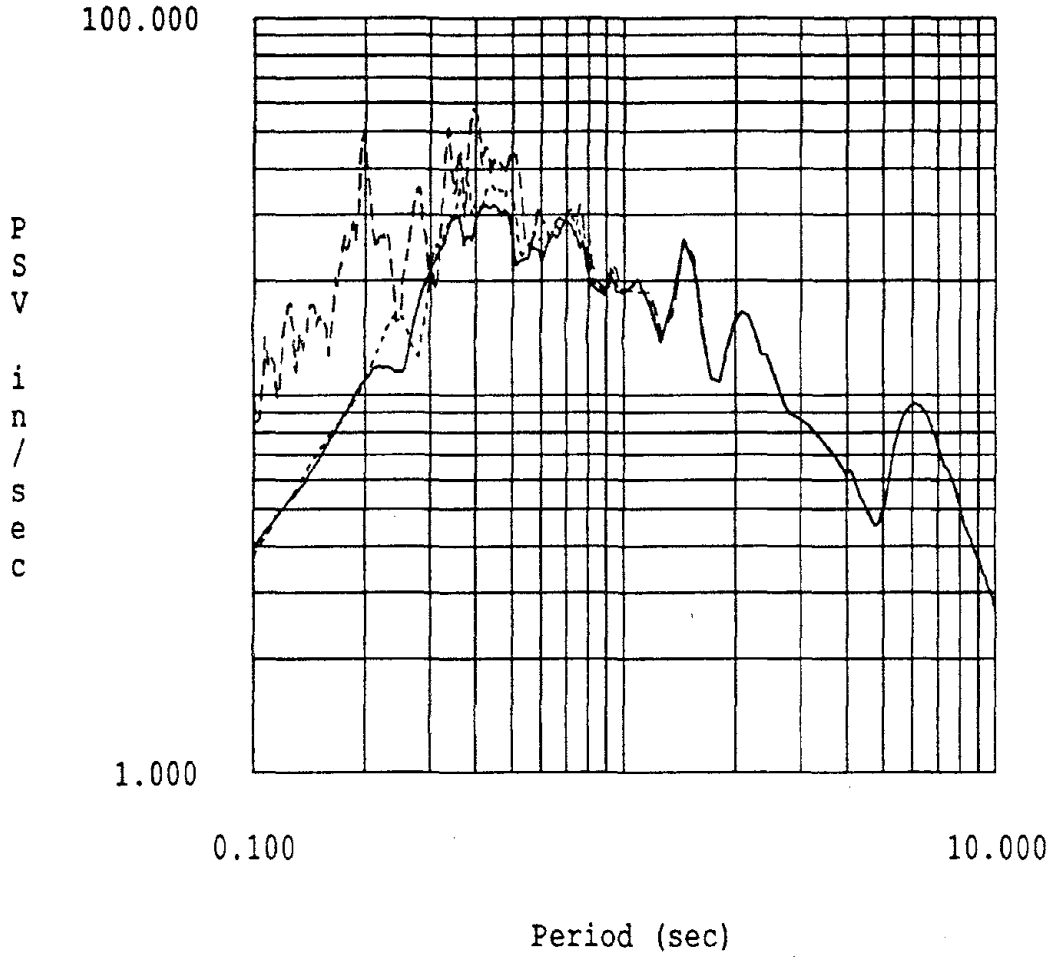

Fig. 9.13: Pseudo Velocity Response Spectrum: Taft 1% damping

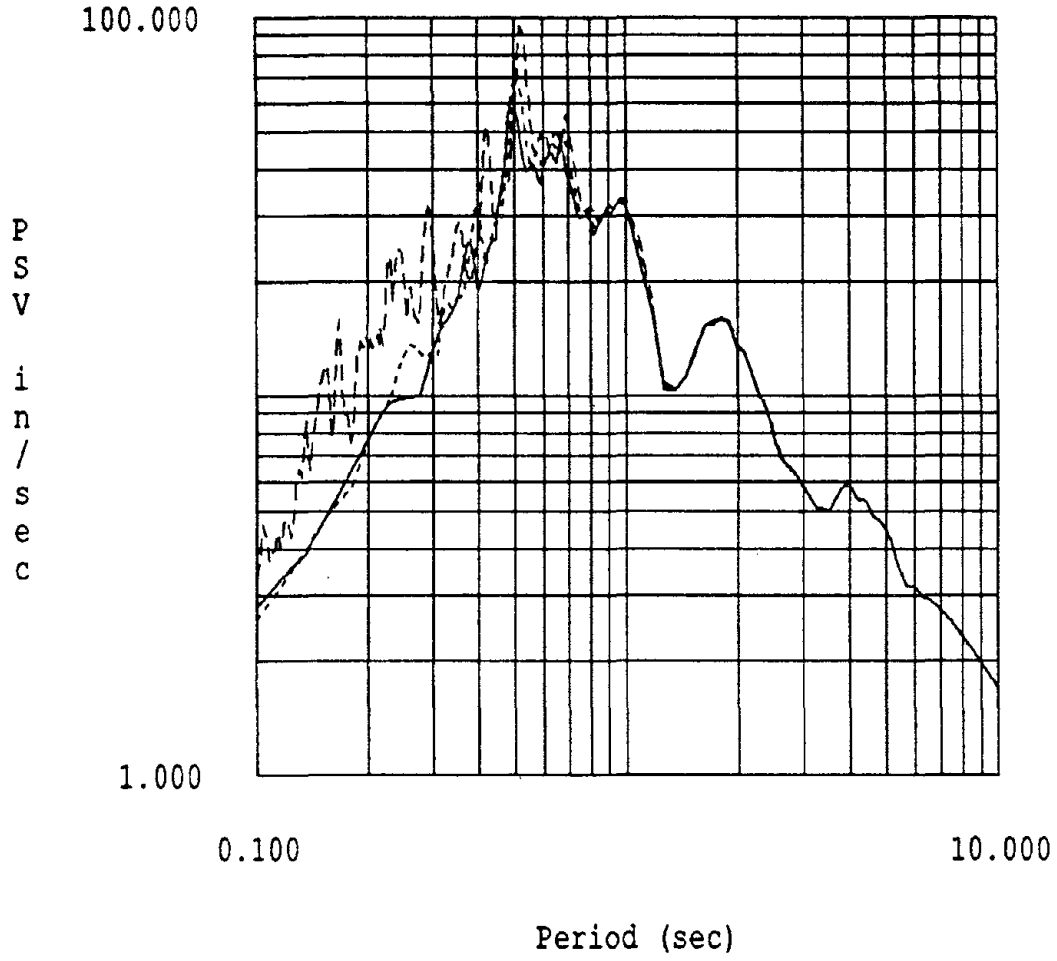

Fig. 9.14: Pseudo Velocity Response Spectrum: Miyagi 1% damping

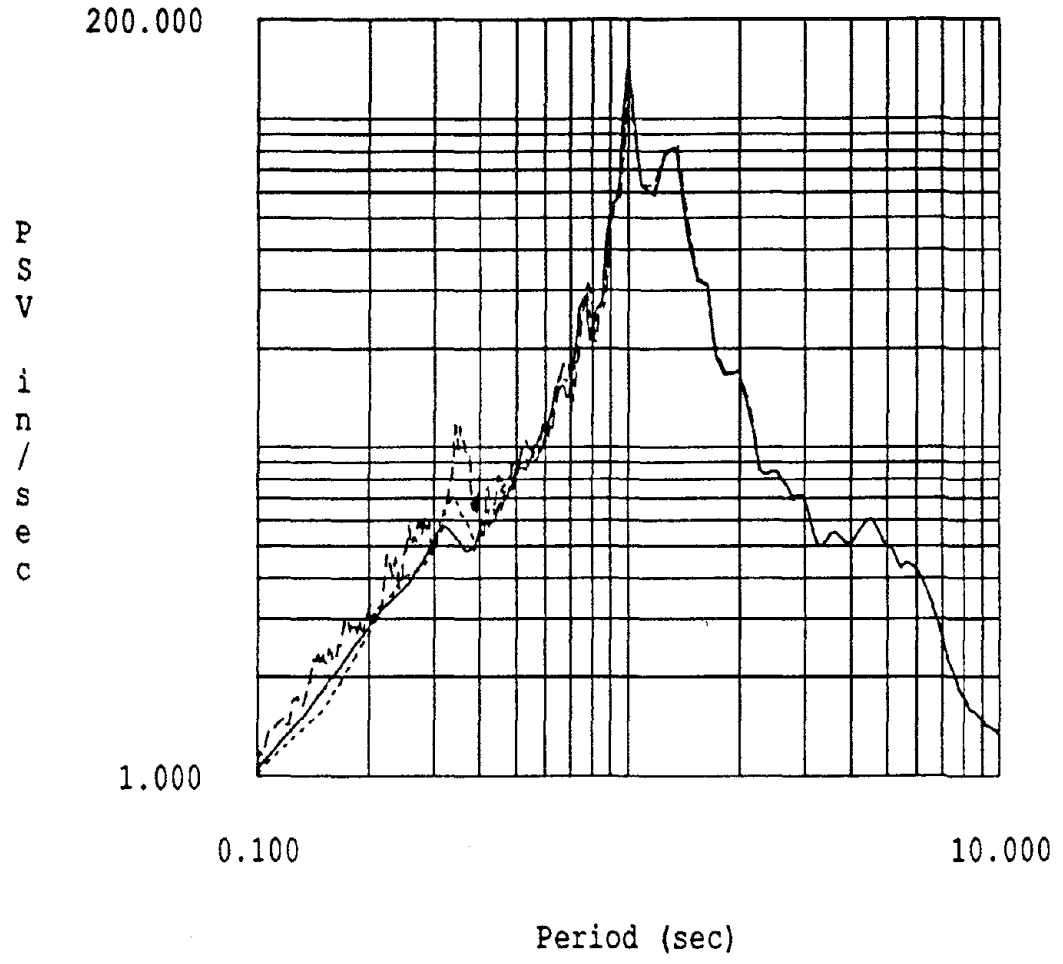

Fig. 9.15: Pseudo Velocity Response Spectrum: Mexico 1% Damping.
Time Scale Factor = 2

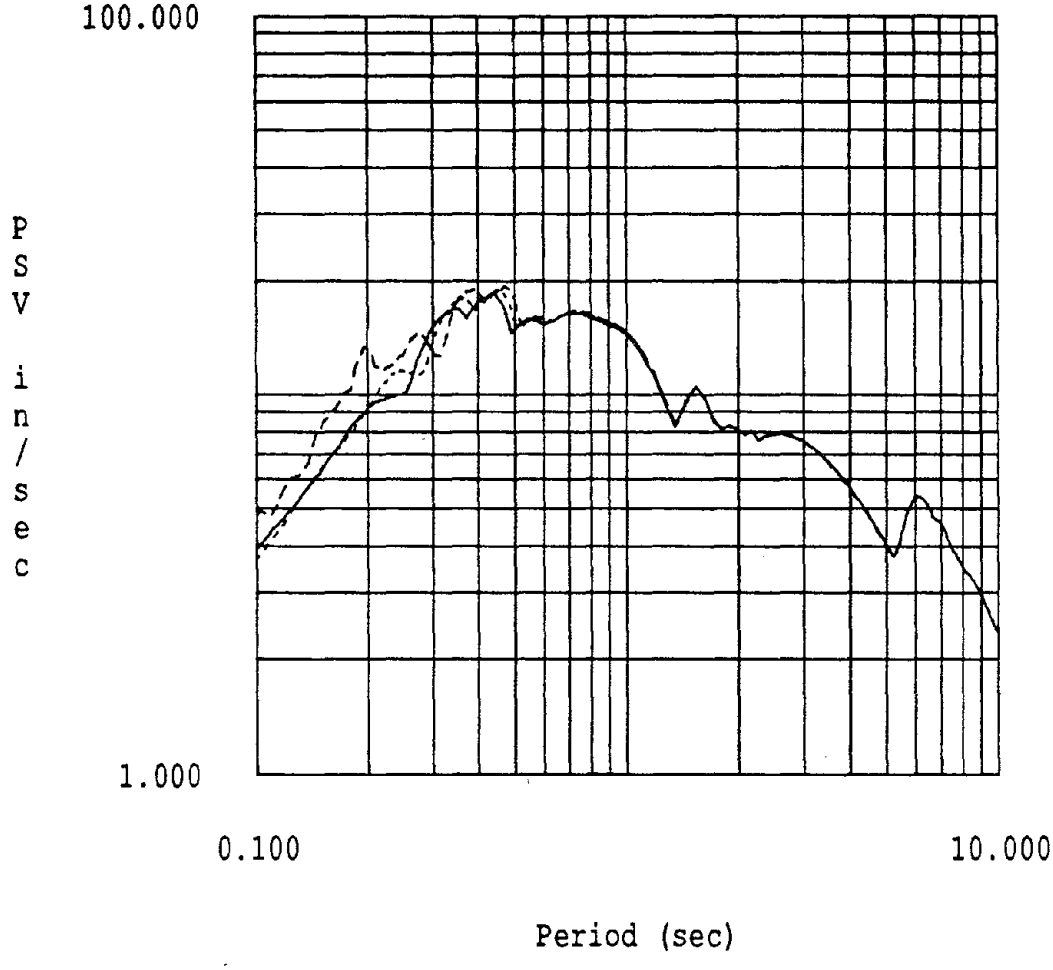

Fig. 9.16: Pseudo Velocity Response Spectrum: Taft 10% damping

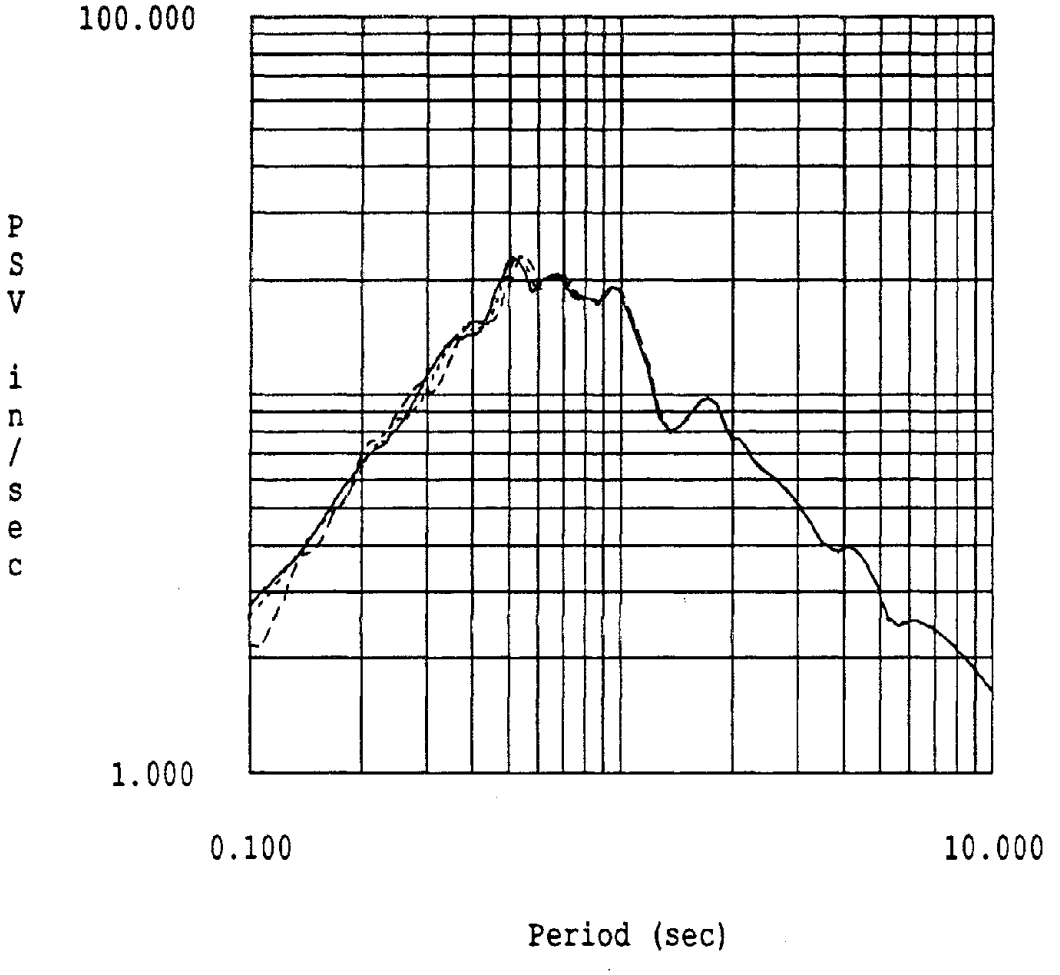

Fig. 9.17: Pseudo Velocity Response Spectrum: Miyagi 10% damping

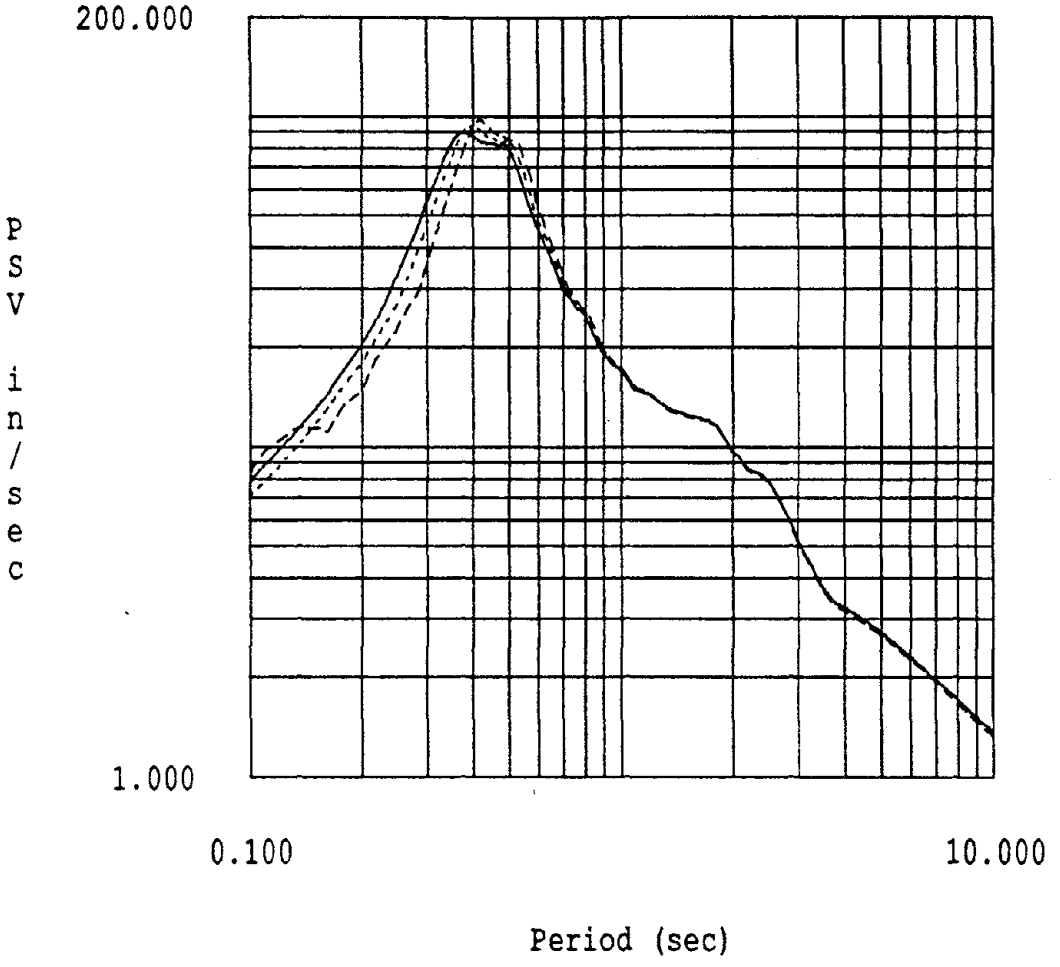

Fig. 9.18: Pseudo Velocity Response Spectrum: Mexico 10% Damping.
Time Scale Factor = 5

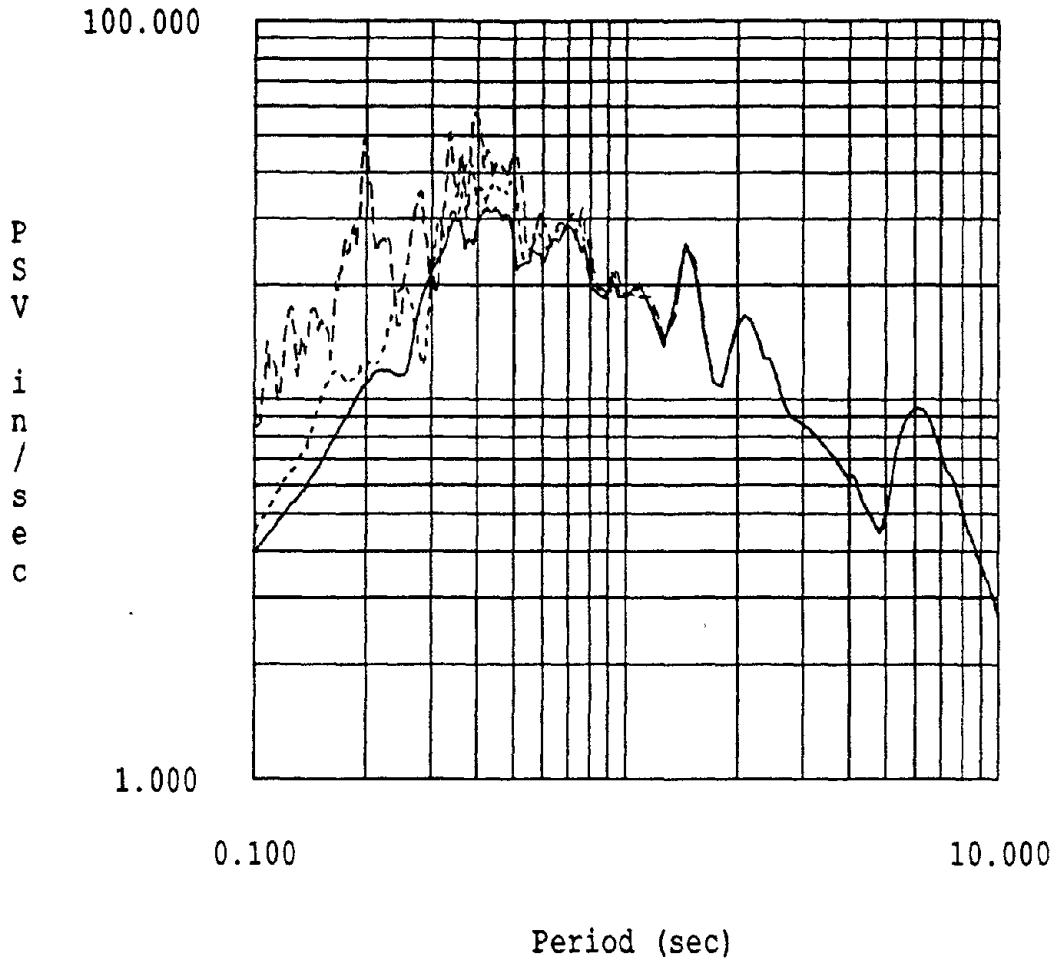

Fig. 9.19: Pseudo Velocity Response Spectrum: Taft 1% damping

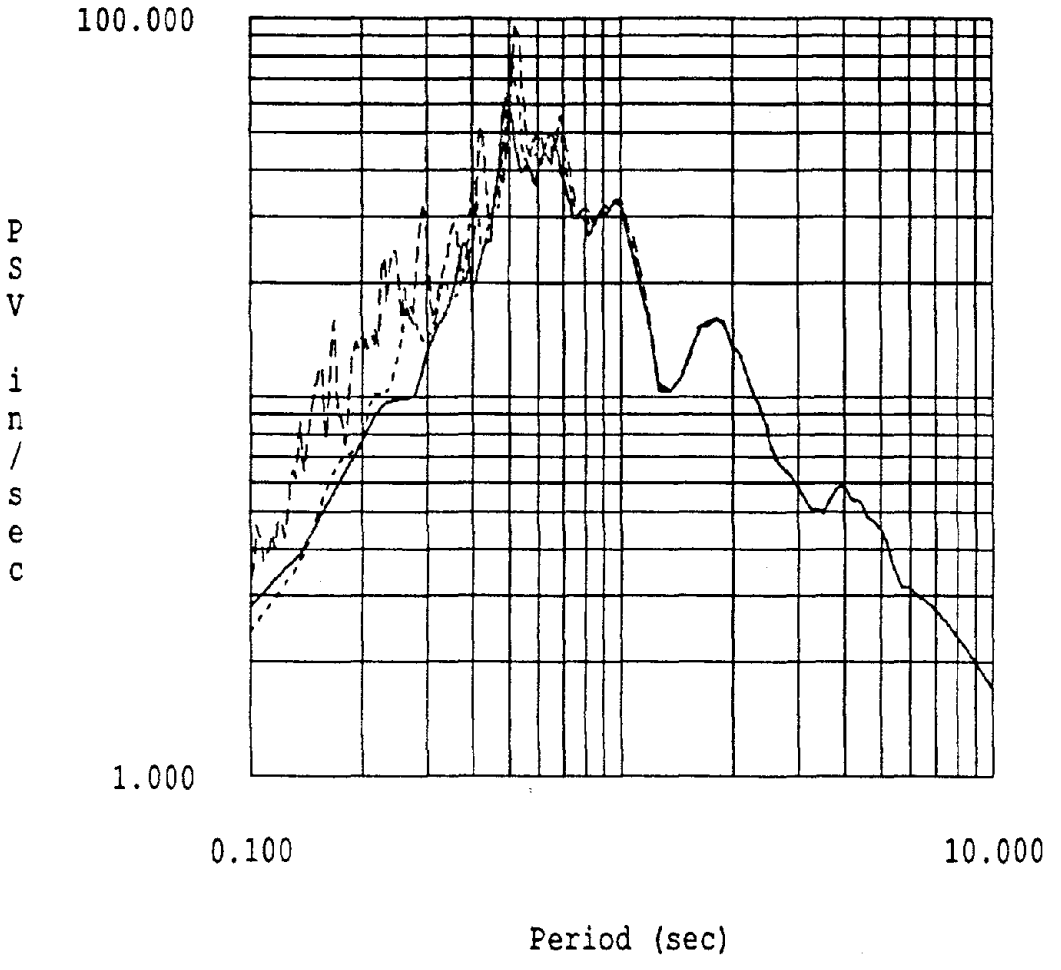

Fig. 9.20: Pseudo Velocity Response Spectrum: Miyagi 1% damping

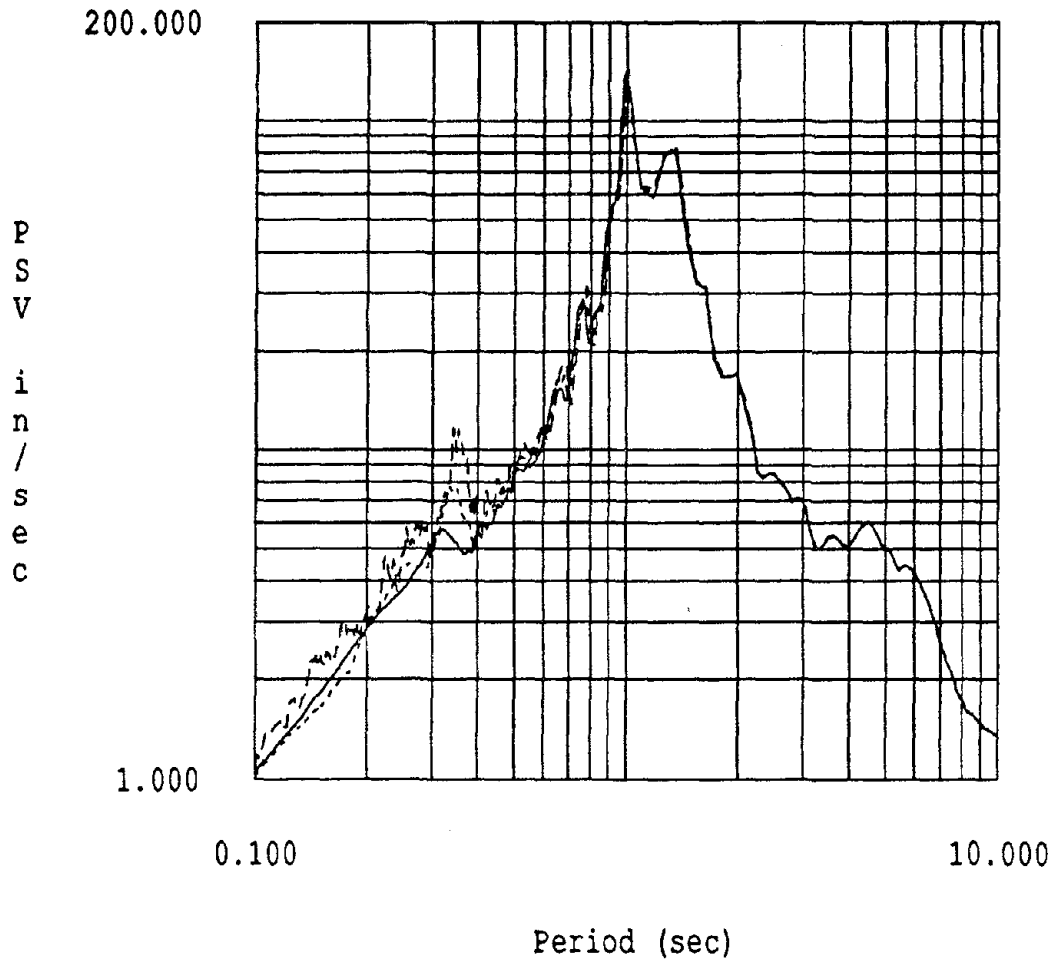

Fig. 9.21: Pseudo Velocity Response Spectrum: Mexico 1% Damping.
Time Scale Factor = 2

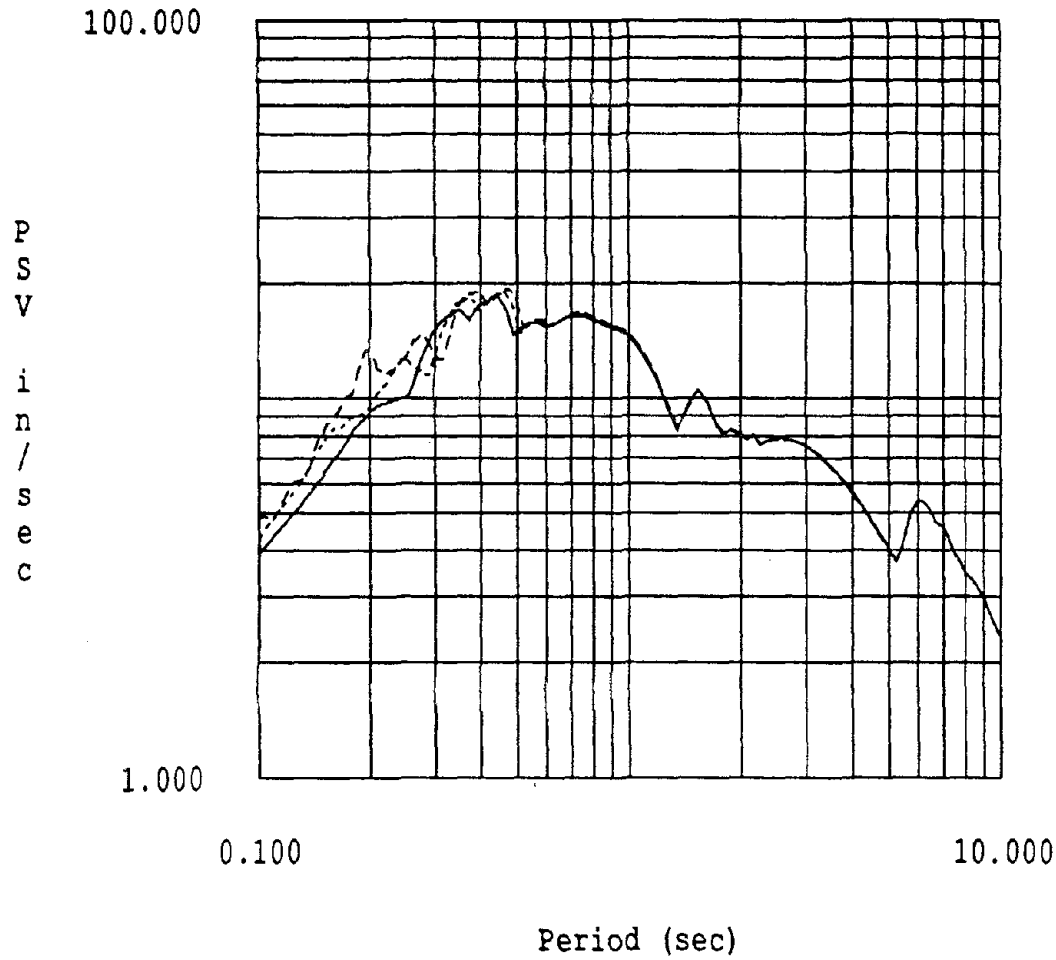

Fig. 9.22: Pseudo Velocity Response Spectrum: Taft 10% damping

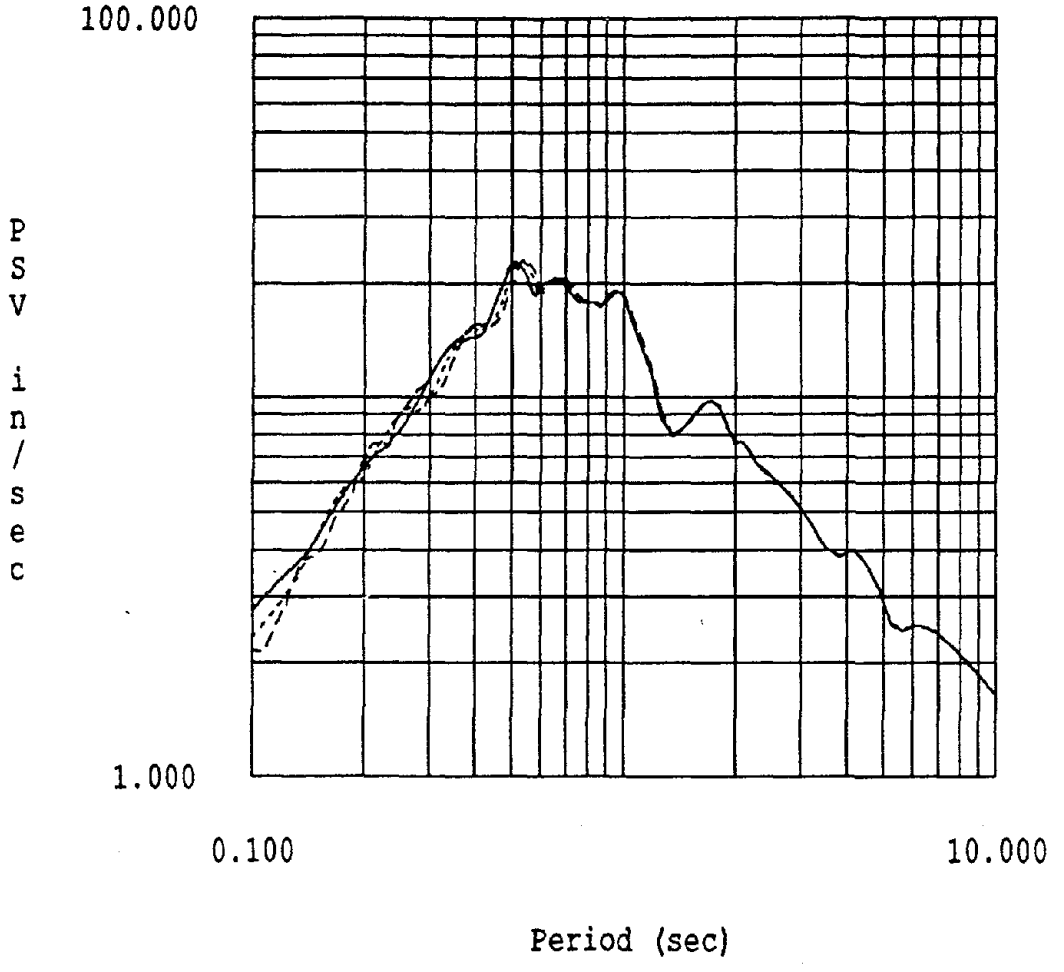

Fig. 9.23: Pseudo Velocity Response Spectrum: Miyagi 10% damping

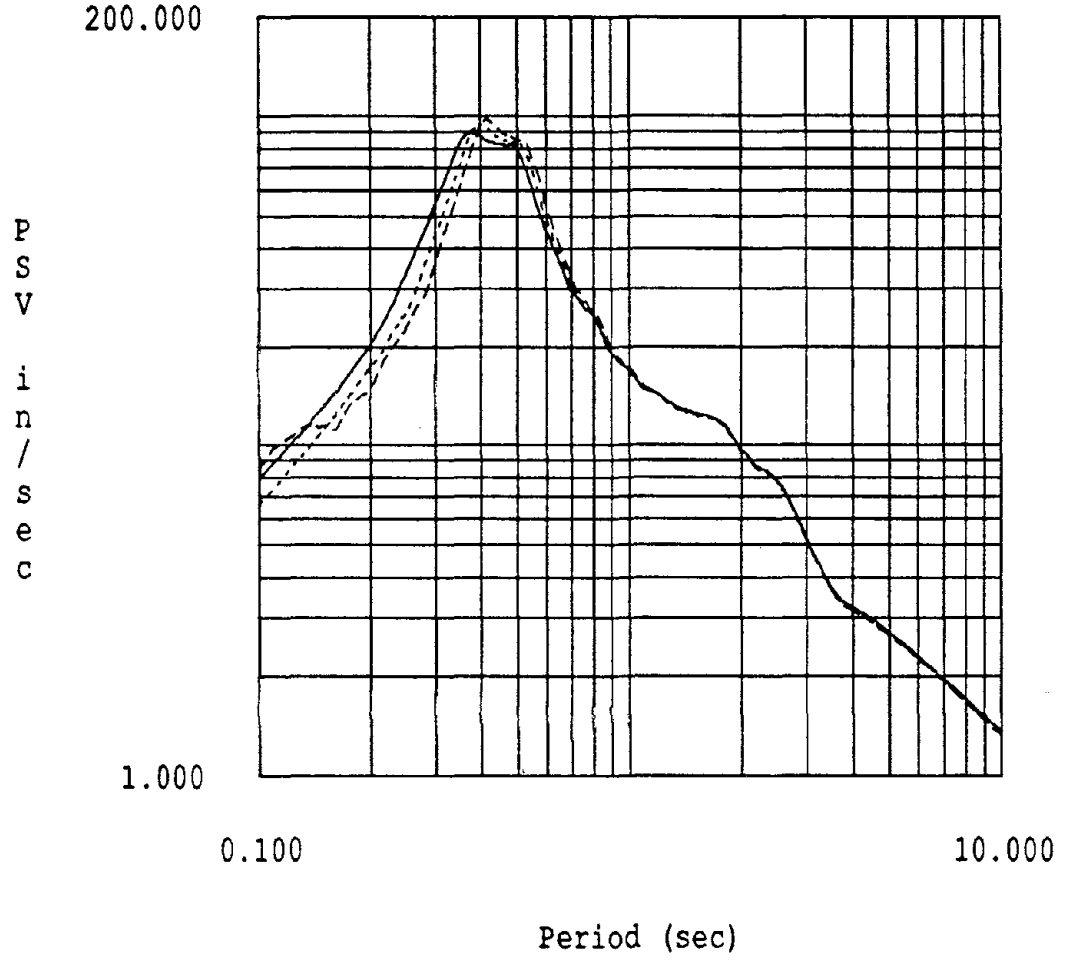

Fig. 9.24: Pseudo Velocity Response Spectrum: Mexico 10% Damping. Time Scale Factor = 5

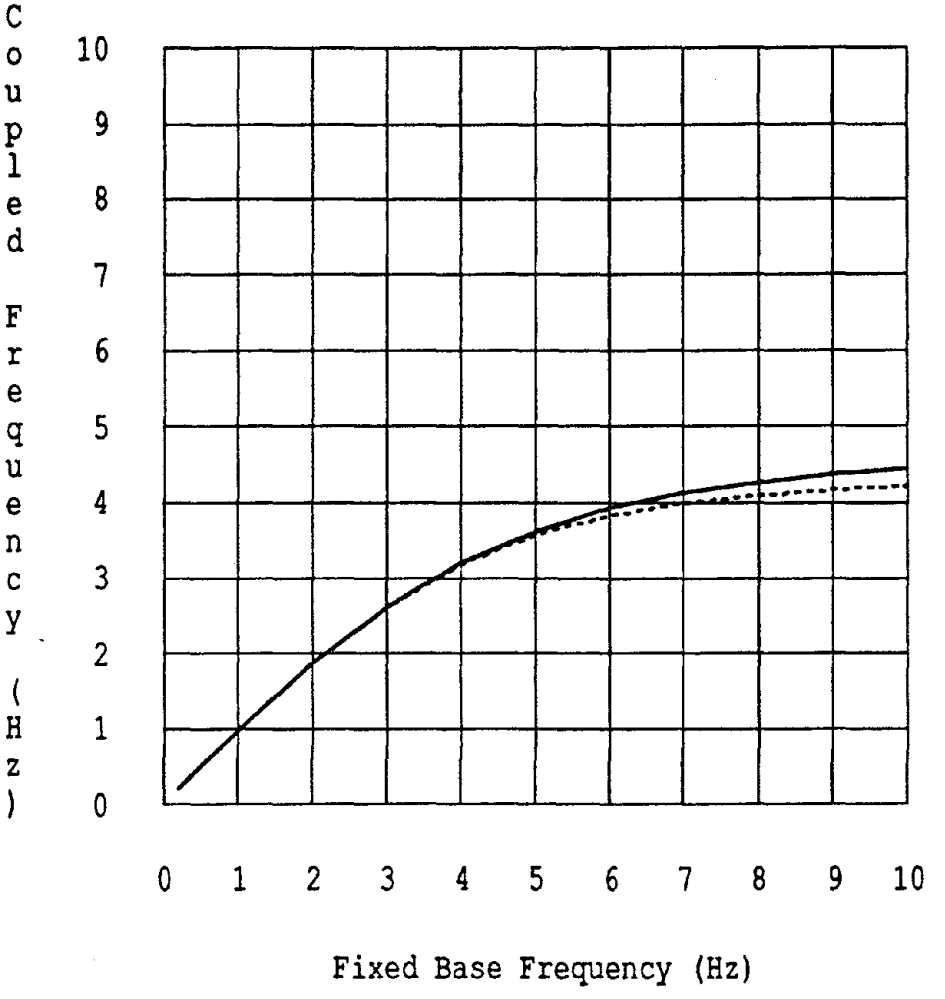

Fig. 9.25: Variation of Coupled System Frequency with Fixed Base Structural Frequency: Hybrid vs. Mechanical Model.

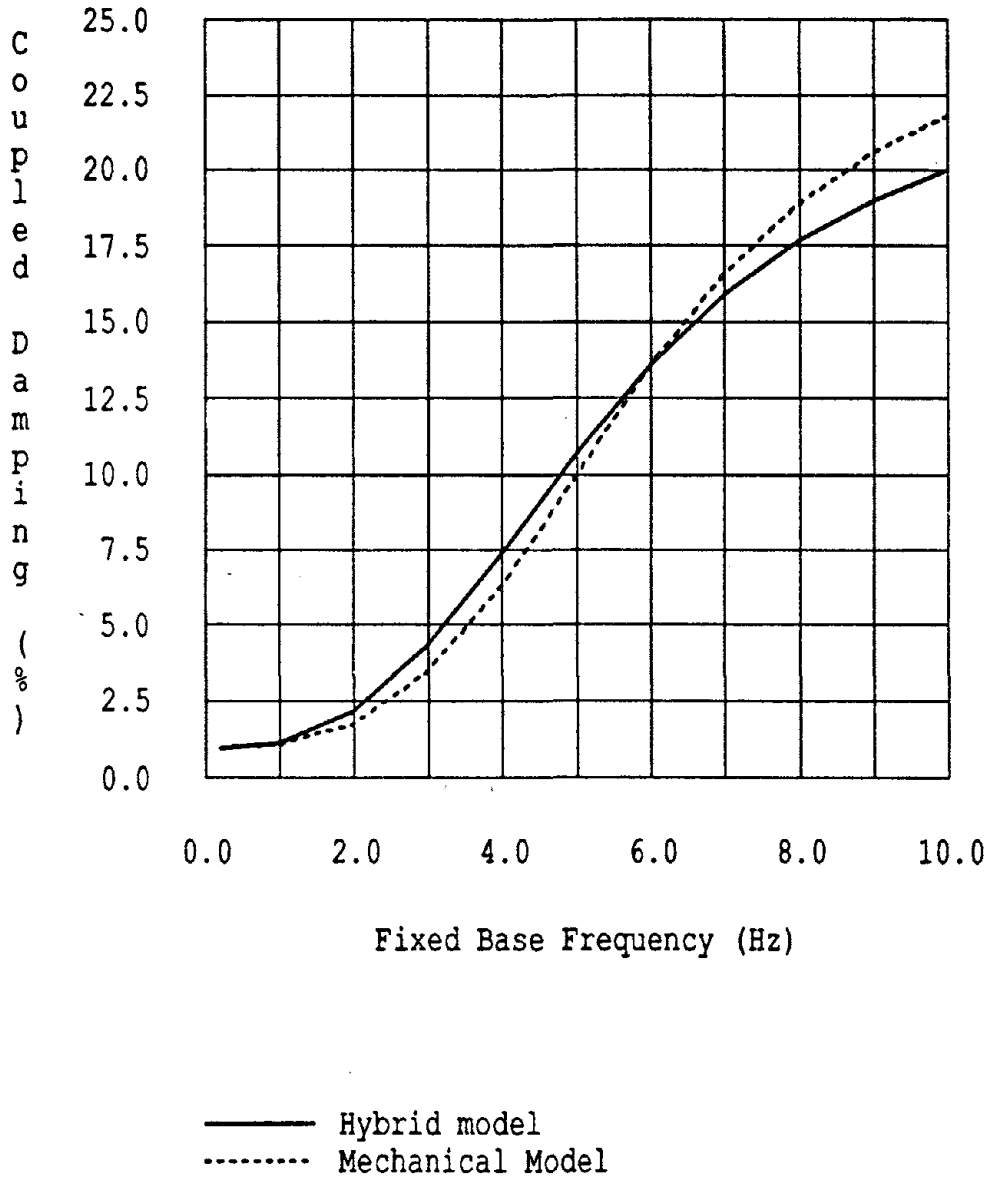

Fig. 9.26: Variation of Coupled System Damping with Fixed Base Structural Frequency for 1 % Fixed Base Damping.

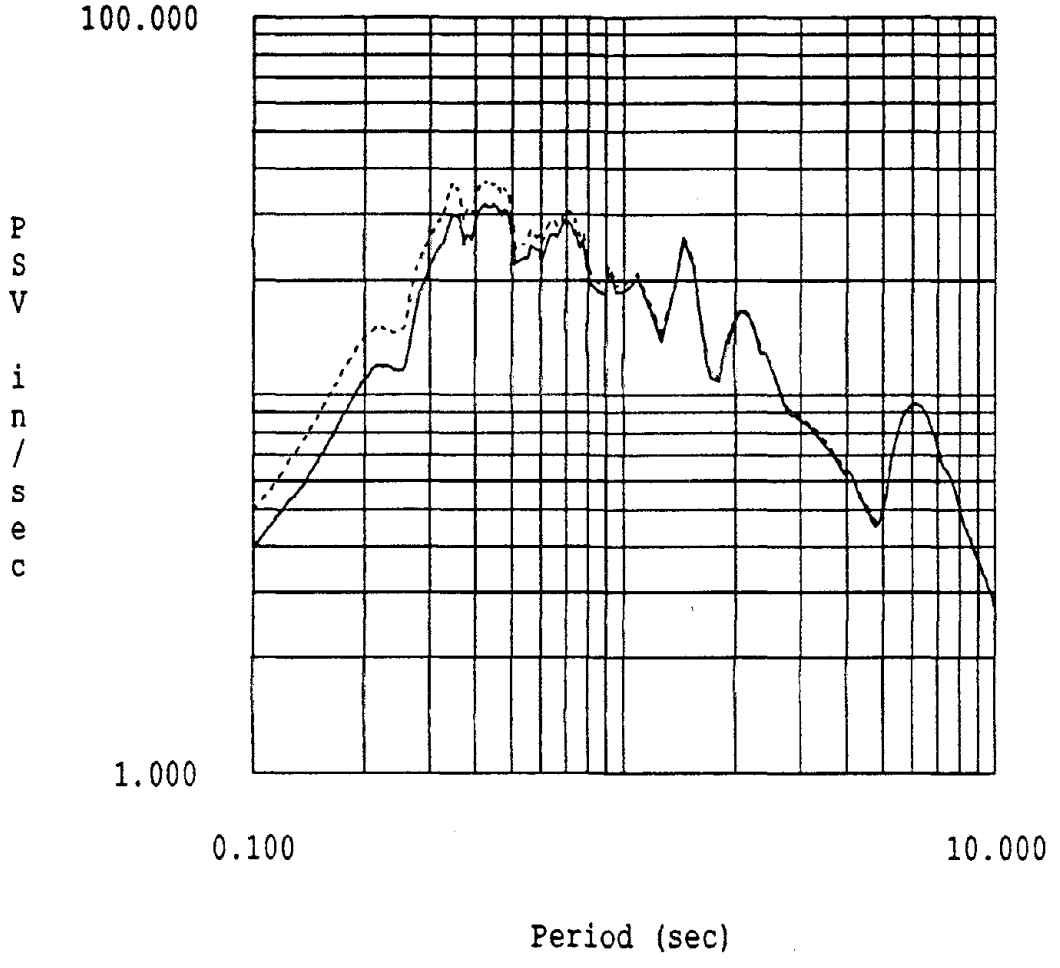

Fig. 9.27: Pseudo Velocity Response Spectrum: Taft 1% damping

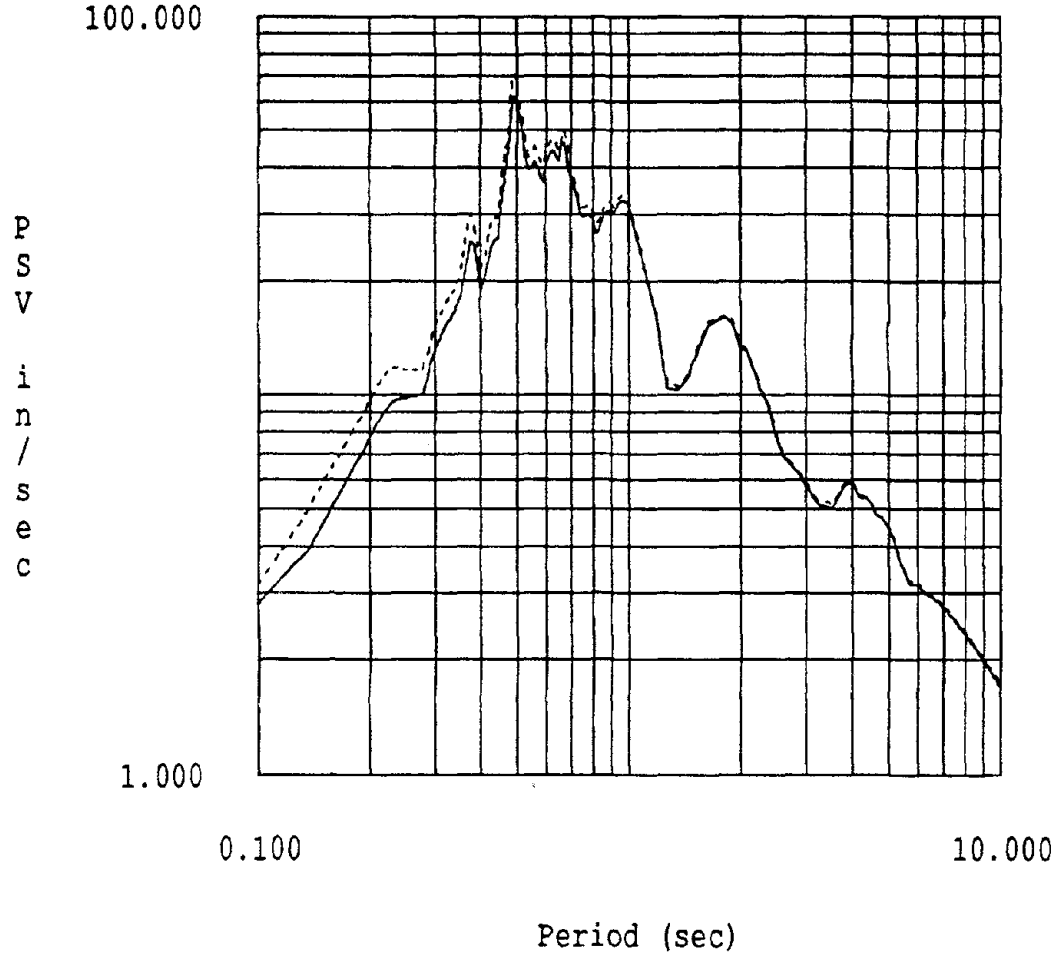

Fig. 9.28: Pseudo Velocity Response Spectrum: Miyagi 1% damping

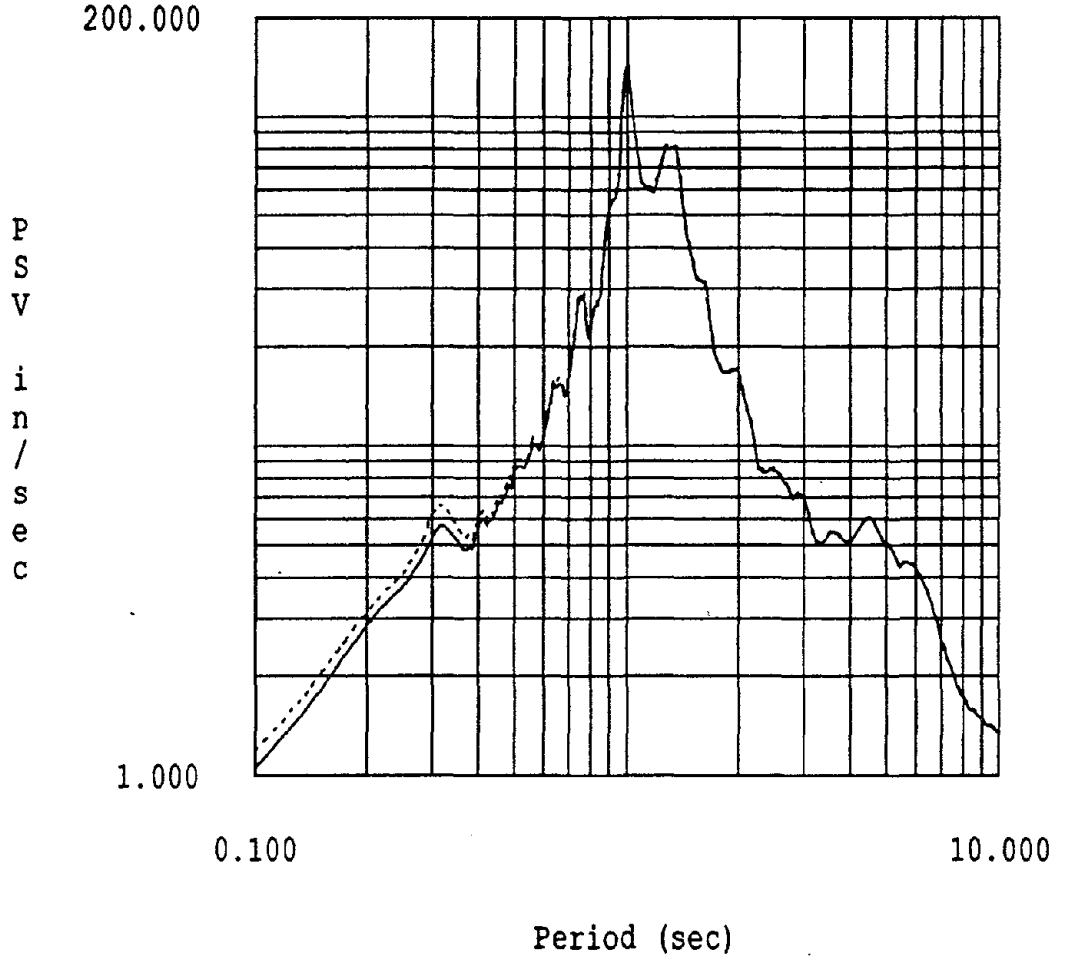

Fig. 9.29: Pseudo Velocity Response Spectrum: Mexico 1% Damping.
Time Scale Factor = 2

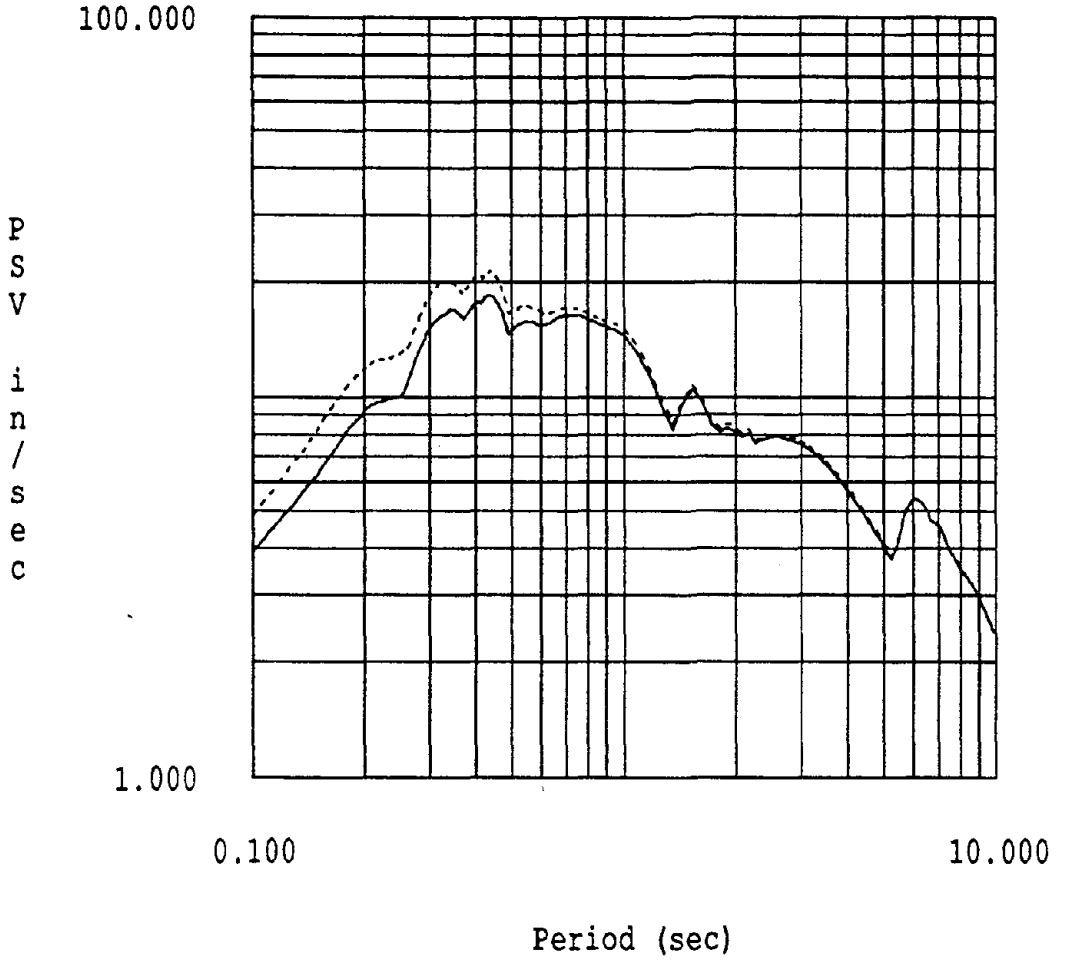

Fig. 9.30: Pseudo Velocity Response Spectrum: Taft 10% damping

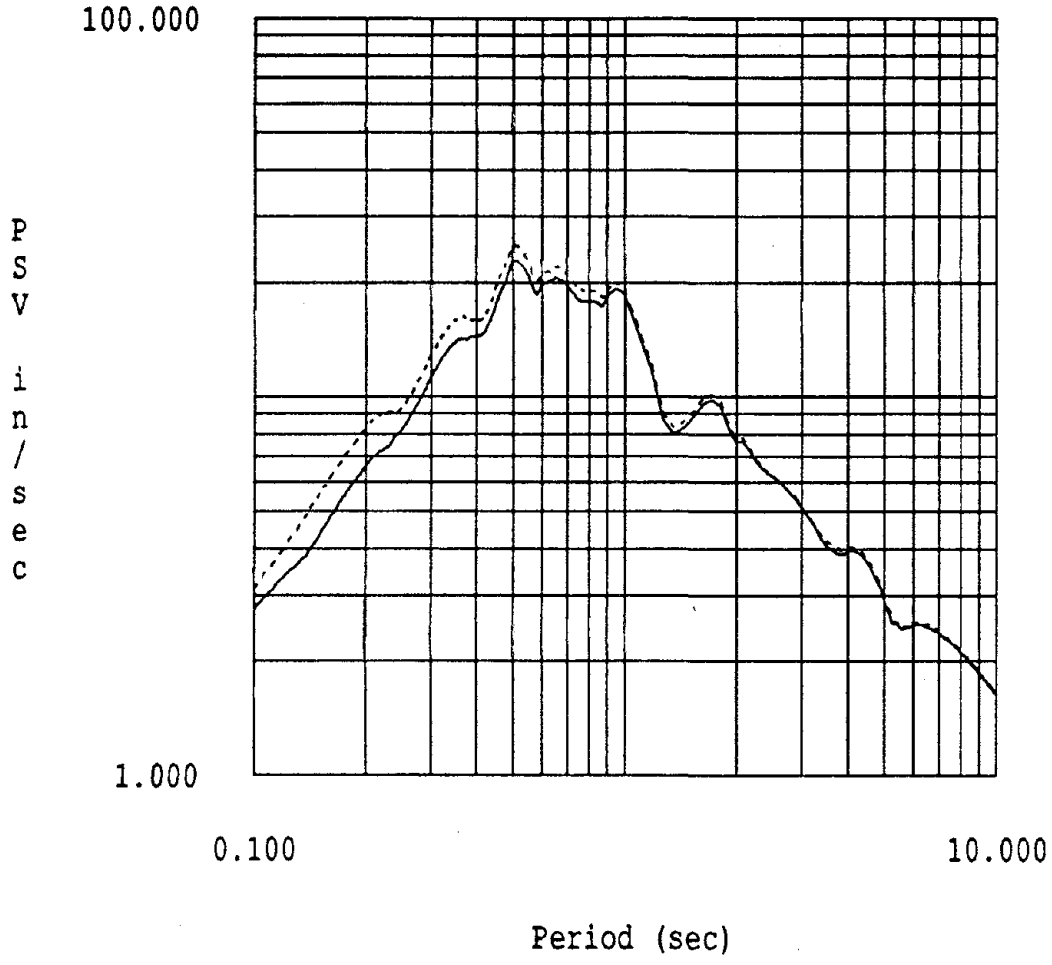

Fig. 9.31: Pseudo Velocity Response Spectrum: Miyagi 10% damping

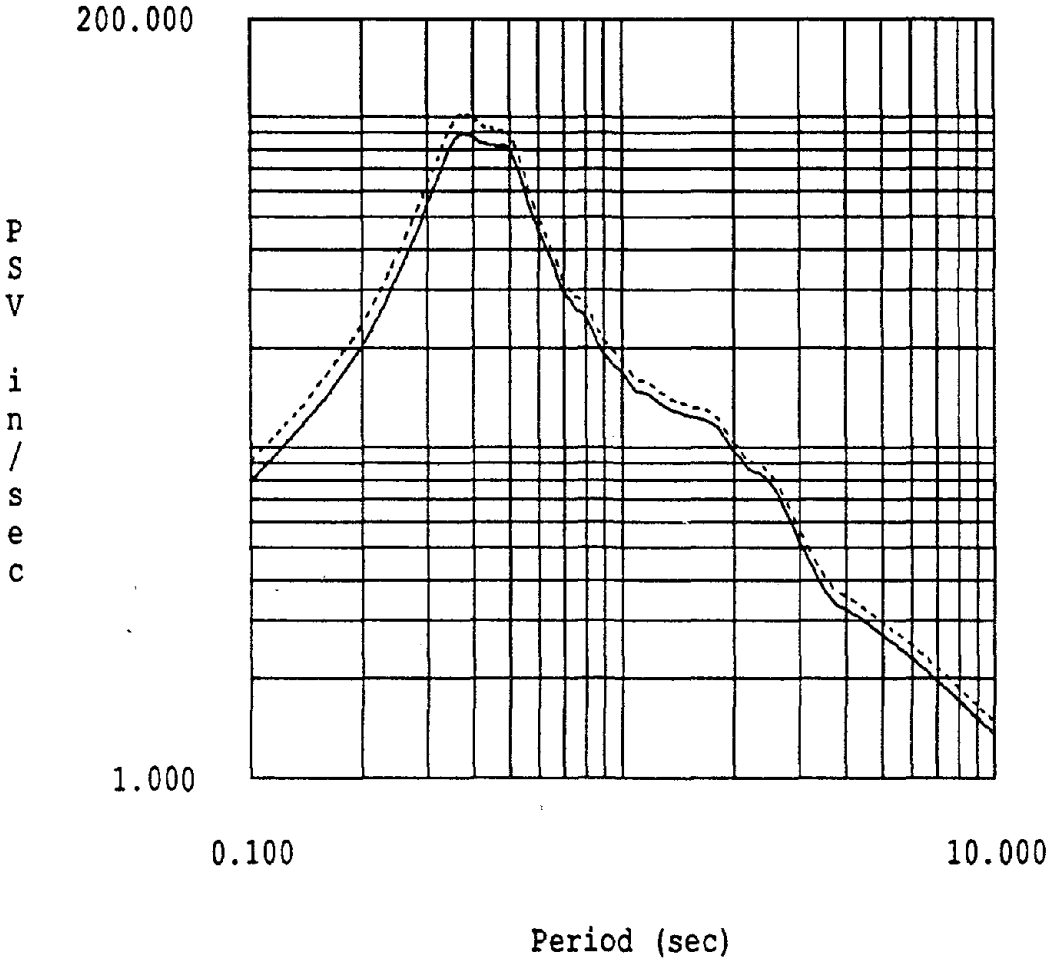

Fig. 9.32: Pseudo Velocity Response Spectrum: Mexico 10% Damping.
Time Scale Factor = 5

Chapter Ten
SUMMARY AND CONCLUSIONS

10.1 SUMMARY

Shaking table interaction was observed experimentally in this research by comparing the table motions that were produced with the input excitation signal, using 3 loading configurations. First, the bare table was studied using random as well as real earthquake input records. Second, a 70 kip concrete mass with a height of 2 ft was studied mainly with white noise excitation. Third, a 68 kip single degree-of-freedom braced steel structure with a fixed-base frequency of 2.87 Hz was tested using random as well as earthquake records. The height of the SDOF structure was about 219 inches from the horizontal actuator position, which was expected to cause a reasonably high overturning moment that will induce the shaking table to undergo significant rocking (pitching). The effect of varying the shaking table control settings was observed during testing by using white noise excitation. Shaking table-structure interaction was analyzed using transfer functions, response spectra and the response of an equivalent SDOF model. In addition these interaction effects were analyzed using an effective acceleration applied to the table mass. Most of the analysis was confined to single degree-of-freedom systems mounted on the shaking table, but in some instances the method was extended to multi-degree-of-freedom systems. Linear analysis of the interaction has been assumed throughout most of the investigation. Appendix C includes a treatment of a nonlinear model and highlights the effects of nonlinearities on the system behavior.

The shaking table itself was modeled using various methods. These included a horizontal feedback control system model, a horizontal feedback model with a filter on the pressure feedback, a horizontal mass-spring-damper model, a rotational mass-spring-damper model, and a combined horizontal and pitching mass-spring-damper model. A hybrid model was also used which included a horizontal feedback control together with a rotational

Preceding page blank

spring and a rotational dashpot. In addition, a horizontal nonlinear feedback model was presented. The single degree-of-freedom structure was assumed to be viscously damped and linear.

Several methods that avoided modeling of the shaking table were also treated in Chapter 4. These included using the measured table acceleration and the measured table pitch as an input to the rigid massless foundation. In this case the fixed-base structural characteristics should be used in defining the model. Another method was used that combines the horizontal and pitching motion of the table in an equivalent or "effective horizontal motion". This method is exact for SDOF structures, and can also yield good results when extended to multi-degree-of-freedom systems.

Several practical methods were described to estimate the shaking table model parameters experimentally as well as to determine the fixed-base structural parameters which may be assumed to vary with the amplitude of earthquake excitation.

Some of the important findings of this report are listed in the section below.

10.2 CONCLUSIONS

- Transfer functions of the bare table and of the table loaded with a heavy concrete mass showed a very reasonable response behavior. The table displacement was very similar to that of the command displacement. Table pitching was insignificant. Transfer functions showed no peaks or notches in this case.
- The shaking table loaded with a tall and heavy SDOF structure demonstrated significant pitching, and a peak and notch appeared in the transfer function between the table horizontal displacement and the command displacement. The notch in the transfer function occurred at the fixed-base structural frequency, the peak occurred near the coupled table-structure frequency. Table pitching was most evident at the coupled table-structure frequency.
- The effect of the peak and notch behavior on the system response was not as significant as had been previously thought, this conclusion was

verified by using the Mexico record which is basically a very narrow banded input.

- The shaking table interaction effects can be expressed as a lowering in the system frequency and as a change in damping, as is frequently the case in soil-structure interaction. For a system with low fixed-base structural damping, the effect of interaction is to increase the structural damping significantly; for structures with higher damping ratios, the interaction can actually decrease the total damping in the system.
- Interaction effects in the EERC shaking table are negligible for structures with periods greater than 1 second (i.e., frequencies lower than 1 Hz).
- Both the horizontal and rocking interaction mechanisms play an important role in the total system interaction for such flexible structures.
- In general, though not always, shaking table interaction tends to reduce the structural response. This is because in most cases the added damping due to interaction more than compensates for the frequency shift.
- Compensation for the reduced frequency effect of interaction can be achieved either by stiffening the structure or by a time-scale elongation in the earthquake record to account for the reduced natural frequency due to interaction. Appropriate reduction in structural damping is harder to achieve; moreover damping is poorly understood in most systems and may not be scaled properly in the test specimens so any shaking table discrepancy in damping has limited significance.
- Linear shaking table system parameters can change significantly with different test specimens or loading conditions. This requires estimating different system parameters for every loading configuration.
- It could be counter productive to try to correct for shaking table interaction using an input signal correction scheme that accounts only for horizontal interaction [36,37]. The reason is that the rocking interaction would not be taken care of, and more important, the modification of the command signal will amplify the input forces near the fixed-base frequency (in the process of correcting for the notch at that frequency).

This amplification of the signal at a frequency the system no longer has, because of the coupling effect, may not change the response significantly; moreover, the correction would also lower the input forces at the coupled table-structure frequency. The combined effect of the correction to the command signal may lead to a reduced response. If a correction scheme is ever justified, it must be based on the effective displacement that includes the pitching effect [Section 4.2.2].

- When a feedback control system is maintaining a zero command signal, as is the case with the pitch controller in the EERC earthquake simulator, it can be modeled as a frequency dependent spring-damper system.

REFERENCES

[1] Bertero, V.V.; Aktan, A. E.; Charney, F.A. and Sause, R. "US-JAPAN Cooperative Earthquake Research Program: Earthquake Simulation Tests And Associated Studies Of A 1/5th Scale Model Of A 7-Story Reinforced Concrete Test Structure" EERC Report No. 84/05, University Of California, Berkeley, 1984.

[2] Tang, David T. "Earthquake simulator study of a steel frame structure, Vol II: Analytical results". EERC report 75/36, October 1975. University of California at Berkeley.

[3] Huckelbridge, Arthur A. "Earthquake simulations tests of a nine story steel frame with columns allowed to uplift. EERC report 77/23, August 1977. University of California at Berkeley.

[4] Ghanaat, Yusof "Study of X-Braced Steel Frame Structures Under Earthquake Simulation". EERC Report 80/08, April 1980. University of California at Berkeley.

[5] Yang, Ming-San "Seismic behavior of an eccentrically x-braced steel structure". EERC report 82/14, September 1982. University of California at Berkeley.

[6] Griffith, M.C.; Aiken, Ian and Kelly, J.M. "Experimental Evaluation of Seismic Isolation of a 9-Story Braced Steel Frame Subject to Uplift. EERC report 88/05 may 1988. University of California at Berkeley.

[7] Rea, Dixon.; Abedi-Hayati, S. and Takahashi, Y., "Dynamic analysis of Electrohydraulic shaking tables", EERC Report No. 77/29, University of California, Berkeley, 1977.

[8] Blondet, M. and Esparza, C., "Analysis of shaking table-structure interaction effects during seismic simulation tests", Earthquake Engineering and Structural Dynamics, Vol. 16, No.4, pp 473-490, May 1988.

[9] Mitchell, L.D., "Improved Methods for the Fast Fourier Transform (FFT) Calculation of the Frequency response Function", Tran. ASME., Jr. Mech. Des., 104, pp 277-279, April 1982.

[10] Ewins, D. J., "Modal Testing: Theory and Practice". Research Studies Press LTD. John Wiley and Sons Inc. 1984 (pp 158-168)

[11] Clough, R.W. and Penzien, J., "Dynamics of Structures" McGraw-Hill, Inc. 1975.

[12] Uang, C.-M.; Bertero V.V. and Clough R.W.,"Correlation Studies using the Equivalent Base Horizontal Acceleration Method", Earthquake Engineering and Structural Dynamics, Vol. 18, No. 1, pp 33-47, January 1989.

[13] Wolf, John P., "Dynamic Soil Structure Interaction". Prentice Hall Inc., 1985.

[14] Veletsos, A.S.; Prasad, A.M. and Tang, Y., "Design Approaches For Soil-Structure Interaction" National Center for Earthquake Engineering Research,

State University of New York at Buffalo. Technical Report NCEER-88-0031. December 1988.

[15] Whitman, R.V. "Equivalent Lumped System for Structure Founded upon Stratum of Soil". Paper submitted to the 4th World Conference on Earthquake Engineering, Santiago, Chile, January 1969.

[16] Castellani, A., "Foundation Compliance Effects on Earthquake Response Spectra". J. Soil Mech. and Foundation Eng. Proc. ASCE, Vol. 96, No. SM4, July 1970.

[17] Parmelee, R.A., "Building Foundation Interaction Effects". J. of Eng. Mech. Div. Proc. ASCE, Vol. 93, No. EM2, April 1967.

[18] Veletsos, A.S. and Meek, J.W., "Dynamic Behavior of Building Foundation Systems", Earthquake Eng. Str. Dyn. Vol. 3, 121-138, 1974.

[19] Beliveau, J.G.; Vigneron, F.R.; Soucy, Y. and Draisey, S., "Modal Parameter Estimation From Base Excitation", Journal of Sound and Vibration, Vol. 107, No. 3, pp 435-449, June 1986.

[20] Merritt, H.E., "Hydraulic Control Systems", John Wiley & Sons, Inc., 1967

[21] Anderson, Wayne "Controlling Electrohydraulic Systems". Marcel Dekker, Inc. New York 1988.

[22] Guillon, M. "Hydraulic Servo Systems: Analysis and Design". New York Plenum Press.

[23] Stringer, John "Hydraulic Systems Analysis: An Introduction" John Wiley & Sons, Inc. New York 1976.

[24] Rinawi, A.M.; Clough, R.W. and Blondet, M. "Pitching and Interaction Effects in EERC Seismic Simulator". Ninth World Conference in Earthquake Engineering, Japan, August 1988.

[25] Rinawi, A.M. "Interaction Effects in EERC shaking Table". CE299 report, University of California, Berkeley. April 1987.

[26] Blondet, M.; Rinawi, A.M. and Esparza, C. "Analytical Models for Earthquake Simulator-Structure Interaction".[Abstract Only] Ninth World Conference in Earthquake Engineering, Japan, August 1988.

[27] Jeunink, I.P., "A Seismic Simulator System at PUCP", Meetechniek Report No. 322-81-05, Stevin-Laboratorium, Delft University, 1983.

[28] Titlo, Report to Prof. R.W. Clough, University of California, Berkeley, 1986.

[29] Kuo, B.C.,"Automatic Control Systems", Fourth Edition, Prentice Hall Inc., 1982.

[30] Levenberg, K.,"A method for the solution of certain non-linear problems in least squares", Quart. Appl. Math., 2, 1944, 164-168

[31] Marquardt, D.W., "An algorithm for least squares estimation of nonlinear parameters", J. SIAM, 11 (2) 1963.

[32] IMSL : International Mathematical Subroutine Library.

[33] Dennis, J.E.; Gay, D.M. and Welsch, R.E., "An Adaptive Nonlinear Least Squares Algorithm", ACM Transactions on Mathematical Software, Vol. 7, No. 3, September 1981.

[34] Penzien, J.; Bouwkamp, J.G.; Clough, R.W. and Rea Dixon "Feasibility Study: Large-Scale Earthquake Simulator Facility", EERC report 67/01, September 1967. University of California at Berkeley.

[35] Trifunac, M.D. and Lee, V., "Routine Computer Processing of Strong Motion Accelerograms", Report No. EERL 73-03, Earthquake Eng. Research Laboratory, California Institute of Technology, Pasadena, October 1973.

[36] Lund, R., "Environmental Simulation with Digitally Controlled Servo-Hydraulics", Institute of Environmental Science, Philadelphia, 1976.

[37] Hwang, J.S.; Chang K.C. and Lee G.C., "The System Characteristics and Performance of a Shaking Table", Technical Report NCEER-87-0004, Dept. Civil Eng., State University of New York at Buffalo, June 1987.

[38] Clough, R.W.; Ghanaat, Y. and Qiu, X.-F, "Dynamic Reservoir Interaction with Monticello Dam", Report No. UCB/EERC 87/21 Earthquake Engineering Research Center, University of California, Berkeley, 1987.

[39] Mau, S.T. and Wang, S., "Arch Dam System Identification Using Vibration Test Data", Earthquake Engineering and Structural Dynamics, Vol. 18, 491-505 (1989).

APPENDIX A

ANALYSIS OF A MECHANICAL MODEL FOR TWO-DIRECTIONAL EARTHQUAKE SIMULATORS

Figure 4.4 shows the mechanical model of the pitching table and identifies its degrees of freedom.

Equilibrating the forces acting on the mass of the structure we get

$$m_s \ddot{x}_s^t + c_s \dot{x}_s^r + k_s x_s^r = 0 \tag{A.1}$$

Summing the horizontal forces on the table platform we get

$$m_t \ddot{x}_t + c_h \dot{x}_t^r + k_h x_t^r - c_s \dot{x}_s^r - k_s x_s^r = 0 \tag{A.2}$$

Summing the moment acting on the platform we get

$$I\ddot{\theta} + c_r \dot{\theta} + k_r \theta - c_s \dot{x}_s^r h - k_s x_s^r h = 0 \tag{A.3}$$

Note that the relative structural displacement and the relative table displacements are defined as

$$x_s^r = x_s^t - x_t - x_r \tag{A.4}$$

$$x_t^r = x_t - x_c \tag{A.5}$$

where x_r is given by

$$x_r = \theta h \tag{A.6}$$

Multiplying Eq. (A.3) by h and rewriting in terms of x_r we get

$$I\ddot{x}_r + c_r \dot{x}_r + k_r x_r - c_s h^2 \dot{x}_s^r - k_s h^2 x_r = 0 \tag{A.7}$$

Dividing Eqs. (A.1) and (A.2) by m_s, and (A.7) by I and making use of the relations

$$\frac{k_s}{m_s} = \omega_s^2 \qquad \frac{c_s}{m_s} = 2\omega_s \xi_s$$

Preceding page blank

$$\frac{k_h}{m_t} = \omega_h^2 \qquad \frac{c_h}{m_t} = 2\omega_h \xi_h \tag{A.8}$$

$$\frac{k_r}{I} = \omega_r^2 \qquad \frac{c_r}{I} = 2\omega_r \xi_r$$

$$\frac{m_s}{m_t} = u \qquad \frac{m_s h^2}{I} = v$$

Equation (A.1) can be rewritten as

$$\ddot{x}_s^r + 2\xi_s \omega_s \dot{x}_s^r + \omega_s^2 x_s^r = -(\ddot{x}_t + \ddot{\theta} h) = -\ddot{x}_{eff} \tag{A.9}$$

where $\ddot{x}_{eff}$ is the effective horizontal table acceleration as described in Section 4.2. Equations (A.2) and (A.3) can be rewritten as

$$\ddot{x}_t^r = -2\xi_h \omega_h \dot{x}_t^r - \omega_h^2 x_t^r + 2\xi_s \omega_s u \dot{x}_s^r + \omega_s^2 u x_s^r - \ddot{x}_c \tag{A.10}$$

$$\ddot{x}_r = -2\xi_r \omega_r \dot{x}_r - \omega_r^2 x_r + 2\xi_s \omega_s v \dot{x}_s^r + \omega_s^2 v x_s^r \tag{A.11}$$

and substituting Equations (A.5), (A.6), (A.10) and (A.11) into (A.9) we get

$$\ddot{x}_s^r = -2\xi_s \omega_s (1+u+v)\dot{x}_s^r - \omega_s^2 (1+u+v) x_s^r \tag{A.12}$$

$$+ 2\xi_h \omega_h \dot{x}_t^r + \omega_h^2 x_t^r + 2\xi_r \omega_r \dot{x}_r + \omega_r^2 x_r$$

Equations (A.12), (A.10) and (A.11) can be rewritten in state equation form as

$$\frac{d}{dt}\begin{Bmatrix} \dot{x}_s^r \\ \dot{x}_t^r \\ \dot{x}_r \\ x_s^r \\ x_t^r \\ x_r \end{Bmatrix} = \begin{bmatrix} -2\xi_s\omega_s(1+u+v) & 2\xi_h\omega_h & 2\xi_r\omega_r & -\omega_s^2(1+u+v) & \omega_h^2 & \omega_r^2 \\ 2\xi_s\omega_s u & -2\xi_h\omega_h & 0 & \omega_s^2 u & -\omega_h^2 & 0 \\ 2\xi_s\omega_s v & 0 & -2\xi_r\omega_r & \omega_s^2 v & 0 & -\omega_r^2 \\ 1 & 0 & 0 & 0 & 0 & 0 \\ 0 & 1 & 0 & 0 & 0 & 0 \\ 0 & 0 & 1 & 0 & 0 & 0 \end{bmatrix} \begin{Bmatrix} \dot{x}_s^r \\ \dot{x}_t^r \\ \dot{x}_r \\ x_s^r \\ x_t^r \\ x_r \end{Bmatrix} + \begin{Bmatrix} 0 \\ -1 \\ 0 \\ 0 \\ 0 \\ 0 \end{Bmatrix} \ddot{x}_c \tag{A.13}$$

which has the same form as Eq. (8.16) and can be solved in a similar manner, as described in Section 8.4.

APPENDIX B

UNI-DIRECTIONAL EARTHQUAKE SIMULATOR WITH FILTER ON FORCE FEEDBACK

B.1 INTRODUCTION

At the time the shaking table at the Earthquake Engineering Research Center was tested, it included in addition to the force, displacement and velocity feedback loops, a filter on the force feedback signal. This filter which is basically a highpass filter did not change the shaking table performance dramatically. In the preceding chapters the filter was neglected in order to reduce the system order from four to three and make the system completely expressed in terms of the open loop frequency f_o, open loop damping ξ_o and open loop gain k_o. The system open loop parameters were then found by a nonlinear least squares method as described in Chapter 6. The third order least squares model was found to fit the system very well (Section 6.7).

B.2 RC FILTER

The characteristics of the RC highpass filter are sketched in Fig. B.1, and for the assumed RC value of 0.01, the frequency response in shown in Fig. B.2. The input output relationship is given by

$$V_{out} = \frac{Z_R}{Z_R + Z_C} V_{in} \tag{B.1}$$

where Z_R and Z_C are the impedances of the resistor R and the capacitor C, respectively. Substituting leads to

$$V_{out} = \frac{R}{R + \frac{1}{jwC}} V_{in} \tag{B.2}$$

In differential equation form the above equation can be rewritten as

$$\dot{V}_{out} = -\frac{V_{out}}{RC} + \dot{V}_{in} \tag{B.3}$$

B.3 MODEL EQUATIONS

The filtered pressure or force feedback signal P_f can be expressed in a manner similar to Eq. (B.3) as

$$\dot{P}_f = -\frac{1}{RC} P_f + \dot{P}_L \tag{B.4}$$

where P_L is the pressure difference across the actuator chamber. Equation (6.6) can be expressed in terms of the differential pressure as

$$\ddot{x}_t = \frac{A}{m_t} P_L \tag{B.5}$$

where A is the actuator piston area.

Equation (6.5a) can be rewritten for this case as

$$\frac{V}{4\beta}\dot{P}_L = -k_{ct}P_L - A\dot{x}_t + k_t(x_c - x_t - k_v\dot{x}_t - k_p P_f) \tag{B.6}$$

Velocity feedback was found to have negligible influence on the response and performance of the EERC table and will be neglected here by setting k_v=0 in the above equation. Equations (B.4-B.6) can be written in state equation form as

$$\frac{d}{dt}\begin{Bmatrix} P_L \\ P_f \\ \dot{x}_t \\ x_t \end{Bmatrix} = \begin{bmatrix} -\frac{4\beta}{V}k_{ct} & -\frac{4\beta}{V}k_t k_p & -\frac{4\beta}{V}A & -\frac{4\beta}{V}k_t \\ -\frac{4\beta}{V}k_{ct} & -\frac{4\beta}{V}k_t k_p - \frac{1}{RC} & -\frac{4\beta}{V}A & -\frac{4\beta}{V}k_t \\ \frac{A}{m_t} & 0 & 0 & 0 \\ 0 & 0 & 1 & 0 \end{bmatrix} \begin{Bmatrix} P_L \\ P_f \\ \dot{x}_t \\ x_t \end{Bmatrix} + \begin{Bmatrix} \frac{4\beta}{V}k_t \\ \frac{4\beta}{V}k_t \\ 0 \\ 0 \end{Bmatrix} x_c \tag{B.7}$$

B.4 SYSTEM PARAMETERS

Table B.1 lists the amplification factors corresponding to different shaking table control settings. The relationship between the error function and the slave spool displacement is shown in Fig. B.2, this verifies the assumption of

the linear relationship between the input force and the slave spool displacement as given by Eq. (6.2). The transfer function of the table velocity over the slave spool displacement, is shown in Fig. B.3. The analytical form of this function can be derived from Eqs. (6.2), (6.3) and 6.6. The latter transfer function will have the form given by the open loop transfer function in Eq. (6.13), except that $\hat{k}_o$ will be replaced by k_q/A. The analytical model fitted in Fig. B.3 has the parameters $k_q/A = 129, f_o = 15.00Hz$ and $\xi_o = 0.126$. From f_o, the oil modulus can be found as β= 94000 psi, then only two parameters need to be determined, k_{ct} and k_t. A nonlinear least squares method was employed to get the best estimates for k_{ct} and k_t which are listed together with all the assumed values for the standard control settings in Table B.5. For the standard shaking table settings, the experimental and fitted transfer functions are shown in Fig. B.4.

B.5 EFFECT OF VARYING DELTA-P

By replacing the DELTA-P gain in Table B.5 by the appropriate values for DELTA-P=5 from Table B.1, the corresponding transfer function is shown in Fig. B.5. The higher Delta-P corresponds to a higher gain k_p. The effect of varying the Delta-P on system stability is shown in Fig. B.6. The case with higher Delta-P has lower phase and gain margins and hence is less stable. (Gain and phase margins were introduced in Chapter 6.) In the absence of the filter on the force feedback, the force feedback (or pressure feedback) gain k_f would normally lead to greater open loop system damping ξ_o as given by Eq. (6.16c); this in turn would lead to a greater gain margin as shown by Eq. (6.20) and hence to a more stable system. In this system, which differs from that in Chapter 6 only by the addition of highpass filter on the force or pressure feedback, the feedback gain effect is reversed and that difference can be attributed to the presence of the filter. We observe from Fig. B.1 that the highpass filter changes the phase of the unfiltered part of the low frequency signal.

HORIZONTAL SETTING	FACTOR
Gain=8	4.58
Gain=9*	5.68
Gain=10	7.07
DELTA-P=0	0
DELTA-P=1.5*	0.0000514
DELTA-P=5	0.000274
RATE=5*	0.157
RATE=10	0.999

Table B.1
Corresponding Factors for the Different Shaking Table Settings.
(* : Standard bare table settings)

VERTICAL SETTING	FACTOR
Gain=0	0.189
Gain=2	0.380
Gain=4*	0.542
DELTA-P=0	0
DELTA-P=2*	0.000116
DELTA-P=4	0.000252
RATE=5	0.192
RATE=10*	1.000

Table B.2
Corresponding Factors for the Different Shaking Table Settings.
(* : Standard bare table settings)

PITCH SETTING	FACTOR
Gain=0*	0.222
Gain=1	0.420
Gain=3	0.745
DELTA-P=0	0
DELTA-P=2*	0.000127
DELTA-P=4	0.000290
RATE=0*	0
RATE=5	0.222
RATE=10	1.015

Table B.3
Corresponding factors for the different shaking table settings.
(* : Standard bare table settings)

ROLL SETTING	FACTOR
Gain=4*	0.743
RATE=10*	0.911

Table B.4
Corresponding factors for the different shaking table settings.
(* : Standard bare table settings)

Delta-P Gain	k_p	0.0000514
Total Horizontal Gain	k_t	663.0
Flow Pressure Coefficient (in^3/s/psi)	k_{ct}	0.0787
RC Filter	RC	0.01
Table Mass (100 kips/(3g))	m_t	86.3
Oil Modulus (psi)	β	94000.0
Actuator Area (in^2)	A	25.4
Oil Volume (in^3)	V	317.5

Table B.5
Bare Table Fitted Parameters

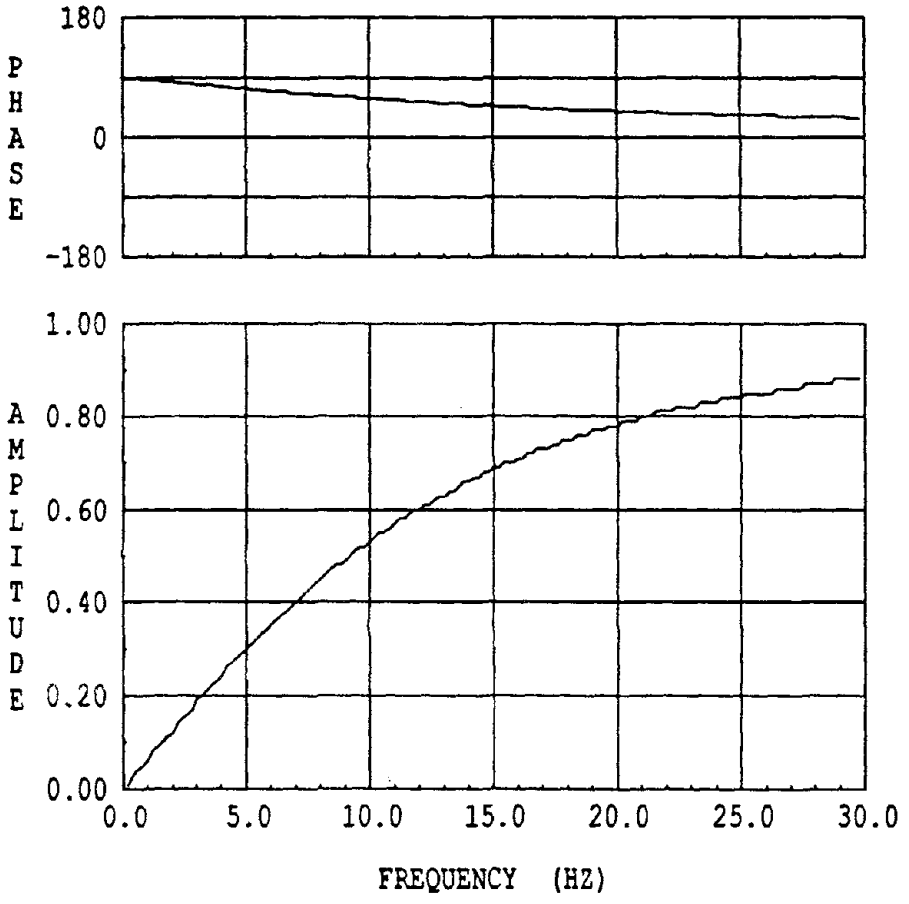

Fig. B.1: Amplitude and Phase Characteristics of The RC Filter used in Force Feedback Loop.

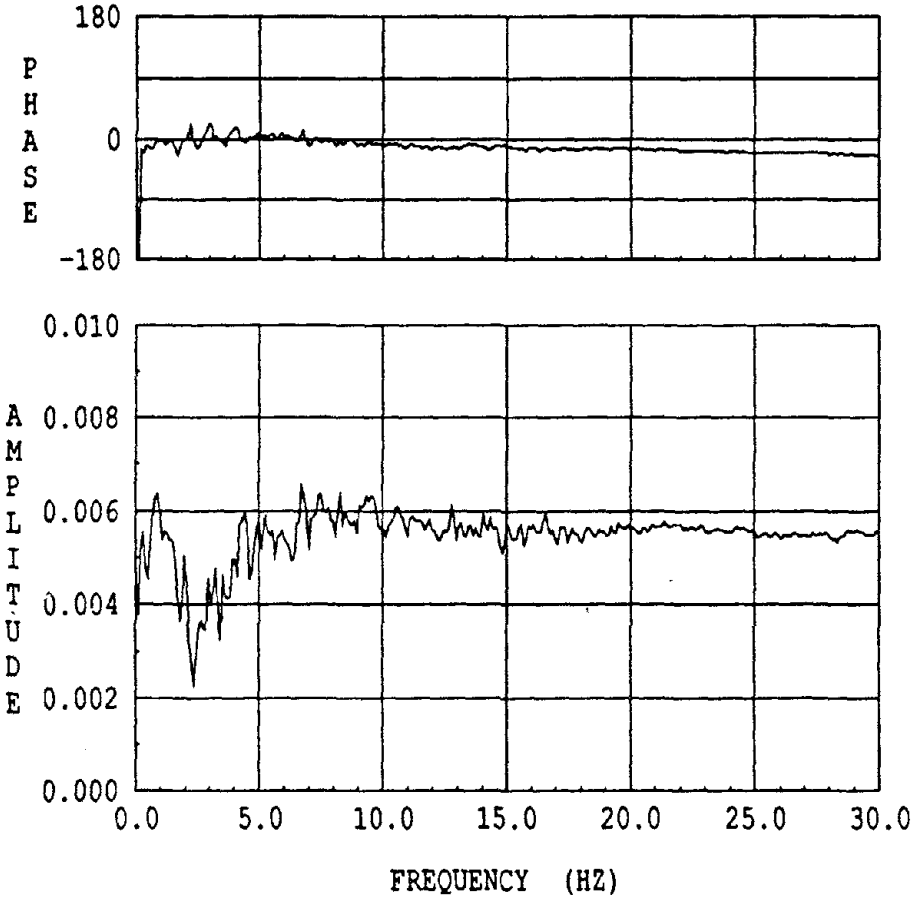

Fig. B.2: Transfer Function of Slave Spool Displacement of Horizontal Actuator H3 over H3 error signal.

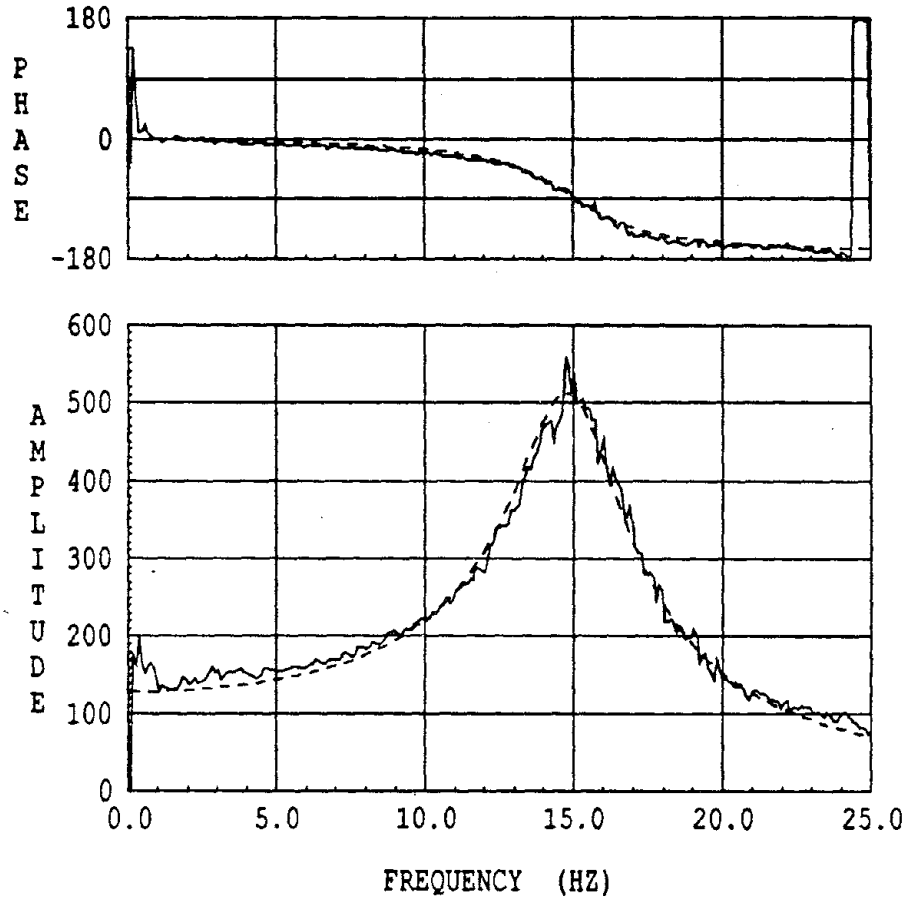

——— Experimental
---- Analytical: Frequency=15.0 Hz, Damp=12.8%, Gain=129

Fig. B.3: Transfer Function of Actuator Velocity over Slave Spool Displacement: Actuator H3.

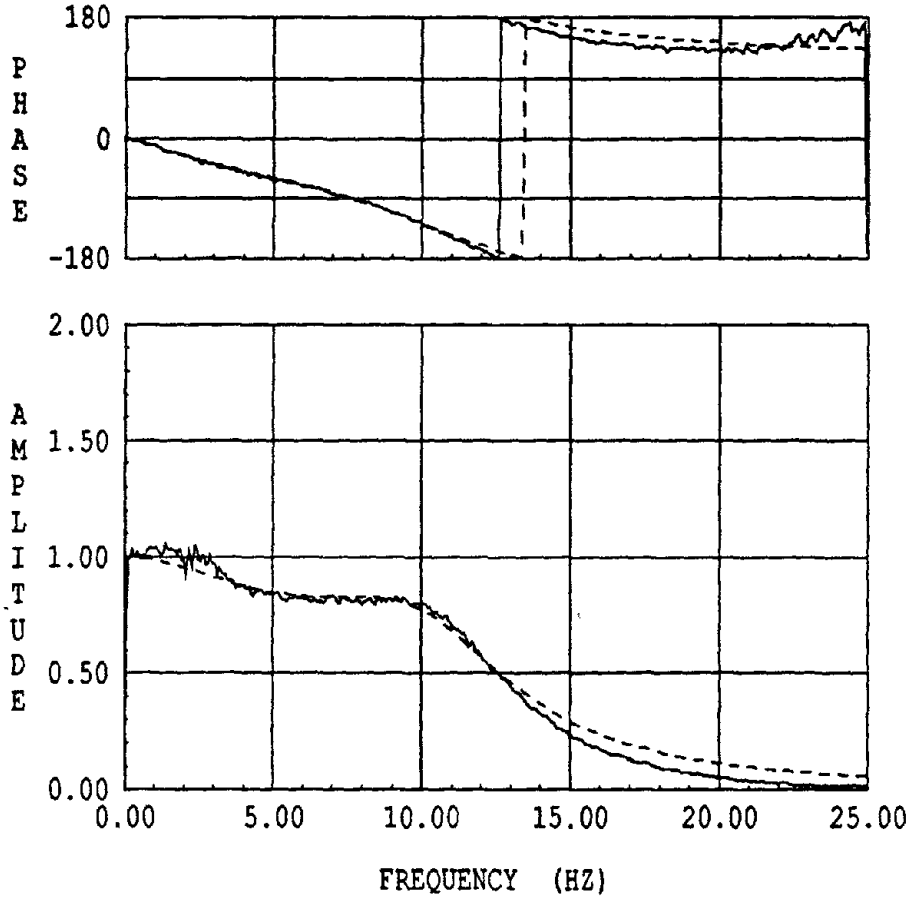

Fig. B.4: Experimental and Analytical Model Prediction of the Table Displacement over Command Displacement. Delta-P=1.5

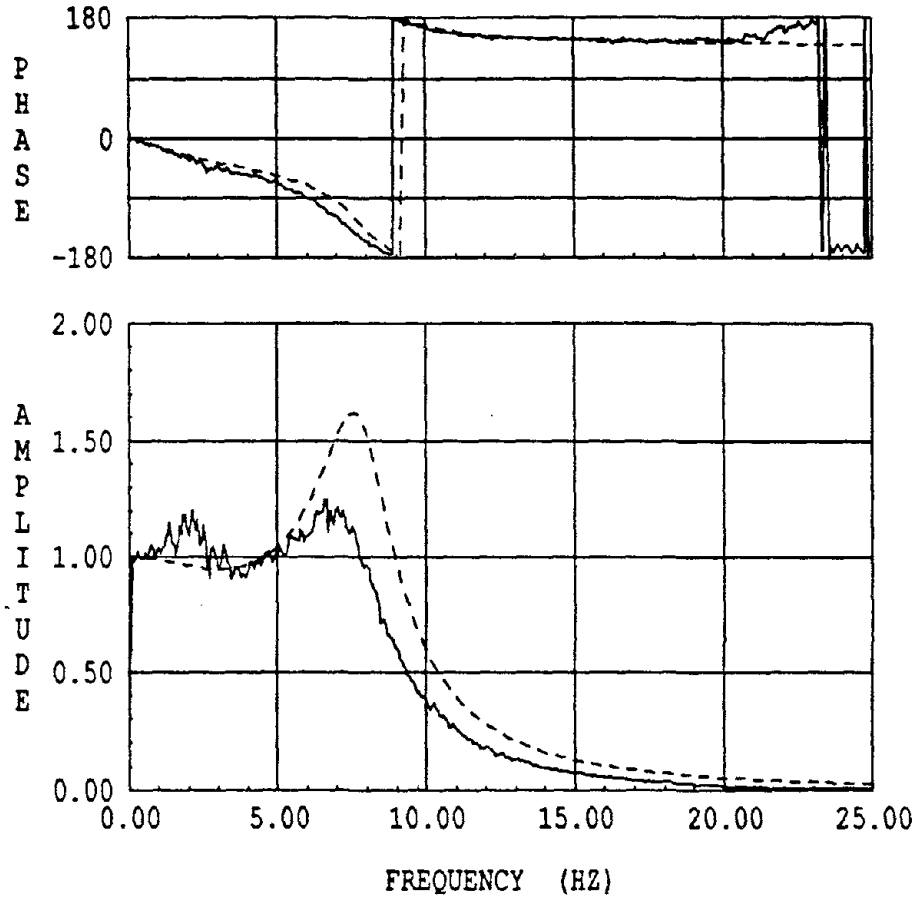

—— Experimental: Delta-P=5
---- Analytical Model

Fig. B.5: Experimental and Analytical Model Prediction of the Table Displacement over Command Displacement. Delta-P=5

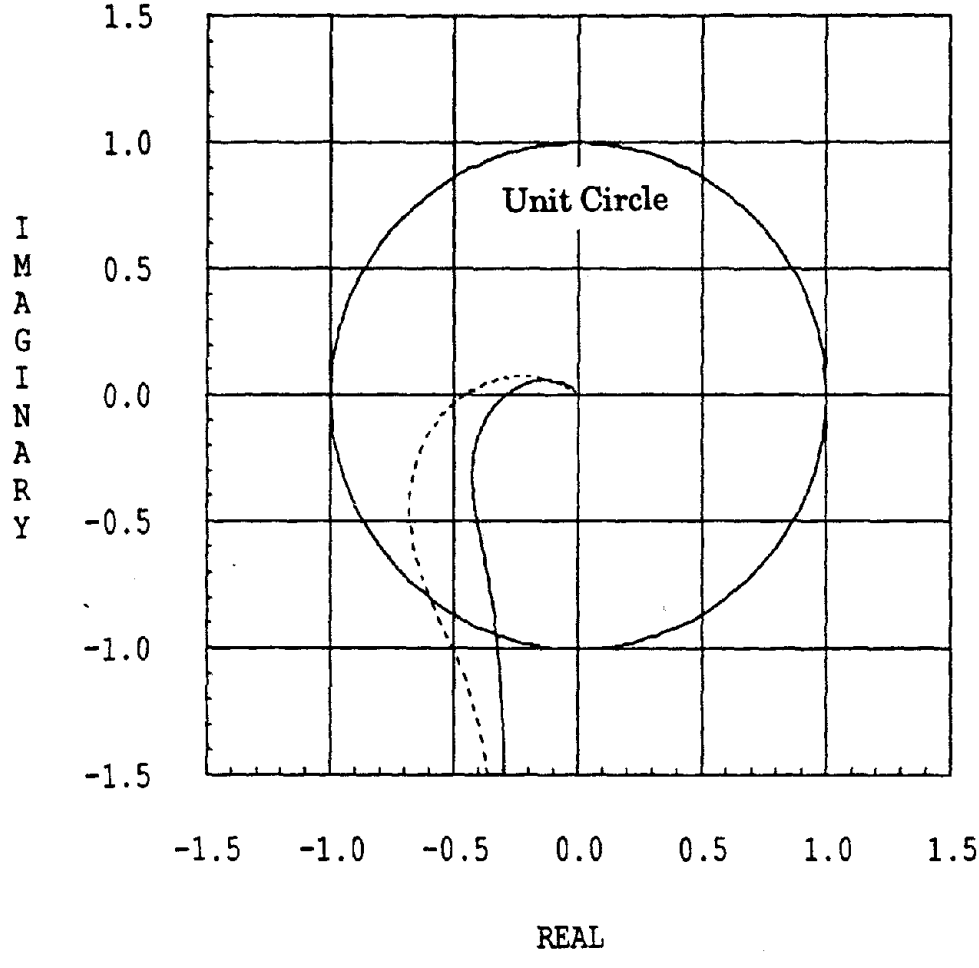

Fig. B.6: Effect of Delta-P Gain on Bare Table Stability: Nyquist Plot

APPENDIX C

NONLINEAR MODEL FOR A UNI-DIRECTIONAL EARTHQUAKE SIMULATOR

C.1 MODEL EQUATIONS

Figure C.1 shows the slave spool and actuator chamber employed in the actuators at EERC. The pilot spool is omitted from the figure for simplicity. It will be assumed that the pilot spool helps linearize the input force-slave spool displacement as in Eq. (6.1). This assumption can be justified on the basis of the results shown in Fig. B.2 and also by the fact that the slave spool mass involved is very small so that the component frequency is much larger than the system frequency.

The flows Q_1 and Q_2 into and out of the actuator chambers consist of an orifice flow and a leakage flow. For positive spool displacement ($x_{sp} > 0$), these flows can be written as

$$Q_1 = C_v x_{sp} \sqrt{P_s - P_1} - C_l P_1 \tag{C.1}$$

$$Q_2 = C_v x_{sp} \sqrt{P_2} - C_l (P_s - P_2) \tag{C.2}$$

and for negative spool displacement the equations become

$$Q_1 = C_v x_{sp} \sqrt{P_1} - C_l (P_s - P_1) \tag{C.3}$$

$$Q_2 = C_v x_{sp} \sqrt{P_s - P_2} - C_l P_2 \tag{C.4}$$

The flow through the orifice is assumed turbulent because of the high velocities associated with this type of flow. While the leakage is assumed to be laminar, a more realistic assumption for the leakage term would be a flow that varies from turbulent to laminar based on the spool displacement x_{sp}. The power of the pressure term could then be varied from 0.5 for small values of x_{sp} to the value of one for the maximum spool displacement x_{vm}. C_v is the valve coefficient and is a function of the discharge coefficient C_d,

orifice area gradient w and the oil density ρ as

$$C_v = \frac{C_d}{\sqrt{\rho}} w\sqrt{2} \tag{C.5}$$

The discharge coefficient $C_d \approx 0.61$ [20] and for petroleum base fluids $\rho \approx 0.78 \times 10^{-4}$ lb-sec^2/in^4. The area gradient can be roughly estimated as the spool perimeter. Alternatively C_v can be obtained from the servovalve flow rating supplied by the manufacturer. The rated flow is normally given at the maximum valve stroke x_{vm} and a standard pressure drop of 1000 psi. The other parameters in Eqs. (C.1) and (C.2) are P_s, the supply pressure (usually 3000 psi), P_1 and P_2 the oil pressure on both sides of the actuator piston as shown in Fig. C.1. C_l is a leakage coefficient of the servovalve and is zero for the ideal case of no leakage. Note that the flow into the actuator is limited by the supply flow and by the maximum valve stroke x_{vm}; which may introduce an additional nonlinearity into the system.

The continuity equations for the flow into the actuator chambers require that

$$Q_1 - C_{ip}(P_1 - P_2) - C_{ep}P_1 = \frac{dV_1}{dt} + \frac{V_1}{\beta_{e1}}\frac{dP_1}{dt} \tag{C.6}$$

$$C_{ip}(P_1 - P_2) - C_{ep}P_2 - Q_2 = \frac{dV_2}{dt} + \frac{V_2}{\beta_{e2}}\frac{dP_2}{dt} \tag{C.7}$$

The left hand terms include the internal leakage (C_{ip} terms) across the actuator piston and external leakage (C_{ep} terms) from the cylinder. The right hand terms include first, the change in volume on one side of the piston due to piston movement and second, the change in volume due to compressibility of the fluid. If the initial piston volumes are V_{o1} and V_{o2}, the volume of oil as a function of the actuator displacement is

$$V_1 = V_{o1} + Ax_t \tag{C.8}$$

$$V_2 = V_{o2} - Ax_t \tag{C.9}$$

where A is the actuator piston area, and x_t is the piston movement. The effective bulk modulus of the oil in each chamber is a function of the

amount of entrained air r and the pressure [20].

$$\frac{1}{\beta_{e1}} = \frac{1}{\beta} + \frac{r}{1.4P_1} \tag{C.10}$$

$$\frac{1}{\beta_{e2}} = \frac{1}{\beta} + \frac{r}{1.4P_2} \tag{C.11}$$

where β is the oil bulk modulus and for petroleum base fluids is about 210,000 psi. r is the ratio of the volume of entrained air to the total volume. The compressibility of the actuator cylinder is neglected and normally it has a minor influence on the effective bulk modulus.

Equilibrating the forces acting on the actuator piston we get

$$A(P_1 - P_2) = m_t \ddot{x}_t + F_r \frac{\dot{x}_t}{|\dot{x}_t|} \tag{C.12}$$

in which m_t is the table mass and F_r is the friction force. The spool displacement x_{sp} is proportional to the difference between the command displacement x_c and the several feedback terms as follows

$$x_{sp} = k_a (x_c - x_t - k_v \dot{x}_t - k_p (P_1 - P_2)) \tag{C.13}$$

where k_v and k_p are the gains for the velocity and pressure feedback. The above equation can be solved using a Runga-Kutta integration scheme to get the output table displacement. The state variables involved are P_1, P_2, x_t and $\dot{x}_t$. The initial value for both pressure terms is $P_s/2$. The initial table displacement and velocity are zero.

C.2 SYSTEM NONLINEARITIES

It is important to identify the system nonlinearities that can be seen from the nonlinear model equations.

- Saturation nonlinearity: This type of nonlinearity occurs when the velocity or acceleration limits are reached. The displacement limit is normally not a problem as that can be avoided in advance by adjustment of the command signal. A typical performance curve for the EERC bare

table is shown in Fig. 2.3. Force limits are imposed by the actuator capacity $(P_1-P_2)A$, in which the maximum pressure is limited by the supply pressure. A negative pressure would cause cavitation and is highly undesirable. On the other hand, actuator velocity is limited by the servovalve flow capacity which is achieved with the maximum spool displacement x_{vm}.

- Effective Bulk Modulus: The Bulk Modulus of oil changes significantly with the amount of entrained air and the operating pressure as given by Eq. (C.10).
- Friction: Mechanical friction is always present in hydraulic systems and constitutes a common nonlinearity.
- Interaction between the pressure supply and the servo load: Sudden velocity changes in the servo valves require high flows from the hydraulic supply; this high flow in turn causes a reduction in the supply pressure which could worsen system performance. The EERC supply consists of four 90 gpm pumps each driven by a 120 hp motor; accumulators can double the peak instantaneous flow rates. However, the demand includes three 170 gpm horizontal actuators and four 90 gpm vertical actuators may exceed the supply flow, and that can cause a drop in the supply pressure.
- Orifice Flow equation: The flow across orifices is normally turbulent in high pressure systems because of the high Reynolds numbers associated with such flows. For turbulent flow, the flow rate is a function of the square root of the pressure difference across the orifice.

C.3 LINEARIZED FLOW EQUATION

By ignoring the leakage terms in Eqns. (C.1-C.4), and assuming the supply pressure as the sum of the two piston pressures P_1 and P_2, Eqs. (C.1-C.4) can be expressed in one single relation as

$$Q_L = \frac{C_v}{\sqrt{2}} x_{sp} \sqrt{P_s - \frac{x_{sp}}{|x_{sp}|} P_L} \tag{C.14}$$

where Q_L is the flow into or out of the actuator chambers and P_L is the pressure difference across the actuator piston. A first order approximation of C.14 is

$$\Delta Q_L = \frac{\partial Q_L}{\partial x_{sp}} \Delta x_{sp} + \frac{\partial Q_L}{\partial P_L} \Delta P_L \tag{C.15}$$

This can be rewritten as

$$\Delta Q_L = k_q \Delta Q_L - k_c^p \Delta P_L \tag{C.16}$$

where the flow gain k_q is given by

$$k_q = \frac{C_v}{\sqrt{2}} \sqrt{P_s - P_L} \tag{C.17}$$

and the flow-pressure coefficient k_c^p is given by

$$k_c^p = \frac{C_v}{\sqrt{2(P_s - P_L)}} x_{sp} \tag{C.18}$$

The term k_c^p in this equation is related to the flow force coefficient k_c which was introduced in Eq. (6.2) as follows

$$k_c^p = k_c A \tag{C.19}$$

where A is the actuator piston area.

It is to be noted that Eq. (C.16) is valid near the operating point of the table. This linearized flow relation was used in model building in Chapter 6.

C.4 VALIDITY OF THE LINEARIZED SYSTEM

In Chapter 6 and throughout this report, the system is assumed linear and the linearized flow equation (Eq. C.16) was used. This presents important simplifications which are valuable in understanding the shaking table system behavior. However, one needs to put the problem in perspective and consider the validity of these assumptions. Some important facts about the linearized system are listed below:

- The flow gain k_q given in Eq. (C.17) is largest at the null position and is reduced when a load is applied. At the maximum design load corresponding to $P_L=\frac{2}{3}P_s$, the k_q value is only 57.7 percent of the no load value.
- The open loop system damping ξ_o given by Eq. (6.14b) is proportional to the flow-pressure coefficient k_c^p. This value is minimum at small spool displacements giving the lowest damping ratio.
- The open loop frequency ω_o as given by Eq. (6.14a) depends on the effective bulk modulus of the oil. This effective bulk modulus is a function of the amount of entrained air and the pressure in the actuator; the entrained air can reduce the bulk modulus by more than 50 percent.
- The open loop frequency is a function of the initial oil volumes on both sides of the actuator piston V_{o1} and V_{o2} [20]:

$$\omega_o^2 = \frac{\beta_e A^2}{m_t}\left(\frac{1}{V_{o1}}+\frac{1}{V_{o2}}\right) \tag{C.20}$$

  The open loop frequency is minimum when $V_{o1}=V_{o2}=0.50V$ where V is the total volume of entrained air in the actuator cylinder. If $V_{o2}=0.25V$ then the natural frequency would be increased by 15 percent.
- Merritt [20] states that: "Small variations (perhaps 2 or 3 to 1) in the gain constant k_q and natural frequency ω_o and very large variations (perhaps 20 or 30 to 1) in the damping ratio of the valve motor dynamics can and do occur...These variations cause the frequency response to float around, so to speak, as the operating point is changed".

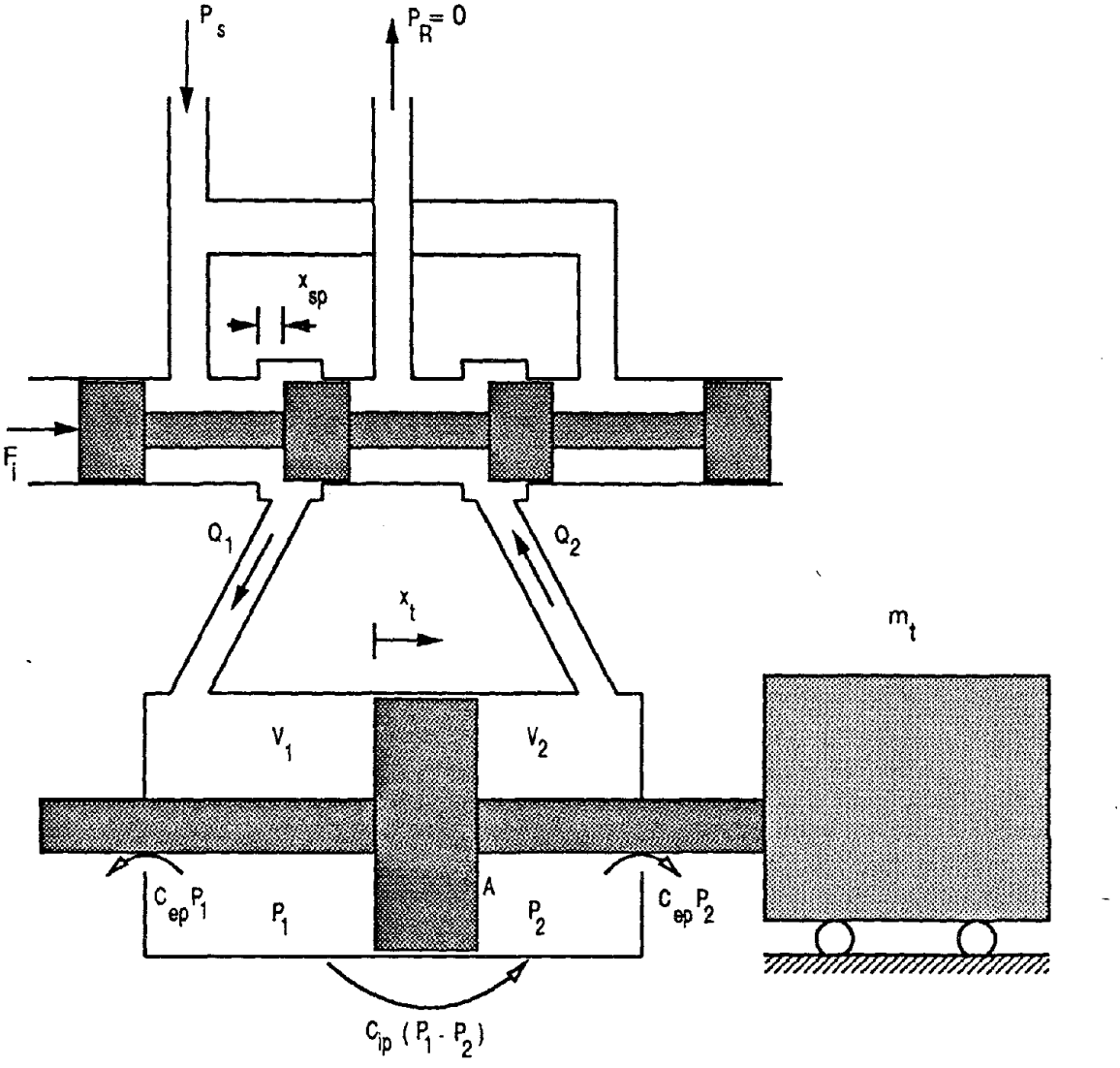

Fig. C.1: Typical slave spool and actuator used in EERC shaking table.

APPENDIX D

IMPROVED AMPLITUDE FITTING FOR FREQUENCY AND DAMPING ESTIMATION

D.1 PROCEDURE

A well separated peak in the transfer function can be approximated by a single mode response as

$$\ddot{y} + 2\omega_n \xi_n \dot{y} + \omega_n^2 y = P_n e^{i\Omega t} \tag{D.1}$$

in which ω_n, ξ_n are the structural frequency and damping for the particular mode. P_n is the participation factor for the mode. At a given input frequency Ω_k, the steady state amplitude of the response y is given by

$$A_k = \frac{P_n}{\sqrt{(\omega_n^2 - \Omega_k^2)^2 + (2\omega_n \xi_n \Omega_k)^2}} = \frac{P_n}{D_k} \tag{D.2}$$

The unknown parameters in the above equation are ω_n, ξ_n and P_n. It is important to note that the above equation is valid only for a transfer function relating the input force (or acceleration) to the output displacement. If that is not the case, the amplitude A_k needs to be scaled by the appropriate power of Ω_k to transform the equation into the above form.

Equation (D.2) can be written as

$$A_k^2 D_k^2 - P_n^2 = 0 \tag{D.3}$$

or as shown in the next section it is better to scale it by the amplitude A_k as follows

$$A_k^3 D_k^2 - A_k P_n^2 = 0 \tag{D.4}$$

Substituting D_k of Eq. (D.2) gives

$$A_k^3 x_1 + A_k^3 \Omega_k^2 x_2 - A_k x_3 = -A_k^3 \Omega_k^4 \tag{D.5}$$

Preceding page blank

where

$$x_1 = \omega_n^4$$

$$x_2 = 4\xi_n^2\omega_n^2 - 2\omega_n^2 \tag{D.6}$$

$$x_3 = P_n^2$$

For a set of frequencies Ω_k , k=1,N; Eq. (D.5) can be written as

$$\begin{bmatrix} A_1^3 & A_1^3\Omega_1^2 & -A_1 \\ A_2^3 & A_2^3\Omega_2^2 & -A_2 \\ A_3^3 & A_3^3\Omega_3^2 & -A_3 \\ . & . & . \\ . & . & . \\ A_N^3 & A_N^3\Omega_N^2 & -A_N \end{bmatrix} \begin{Bmatrix} x_1 \\ x_2 \\ x_3 \end{Bmatrix} = \begin{Bmatrix} -A_1^3\Omega_1^4 \\ -A_2^3\Omega_2^4 \\ -A_3^3\Omega_3^4 \\ . \\ . \\ -A_N^3\Omega_N^4 \end{Bmatrix} \tag{D.7}$$

or by an equation of the form

$$\mathbf{A\,x = B} \tag{D.8}$$

The least squares solution of Eq. (D.8) is

$$\mathbf{A^T A\,x = A^T B} \tag{D.9}$$

which can be simplified as

$$\begin{bmatrix} \sum_{k=1}^{N} A_k^6 & \sum_{k=1}^{N} A_k^6\Omega_k^2 & -\sum_{k=1}^{N} A_k^4 \\ \sum_{k=1}^{N} A_k^6\Omega_k^2 & \sum_{k=1}^{N} A_k^6\Omega_k^4 & -\sum_{k=1}^{N} A_k^4\Omega_k^2 \\ -\sum_{k=1}^{N} A_k^4 & -\sum_{k=1}^{N} A_k^4\Omega_k^2 & \sum_{k=1}^{N} A_k^2 \end{bmatrix} \begin{Bmatrix} x_1 \\ x_2 \\ x_3 \end{Bmatrix} = \begin{Bmatrix} -\sum_{k=1}^{N} A_k^6\Omega_k^4 \\ -\sum_{k=1}^{N} A_k^6\Omega_k^6 \\ \sum_{k=1}^{N} A_k^4\Omega_k^4 \end{Bmatrix} \tag{D.10}$$

Once the above equation is solved, the modal parameters can be computed from

$$\omega_n = (x_1)^{1/4}$$

$$\xi_n = \sqrt{\frac{x_2}{4\omega_n^2} + \frac{1}{2}} \tag{D.11}$$

$$P_n = \sqrt{x_3}$$

It is important to note that Eq. (D.10) contains high powers of the experimental amplitude A_k. In order to avoid overflow it is suggested that all the A_k values be normalized such that

$$Max\,(A_k) = 1 \qquad \text{(D.11b)}$$

by dividing all A_k values by the maximum value. The same normalizing factor should then be applied to the resulting value P_n as is apparent from Eq. (D.2).

D.2 GLOBAL FREQUENCY AND DAMPING

It is frequently the case that several measurements could be used to estimate the frequency and damping of a particular mode. For example the responses at different nodes in system are usually measured in order to establish the mode shapes. Technically the transfer function at any of these locations may be used to get the frequency and damping. The frequency and damping estimates obtained from different transfer functions corresponding to different locations would normally be different. The question of which values to use would then be encountered. Fortunately it is possible to combine all the response transfer functions such that average or global parameters can be determined.

Let us assume that the measured transfer function amplitudes at node A and C are A_k and C_k respectively. Equation (D.7) can be rewritten to include the responses C_k by recognizing that x_1 and x_2 are functions of ω_n and ξ_n only and hence are global parameters. The parameter x_3 on the other hand is a function of the participation factor at the particular node and would have two different values x_3^A and x_3^C for the different locations. If we write Eq. (D.5) for each point on the transfer functions at nodes A and C we get

$$\begin{bmatrix} A_1^3 & A_1^3\Omega_1^2 & -A_1 & 0 \\ A_2^3 & A_2^3\Omega_2^2 & -A_2 & 0 \\ A_3^3 & A_3^3\Omega_3^2 & -A_3 & 0 \\ . & . & . & . \\ A_N^3 & A_N^3\Omega_N^2 & -A_N & 0 \\ C_1^3 & C_1^3\Omega_1^2 & 0 & -C_1 \\ C_2^3 & C_2^3\Omega_2^2 & 0 & -C_2 \\ C_3^3 & C_3^3\Omega_3^2 & 0 & -C_3 \\ . & . & . & . \\ C_N^3 & C_N^3\Omega_N^2 & 0 & -C_N \end{bmatrix} \begin{Bmatrix} x_1 \\ x_2 \\ x_3^A \\ x_3^C \end{Bmatrix} = \begin{Bmatrix} -A_1^3\Omega_1^4 \\ -A_2^3\Omega_2^4 \\ -A_3^3\Omega_3^4 \\ . \\ -A_N^3\Omega_N^4 \\ -C_1^3\Omega_1^4 \\ -C_2^3\Omega_2^4 \\ -C_3^3\Omega_3^4 \\ . \\ -C_N^3\Omega_N^4 \end{Bmatrix} \tag{D.11c}$$

Equation (D.11c) is similar in form to Eq. (D.7) and can be solved similarly for the four unknowns. Note that it was assumed here that the number of points in each function is N and both have the same frequencies. It should be straight forward to generalize Eq. (D.11c) to include different N values and frequency points for different transfer functions. The procedure can also be generalized to include more transfer functions by adding an additional participation factor for each new curve.

D.3 JUSTIFICATION FOR SCALING (WEIGHTING)

Equation (D.2) cannot be exact because of errors that inevitably exist in the experimental data, so it may be written as

$$A_k + \varepsilon_1^k = \frac{P_n}{D_k} \tag{D.12}$$

where ε_1^k is the error in the amplitude. But as seen in Section D.1, the square root in D_k complicates the equation so that expressing in terms of the squares of the amplitude gives

$$A_k^2 + \varepsilon_2^k = \frac{P_n^2}{D_k^2} \tag{D.13}$$

where ε_2^k is the error in the square of the amplitude A_k^2. It can be easily

shown that

$$\varepsilon_2^k = 2\varepsilon_1^k A_k \tag{D.14}$$

by neglecting the second order error term. Equation (D.13) can be expressed as

$$A_k^2 D_k^2 - P_n^2 = \varepsilon_2^k D_k^2 \tag{D.15}$$

If Eq. (D.3) is used to solve for the unknowns, the minimized error would be

$$\sum_{k=1}^{N} (\varepsilon_2^k D_k^2)^2 \tag{D.16}$$

D_k^2 can be considered a weighting factor corresponding to the point at frequency Ω_k. But since D_k is minimum at resonance, the points near resonance are given a lower weighing factor than those away from the peak. This is normally undesirable since points further from the peak are contaminated by residues from adjacent modes.

The term $\varepsilon_2^k D_k^2$ in Eq. (D.15) can be written using Eq. (D.14) as

$$\varepsilon_2^k D_k^2 = 2\varepsilon_1^k A_k D_k^2 \tag{D.17}$$

or as

$$\varepsilon_2^k D_k^2 = \frac{2\varepsilon_1^k}{A_k}(A_k^2 D_k^2) \tag{D.18}$$

But $A_k^2 D_k^2$ in Eq. (D.18) can be approximated from Eq. (D.13) by P_n^2 so that Eq. (D.15) can be written as

$$A_k^2 D_k^2 - P_n^2 = \frac{2\varepsilon_1^k P_n^2}{A_k} \tag{D.19}$$

If Eq. (D.19) is multiplied by A_k we get

$$A_k^3 D_k^2 - A_k P_n^2 = 2\varepsilon_1^k P_n^2 \tag{D.20}$$

Equation (D.20) shows that if Eq. (D.4) is solved using the least squares method, the error minimized is

$$\sum_{k=1}^{N} (2\varepsilon_1^k P_n^2)^2 \tag{D.21}$$

but since P_n is a constant, the function $\sum_{k=1}^{N} (\varepsilon_1^k)^2$ which is the error term in Eq. (D.12), is actually minimized.

This method is an extended or weighted version of the procedure used by Clough et al. [38] and Mau and Wang [39].

D.4 EXAMPLES

The frequencies and damping ratios listed in Table D.1 were obtained using this procedure. The corresponding values in Table 3.1 were obtained by circle fitting or amplitude fitting [38]. For the Taft 200 case listed in Table D.1, the experimental and analytical curves are shown in Fig. D.1 for the fixed-base structure case. Fig. D.2 shows the results obtained if Eq. (D.3) is used instead of Eq. (D.4). Note that the analytical curve in Figure D.2 fits the lower amplitude values very well but gives a much larger error for the points near resonance. The analytical curve in Fig. D.1 provides a better overall fit. The damping ratio used in Fig. D.1 is 1.2 percent and that in Fig. D.2 is 0.67 percent. If the procedure described in [39] is used, a negative damping ratio would have been obtained because the lower amplitudes are much more weighted than those in Eq. (D.3). Since the transfer function used here represents a displacement/displacement ratio, it was converted into a displacement/force ratio by dividing the amplitude at each frequency by Ω^2 before fitting.

The fitted curve in Fig. B.3 was also computed using the procedure described in this section.

EARTHQUAKE RECORD	Fixed base		Base rotation coupling		Transl. and rot. coupling	
	FREQ (Hz)	DAMP (%)	FREQ (Hz)	DAMP (%)	FREQ (Hz)	DAMP (%)
Miyagi span 270	2.91	1.1	2.72	2.3	2.62	2.2
Miyagi span 350	2.91	1.3	2.71	2.4	2.60	2.5
Taft span 200	2.89	1.2	2.70	0.7	2.57	2.4

Table D.1: Vibration characteristics of the structure for three boundary conditions and three different records. Updated values of those in Table 3.1 using the procedure described here.

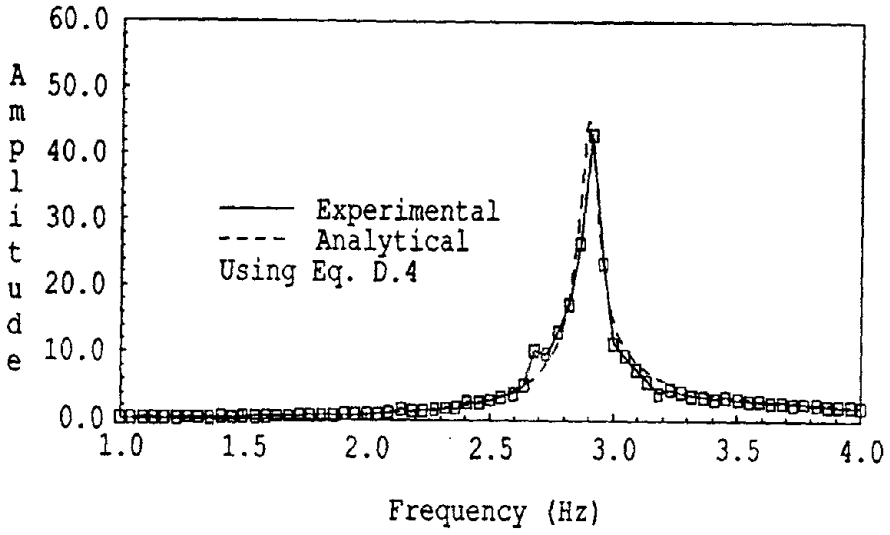

Fig. D.1: Transfer Function of Relative Structural Displacement over Effective Base Displacement.

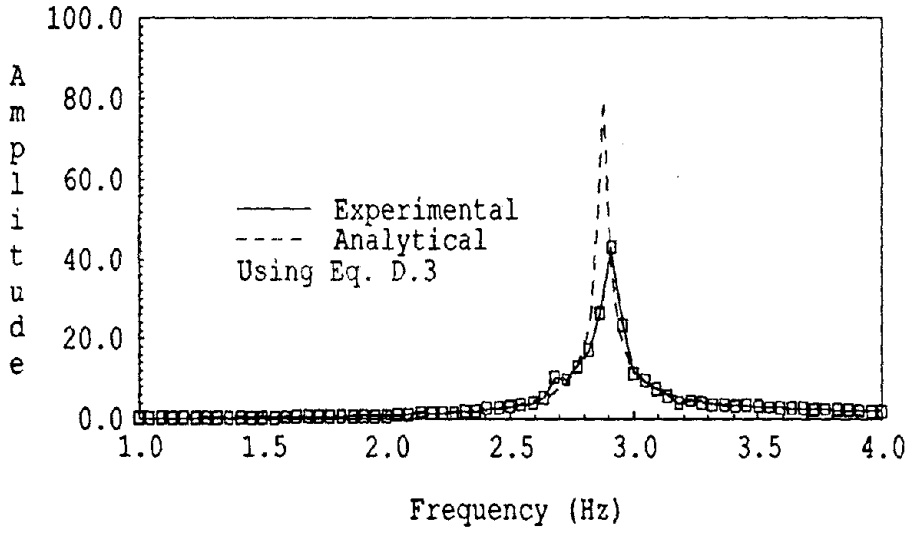

Fig. D.2: Transfer Function of Relative Structural Displacement over Effective Base Displacement.

EARTHQUAKE ENGINEERING RESEARCH CENTER REPORT SERIES

EERC reports are available from the National Information Service for Earthquake Engineering(NISEE) and from the National Technical Information Service(NTIS). Numbers in parentheses are Accession Numbers assigned by the National Technical Information Service; these are followed by a price code. Contact NTIS, 5285 Port Royal Road, Springfield Virginia, 22161 for more information. Reports without Accession Numbers were not available from NTIS at the time of printing. For a current complete list of EERC reports (from EERC 67-1) and availablity information, please contact University of California, EERC, NISEE, 1301 South 46th Street, Richmond, California 94804.

UCB/EERC-81/01 "Control of Seismic Response of Piping Systems and Other Structures by Base Isolation," by Kelly, J.M., January 1981, (PB81 200 735)A05.

UCB/EERC-81/02 "OPTNSR- An Interactive Software System for Optimal Design of Statically and Dynamically Loaded Structures with Nonlinear Response," by Bhatti, M.A., Ciampi, V. and Pister, K.S., January 1981, (PB81 218 851)A09.

UCB/EERC-81/03 "Analysis of Local Variations in Free Field Seismic Ground Motions," by Chen, J.-C., Lysmer, J. and Seed, H.B., January 1981, (AD-A099508)A13.

UCB/EERC-81/04 "Inelastic Structural Modeling of Braced Offshore Platforms for Seismic Loading," by Zayas, V.A., Shing, P.-S.B., Mahin, S.A. and Popov, E.P., January 1981, INEL4, (PB82 138 777)A07.

UCB/EERC-81/05 "Dynamic Response of Light Equipment in Structures," by Der Kiureghian, A., Sackman, J.L. and Nour-Omid, B., April 1981, (PB81 218 497)A04.

UCB/EERC-81/06 "Preliminary Experimental Investigation of a Broad Base Liquid Storage Tank," by Bouwkamp, J.G., Kollegger, J.P. and Stephen, R.M., May 1981, (PB82 140 385)A03.

UCB/EERC-81/07 "The Seismic Resistant Design of Reinforced Concrete Coupled Structural Walls," by Aktan, A.E. and Bertero, V.V., June 1981, (PB82 113 358)A11.

UCB/EERC-81/08 "Unassigned," by Unassigned, 1981.

UCB/EERC-81/09 "Experimental Behavior of a Spatial Piping System with Steel Energy Absorbers Subjected to a Simulated Differential Seismic Input," by Stiemer, S.F., Godden, W.G. and Kelly, J.M., July 1981, (PB82 201 898)A04.

UCB/EERC-81/10 "Evaluation of Seismic Design Provisions for Masonry in the United States," by Sveinsson, B.I., Mayes, R.L. and McNiven, H.D., August 1981, (PB82 166 075)A08.

UCB/EERC-81/11 "Two-Dimensional Hybrid Modelling of Soil-Structure Interaction," by Tzong, T.-J., Gupta, S. and Penzien, J., August 1981, (PB82 142 118)A04.

UCB/EERC-81/12 "Studies on Effects of Infills in Seismic Resistant R/C Construction," by Brokken, S. and Bertero, V.V., October 1981, (PB82 166 190)A09.

UCB/EERC-81/13 "Linear Models to Predict the Nonlinear Seismic Behavior of a One-Story Steel Frame," by Valdimarsson, H., Shah, A.H. and McNiven, H.D., September 1981, (PB82 138 793)A07.

UCB/EERC-81/14 "TLUSH: A Computer Program for the Three-Dimensional Dynamic Analysis of Earth Dams," by Kagawa, T., Mejia, L.H., Seed, H.B. and Lysmer, J., September 1981, (PB82 139 940)A06.

UCB/EERC-81/15 "Three Dimensional Dynamic Response Analysis of Earth Dams," by Mejia, L.H. and Seed, H.B., September 1981, (PB82 137 274)A12.

UCB/EERC-81/16 "Experimental Study of Lead and Elastomeric Dampers for Base Isolation Systems," by Kelly, J.M. and Hodder, S.B., October 1981, (PB82 166 182)A05.

UCB/EERC-81/17 "The Influence of Base Isolation on the Seismic Response of Light Secondary Equipment," by Kelly, J.M., April 1981, (PB82 255 266)A04.

UCB/EERC-81/18 "Studies on Evaluation of Shaking Table Response Analysis Procedures," by Blondet, J. M., November 1981, (PB82 197 278)A10.

UCB/EERC-81/19 "DELIGHT.STRUCT: A Computer-Aided Design Environment for Structural Engineering," by Balling, R.J., Pister, K.S. and Polak, E., December 1981, (PB82 218 496)A07.

UCB/EERC-81/20 "Optimal Design of Seismic-Resistant Planar Steel Frames," by Balling, R.J., Ciampi, V. and Pister, K.S., December 1981, (PB82 220 179)A07.

UCB/EERC-82/01 "Dynamic Behavior of Ground for Seismic Analysis of Lifeline Systems," by Sato, T. and Der Kiureghian, A., January 1982, (PB82 218 926)A05.

UCB/EERC-82/02 "Shaking Table Tests of a Tubular Steel Frame Model," by Ghanaat, Y. and Clough, R.W., January 1982, (PB82 220 161)A07.

UCB/EERC-82/03 "Behavior of a Piping System under Seismic Excitation: Experimental Investigations of a Spatial Piping System supported by Mechanical Shock Arrestors," by Schneider, S., Lee, H.-M. and Godden, W. G., May 1982, (PB83 172 544)A09.

UCB/EERC-82/04 "New Approaches for the Dynamic Analysis of Large Structural Systems," by Wilson, E.L., June 1982, (PB83 148 080)A05.

UCB/EERC-82/05 "Model Study of Effects of Damage on the Vibration Properties of Steel Offshore Platforms," by Shahrivar, F. and Bouwkamp, J.G., June 1982, (PB83 148 742)A10.

UCB/EERC-82/06 "States of the Art and Pratice in the Optimum Seismic Design and Analytical Response Prediction of R/C Frame Wall Structures," by Aktan, A.E. and Bertero, V.V., July 1982, (PB83 147 736)A05.

UCB/EERC-82/07 "Further Study of the Earthquake Response of a Broad Cylindrical Liquid-Storage Tank Model," by Manos, G.C. and Clough, R.W., July 1982, (PB83 147 744)A11.

UCB/EERC-82/08 "An Evaluation of the Design and Analytical Seismic Response of a Seven Story Reinforced Concrete Frame," by Charney, F.A. and Bertero, V.V., July 1982, (PB83 157 628)A09.

UCB/EERC-82/09 "Fluid-Structure Interactions: Added Mass Computations for Incompressible Fluid," by Kuo, J.S.-H., August 1982, (PB83 156 281)A07.

UCB/EERC-82/10 "Joint-Opening Nonlinear Mechanism: Interface Smeared Crack Model," by Kuo, J.S.-H., August 1982, (PB83 149 195)A05.

UCB/EERC-82/11 "Dynamic Response Analysis of Techi Dam," by Clough, R.W., Stephen, R.M. and Kuo, J.S.-H., August 1982, (PB83 147 496)A06.

UCB/EERC-82/12 "Prediction of the Seismic Response of R/C Frame-Coupled Wall Structures," by Aktan, A.E., Bertero, V.V. and Piazzo, M., August 1982, (PB83 149 203)A09.

UCB/EERC-82/13 "Preliminary Report on the Smart 1 Strong Motion Array in Taiwan," by Bolt, B.A., Loh, C.H., Penzien, J. and Tsai, Y.B., August 1982, (PB83 159 400)A10.

UCB/EERC-82/14 "Seismic Behavior of an Eccentrically X-Braced Steel Structure," by Yang, M.S., September 1982, (PB83 260 778)A12.

UCB/EERC-82/15 "The Performance of Stairways in Earthquakes," by Roha, C., Axley, J.W. and Bertero, V.V., September 1982, (PB83 157 693)A07.

UCB/EERC-82/16 "The Behavior of Submerged Multiple Bodies in Earthquakes," by Liao, W.-G., September 1982, (PB83 158 709)A07.

UCB/EERC-82/17 "Effects of Concrete Types and Loading Conditions on Local Bond-Slip Relationships," by Cowell, A.D., Popov, E.P. and Bertero, V.V., September 1982, (PB83 153 577)A04.

UCB/EERC-82/18 "Mechanical Behavior of Shear Wall Vertical Boundary Members: An Experimental Investigation," by Wagner, M.T. and Bertero, V.V., October 1982, (PB83 159 764)A05.

UCB/EERC-82/19 "Experimental Studies of Multi-support Seismic Loading on Piping Systems," by Kelly, J.M. and Cowell, A.D., November 1982, (PB90 262 684)A07.

UCB/EERC-82/20 "Generalized Plastic Hinge Concepts for 3D Beam-Column Elements," by Chen, P. F.-S. and Powell, G.H., November 1982, (PB83 247 981)A13.

UCB/EERC-82/21 "ANSR-II: General Computer Program for Nonlinear Structural Analysis," by Oughourlian, C.V. and Powell, G.H., November 1982, (PB83 251 330)A12.

UCB/EERC-82/22 "Solution Strategies for Statically Loaded Nonlinear Structures," by Simons, J.W. and Powell, G.H., November 1982, (PB83 197 970)A06.

UCB/EERC-82/23 "Analytical Model of Deformed Bar Anchorages under Generalized Excitations," by Ciampi, V., Eligehausen, R., Bertero, V.V. and Popov, E.P., November 1982, (PB83 169 532)A06.

UCB/EERC-82/24 "A Mathematical Model for the Response of Masonry Walls to Dynamic Excitations," by Sucuoglu, H., Mengi, Y. and McNiven, H.D., November 1982, (PB83 169 011)A07.

UCB/EERC-82/25 "Earthquake Response Considerations of Broad Liquid Storage Tanks," by Cambra, F.J., November 1982, (PB83 251 215)A09.

UCB/EERC-82/26 "Computational Models for Cyclic Plasticity, Rate Dependence and Creep," by Mosaddad, B. and Powell, G.H., November 1982, (PB83 245 829)A08.

UCB/EERC-82/27 "Inelastic Analysis of Piping and Tubular Structures," by Mahasuverachai, M. and Powell, G.H., November 1982, (PB83 249 987)A07.

UCB/EERC-83/01 "The Economic Feasibility of Seismic Rehabilitation of Buildings by Base Isolation," by Kelly, J.M., January 1983, (PB83 197 988)A05.

UCB/EERC-83/02 "Seismic Moment Connections for Moment-Resisting Steel Frames.," by Popov, E.P., January 1983, (PB83 195 412)A04.

UCB/EERC-83/03 "Design of Links and Beam-to-Column Connections for Eccentrically Braced Steel Frames," by Popov, E.P. and Malley, J.O., January 1983, (PB83 194 811)A04.

UCB/EERC-83/04 "Numerical Techniques for the Evaluation of Soil-Structure Interaction Effects in the Time Domain," by Bayo, E. and Wilson, E.L., February 1983, (PB83 245 605)A09.

UCB/EERC-83/05 "A Transducer for Measuring the Internal Forces in the Columns of a Frame-Wall Reinforced Concrete Structure," by Sause, R. and Bertero, V.V., May 1983, (PB84 119 494)A06.

UCB/EERC-83/06 "Dynamic Interactions Between Floating Ice and Offshore Structures," by Croteau, P., May 1983, (PB84 119 486)A16.

UCB/EERC-83/07 "Dynamic Analysis of Multiply Tuned and Arbitrarily Supported Secondary Systems," by Igusa, T. and Der Kiureghian, A., July 1983, (PB84 118 272)A11.

UCB/EERC-83/08 "A Laboratory Study of Submerged Multi-body Systems in Earthquakes," by Ansari, G.R., June 1983, (PB83 261 842)A17.

UCB/EERC-83/09 "Effects of Transient Foundation Uplift on Earthquake Response of Structures," by Yim, C.-S. and Chopra, A.K., June 1983, (PB83 261 396)A07.

UCB/EERC-83/10 "Optimal Design of Friction-Braced Frames under Seismic Loading," by Austin, M.A. and Pister, K.S., June 1983, (PB84 119 288)A06.

UCB/EERC-83/11 "Shaking Table Study of Single-Story Masonry Houses: Dynamic Performance under Three Component Seismic Input and Recommendations," by Manos, G.C., Clough, R.W. and Mayes, R.L., July 1983, (UCB/EERC-83/11)A08.

UCB/EERC-83/12 "Experimental Error Propagation in Pseudodynamic Testing," by Shiing, P.B. and Mahin, S.A., June 1983, (PB84 119 270)A09.

UCB/EERC-83/13 "Experimental and Analytical Predictions of the Mechanical Characteristics of a 1/5-scale Model of a 7-story R/C Frame-Wall Building Structure," by Aktan, A.E., Bertero, V.V., Chowdhury, A.A. and Nagashima, T., June 1983, (PB84 119 213)A07.

UCB/EERC-83/14 "Shaking Table Tests of Large-Panel Precast Concrete Building System Assemblages," by Oliva, M.G. and Clough, R.W., June 1983, (PB86 110 210/AS)A11.

UCB/EERC-83/15 "Seismic Behavior of Active Beam Links in Eccentrically Braced Frames," by Hjelmstad, K.D. and Popov, E.P., July 1983, (PB84 119 676)A09.

UCB/EERC-83/16 "System Identification of Structures with Joint Rotation," by Dimsdale, J.S., July 1983, (PB84 192 210)A06.

UCB/EERC-83/17 "Construction of Inelastic Response Spectra for Single-Degree-of-Freedom Systems," by Mahin, S. and Lin, J., June 1983, (PB84 208 834)A05.

UCB/EERC-83/18 "Interactive Computer Analysis Methods for Predicting the Inelastic Cyclic Behaviour of Structural Sections," by Kaba, S. and Mahin, S., July 1983, (PB84 192 012)A06.

UCB/EERC-83/19 "Effects of Bond Deterioration on Hysteretic Behavior of Reinforced Concrete Joints," by Filippou, F.C., Popov, E.P. and Bertero, V.V., August 1983, (PB84 192 020)A10.

UCB/EERC-83/20 "Correlation of Analytical and Experimental Responses of Large-Panel Precast Building Systems," by Oliva, M.G., Clough, R.W., Velkov, M. and Gavrilovic, P., May 1988, (PB90 262 692)A06.

UCB/EERC-83/21 "Mechanical Characteristics of Materials Used in a 1/5 Scale Model of a 7-Story Reinforced Concrete Test Structure," by Bertero, V.V., Aktan, A.E., Harris, H.G. and Chowdhury, A.A., October 1983, (PB84 193 697)A05.

UCB/EERC-83/22 "Hybrid Modelling of Soil-Structure Interaction in Layered Media," by Tzong, T.-J. and Penzien, J., October 1983, (PB84 192 178)A08.

UCB/EERC-83/23 "Local Bond Stress-Slip Relationships of Deformed Bars under Generalized Excitations," by Eligehausen, R., Popov, E.P. and Bertero, V.V., October 1983, (PB84 192 848)A09.

UCB/EERC-83/24 "Design Considerations for Shear Links in Eccentrically Braced Frames," by Malley, J.O. and Popov, E.P., November 1983, (PB84 192 186)A07.

UCB/EERC-84/01 "Pseudodynamic Test Method for Seismic Performance Evaluation: Theory and Implementation," by Shing, P.-S.B. and Mahin, S.A., January 1984, (PB84 190 644)A08.

UCB/EERC-84/02 "Dynamic Response Behavior of Kiang Hong Dian Dam," by Clough, R.W., Chang, K.-T., Chen, H.-Q. and Stephen, R.M., April 1984, (PB84 209 402)A08.

UCB/EERC-84/03 "Refined Modelling of Reinforced Concrete Columns for Seismic Analysis," by Kaba, S.A. and Mahin, S.A., April 1984, (PB84 234 384)A06.

UCB/EERC-84/04 "A New Floor Response Spectrum Method for Seismic Analysis of Multiply Supported Secondary Systems," by Asfura, A. and Der Kiureghian, A., June 1984, (PB84 239 417)A06.

UCB/EERC-84/05 "Earthquake Simulation Tests and Associated Studies of a 1/5th-scale Model of a 7-Story R/C Frame-Wall Test Structure," by Bertero, V.V., Aktan, A.E., Charney, F.A. and Sause, R., June 1984, (PB84 239 409)A09.

UCB/EERC-84/06 "Unassigned," by Unassigned, 1984.

UCB/EERC-84/07 "Behavior of Interior and Exterior Flat-Plate Connections subjected to Inelastic Load Reversals," by Zee, H.L. and Moehle, J.P., August 1984, (PB86 117 629/AS)A07.

UCB/EERC-84/08 "Experimental Study of the Seismic Behavior of a Two-Story Flat-Plate Structure," by Moehle, J.P. and Diebold, J.W., August 1984, (PB86 122 553/AS)A12.

UCB/EERC-84/09 "Phenomenological Modeling of Steel Braces under Cyclic Loading," by Ikeda, K., Mahin, S.A. and Dermitzakis, S.N., May 1984, (PB86 132 198/AS)A08.

UCB/EERC-84/10 "Earthquake Analysis and Response of Concrete Gravity Dams," by Fenves, G. and Chopra, A.K., August 1984, (PB85 193 902/AS)A11.

UCB/EERC-84/11 "EAGD-84: A Computer Program for Earthquake Analysis of Concrete Gravity Dams," by Fenves, G. and Chopra, A.K., August 1984, (PB85 193 613/AS)A05.

UCB/EERC-84/12 "A Refined Physical Theory Model for Predicting the Seismic Behavior of Braced Steel Frames," by Ikeda, K. and Mahin, S.A., July 1984, (PB85 191 450/AS)A09.

UCB/EERC-84/13 "Earthquake Engineering Research at Berkeley - 1984," by EERC, August 1984, (PB85 197 341/AS)A10.

UCB/EERC-84/14 "Moduli and Damping Factors for Dynamic Analyses of Cohesionless Soils," by Seed, H.B., Wong, R.T., Idriss, I.M. and Tokimatsu, K., September 1984, (PB85 191 468/AS)A04.

UCB/EERC-84/15 "The Influence of SPT Procedures in Soil Liquefaction Resistance Evaluations," by Seed, H.B., Tokimatsu, K., Harder, L.F. and Chung, R.M., October 1984, (PB85 191 732/AS)A04.

UCB/EERC-84/16 "Simplified Procedures for the Evaluation of Settlements in Sands Due to Earthquake Shaking," by Tokimatsu, K. and Seed, H.B., October 1984, (PB85 197 887/AS)A03.

UCB/EERC-84/17 "Evaluation of Energy Absorption Characteristics of Highway Bridges Under Seismic Conditions - Volume I (PB90 262 627)A16 and Volume II (Appendices) (PB90 262 635)A13," by Imbsen, R.A. and Penzien, J., September 1986.

UCB/EERC-84/18 "Structure-Foundation Interactions under Dynamic Loads," by Liu, W.D. and Penzien, J., November 1984, (PB87 124 889/AS)A11.

UCB/EERC-84/19 "Seismic Modelling of Deep Foundations," by Chen, C.-H. and Penzien, J., November 1984, (PB87 124 798/AS)A07.

UCB/EERC-84/20 "Dynamic Response Behavior of Quan Shui Dam," by Clough, R.W., Chang, K.-T., Chen, H.-Q., Stephen, R.M., Ghanaat, Y. and Qi, J.-H., November 1984, (PB86 115177/AS)A07.

UCB/EERC-85/01 "Simplified Methods of Analysis for Earthquake Resistant Design of Buildings," by Cruz, E.F. and Chopra, A.K., February 1985, (PB86 112299/AS)A12.

UCB/EERC-85/02 "Estimation of Seismic Wave Coherency and Rupture Velocity using the SMART 1 Strong-Motion Array Recordings," by Abrahamson, N.A., March 1985, (PB86 214 343)A07.

UCB/EERC-85/03 "Dynamic Properties of a Thirty Story Condominium Tower Building," by Stephen, R.M., Wilson, E.L. and Stander, N., April 1985, (PB86 118965/AS)A06.

UCB/EERC-85/04 "Development of Substructuring Techniques for On-Line Computer Controlled Seismic Performance Testing," by Dermitzakis, S. and Mahin, S., February 1985, (PB86 132941/AS)A08.

UCB/EERC-85/05 "A Simple Model for Reinforcing Bar Anchorages under Cyclic Excitations," by Filippou, F.C., March 1985, (PB86 112 919/AS)A05.

UCB/EERC-85/06 "Racking Behavior of Wood-framed Gypsum Panels under Dynamic Load," by Oliva, M.G., June 1985, (PB90 262 643)A04.

UCB/EERC-85/07 "Earthquake Analysis and Response of Concrete Arch Dams," by Fok, K.-L. and Chopra, A.K., June 1985, (PB86 139672/AS)A10.

UCB/EERC-85/08 "Effect of Inelastic Behavior on the Analysis and Design of Earthquake Resistant Structures," by Lin, J.P. and Mahin, S.A., June 1985, (PB86 135340/AS)A08.

UCB/EERC-85/09 "Earthquake Simulator Testing of a Base-Isolated Bridge Deck," by Kelly, J.M., Buckle, I.G. and Tsai, H.-C., January 1986, (PB87 124 152/AS)A06.

UCB/EERC-85/10 "Simplified Analysis for Earthquake Resistant Design of Concrete Gravity Dams," by Fenves, G. and Chopra, A.K., June 1986, (PB87 124 160/AS)A08.

UCB/EERC-85/11 "Dynamic Interaction Effects in Arch Dams," by Clough, R.W., Chang, K.-T., Chen, H.-Q. and Ghanaat, Y., October 1985, (PB86 135027/AS)A05.

UCB/EERC-85/12 "Dynamic Response of Long Valley Dam in the Mammoth Lake Earthquake Series of May 25-27, 1980," by Lai, S. and Seed, H.B., November 1985, (PB86 142304/AS)A05.

UCB/EERC-85/13 "A Methodology for Computer-Aided Design of Earthquake-Resistant Steel Structures," by Austin, M.A., Pister, K.S. and Mahin, S.A., December 1985, (PB86 159480/AS)A10 .

UCB/EERC-85/14 "Response of Tension-Leg Platforms to Vertical Seismic Excitations," by Liou, G.-S., Penzien, J. and Yeung, R.W., December 1985, (PB87 124 871/AS)A08.

UCB/EERC-85/15 "Cyclic Loading Tests of Masonry Single Piers: Volume 4 - Additional Tests with Height to Width Ratio of 1," by Sveinsson, B., McNiven, H.D. and Sucuoglu, H., December 1985.

UCB/EERC-85/16 "An Experimental Program for Studying the Dynamic Response of a Steel Frame with a Variety of Infill Partitions," by Yanev, B. and McNiven, H.D., December 1985, (PB90 262 676)A05.

UCB/EERC-86/01 "A Study of Seismically Resistant Eccentrically Braced Steel Frame Systems," by Kasai, K. and Popov, E.P., January 1986, (PB87 124 178/AS)A14.

UCB/EERC-86/02 "Design Problems in Soil Liquefaction," by Seed, H.B., February 1986, (PB87 124 186/AS)A03.

UCB/EERC-86/03 "Implications of Recent Earthquakes and Research on Earthquake-Resistant Design and Construction of Buildings," by Bertero, V.V., March 1986, (PB87 124 194/AS)A05.

UCB/EERC-86/04 "The Use of Load Dependent Vectors for Dynamic and Earthquake Analyses," by Leger, P., Wilson, E.L. and Clough, R.W., March 1986, (PB87 124 202/AS)A12.

UCB/EERC-86/05 "Two Beam-To-Column Web Connections," by Tsai, K.-C. and Popov, E.P., April 1986, (PB87 124 301/AS)A04.

UCB/EERC-86/06 "Determination of Penetration Resistance for Coarse-Grained Soils using the Becker Hammer Drill," by Harder, L.F. and Seed, H.B., May 1986, (PB87 124 210/AS)A07.

UCB/EERC-86/07 "A Mathematical Model for Predicting the Nonlinear Response of Unreinforced Masonry Walls to In-Plane Earthquake Excitations," by Mengi, Y. and McNiven, H.D., May 1986, (PB87 124 780/AS)A06.

UCB/EERC-86/08 "The 19 September 1985 Mexico Earthquake: Building Behavior," by Bertero, V.V., July 1986.

UCB/EERC-86/09 "EACD-3D: A Computer Program for Three-Dimensional Earthquake Analysis of Concrete Dams," by Fok, K.-L., Hall, J.F. and Chopra, A.K., July 1986, (PB87 124 228/AS)A08.

UCB/EERC-86/10 "Earthquake Simulation Tests and Associated Studies of a 0.3-Scale Model of a Six-Story Concentrically Braced Steel Structure," by Uang, C.-M. and Bertero, V.V., December 1986, (PB87 163 564/AS)A17.

UCB/EERC-86/11 "Mechanical Characteristics of Base Isolation Bearings for a Bridge Deck Model Test," by Kelly, J.M., Buckle, I.G. and Koh, C.-G., November 1987, (PB90 262 668)A04.

UCB/EERC-86/12 "Effects of Axial Load on Elastomeric Isolation Bearings," by Koh, C.-G. and Kelly, J.M., November 1987.

UCB/EERC-87/01 "The FPS Earthquake Resisting System: Experimental Report," by Zayas, V.A., Low, S.S. and Mahin, S.A., June 1987.

UCB/EERC-87/02 "Earthquake Simulator Tests and Associated Studies of a 0.3-Scale Model of a Six-Story Eccentrically Braced Steel Structure," by Whittaker, A., Uang, C.-M. and Bertero, V.V., July 1987.

UCB/EERC-87/03 "A Displacement Control and Uplift Restraint Device for Base-Isolated Structures," by Kelly, J.M., Griffith, M.C. and Aiken, I.D., April 1987.

UCB/EERC-87/04 "Earthquake Simulator Testing of a Combined Sliding Bearing and Rubber Bearing Isolation System," by Kelly, J.M. and Chalhoub, M.S., 1987.

UCB/EERC-87/05 "Three-Dimensional Inelastic Analysis of Reinforced Concrete Frame-Wall Structures," by Moazzami, S. and Bertero, V.V., May 1987.

UCB/EERC-87/06 "Experiments on Eccentrically Braced Frames with Composite Floors," by Ricles, J. and Popov, E., June 1987.

UCB/EERC-87/07 "Dynamic Analysis of Seismically Resistant Eccentrically Braced Frames," by Ricles, J. and Popov, E., June 1987.

UCB/EERC-87/08 "Undrained Cyclic Triaxial Testing of Gravels-The Effect of Membrane Compliance," by Evans, M.D. and Seed, H.B., July 1987.

UCB/EERC-87/09 "Hybrid Solution Techniques for Generalized Pseudo-Dynamic Testing," by Thewalt, C. and Mahin, S.A., July 1987.

UCB/EERC-87/10 "Ultimate Behavior of Butt Welded Splices in Heavy Rolled Steel Sections," by Bruneau, M., Mahin, S.A. and Popov, E.P., September 1987.

UCB/EERC-87/11 "Residual Strength of Sand from Dam Failures in the Chilean Earthquake of March 3, 1985," by De Alba, P., Seed, H.B., Retamal, E. and Seed, R.B., September 1987.

UCB/EERC-87/12 "Inelastic Seismic Response of Structures with Mass or Stiffness Eccentricities in Plan," by Bruneau, M. and Mahin, S.A., September 1987, (PB90 262 650)A14.

UCB/EERC-87/13 "CSTRUCT: An Interactive Computer Environment for the Design and Analysis of Earthquake Resistant Steel Structures," by Austin, M.A., Mahin, S.A. and Pister, K.S., September 1987.

UCB/EERC-87/14 "Experimental Study of Reinforced Concrete Columns Subjected to Multi-Axial Loading," by Low, S.S. and Moehle, J.P., September 1987.

UCB/EERC-87/15 "Relationships between Soil Conditions and Earthquake Ground Motions in Mexico City in the Earthquake of Sept. 19, 1985," by Seed, H.B., Romo, M.P., Sun, J., Jaime, A. and Lysmer, J., October 1987.

UCB/EERC-87/16 "Experimental Study of Seismic Response of R. C. Setback Buildings," by Shahrooz, B.M. and Moehle, J.P., October 1987.

UCB/EERC-87/17 "The Effect of Slabs on the Flexural Behavior of Beams," by Pantazopoulou, S.J. and Moehle, J.P., October 1987, (PB90 262 700)A07.

UCB/EERC-87/18 "Design Procedure for R-FBI Bearings," by Mostaghel, N. and Kelly, J.M., November 1987, (PB90 262 718)A04.

UCB/EERC-87/19 "Analytical Models for Predicting the Lateral Response of R C Shear Walls: Evaluation of their Reliability," by Vulcano, A. and Bertero, V.V., November 1987.

UCB/EERC-87/20 "Earthquake Response of Torsionally-Coupled Buildings," by Hejal, R. and Chopra, A.K., December 1987.

UCB/EERC-87/21 "Dynamic Reservoir Interaction with Monticello Dam," by Clough, R.W., Ghanaat, Y. and Qiu, X-F., December 1987.

UCB/EERC-87/22 "Strength Evaluation of Coarse-Grained Soils," by Siddiqi, F.H., Seed, R.B., Chan, C.K., Seed, H.B. and Pyke, R.M., December 1987.

UCB/EERC-88/01 "Seismic Behavior of Concentrically Braced Steel Frames," by Khatib, I., Mahin, S.A. and Pister, K.S., January 1988.

UCB/EERC-88/02 "Experimental Evaluation of Seismic Isolation of Medium-Rise Structures Subject to Uplift," by Griffith, M.C., Kelly, J.M., Coveney, V.A. and Koh, C.G., January 1988.

UCB/EERC-88/03 "Cyclic Behavior of Steel Double Angle Connections," by Astaneh-Asl, A. and Nader, M.N., January 1988.

UCB/EERC-88/04 "Re-evaluation of the Slide in the Lower San Fernando Dam in the Earthquake of Feb. 9, 1971," by Seed, H.B., Seed, R.B., Harder, L.F. and Jong, H.-L., April 1988.

UCB/EERC-88/05 "Experimental Evaluation of Seismic Isolation of a Nine-Story Braced Steel Frame Subject to Uplift," by Griffith, M.C., Kelly, J.M. and Aiken, I.D., May 1988.

UCB/EERC-88/06 "DRAIN-2DX User Guide.," by Allahabadi, R. and Powell, G.H., March 1988.

UCB/EERC-88/07 "Theoretical and Experimental Studies of Cylindrical Water Tanks in Base-Isolated Structures," by Chalhoub, M.S. and Kelly, J.M., April 1988.

UCB/EERC-88/08 "Analysis of Near-Source Waves: Separation of Wave Types using Strong Motion Array Recordings," by Darragh, R.B., June 1988.

UCB/EERC-88/09 "Alternatives to Standard Mode Superposition for Analysis of Non-Classically Damped Systems," by Kusainov, A.A. and Clough, R.W., June 1988.

UCB/EERC-88/10 "The Landslide at the Port of Nice on October 16, 1979," by Seed, H.B., Seed, R.B., Schlosser, F., Blondeau, F. and Juran, I., June 1988.

UCB/EERC-88/11 "Liquefaction Potential of Sand Deposits Under Low Levels of Excitation," by Carter, D.P. and Seed, H.B., August 1988.

UCB/EERC-88/12 "Nonlinear Analysis of Reinforced Concrete Frames Under Cyclic Load Reversals," by Filippou, F.C. and Issa, A., September 1988.

UCB/EERC-88/13 "Implications of Recorded Earthquake Ground Motions on Seismic Design of Building Structures," by Uang, C.-M. and Bertero, V.V., November 1988.

UCB/EERC-88/14 "An Experimental Study of the Behavior of Dual Steel Systems," by Whittaker, A.S. , Uang, C.-M. and Bertero, V.V., September 1988.

UCB/EERC-88/15 "Dynamic Moduli and Damping Ratios for Cohesive Soils," by Sun, J.I., Golesorkhi, R. and Seed, H.B., August 1988.

UCB/EERC-88/16 "Reinforced Concrete Flat Plates Under Lateral Load: An Experimental Study Including Biaxial Effects," by Pan, A. and Moehle, J., October 1988.

UCB/EERC-88/17 "Earthquake Engineering Research at Berkeley - 1988," by EERC, November 1988.

UCB/EERC-88/18 "Use of Energy as a Design Criterion in Earthquake-Resistant Design," by Uang, C.-M. and Bertero, V.V., November 1988.

UCB/EERC-88/19 "Steel Beam-Column Joints in Seismic Moment Resisting Frames," by Tsai, K.-C. and Popov, E.P., November 1988.

UCB/EERC-88/20 "Base Isolation in Japan, 1988," by Kelly, J.M., December 1988.

UCB/EERC-89/01 "Behavior of Long Links in Eccentrically Braced Frames," by Engelhardt, M.D. and Popov, E.P., January 1989.

UCB/EERC-89/02 "Earthquake Simulator Testing of Steel Plate Added Damping and Stiffness Elements," by Whittaker, A., Bertero, V.V., Alonso, J. and Thompson, C., January 1989.

UCB/EERC-89/03 "Implications of Site Effects in the Mexico City Earthquake of Sept. 19, 1985 for Earthquake-Resistant Design Criteria in the San Francisco Bay Area of California," by Seed, H.B. and Sun, J.I., March 1989.

UCB/EERC-89/04 "Earthquake Analysis and Response of Intake-Outlet Towers," by Goyal, A. and Chopra, A.K., July 1989.

UCB/EERC-89/05 "The 1985 Chile Earthquake: An Evaluation of Structural Requirements for Bearing Wall Buildings," by Wallace, J.W. and Moehle, J.P., July 1989.

UCB/EERC-89/06 "Effects of Spatial Variation of Ground Motions on Large Multiply-Supported Structures," by Hao, H., July 1989.

UCB/EERC-89/07 "EADAP - Enhanced Arch Dam Analysis Program: Users's Manual," by Ghanaat, Y. and Clough, R.W., August 1989.

UCB/EERC-89/08 "Seismic Performance of Steel Moment Frames Plastically Designed by Least Squares Stress Fields," by Ohi, K. and Mahin, S.A., August 1989.

UCB/EERC-89/09 "Feasibility and Performance Studies on Improving the Earthquake Resistance of New and Existing Buildings Using the Friction Pendulum System," by Zayas, V., Low, S., Mahin, S.A. and Bozzo, L., July 1989.

UCB/EERC-89/10 "Measurement and Elimination of Membrane Compliance Effects in Undrained Triaxial Testing," by Nicholson, P.G., Seed, R.B. and Anwar, H., September 1989.

UCB/EERC-89/11 "Static Tilt Behavior of Unanchored Cylindrical Tanks," by Lau, D.T. and Clough, R.W., September 1989.

UCB/EERC-89/12 "ADAP-88: A Computer Program for Nonlinear Earthquake Analysis of Concrete Arch Dams," by Fenves, G.L., Mojtahedi, S. and Reimer, R.B., September 1989.

UCB/EERC-89/13 "Mechanics of Low Shape Factor Elastomeric Seismic Isolation Bearings," by Aiken, I.D., Kelly, J.M. and Tajirian, F.F., November 1989.

UCB/EERC-89/14 "Preliminary Report on the Seismological and Engineering Aspects of the October 17, 1989 Santa Cruz (Loma Prieta) Earthquake," by EERC, October 1989.

UCB/EERC-89/15 "Experimental Studies of a Single Story Steel Structure Tested with Fixed, Semi-Rigid and Flexible Connections," by Nader, M.N. and Astaneh-Asl, A., August 1989, (PB91 229 211/AS)A10.

UCB/EERC-89/16 "Collapse of the Cypress Street Viaduct as a Result of the Loma Prieta Earthquake," by Nims, D.K., Miranda, E., Aiken, I.D., Whittaker, A.S. and Bertero, V.V., November 1989, (PB91 217 935/AS)A05.

UCB/EERC-90/01 "Mechanics of High-Shape Factor Elastomeric Seismic Isolation Bearings," by Kelly, J.M., Aiken, I.D. and Tajirian, F.F., March 1990.

UCB/EERC-90/02 "Javid's Paradox: The Influence of Preform on the Modes of Vibrating Beams," by Kelly, J.M., Sackman, J.L. and Javid, A., May 1990, (PB91 217 943/AS)A03.

UCB/EERC-90/03 "Earthquake Simulator Testing and Analytical Studies of Two Energy-Absorbing Systems for Multistory Structures," by Aiken, I.D. and Kelly, J.M., October 1990.

UCB/EERC-90/04 "Damage to the San Francisco-Oakland Bay Bridge During the October 17, 1989 Earthquake," by Astaneh, A., June 1990.

UCB/EERC-90/05 "Preliminary Report on the Principal Geotechnical Aspects of the October 17, 1989 Loma Prieta Earthquake," by Seed, R.B., Dickenson, S.E., Riemer, M.F., Bray, J.D., Sitar, N., Mitchell, J.K., Idriss, I.M., Kayen, R.E., Kropp, A., Harder, L.F., Jr. and Power, M.S., April 1990.

UCB/EERC-90/06 "Models of Critical Regions in Reinforced Concrete Frames Under Seismic Excitations," by Zulfiqar, N. and Filippou, F., May 1990.

UCB/EERC-90/07 "A Unified Earthquake-Resistant Design Method for Steel Frames Using ARMA Models," by Takewaki, I., Conte, J.P., Mahin, S.A. and Pister, K.S., June 1990.

UCB/EERC-90/08 "Soil Conditions and Earthquake Hazard Mitigation in the Marina District of San Francisco," by Mitchell, J.K., Masood, T., Kayen, R.E. and Seed, R.B., May 1990.

UCB/EERC-90/09 "Influence of the Earthquake Ground Motion Process and Structural Properties on Response Characteristics of Simple Structures," by Conte, J.P., Pister, K.S. and Mahin, S.A., July 1990.

UCB/EERC-90/10 "Experimental Testing of the Resilient-Friction Base Isolation System," by Clark, P.W. and Kelly, J.M., July 1990.

UCB/EERC-90/11 "Seismic Hazard Analysis: Improved Models, Uncertainties and Sensitivities," by Araya, R. and Der Kiureghian, A., March 1988.

UCB/EERC-90/12 "Effects of Torsion on the Linear and Nonlinear Seismic Response of Structures," by Sedarat, H. and Bertero, V.V., September 1989.

UCB/EERC-90/13 "The Effects of Tectonic Movements on Stresses and Deformations in Earth Embankments," by Bray, J. D., Seed, R. B. and Seed, H. B., September 1989.

UCB/EERC-90/14 "Inelastic Seismic Response of One-Story, Asymmetric-Plan Systems," by Goel, R.K. and Chopra, A.K., October 1990.

UCB/EERC-90/15 "Dynamic Crack Propagation: A Model for Near-Field Ground Motion.," by Seyyedian, H. and Kelly, J.M., 1990.

UCB/EERC-90/16 "Sensitivity of Long-Period Response Spectra to System Initial Conditions," by Blasquez, R., Ventura, C. and Kelly, J.M., 1990.

UCB/EERC-90/17 "Behavior of Peak Values and Spectral Ordinates of Near-Source Strong Ground-Motion over a Dense Array," by Niazi, M., June 1990.

UCB/EERC-90/18 "Material Characterization of Elastomers used in Earthquake Base Isolation," by Papoulia, K.D. and Kelly, J.M., 1990.

UCB/EERC-90/19 "Cyclic Behavior of Steel Top-and-Bottom Plate Moment Connections," by Harriott, J.D. and Astaneh, A., August 1990, (PB91 229 260/AS)A05.

UCB/EERC-90/20 "Seismic Response Evaluation of an Instrumented Six Story Steel Building," by Shen, J.-H. and Astaneh, A., December 1990.

UCB/EERC-90/21 "Observations and Implications of Tests on the Cypress Street Viaduct Test Structure," by Bollo, M., Mahin, S.A., Moehle, J.P., Stephen, R.M. and Qi, X., December 1990.

UCB/EERC-91/01 "Experimental Evaluation of Nitinol for Energy Dissipation in Structures," by Nims, D.K., Sasaki, K.K. and Kelly, J.M., 1991.

UCB/EERC-91/02 "Displacement Design Approach for Reinforced Concrete Structures Subjected to Earthquakes," by Qi, X. and Moehle, J.P., January 1991.

UCB/EERC-91/03 "Shake Table Tests of Long Period Isolation System for Nuclear Facilities at Soft Soil Sites," by Kelly, J.M., March 1991.

UCB/EERC-91/04 "Dynamic and Failure Characteristics of Bridgestone Isolation Bearings," by Kelly, J.M., April 1991.

UCB/EERC-91/05 "Base Sliding Response of Concrete Gravity Dams to Earthquakes," by Chopra, A.K. and Zhang, L., May 1991.

UCB/EERC-91/06 "Computation of Spatially Varying Ground Motion and Foundation-Rock Impedance Matrices for Seismic Analysis of Arch Dams," by Zhang, L. and Chopra, A.K., May 1991.

UCB/EERC-91/07 "Estimation of Seismic Source Processes Using Strong Motion Array Data," by Chiou, S.-J., July 1991.

UCB/EERC-91/08 "A Response Spectrum Method for Multiple-Support Seismic Excitations," by Der Kiureghian, A. and Neuenhofer, A., August 1991.

UCB/EERC-91/09 "A Preliminary Study on Energy Dissipating Cladding-to-Frame Connection," by Cohen, J.M. and Powell, G.H., September 1991.

UCB/EERC-91/10 "Evaluation of Seismic Performance of a Ten-Story RC Building During the Whittier Narrows Earthquake," by Miranda, E. and Bertero, V.V., October 1991.

UCB/EERC-91/11 "Seismic Performance of an Instrumented Six Story Steel Building," by Anderson, J.C. and Bertero, V.V., November 1991.

UCB/EERC-91/12 "Performance of Improved Ground During the Loma Prieta Earthquake," by Mitchell, J.K. and Wentz, Jr., F.J., October 1991.

UCB/EERC-91/13 "Shaking Table - Structure Interaction," by Rinawi, A.M. and Clough, R.W., October 1991.